VOLUME 83 NO. ST2
MARCH 1957

JOURNAL of the

Structural Division

PROCEEDINGS OF THE

AMERICAN SOCIETY
OF CIVIL ENGINEERS

BASIC REQUIREMENTS FOR MANUSCRIPTS

This Journal represents an effort by the Society to deliver information to the reader with the greatest possible speed. To this end the material herein has none of the usual editing required in more formal publications.

Original papers and discussions of current papers should be submitted to the Manager of Technical Publications, ASCE. The final date on which a discussion should reach the Society is given as a footnote with each paper. Those who are planning to submit material will expedite the review and publication procedures by complying with the following basic requirements:

1. Titles should have a length not exceeding 50 characters and spaces.

2. A 50-word summary should accompany the paper.

3. The manuscript (a ribbon copy and two copies) should be double-spaced on one side of 8½-in. by 11-in. paper. Papers that were originally prepared for oral presentation must be rewritten into the third person before being submitted.

4. The author's full name, Society membership grade, and footnote reference stating present employment should appear on the first page of the paper.

5. Mathematics are reproduced directly from the copy that is submitted. Because of this, it is necessary that capital letters be drawn, in black ink, 3/16-in. high (with all other symbols and characters in the proportions dictated by standard drafting practice) and that no line of mathematics be longer than 6½-in. Ribbon copies of typed equations may be used but they will be proportionately smaller in the printed version.

6. Tables should be typed (ribbon copies) on one side of 8½-in. by 11-in. paper within a 6½-in. by 10½-in. invisible frame. Small tables should be grouped within this frame. Specific reference and explanation should be made in the text for each table.

7. Illustrations should be drawn in black ink on one side of 8½-in. by 11-in. paper within an invisible frame that measures 6½-in. by 10½-in.; the caption should also be included within the frame. Because illustrations will be reduced to 69% of the original size, the capital letters should be 3/16-in. high. Photographs should be submitted as glossy prints in a size that is less than 6½-in. by 10½-in. Explanations and descriptions should be made within the text for each illustration.

8. Papers should average about 12,000 words in length and should be no longer than 18,000 words. As an approximation, each full page of typed text, table, or illustration is the equivalent of 300 words.

Further information concerning the preparation of technical papers is contained in the "Technical Publications Handbook" which can be obtained from the Society.

Reprints from this Journal may be made on condition that the full title of the paper, name of author, page reference (or paper number), and date of publication by the Society are given. The Society is not responsible for any statement made or opinion expressed in its publications.

This Journal is published bi-monthly by the American Society of Civil Engineers. Publication office is at 2500 South State Street, Ann Arbor, Michigan. Editorial and General Offices are at 33 West 39 Street, New York 18, New York. $4.00 of a member's dues are applied as a subscription to this Journal. Second-class mail privileges are authorized at Ann Arbor, Michigan.

HY,PO,SA,ST.

Journal of the

STRUCTURAL DIVISION

Proceedings of the American Society of Civil Engineers

STRUCTURAL DIVISION
COMMITTEE ON PUBLICATIONS
Josef Sorkin, Chairman; Mace H. Bell; Thomas R. Kuesel;
K. W. Lange; Wayne C. Lewis; Nathan W. Morgan;
Alfred L. Parme; Kenneth R. White; David M. Wilson.

CONTENTS

March, 1957

	Number
The Vibration of Simple Span Highway Bridges by John M. Biggs, Herbert S. Suer, and Jacobus M. Louw	1186
Analysis of Multiple-Span Continuous Trusses by Benjamin C. F. Wei	1187
Resistance to Overturning of Single, Short Piles by E. Czerniak	1188
Confirmation of Inelastic Stress Distribution in Concrete by Eivind Hognestad	1189
Design of Flexible Steel Arches by Interaction Diagrams by Haaren A. Miklofsky and Omar J. Sotillo	1190
Prestressed Truss-Beams by Ralph L. Barnett	1191
Discussion	1192

Copyright 1957 by the American Society of Civil Engineers.

Paper 1186 ST 2

Journal of the
STRUCTURAL DIVISION
Proceedings of the American Society of Civil Engineers

THE VIBRATION OF SIMPLE SPAN HIGHWAY BRIDGES

John M. Biggs,[1] A.M. ASCE., Herbert S. Suer,[2] J.M. ASCE.,
and Jacobus M. Louw[3]
(Proc. Paper 1186)

SYNOPSIS

The purpose of the investigation reported herein is to develop an analytical method by which the magnitude and character of highway bridge vibration due to the passage of heavy vehicles can be predicted. A method of analysis based upon certain simplifying assumptions is presented. The accuracy of the method and the validity of the assumptions are investigated by comparison with laboratory tests on model bridges. Tests of actual structures are used to prove the applicability of the method to field conditions. These tests also serve to indicate the field conditions which should be assumed for design purposes. Theoretical results obtained by both analog and digital computers are presented to show the effects of the various parameters involved. Finally, the problem is reduced to its simplest form and charts are provided which can be used to predict maximum dynamic deflections. The investigation is limited to simple-span girder and stringer bridges loaded by single two-axle vehicles.

NOTATION

The letter symbols used in this paper are defined where they first appear and are assembled for convenience of reference in the Appendix.

Note: Discussion open until August 1, 1957. Paper 1186 is part of the copyrighted Journal of the Structural Division of the American Society of Civil Engineers, Vol. 83, No. ST 2, March, 1957.

1. Associate Prof. of Structural Eng., Massachusetts Inst. of Technology, Cambridge, Mass.
2. Senior Structural Research Engr., North American Aviation, Inc., Downey, Calif.; formerly Research Asst., Massachusetts Inst. of Technology, Cambridge, Mass.
3. Research Asst., Massachusetts Inst. of Technology, Cambridge, Mass., and post-M.Sc. Fellow of The South African Council for Scientific and Industrial Research.

INTRODUCTION

The information currently available on highway bridge vibration is extremely meagre. Previous theoretical developments[4,5] were either directed toward railway bridge vibration or did not consider the actual field conditions which are part of the engineering problem. This paper attempts to bridge the gap between theory and field test results. The latter are useful as check points for the theory but cannot alone provide a solution to the problem.

Earlier field tests by the authors[6] lead to certain conculsions which form the basis for the investigation reported herein. The most important of these was the conclusion that the major factor which influences the amplitude of vibration is the vertical oscillation of the vehicle on its own springs as it approaches the span. Although the magnitude of this oscillation depends upon the roughness of the approach roadway, this factor is of primary importance even on surfaces normally considered to be "smooth." Except in extreme cases the condition of the surface on the bridge itself is of less importance and merely augments the initial oscillation of the vehicle.

The conclusion stated above indicates that the dynamic behavior of the vehicle is a primary consideration in the study of bridge vibration. The laboratory and field tests reported herein therefore involve dynamic measurements on both bridge and vehicle. The theoretical development below takes into account the dynamic characteristics of the vehicle as well as those of the bridge.

Theoretical Analysis

The analysis presented here does not represent a new theoretical development but is rather a simplification of previously derived theory. The manner in which it is presented is intended to convey a clear physical concept of the behavior. The basic equations derived, however, are essentially a simplified form of those used by Inglis, Hillerborg, and others.[7]

The form of the equations given below is believed to be such as to permit solution by the simplest possible computational methods. The equations are not theoretically exact but are sufficiently accurate to predict bridge vibrations for practical purposes. This is particularly true because the dynamic loading conditions for an actual structure can never be accurately predicted.

The method of analysis is based upon the following simplifications and assumptions:

---

4. "A Mathematical Treatise on Vibration in Railway Bridges," by C. E. Inglis, Cambridge University Press, London, 1934.
5. "Dynamic Influences of Smoothly Running Loads on Simply Supported Girders," by A. Hillerborg, Institution of Structural Engineering and Bridge Building, Royal Institute of Technology, Stockholm, 1951.
6. "Vibration Measurements on Five Simple Span Bridges," by J. M. Biggs and H. S. Suer, Highway Research Board, Bulletin No. 124, 1956.
7. "Highway-Bridge Impact Problems," by T. P. Tung, L. E. Goodman, T. Y. Chen, and N. M. Newmark, Highway Research Board, Bulletin No. 124, 1956.

1. Only the first mode of vibration is considered and the bridge is represented as a simple beam. Thus the bridge may be replaced by a single-degree-of-freedom system. The error resulting from this simplification is not serious if we are only concerned with the dynamic deflection at mid-span.

2. The vehicle is assumed to have only one degree of freedom. Actually a two-axle vehicle has many degrees of freedom since the mass is usually supported on four springs and four or more flexible tires. It is believed, however, that the important vehicle motion with respect to bridge vibration occurs when all of these elements are acting in phase.

3. The entire weight of the vehicle is assumed to be located at the center of gravity of the vehicle mass. The effect of the two axles could be considered in the procedure given below but this appears to be an unnecessary refinement.

4. Viscous damping is assumed in both bridge and vehicle.

Based upon these assumptions the system is simplified to that shown in Fig. 1 with the following notation:

V = velocity of vehicle
L = span of bridge
y_c = deflection at mid-span at any time
x = distance of vehicle from end of span
ω = crossing frequency = $\frac{\pi V}{L}$

At time t = 0 the center of gravity of the vehicle is at the end of the span. Since it is assumed that the deflected shape is at all times sinusoidal the bridge deflection beneath the vehicle is $y_c \sin(\omega t)$.

The vehicle is represented by the single-degree system shown in Fig. 2, in which,

M_{vs} = sprung mass of vehicle
M_{vu} = unsprung mass of vehicle
k_v = spring constant of vehicle suspension system
z = absolute deflection of sprung vehicle mass measured from the neutral position

The distortion of the vehicle spring is given by,

$$z - y_c \sin(\omega t) = \Delta \tag{1}$$

The force in the spring is,

$$k_v \Delta + M_{vs} g \tag{2}$$

Thus the equation of motion for the sprung mass is,

$$- k_v \Delta - c_v \dot{\Delta} = M_{vs} \ddot{z} \tag{3}$$

in which c_v is the coefficient of damping.

A typical vehicle actually has no unsprung mass since the tires behave as springs. The term is included in this general derivation in order to compare the theory with the model results presented below.

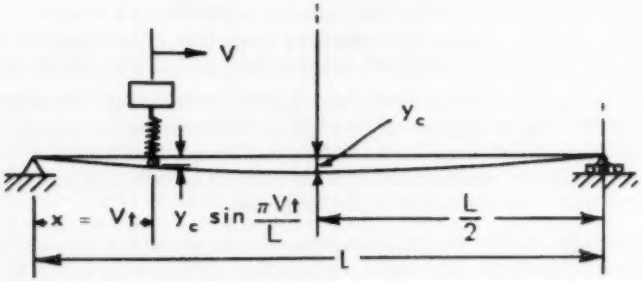

FIG. 1 IDEALIZED DYNAMIC SYSTEM

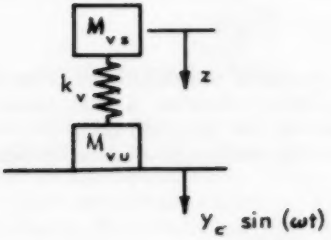

FIG. 2 IDEALIZED VEHICLE

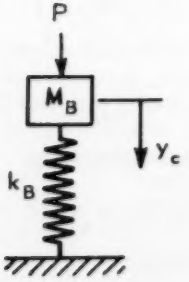

FIG. 3 IDEALIZED BRIDGE

The bridge may be represented by the single-degree system shown in Fig. 3 where P, M_B, and k_B are the load, mass, and spring stiffness of the equivalent system. The deflection of the equivalent mass is taken to be the same as the actual mid-span deflection of the bridge. Considering only the first mode of vibration it may be shown that the parameters of the equivalent system are as follows:

$$M_B = \frac{1}{2} M_B^T + M_{vu} \sin^2(\omega t) \tag{4}$$

where M_B^T is the total mass of the bridge,

$$P = (M_v g + k_v \Delta) \sin \omega t, \tag{5}$$

and

$$k_B = \frac{\pi^4 EI}{2L^3} \tag{6}$$

where EI is the rigidity of the actual bridge. The natural frequency of the equivalent system when the vehicle is not on the span is given by,

$$p_B = \sqrt{\frac{k_B}{M_B}} = \sqrt{\frac{\pi^4 EI}{M_B^T L^3}} \tag{7}$$

which is exactly the same as that of the first mode of the actual structure.

The equation of motion for the equivalent bridge system may then be written,

$$(M_v g + k_v \Delta) \sin(\omega t) - k_B y_c - c_B \dot{y}_c = M_B \ddot{y}_c \tag{8}$$

in which c_B is the coefficient of bridge damping.

In order to obtain a solution for y_c as a function of time Eqs. (3) and (8) are solved simultaneously while making use of Eq. (1). To take into account the vibration of the vehicle itself as it enters the span the initial conditions Δ_o and $\dot{\Delta}_o$ are inserted in the equations at t = 0.

Eqs. (3) and (8) cannot be solved directly in any convenient form. For this reason approximate methods of solution must be employed. One such method is numerical integration—a common device in the solution of dynamic problems—which produces a continuous record of deflection during the entire crossing. If done by hand computation this method is very laborious and not practical unless a limited number of solutions are desired. However, it is easily handled by digital computer and the final theoretical results of this paper were obtained in that manner.

Solutions may also be obtained by analog computer. This device is not as accurate as numerical integration but is more convenient for qualitative investigations of the effect of parameter variation. This procedure was used to obtain some of the results presented below.

Model Studies

Before attempting to obtain confirmation of the theoretical analysis by

field tests on actual structures, a series of small-scale laboratory tests was conducted to check the accuracy of the theoretical solution under carefully controlled conditions.[8] In this way the basic mathematical assumptions of the method were investigated without the uncertain conditions always present in actual field tests.

A single bridge model consisting of a simple beam with weights hung uniformly to provide mass was tested. The model was designed to represent a typical two-lane girder bridge of approximately 90-foot span. The natural frequency and the static deflection of the model are the same as for the prototype. The vehicle model simulated a 20-ton two-axle truck. Measurements were taken of the mid-span deflection and, simultaneously, the force in the vehicle spring. Tests were made varying the vehicle velocity, frequency, damping, and initial oscillation.

Test Apparatus

A general view of the testing apparatus is shown in Fig. 4. The model

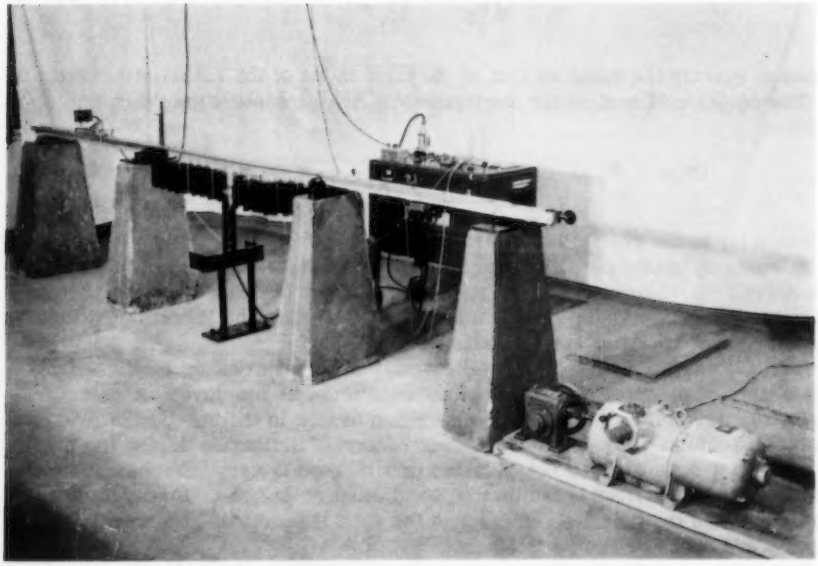

FIG. 4 MODEL TEST APPARATUS

8. "Model Investigation of Effects of Vehicular Vibrations on Simple Span Bridges," R. M. Connell and R. J. Lamp, M.I.T. Master's Thesis, June, 1955.

beam consisted of two pieces of steel stock fastened together by screws in such a manner as to introduce a camber equal to the total dead load deflection. The required mass of the model was obtained by hanging weights uniformly along the span. The fundamental natural frequency of the weighted beam was measured as 4.05 cps. Two approach sections were provided for accelerating and decelerating the vehicle.

The model vehicle consisted of an aluminum chassis on two axles which supported a cantilever beam of spring steel to which a steel mass was attached. The sprung mass was 85 per cent of the total weight of which 20 per cent was on the front axle. Damping in the vehicle was provided by a friction device on the suspended mass. Three springs were used in the model which provided natural vehicle frequencies of 2.27, 3.07, and 3.87 cps. The vehicle was pulled across the beam at constant speed by a synchronous motor with a master speed control. Tests were run at velocities corresponding to vehicle speeds on the prototype of 30, 40, and 50 mph.

It was desired to reproduce in the model the condition which is the major cause of actual bridge vibration, namely, an initial oscillation of the vehicle as it enters the span. This was accomplished by a removable hold-down arm which introduced a known deflection of the sprung mass. As the vehicle entered the span this arm was suddenly removed by a mechanical device. Thus the initial amplitude of harmonic motion was known.

The dynamic mid-span deflection of the bridge model was measured by a Shaevitz Transformer. The oscillations of the sprung vehicle mass were obtained by SR-4 strain gages mounted near the fixed end of the cantilever spring. Thus the dynamic force applied to the chassis at any time was known. The two measurements were simultaneously recorded by an oscillograph.

Model Test Results

Typical experimental results are shown by the dashed curves in Figs. 5 and 6. The upper portion of each figure indicates the per cent variation in total force applied by the vehicle to the bridge. The abscissa for all curves indicates the position of the vehicle center of gravity in terms of span which may also be considered to be a time scale. For convenience the ordinate of the deflection curves has been taken as the ratio of dynamic to maximum static mid-span deflection. The natural vehicle frequency was 3.87 cps for the test run shown in Fig. 5 and 3.07 cps for that shown in Fig. 6. The vehicle velocity for both test runs corresponded to 30 mph on the prototype.

The theoretical curves of Figs. 5 and 6 were obtained by numerical integration of Eqs. (3) and (8) using the initial conditions imposed on the model. The upper curve is given by,

$$\frac{100 \times k_v \Delta}{M_v g} \tag{9}$$

using the notation of the theoretical analysis. The ordinate of the lower curve is $\frac{y_c}{\delta_{st}}$ or $\frac{y_c k_B}{M_v g}$ where δ_{st} is the maximum static deflection at mid-span.

As indicated by the typical model results shown, there is good agreement between analysis and experiment for both bridge and vehicle behavior. The

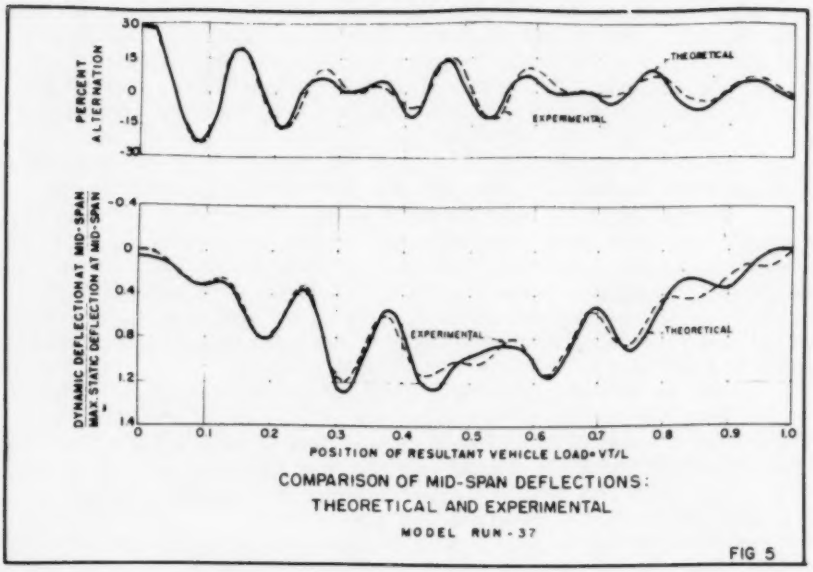

COMPARISON OF MID-SPAN DEFLECTIONS:
THEORETICAL AND EXPERIMENTAL
MODEL RUN - 37

FIG 5

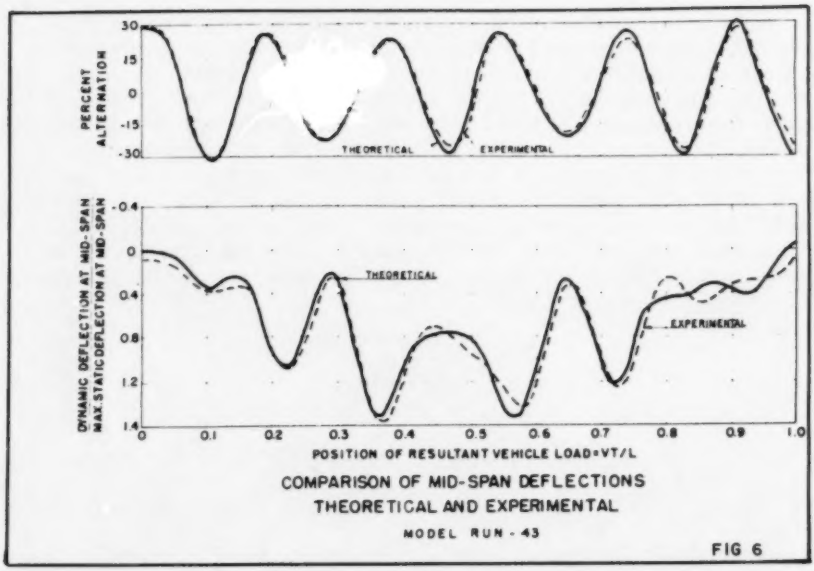

COMPARISON OF MID-SPAN DEFLECTIONS
THEORETICAL AND EXPERIMENTAL
MODEL RUN - 43

FIG 6

most obvious discrepancies in bridge deflection occur when the amplitude of vibration is small. However, the magnitude of these smaller amplitudes is not significant. It is concluded that the basic method of analysis is satisfactory. More specifically, the following conclusions are drawn: (1) For the computation of mid-span deflection the bridge may be represented by a single-degree-of-freedom system without appreciable error, and (2) for the type of bridge and vehicle represented by the model the separate axle loads may be replaced by a single concentrated load.

It is significant that the bridge deflection records obtained from the model are remarkably similar to those observed in actual field tests. This indicates that the conditions imposed on the model represent the major cause of actual bridge vibration.

Field Tests

Having concluded that the theoretical analysis gives satisfactory results for the idealized system represented by the model, it was then necessary to determine whether this system truly represents an actual bridge. More specifically, it was necessary to prove the following: (1) That an actual bridge could be idealized as a simple beam; (2) that an actual vehicle could be idealized as a single-degree-of-freedom system; and (3) that the surface roughness on the bridge was of secondary importance and could be ignored.

To accomplish this purpose two bridges were tested—one of the stringer type and the other a typical through girder bridge.[9] In each case the mid-span deflection was measured during the passage of a single heavy vehicle. The truck was also instrumented in order to obtain a continuous record of the dynamic force applied to the bridge. Approximately 25 test runs at various vehicle speeds were made on each of the two bridges.

The two structures selected for testing were the Main Street and South Street Bridges in Townsend, Massachusetts. The cross sections of the bridges are shown in Figs. 7 and 8. The Main Street Bridge has a skew of 21-1/2 degrees and the South Street Bridge a skew of 17 degrees. These particular bridges were selected because they are typical medium-span structures and because they presented a minimum of testing difficulties.

The test vehicle was a 1952 two-axle (6-wheel) Sterling White ten-ton dump truck. This truck has a wheel base of 13 feet, a tread of 6 ft 6 in., 11:00-24 front wheel tires and 12:00-24 rear wheel tires. The suspension system consists of leaf springs with a pair of auxiliary springs on the rear axle which are engaged under heavy load. The truck was loaded with steel snow-plow blades to produce a total weight of 41,624 lbs of which 33,875 lbs was on the rear axle.

Testing Procedure

Mid-span dynamic deflections were measured by deflectometers each of which consists of a small calibrated beam mounted within a tower which is placed beneath the structure. Also within the tower is a long rod held tightly between the beam and the underside of the bridge. As the bridge deflects the

9. "Dynamic Response of Simple Span Highway Bridges to Moving Vehicle Loads," by H. S. Suer, Doctor's Thesis, Massachusetts Institute of Technology, Sept., 1955.

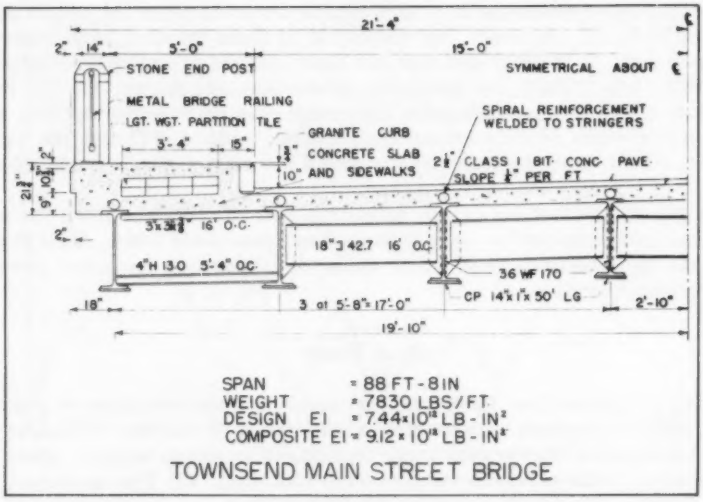

SPAN = 88 FT - 8 IN
WEIGHT = 7830 LBS/FT
DESIGN EI = 7.44×10^{12} LB - IN^2
COMPOSITE EI = 9.12×10^{12} LB - IN^2

TOWNSEND MAIN STREET BRIDGE

FIG. 7

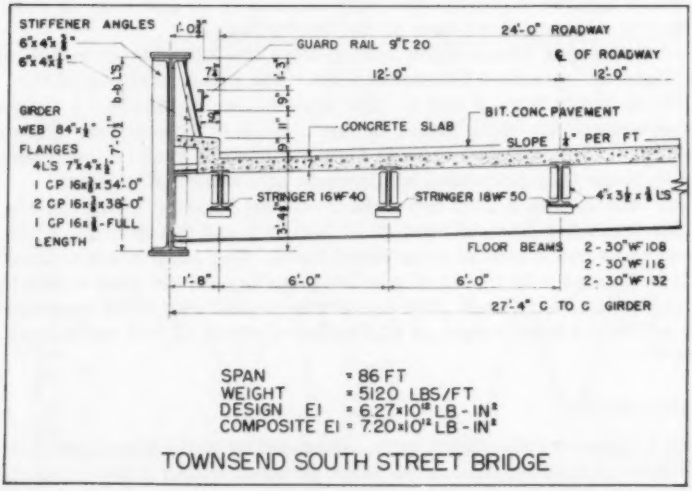

SPAN = 86 FT
WEIGHT = 5120 LBS/FT
DESIGN EI = 6.27×10^{12} LB - IN^2
COMPOSITE EI = 7.20×10^{12} LB - IN^2

TOWNSEND SOUTH STREET BRIDGE

FIG. 8

calibrated beam is also forced to deflect and the resulting strains are measured by SR-4 strain gages. The responses of these gages were fed into a Sanborn Strain Gage Amplifier and Recording System.

The testing of each bridge began with the measurement of static deflections which are given on the figures of test results. In both static and dynamic tests the vehicle was located in the center of the roadway. At the Townsend Main Street Bridge deflections were measured at mid-span of the stringer nearest the center line and at mid-span of the exterior stringer. At the Townsend South Street Bridge measurements were taken at mid-span of both girders. Moving load tests were conducted at various vehicle speeds and in both directions. During the tests care was taken to ensure that the vehicle speed was as constant as possible and that the truck maintained the centerline position.

Instrumentation of the truck consisted of strain gages used to measure the bending strains in the rear axle and, in addition, an accelerometer mounted at the center of the same axle. The responses of both strain gages and accelerometer were recorded by a portable Sanborn System placed in the bed of the truck. This procedure was based on the assumption that the variations in the front wheel loads were negligible compared to the total vehicle weight. This approximation was possible because only 19 per cent of the total weight was on the front axle.

Four strain gages were mounted on the axle and calibrated under static loading so as to provide values of the total axle load. This was accomplished by weighing the individual wheel reactions as the truck was loaded. Under dynamic conditions, however, corrections must be made for the inertia forces on the axle. For this purpose it was assumed that the entire mass of the axle assembly is concentrated at the center of the wheels. The error involved is not appreciable since 90 per cent of the total weight is concentrated at these points.

With these assumptions it may be shown that the sum of the two dynamic wheel loads is equal to that indicated by the strain gages minus the inertia force on the axle assembly. The latter is equal to the measured acceleration times the total mass of the assembly. This measurement was taken at the center of the axle. Although it is approximate for the individual wheels this acceleration is essentially correct for the total axle load. This procedure neglects the bending vibration of the axle itself. However, the natural frequency of this vibration is much higher than that of the rigid-body motion of the axle and has a negligible effect on the wheel loads.

A more serious error results from the fact that the resultant wheel load may not act at the same point along the axle as it did during the static calibration. This would occur if the roadway surface at each wheel was not parallel to the axle. Investigation reveals, however, that the possible error involved is not too large to be tolerated.

A completely satisfactory vehicle instrumentation is very difficult to achieve. In this study, however, it was not necessary to obtain exact measurement of the dynamic wheel loads but only to obtain an indication of the vehicle behavior. For this purpose the instrumentation proved to be satisfactory.

The average velocity and position of the test vehicle were determined by the use of two simple switching devices placed in the roadway at both ends of the structure. Each device consisted of a vertical strip of spring steel mounted so as to close a microswitch when bent by the passing vehicle. The

closed circuit caused a "pip" on the paper recording the bridge deflection. A similar device was mounted on the vehicle to provide a signal for the recording apparatus in the truck.

Test Results

The dynamic properties of the test vehicle were determined independently of the test runs on the bridges. The truck was run slowly over a large obstruction and the resulting free vibration recorded. The variation in the rear axle load showed a consistent natural frequency of approximately 2.3 cps. This same natural frequency was predominant on all test runs although the motion was never purely harmonic. Additional records obtained prior to and after crossing of the bridges indicated that the truck normally vibrates at essentially this frequency as it moves along the highway. This is not a practical way to determine the natural frequency, however, since local surface conditions introduce forcing functions which prevent a truly free vibration.

An attempt was made to compute the natural truck frequency from spring and tire stiffnesses measured statically. This computed frequency was considerably lower than that actually measured. The difference is believed to be due to greater interleaf spring friction during short-term load variations. To verify this conclusion vertical acceleration measurements were made simultaneously on the axle and body of the vehicle as it moved along the roadway. With moderate roadway surface conditions the two accelerations were found to be almost identical in amplitude, frequency, and phase, thus indicating that the leaf springs were almost entirely inactive and that the tires were providing most of the springing. The effectiveness of the springs obviously depends upon the age and condition of the vehicle.

The damping characteristic of the vehicle was found to vary considerably. However, an average viscous damping coefficient of 70.0 lb-sec per inch appeared to be reasonable.

The natural frequencies of the test bridges were obtained from the free vibrations remaining after the vehicle had left the span. These were found to be 3.77 cps for the Main Street Bridge and 4.17 cps for the South Street Bridge.

Typical experimental results for the dynamic tests on the two bridges are shown by the dashed lines in Figs. 9-12. The upper traces are those produced by the portable recorder in the vehicle while the lower traces are the records of bridge deflection which were obtained simultaneously. For convenience in analyzing the data analytical solutions are superimposed on the experimental curves. Many more records were obtained but they would provide little more information than those presented since the general characteristics of vibration were similar.

The records shown have been replotted from the original traces to provide more convenient scales. The ordinate is the ratio of dynamic to maximum static deflection. The abscissa is the position of the center of gravity of the vehicle in terms of span length. The latter may also be considered to be a time scale.

On the figures for the South Street Bridge the midspan deflections of both girders are shown on the same scale since the maximum static deflections are essentially equal. Only the deflection of the stringer nearest the center line is plotted for the Main Street Bridge.

The experimental load variation curves were computed from the strain and

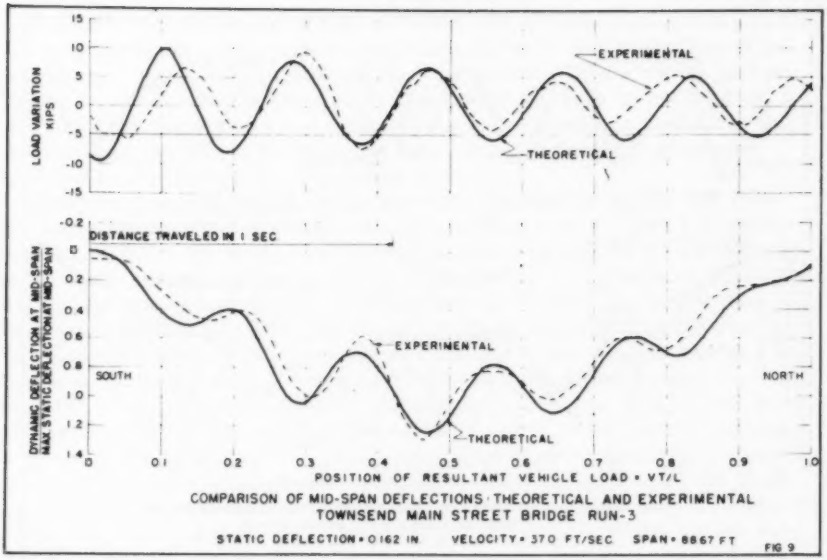

COMPARISON OF MID-SPAN DEFLECTIONS THEORETICAL AND EXPERIMENTAL
TOWNSEND MAIN STREET BRIDGE RUN-3

STATIC DEFLECTION = 0.162 IN. VELOCITY = 37.0 FT/SEC. SPAN = 88.67 FT

FIG 9

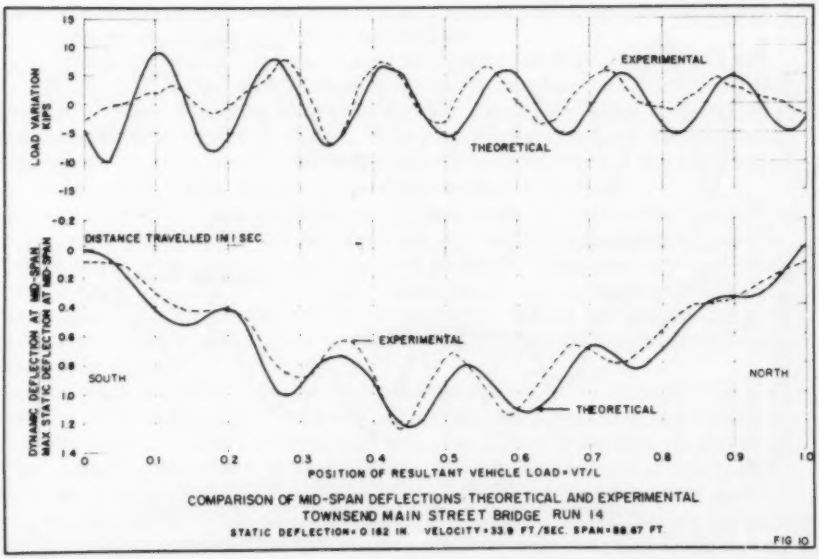

COMPARISON OF MID-SPAN DEFLECTIONS THEORETICAL AND EXPERIMENTAL
TOWNSEND MAIN STREET BRIDGE RUN 14

STATIC DEFLECTION = 0.162 IN. VELOCITY = 33.9 FT/SEC. SPAN = 88.67 FT

FIG 10

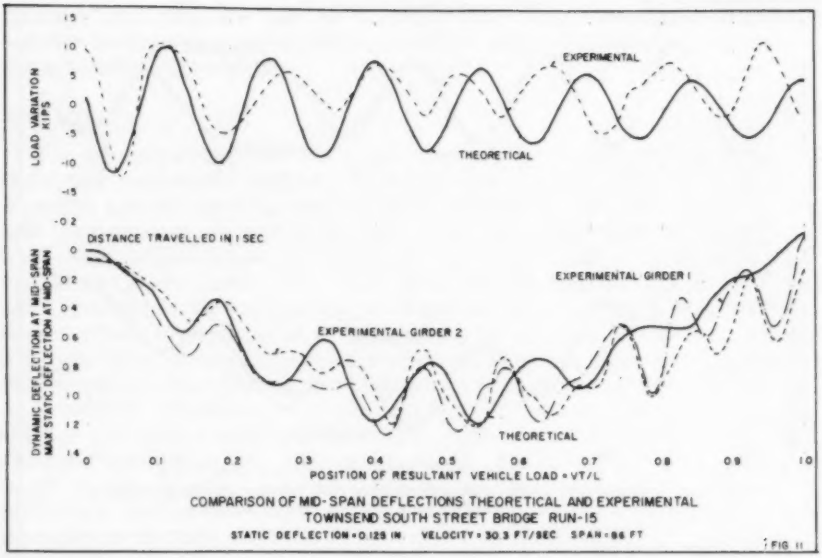

COMPARISON OF MID-SPAN DEFLECTIONS THEORETICAL AND EXPERIMENTAL
TOWNSEND SOUTH STREET BRIDGE RUN-15

STATIC DEFLECTION = 0.125 IN. VELOCITY = 30.3 FT/SEC SPAN = 86 FT

FIG 11

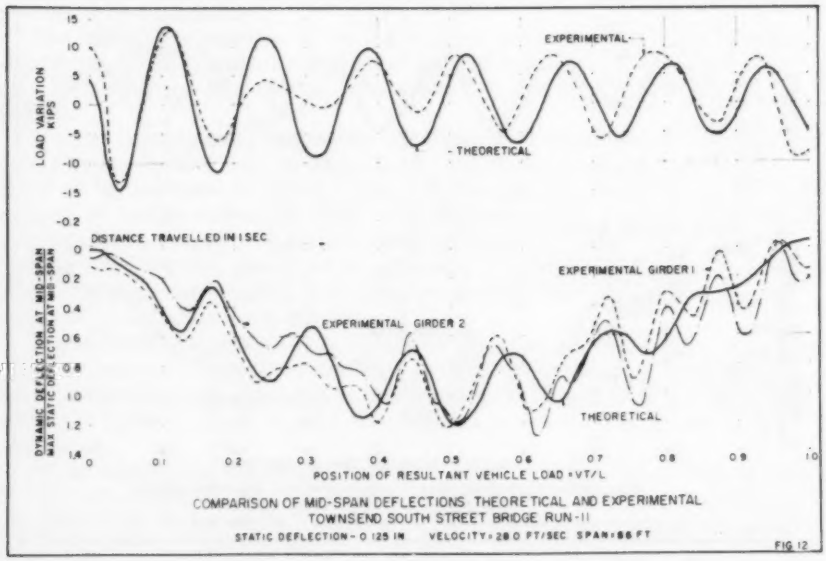

COMPARISON OF MID-SPAN DEFLECTIONS THEORETICAL AND EXPERIMENTAL
TOWNSEND SOUTH STREET BRIDGE RUN-11

STATIC DEFLECTION = 0.125 IN. VELOCITY = 28.0 FT/SEC SPAN = 86 FT

FIG 12

acceleration measurements on the rear axle. As discussed previously it was assumed that these measurements represent the total load variations of the test vehicle. These curves indicate the time variation of the actual load applied by the vehicle to the structure. The load at any time is the total static weight of the vehicle plus the ordinate to the curve given. In computing the load variation the inertia force on the axle computed from the measured acceleration generally had a secondary effect.

It may be observed that the behavior of the vehicle during the test runs was somewhat erratic. However, an average frequency of about 2.3 cps is apparent. This is the measured natural frequency of the truck. The erratic nature of the records is due primarily to the surface roughness on the bridge although the nonlinear behavior of the springs may be a contributing factor. The vehicle vibration is less uniform on the South Street Bridge than on the Main Street Bridge. This is directly attributable to the rougher roadway surface on the former. In fact, the roadway on the South Street Bridge was considerably rougher than that usually found on such bridges. It is important to note that in spite of this fact the load variation curve is reasonably uniform.

Although the amplitudes of vehicle oscillation varied considerably there is apparently an order of magnitude associated with each bridge. At the South Street Bridge the initial amplitude of load variation averaged about 15 kips or 35 per cent of the total weight. The variation at the Main Street Bridge was 5 to 10 kips or an average of 17.5 per cent of the total weight. There was a critical range of vehicle speed at which large oscillations occurred. Obviously for a certain character of roadway surface and a given natural vehicle frequency there is a critical velocity which induces maximum load variations.

It is important to note that in general the major portion of the load variation is caused by surface roughness on the approaches rather than on the bridge itself. The records for both structures indicate that the character of the expansion joints at the entrance to the span have an important influence on the subsequent amplitude of vehicle oscillation.

The bridge deflection records shown as dashed lines in Figs. 9-12 have been replotted from the oscillograph traces with no alteration except for the change in scales. It may be observed that the bridge vibration is generally in phase with the load variation curve. It is also obvious that the amplitude of bridge vibration is related to the amplitude of load variation. Sizable variations in the applied load always cause large bridge vibrations.

Figs. 11 and 12 for the South Street Bridge show the deflection records for both girders. In all cases the two records are displaced horizontally due to the skew in the same manner as the crawl or static deflection curves. The vibration superimposed on the crawl deflection, however, is essentially the same in phase and amplitude for the two girders. Minor variations are probably due to rolling of the vehicle about its longitudinal axis induced by local surface conditions.

On the Main Street Bridge the deflection of the exterior stringer was also measured but is not shown. With the vehicle on the center line the maximum static deflection observed was only 36 per cent of that measured on the centerline stringer. However, the vibrations of the two stringers under dynamic conditions were almost completely in phase and the amplitudes were more nearly equal than were the static deflections. This indicates that as far as the vibration is concerned the bridge behaves transversely more as a rigid body than it does under static loading. Records of the free vibration after the crossing of the vehicle show identical amplitudes for the two stringers.

Comparison with Theoretical Analysis

The theoretical solutions shown by the solid lines in Figs. 9-14 are based upon the equations previously given. Two different approaches are used. In the first intermediate step the dynamic bridge deflection is computed making use of the measured load variation. This serves to verify the applicability of the analytical method to actual bridges. In the second approach the vehicle behavior is idealized and the solution is completely theoretical except for the initial conditions and the values of bridge and vehicle stiffnesses. This second approach serves to investigate the feasibility of idealizing the vehicle for practical purposes.

In the solutions based upon the measured load variation only Eq. (8) was used. The term $k_v\Delta$ was replaced by the actual measured load variation and the equation was solved by numerical integration. The effective mass of the bridge, M_B, was computed from the design drawings. The rigidity, EI, in Eq. (6) was determined from the measured static deflection. The damping term in Eq. (8) was neglected since this is of minor importance.

Samples of this type of analysis are shown in Figs. 13 and 14. In the solution for the South Street Bridge no attempt is made to distinguish between the two girders since the bridge is idealized as a single beam. Only the interior stringer of the Main Street Bridge is considered. In both cases the agreement between theory and experiment is satisfactory. The maximum dynamic deflections are almost identical although there is less agreement when the amplitude of vibration is small. The discrepancies are no more than would be normally expected in any comparison of theory with actual field tests. It is concluded that the basic method of analysis is satisfactory for field conditions. To obtain a completely theoretical solution it is only necessary to idealize the vehicle behavior in a satisfactory manner.

The theoretical results shown in Figs. 9-12 were obtained using the complete analytical method without modification. For the vehicle stiffness, k_v, and damping coefficient, c_v, the experimental values were used. The oscillation of the vehicle at $t = 0$ was defined by the initial conditions Δ_o and $\dot{\Delta}_o$. These initial conditions were rather arbitrarily assumed so as to match as much of the experimental load variation curve as possible. The upper theoretical curves in the figures are plots of $k_v\Delta$ obtained from the analysis.

As expected the agreement between this completely theoretical approach and the experimental results is generally not as good as for the solution based upon the measured load variation. However, the comparison is still satisfactory. The agreement between theory and experiment is remarkably good for the Main Street Bridge. Better agreement on the South Street Bridge could probably not be expected because of the extremely rough roadway on the structure and because of the obvious effect of skew on the behavior of girder bridges. Most of the discrepancies in the bridge deflection records involve a phase shift rather than a difference in amplitude. For practical purposes these phase shifts are of little importance. It is also significant that the larger the vibration the more accurate the theoretical analysis becomes.

The differences between the theoretical and experimental bridge deflection curves are due primarily to the difference between the actual and the idealized load variation. The latter difference is largely due to surface roughness on the bridge deck. This is much more pronounced on the South Street Bridge which had the rougher roadway. Although the effect of the surface condition is quite obvious it does not change significantly the maximum amplitude or the general character of the bridge vibration.

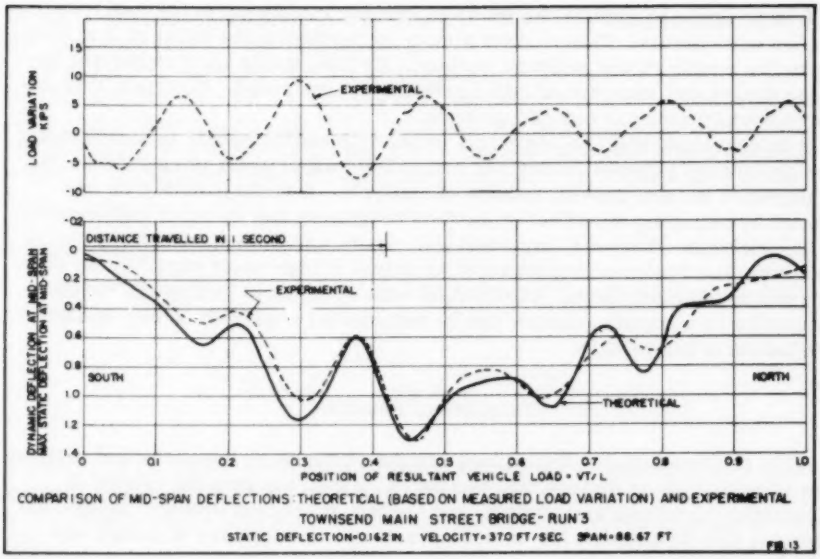

COMPARISON OF MID-SPAN DEFLECTIONS THEORETICAL (BASED ON MEASURED LOAD VARIATION) AND EXPERIMENTAL
TOWNSEND MAIN STREET BRIDGE - RUN 3
STATIC DEFLECTION = 0.162 IN. VELOCITY = 37.0 FT/SEC. SPAN = 88.67 FT

FIG 13

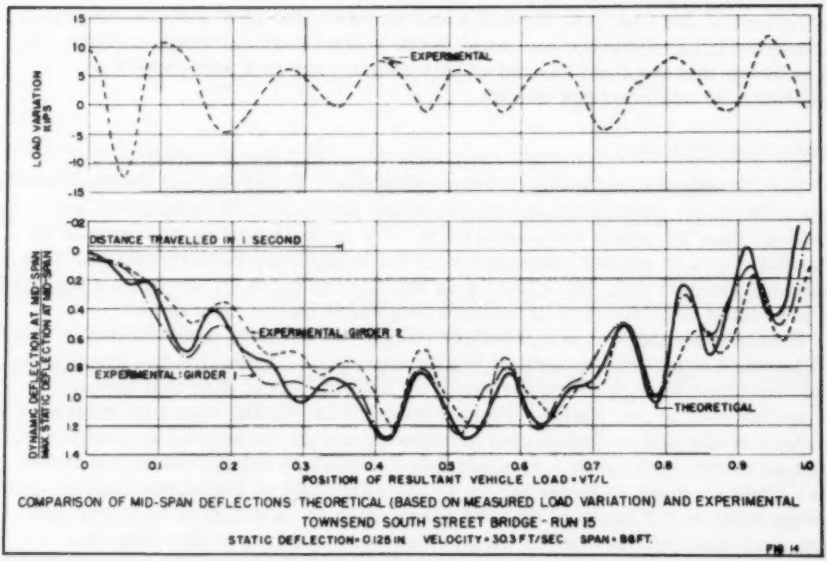
LOAD VARIATION K.P.S
EXPERIMENTAL
DISTANCE TRAVELLED IN 1 SECOND
EXPERIMENTAL GIRDER 2
EXPERIMENTAL GIRDER 1
THEORETICAL
DYNAMIC DEFLECTION AT MID-SPAN / MAX STATIC DEFLECTION AT MID-SPAN
POSITION OF RESULTANT VEHICLE LOAD = VT/L

COMPARISON OF MID-SPAN DEFLECTIONS THEORETICAL (BASED ON MEASURED LOAD VARIATION) AND EXPERIMENTAL
TOWNSEND SOUTH STREET BRIDGE - RUN 15
STATIC DEFLECTION = 0.128 IN. VELOCITY = 30.3 FT/SEC. SPAN = 88 FT.

FIG 14

It is possible to include the effect of surface roughness in the analytical method used herein. This is done simply by modifying the value of Δ according to the profile of the roadway surface. By this device the comparison between theory and experiment could probably be improved. However, this appears unwarranted for design purposes.

It is concluded that the analytical method presented herein is satisfactory. The agreement between theory and actual field experiment is as good as can be expected for any general method of analysis. It could possibly be improved by including the effect of surface roughness and by other refinements in the analysis. However, experimental errors and the inherent difficulty of idealizing the dynamic properties of an actual bridge make significantly closer agreement improbable. For bridges with reasonable degrees of surface roughness an adequate solution can be obtained by considering only an initial oscillation of the vehicle.

Theoretical Results

This section contains theoretical results obtained by the analytical method. The investigation is divided into two parts. First, the general effects of parameter variations are studied, and second, maximum dynamic bridge deflections are determined for various practical combinations of bridge and vehicle parameters.

The first part of the investigation was accomplished by use of an analog computer. This is the best device for a study of the effect of parameter variation but does not provide sufficient accuracy for final results. For this reason a digital computer was used in the second part referred to above. It is believed that the final results of this chapter are in a form which is practical for use in bridge design.

Basic Assumptions

The assumptions upon which these results are based include the theoretical approximations used in the derivation of the equations. It is believed that none of these introduce serious errors. The most important assumption is that the effect of roadway roughness on the bridge may be disregarded. The analysis includes only the effect of an initial oscillation of the vehicle which is presumed to be induced by surface roughness on the approaches.

It is obvious that severe pavement roughness or large obstructions on the bridge deck would cause serious bridge vibrations. However, the magnitude and character of such vibration would be little different than that induced by an initial vehicle oscillation. Furthermore, it is questionable that extreme surface conditions or actual obstructions should be considered in design at normal working stresses. An allowance for surface roughness on the structure could be made in the selection of the amplitude of initial oscillation. For design purposes it appears that the assumption of an initial vehicle oscillation is an adequate device for the prediction of dynamic bridge behavior.

In these theoretical computations damping in both the bridge and vehicle have been neglected. The damping coefficients of typical highway bridges are generally small and have very little effect on the vibration during the crossing of a vehicle. Damping in the vehicle is ignored because it may be counteracted by the surface roughness which may continuously excite the vehicle oscillation. Such being the case the inclusion of a vehicle damping coefficient

appears to be an unnecessary complication. Even if it were included it would be important only for the longer spans.

It is further assumed that the distinction between sprung and unsprung vehicle masses may be ignored and that the entire mass is spring supported. This is probably correct since the vehicle experiments indicated that much of the springing was in the tires rather than the leaf springs. In any case the effect of the unsprung mass is secondary because it is a small part of the total mass.

Parameters

A more convenient form of the theoretical equations is obtained by introducing the relationships,

$$p_v^2 = \frac{k_v}{M_v} \quad , \quad p_B^2 = \frac{K_B}{M_B} = \frac{M_v g}{M_B \delta_{st}}$$

where p_v is the natural vehicle frequency and p_B is the natural bridge frequency. Substituting Eq. (1) into Eqs. (3) and (8), eliminating the damping terms, replacing M_{vs} by M_v, and introducing the above relationships we obtain,

$$\frac{\ddot{y}_c}{\delta_{st}} = p_B^2 \left(\sin \omega t - \frac{y_c}{\delta_{st}}\right) + p_v^2 \frac{M_v}{M_B} \left(\frac{z}{\delta_{st}} - \frac{y_c}{\delta_{st}} \sin \omega t\right) \sin \omega t \quad (10)$$

$$\frac{\ddot{z}}{\delta_{st}} = - p_v^2 \left(\frac{z}{\delta_{st}} - \frac{y_c}{\delta_{st}} \sin \omega t\right) \quad (11)$$

All displacements are divided by the maximum static bridge deflection, δ_{st}, which is equal to $M_v g / p_B^2 M_B$. The parameters upon which the dynamic deflection and amplitude of vibration depend are taken as follows: ω, M_v/M_B, p_v, and p_B/p_v. In addition there are the initial conditions z_o, $\dot{z}_o$, y_{co}, and $\dot{y}_{co}$. The initial bridge conditions y_{co} and $\dot{y}_{co}$ are always taken as zero. The initial vehicle conditions z_o and $\dot{z}_o$ depend upon the maximum initial amplitude of vehicle oscillation, z_m, and the phase angle, ϕ. For convenience in presenting the results z_m is replaced by,

$$\beta = \frac{k_v z_m}{M_v g} = \left(\frac{p_v}{p_B} \right)^2 \frac{M_v}{M_B} \frac{z_m}{\delta_{st}} \quad (12)$$

where β is the maximum fractional variation in the applied load before entering the span. The phase angle is defined as the angular distance in terms of vehicle vibration from the end of the span to the point at which the vehicle mass has zero displacement and maximum downward velocity. Thus,

$$z_o = z_m \sin \phi \quad (13)$$

$$\dot{z}_o = z_m p_v \cos \phi \quad (14)$$

Parameter Ranges

In the results which follow each of the parameters is varied through a range of values which includes those encountered in most simple span highway bridges.

The initial oscillation of the vehicle which is defined by the parameter β is the most important of all the factors which determine the magnitude of vibration. Unfortunately, however, it is also the most uncertain factor in a particular case. The magnitude of β depends entirely upon the severity and the character of the surface roughness on the approach to the bridge. In the field tests described previously the maximum value observed was approximately 0.4 or, in other words, the maximum dynamic variation in total load was about 40 per cent of the static vehicle weight. The probability of the occurrence of larger values of β could only be determined by a statistical study of surfaces and vehicles. For the purposes of this investigation β is varied from 0.1 to 0.6.

The mass ratio M_V/M_B is varied from 0.05 to 0.5. It should be noted that M_B is one-half the total mass of the bridge. Therefore the two limiting values of mass ratio represent cases in which the vehicle weighs 2.5 per cent and 25 per cent of the total weight of the bridge.

The natural vehicle frequencies (p_V) considered vary from 2π to 6π radians per second or 1 to 3 cycles per second. No general study of vehicles has been made but it is believed that most heavy vehicles are included within this range.

A variation in natural bridge frequency (p_B) between 4π and 16π radians per second or 2 and 8 cycles per second is considered. In general the lower values correspond to long-span structures and the higher values to bridges of short span. The range of frequency ratio, p_B/p_V, for which results are given is from 0.67 to 7.0.

For each combination of the other parameters the crossing frequency ω is varied in order to determine the maximum possible dynamic deflection and amplitude of vibration. In order to keep the results within a practical range limitations were placed on the variation of this parameter. These limits were derived in the following manner. The range of vehicle velocities is taken as 20 to 50 miles per hour. Lower speeds would probably not involve appreciable vehicle oscillations and higher speeds probably need not be considered. It was assumed that the natural bridge frequency is related to the length of span according to the approximate empirical formula, $p_B = \frac{2200}{L}$. Using this expression and the assumed range of vehicle speeds in the equation $\omega = \pi V/L$ the range of crossing frequency considered in the computations is,

$$\omega = 0.04\, p_B \text{ to } \omega = 0.10\, p_B.$$

The approximate and rather arbitrary nature of these limits is justified by the results which indicate that the range of ω is not of primary importance.

Variations in phase angle, ϕ, are also considered. No limitations are imposed since any value could occur under field conditions.

Effect of Parameter Variations

The effect of vehicle velocity on maximum dynamic deflection was

investigated using the analog computer. These results for various combinations of p_V and p_B are shown in Fig. 15. In all cases it will be noted that the curves have a wave form and that there are critical values of ω at which maximum deflections occur. When the frequency ratio is unity the highest peaks and hence the largest bridge deflections occur at slow vehicle speeds. For frequency ratios of two or greater, however, the peak values increase with increasing velocity. For frequency ratios between unity and two, maximum deflection occurs at velocities between these two extremes. In terms of the limitations imposed on values of ω, maximum deflection occurs near $\omega = .04\ p_B$ for frequency ratios of unity, near $\omega = .10\ p_B$ for ratios above two, and at intermediate values for frequency ratios between one and two. For the higher frequency ratios the peaks occur when the velocity is such that the vehicle mass has a maximum downward displacement at mid-span.

It should not be expected that field tests of actual structures would produce maximum deflection-velocity curves identical to those of Fig. 15. These theoretical curves were obtained for a constant value of β. In field tests the value of β would probably vary in some unpredictable manner with vehicle speed.

The effect of vehicle phase angle on maximum deflection was also investigated by analog computer. Some of these results are shown in Fig. 16. It is obvious that the phase angle has a definite effect and should be considered when determining maximum possible deflections.

The following results beginning with Fig. 17 are maximum dynamic deflections for particular combinations of parameters which define a particular bridge and vehicle. Each value given is intended to be the maximum possible deflection for those parameters. This involves in each case the selection of the most critical values of ω and ϕ. The problem is difficult because there is an infinite number of combinations of these two parameters. The critical values were estimated by analog studies and by certain theoretical considerations. The final results plotted below were then obtained by digital computer. In a final attempt to ensure that the deflections were truly maximums digital computer solutions were obtained for several combinations of ω and ϕ in each case.

For large frequency ratios the critical condition is not difficult to determine because the bridge and vehicle are essentially two independent dynamic systems. In this case the bridge vibration may be approximately considered to be the addition of two parts: (1) The vibration due to a constant force crossing the span and, (2), a vibration in phase with the oscillation of the vehicle. The critical values of ω and ϕ are those for which these two parts have maximum downward amplitudes at the same point near mid-span.

When the frequency ratio is less than approximately 2.5 the two systems cannot be considered independently and the theoretical determination of the critical condition becomes more difficult. The behavior of the bridge is somewhat analogous to the familiar "beat" of a linear two-degree system. However, the variable coefficients of the equations for the bridge problem make it difficult to interpret this analogy.

It is believed that the values plotted in Fig. 17, 18, and 19 are near the absolute maximum deflections. However, it is probable that for frequency ratios less than 2.5 the points should be slightly higher.

The effect of frequency ratio is shown in Fig. 17 where results are given for constant values of β and M_V/M_B. It may be observed that for ratios above 2.5 the curve is smooth and that the dynamic deflection varies from

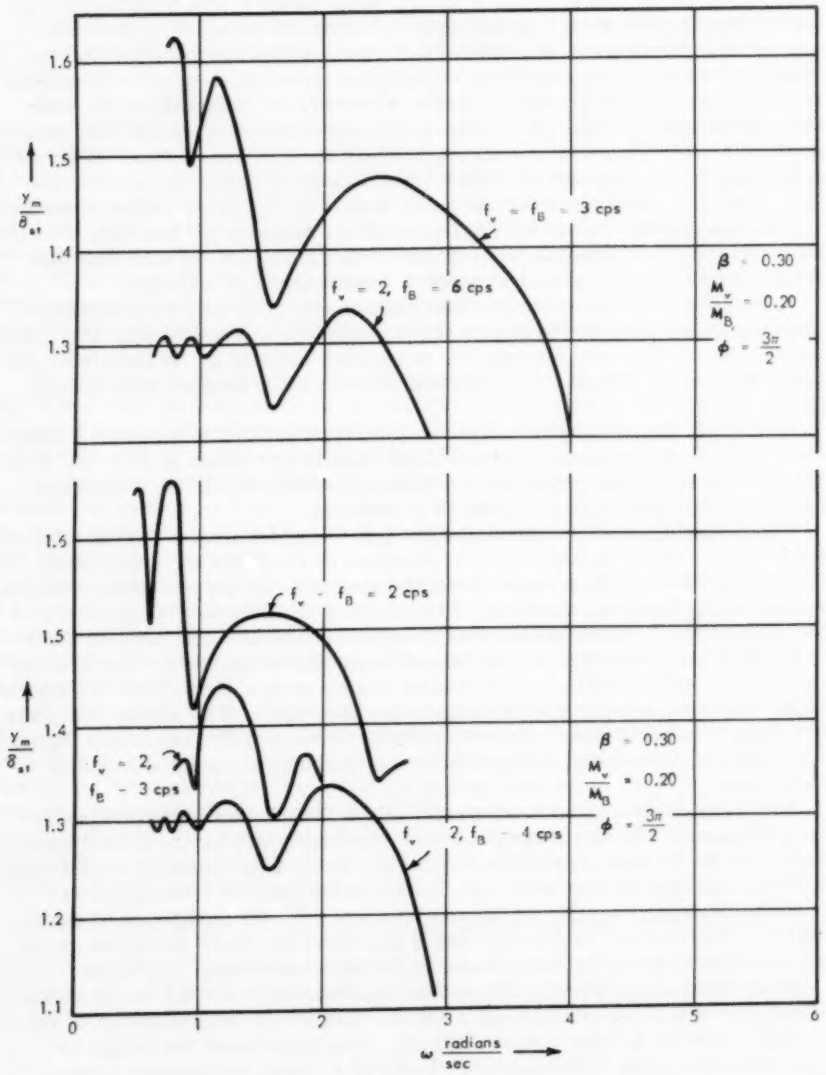

FIG. 15 EFFECT OF ω ON MAXIMUM DEFLECTION

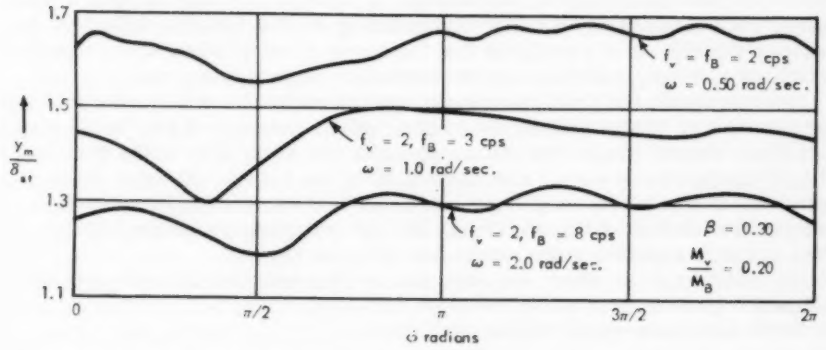

FIG. 16 EFFECT OF PHASE ANGLE ON MAXIMUM DEFLECTION

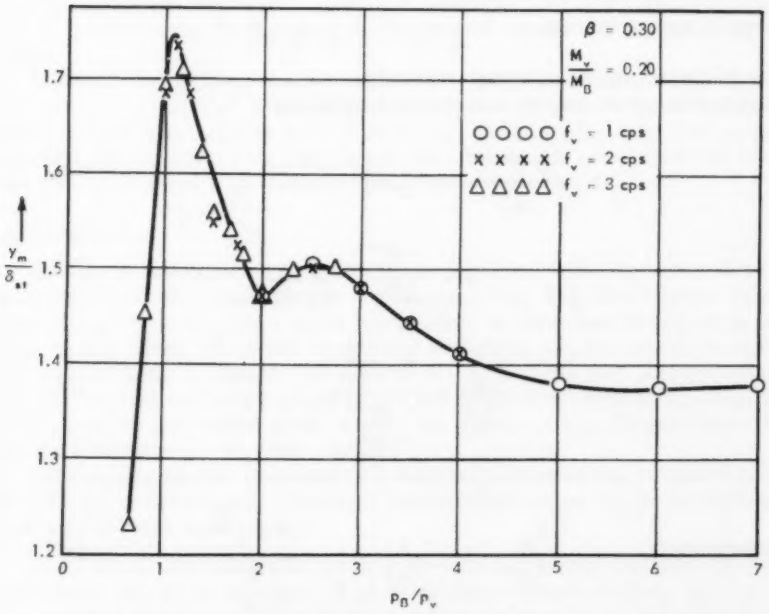

FIG. 17 EFFECT OF FREQUENCY RATIO ON MAXIMUM DEFLECTION

about 1.375 to 1.50 of the static deflection. For ratios below 2.5 the curve is more irregular but generally increases to a maximum of about 1.74 at a frequency ratio slightly above unity. Below this point the dynamic deflection decreases rapidly. It is significant that the curve is independent of the actual values of p_V and p_B and that only the frequency ratio is important.

The reason for the peak near $p_B/p_V = 1$ is apparent when one considers the behavior of bridge and vehicle in this region. Because of the "beat" effect which occurs only at low frequency ratios the oscillation of the vehicle almost disappears at one or more points along the bridge. At these same points the bridge vibration greatly increases because most of the energy originally contained in the vehicle oscillation is transferred to the bridge. This effect is apparent in the model run shown in Fig. 5.

The validity of the above argument can be demonstrated theoretically as follows:

Total initial energy in vehicle oscillation =

$$= \frac{1}{2} k_V z_m^2 = \frac{1}{2} \frac{M_V \beta^2 g^2}{p_V^2}$$

Energy in bridge vibration = $\frac{1}{2} k_B A^2 = \frac{1}{2} M_B p_B^2 A^2$,

where A is the amplitude of bridge vibration.

Assuming complete energy transfer and equating,

$$\frac{M_V \beta^2 g^2}{p_V^2} = M_B p_B^2 A^2$$

$$A = \sqrt{\frac{M_V}{M_B}} \frac{\beta g}{p_V p_B}$$

$$\frac{A}{\delta_{st}} = \frac{\beta \left(\frac{p_B}{p_V} \right)}{\sqrt{\frac{M_V}{M_B}}} \qquad (15)$$

Approximately, $$\frac{y_m}{\delta_{st}} = 1 + \frac{A}{\delta_{st}} = 1 + \frac{\beta \left(\frac{p_B}{p_V} \right)}{\sqrt{\frac{M_V}{M_B}}} \qquad (16)$$

For $\frac{p_B}{p_V} = 1$, $\frac{M_V}{M_B} = 0.2$ and $\beta = 0.3$, $\frac{y}{\delta_{st}}$ may be computed by Eq. (16) to be 1.68. This value is very close to the maximum shown in Fig. 17. The latter is somewhat greater because of the vibration caused by the simple passage of a constant force which is independent of β.

It should be noted that a frequency ratio of unity does not represent a true

resonant condition in which deflections approach infinity. In the case under study energy is not continuously fed into the system and the energy contained in the bridge vibration is limited to that which was originally contained in the vehicle.

The effect of β which represents the initial amplitude of vehicle oscillation is shown in Fig. 18, where curves are plotted for three different combinations of p_V and p_B. It is apparent that in all cases the effect of β is linear. The curves indicate that this effect becomes slightly greater as the frequency ratio approaches unity. For the higher frequency ratios y_m/δ_{st} is essentially equal to $(1.1 + \beta)$.

The effect of mass ratio, M_V/M_B, is shown in Fig. 19. It may be seen that for high frequency ratios the value of mass ratio has no effect on maximum deflection. The effect becomes apparent, however, as the frequency ratio decreases and becomes quite significant for a frequency ratio of unity. It is important to note that for high mass ratios the maximum deflection ratio does not vary appreciably with frequency ratio. This indicates that if the curve of Fig. 17 had been computed for a higher mass ratio the peak near $p_B/p_V = 1$ would not have appeared. The reason for this effect can be deduced from Eq. (16) which indicates that as the mass ratio increases the maximum dynamic deflection decreases. Even if the complete energy transfer takes place the deflection is no larger than would be expected with high frequency ratio.

It should be recalled that all results are given in terms of the deflection ratio, y_m/δ_{st}. A high value of this ratio may not be significant if δ_{st} is small. This may apply to the curve in Fig. 19 for $p_B/p_V = 1$. The large deflection ratios may not be significant since the small mass ratio for which they were obtained may indicate small static deflections.

Application

In Fig. 20 the curves previously presented have been re-drawn in a manner convenient for actual design application. Fig. 20(a) is simply a reproduction of Fig. 17 and is completely independent of the actual values of p_V and p_B. In Fig. 20(b), which has been taken from Fig. 18, the values on each curve have been divided by the value at $\beta = 0.3$. Thus Fig. 20(b) provides correction factors to be applied to results taken from Fig. 20(a). Fig. 20(c) also provides correction factors since the values of Fig. 19 have been divided by the deflection for $M_V/M_B = 0.2$.

To summarize, the following is a detailed outline of the proposed procedure for predicting the maximum dynamic deflection for an actual bridge and a single two-axle vehicle.

1. Compute the maximum static deflection for a single design vehicle on the center line of the roadway (δ_{st}) using conventional methods except that the moment of inertia should be taken as the composite value including all secondary elements of steel or concrete which could conceivably contribute to the stiffness.[6] However, in the case of a wide stringer bridge the contribution of the exterior stringers is questionable. The above recommendation is based on the belief that composite action occurs in deck stringer bridges even though shear connectors are not provided. It should be recognized, however, that this may be only partly true of older bridges.

2. Compute the natural frequency of the structure which may be

---

6. Footnote 6 appears on page 1186-2.

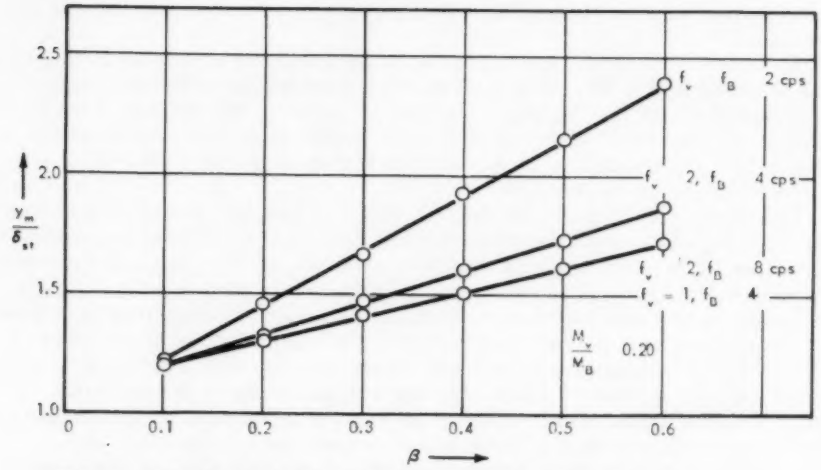

FIG. 18 EFFECT OF β ON MAXIMUM DYNAMIC DEFLECTION

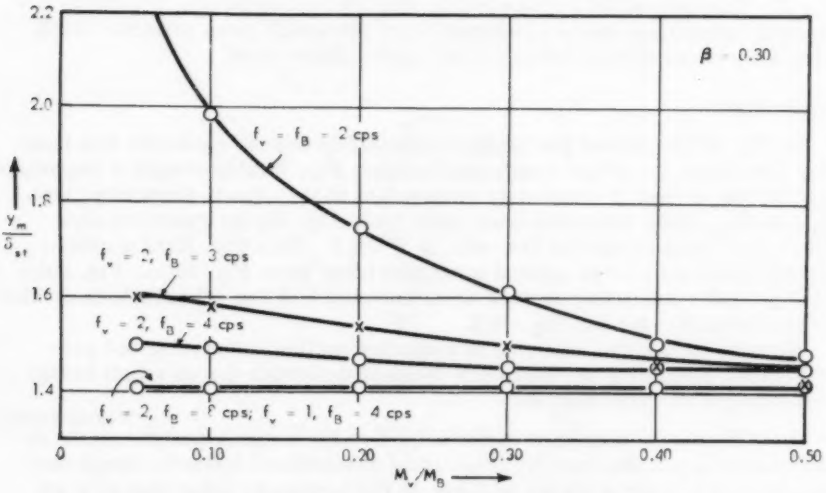

FIG. 19 EFFECT OF MASS RATIO ON MAXIMUM DEFLECTION

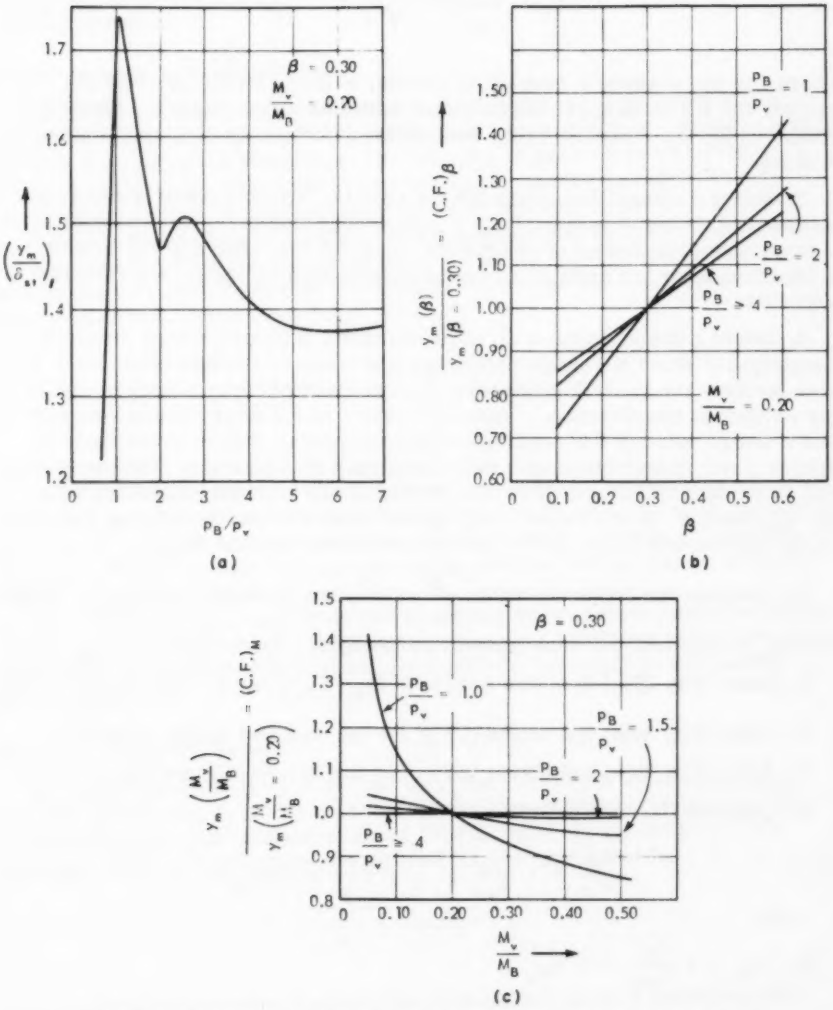

FIG. 20 DESIGN CURVES FOR MAXIMUM DYNAMIC DEFLECTION

approximated by,

$$f_B = \frac{1.2\,\pi}{2L^2}\sqrt{\frac{EI\,g}{W}} \quad \text{cps} \qquad (17)$$

where I is the composite moment of inertia, W is the weight per foot of bridge, and 1.2 is an approximate factor based on test results.[6] I should be computed for the complete cross section even in the case of wide stringer bridges.

3. Select a natural frequency for the vehicle. Further study is required on this subject but it is tentatively recommended that the designer consider a range of vehicle frequencies between 1 and 2.5 cps. For a given natural bridge frequency the most severe vehicle frequency is easily observed in Fig. 20(a).

4. Select a design value of β. Determination of proper values requires considerable study of vehicle properties and roadway surface conditions. It also involves the general philosophy of design and should probably be left to the writers of specifications. Actual β-values of 0.4 are probably common and a design value of 0.5 would not be unreasonable. It is possible that the proper β-value decreases with increasing span of the bridge. This would result from the fact that roadway deck surfaces are generally smoother than the approaches. In the case of long spans, large vehicle oscillations induced on the approaches might not be maintained during the crossing.

5. Compute the frequency ratio, $\frac{p_B}{p_V}$ or $\frac{f_B}{f_V}$, and the mass ratio, $\frac{M_V}{M_B}$. Note that M_B is one-half the total mass of the bridge.

6. Enter Fig. 20(a) to obtain a value of $(y_m/\delta_{st})_1$ for $\beta = 0.3$ and $\frac{M_V}{M_B} = 0.2$.

7. Enter Fig. 20(b) and obtain $(CF)_\beta$ for the selected design value of β.

8. Enter Fig. 20(c) and obtain $(CF)_M$ for the computed mass ratio.

9. Compute the final deflection ratio by,

$$\frac{y_m}{\delta_{st}} = \left(\frac{y_m}{\delta_{st}}\right)_1 \times (CF)_\beta \times (CF)_M \qquad (18)$$

10. $y_m = \left(\frac{y_m}{\delta_{st}}\right) \times \delta_{st}$

Step (9) in the above procedure is not exact since it is assumed that the two correction factors are independent of each other. Although not proven this is believed to be essentially correct.

It should be noted that the dynamic deflection ratio obtained by the above procedure is for a single two-axle vehicle on the roadway center line. The deflection ratio for more than one vehicle or for a single vehicle off the center line would be somewhat less. Vehicles having more than two axles must be considered in future studies.

The results presented herein together with other similar and related

---

6. Footnote 6 appears on page 1186-2.

investigations will eventually lead to specification criteria to guard against excessive vibration. In the meantime the above procedure is believed to be a practical means of investigating the susceptibility of a particular bridge design to vibration.

Maximum Amplitude of Vibration

One of the reasons for studies of bridge vibration is the possible effect of excessive vibration on pedestrians. This may result in public complaint and perhaps distrust of the structure. The reaction of persons to vibration is determined not by maximum deflection but by the amplitude and frequency of the oscillation which is superimposed on the crawl deflection curve.

The amplitude of this oscillation varies continuously as the vehicle crosses the span and the most significant value is not easily determined. However, it may be conservatively taken as the difference between the maximum dynamic and the maximum static deflection. Thus,

$$A = \left[\left(\frac{y_m}{\delta_{st}} \right) - 1 \right] \delta_{st} \tag{19}$$

where y_m/δ_{st} is determined by Eq. (18).

The frequency of the oscillation may vary between the natural frequency of the bridge and that of the vehicle. The largest amplitudes, however, generally occur at the natural vehicle frequency. Since persons are more susceptible to high frequencies it would be conservative to assume that the higher of the two natural frequencies applies.

The combinations of amplitude and frequency which people find objectionable are as yet undetermined. This subject has been studied in connection with automobile design[10] but these results probably do not apply to the case of bridge vibration.

Maximum Dynamic Stress

Although this investigation was not directed toward the determination of dynamic stresses it is possible to draw some general conclusions from the results obtained. The maximum static bending moment due to the vehicle represented by a single concentrated load may be expressed by,

$$M_{st} = \frac{12\ EI}{L^2}\ \delta_{st} \tag{20}$$

Considering the sinusoidal shape of the fundamental mode of vibration, the mid-span bending moment due to the dynamic increment of deflection is given by,

$$M' = EI\ A\ \frac{\pi^2}{L^2} \tag{21}$$

10. "Vehicle Vibration Limits to Fit the Passenger," by R. N. Janeway, SAE Special Publication, March, 1948.

where A is the dynamic increase in mid-span deflection. Combining these two expressions and Eq. (19) we obtain,

$$\frac{M_m}{M_{st}} = 1 + 0.82 \left(\frac{y_m}{\delta_{st}} - 1 \right) \qquad (22)$$

where M_m is the maximum dynamic bending moment at mid-span. This equation is approximate since only the first mode of vibration is included. In general the higher modes contribute more to the bending moment than to the deflection.

In most cases Eq. (22) should not be used to predict maximum dynamic bending stresses without modification of the value of y_m/δ_{st} given by Eq. (18). The latter equation gives deflection ratios for a single vehicle which is not the design condition for most bridge elements. Numerical addition of the dynamic effects of two or more vehicles requires the improbable condition that the oscillation of all are in exact phase. In addition, this study has been limited to the case of a single two-axle vehicle traveling on the center line of the roadway. If the vehicle is not so positioned it is probable that the dynamic increase in the most heavily loaded girder is less than that indicated above. For these reasons Eq. (22) gives a moment ratio which is probably conservative for most design cases.

CONCLUSIONS

The following conclusions may be drawn from the data presented herein:

1. The proposed simplified method of analysis is sufficiently accurate for engineering purposes. Reasonable agreement was obtained with both laboratory and field tests. The method may be used for both stringer and girder bridges.

2. From the field tests it is concluded that the major cause of vibration is the initial oscillation of the vehicle on its own springs and that for design purposes the effect of surface roughness on the bridge may be neglected.

3. Theoretical results based upon conclusion (2) indicate that the initial amplitude of vehicle oscillation is by far the most important factor which influences the magnitude of bridge vibration.

4. In addition, however, large vibrations generally occur when the natural frequency of the vehicle is close to that of the bridge.

5. The only other factor which influences the deflection ratio, y_m/δ_{st}, is the mass ratio, M_V/M_B, and this is important only when the frequency ratio is near unity.

6. All results have been given in terms of the deflection ratio, y_m/δ_{st}. It is obvious that a bridge designed with a large static deflection may be expected to experience large amplitudes of vibration.

7. The present tendency toward long-span and slender bridges should be regarded with caution. For such structures the combination of low natural frequency approaching that of heavy vehicles and roadway roughness on the approaches may result in excessive vibration. It should be noted, however,

that the verifying laboratory and field tests cited herein were all for medium-span bridges. Additional verification is needed for extremely long spans.

ACKNOWLEDGMENTS

This paper is based upon research undertaken by the Joint Highway Research Project established at the Massachusetts Institute of Technology by a grant from the Massachusetts Department of Public Works. The authors are indebted to the personnel of the Department Staff for their cooperation. At M.I.T. Saul Namyet, Assistant Professor of Structural Engineering, and R. G. Gray, Research Assistant, were most helpful in programming the problem for the digital computer.

APPENDIX

Notation

- L Span of bridge
- I Composite moment of inertia of bridge
- W Weight per foot of bridge
- M_B^T Total mass of bridge
- M_B Effective mass of bridge
- k_B Spring stiffness of bridge
- p_B Fundamental natural frequency of bridge, rads/sec
- f_B Fundamental natural frequency of bridge, cps
- c_B Damping coefficient of bridge
- y_c Dynamic mid-span bridge deflection
- $\dot{y}_c$ dy_c/dt
- $\ddot{y}_c$ d^2y_c/dt^2
- y_b Maximum dynamic mid-span bridge deflection
- A Amplitude of bridge vibration
- δ_{st} Maximum static mid-span bridge deflection
- E Modulus of Elasticity
- V Velocity of vehicle
- x Distance of vehicle from end of span
- ω Crossing frequency, $\pi V/L$
- M_v Mass of vehicle
- M_{vs} Sprung mass of vehicle
- M_{vu} Unsprung mass of vehicle

k_v Spring constant of vehicle

p_v Fundamental natural frequency of vehicle, rads/sec

f_v Fundamental natural frequency of vehicle, cps

c_v Vehicle damping coefficient

z Deflection of sprung vehicle mass

Δ Vehicle mass deflection relative to bridge

z_o Initial vehicle mass deflection

β Initial load variation parameter

y_m/δ_{st} Deflection ratio

p_B/p_v Frequency ratio

M_v/M_B Mass ratio

Journal of the
STRUCTURAL DIVISION
Proceedings of the American Society of Civil Engineers

ANALYSIS OF MULTIPLE-SPAN CONTINUOUS TRUSSES

Benjamin C. F. Wei,[1] J.M. ASCE
(Proc. Paper 1187)

SYNOPSIS

This paper presents the method of the moment influence line as the basic tool in analysing continuous trusses. This method, as compared to the conventional analysis of continuous trusses by the removal of reaction redundants, has the advantages that the computation for the stresses due to each unit loading is limited to two spans regardless of the number of spans in the truss, and that the constants for the solution of simultaneous equations are easily obtained by one simple operation. These advantages result in a saving of a considerable amount of time for the analysis of long-span continuous trusses of more than 2-spans, particularly those with unsymmetrical proportions. Computations for elastic weights and constants for the simultaneous equations are given in simple tabular form, suitable for use in actual design. A numerical example showing the complete analysis of moment influence lines for a 4-span continuous truss is presented.

INTRODUCTION

Since the time Gustave Lindenthal designed the Sciotoville Bridge, the continuous truss as a form of load-carrying member has gradually gained popularity among bridge engineers. Only very recently, from 1953 to 1955, a number of notable continuous truss highway bridges have been designed, among which are the 500-800-500 ft. continuous deck truss at Kingston, N. Y.,[2] the four-span continuous approach trusses at Mackinac Straits, Michigan,[3] and the Newark Bay Bridge at the extension of the New Jersey Turnpike. The

Note: Discussion open until August 1, 1957. Paper 1187 is part of the copyrighted Journal of the Structural Division of the American Society of Civil Engineers, Vol. 83, No. ST 2, March, 1957.

1. Prin. Designing Engr. on Structures, Hydrocarbon Research Inc., New York, N. Y.
2. W. E. Joyce & C. H. Gronquist, 'Design of the Kingston Bridge over the Hudson River,' ASCE Proc. Paper #681, May 1955.
3. D. B. Steinman, 'Mackinac Straits Bridge,' ASCE Proc. Paper #559, Dec. 1954.

increasing popularity of the continuous truss in bridge design demands a practical method of analysis that is accurate, systematic, easy to work, and yet simple enough to be plainly understandable in its principle of application. The conventional method of removing the reaction redundant is a good method, easily visualized and readily workable. This method has been widely used for analysing continuous trusses, and the principle of the analysis has been demonstrated in most standard texts of structural theory.[4] However, the method involves a considerable amount of arithmetic in the solution of influence ordinates, particularly for multiple-span continuous trusses of many panels and with unsymmetrical elevations. It is a well-known fact that the design of continuous trusses is a cut-and-trial procedure, meaning that any change of area of a member of the truss in the various stages of design would affect the balance of the structure and hence would call for a revised calculation. Ordinarily at least two or three cycles of computation are necessary to obtain the final influence line to be used in design. The method of the moment influence line aims chiefly at simplifying and reducing the arithmetic involved in computing the influence ordinates, and hence reducing proportionately the chance of error. This method is specially adaptable to design offices, since any simplification of work and saving of time for one cycle of computation would be multiplied by the number of cycles required for the entire repetitive analysis of the structure. It must be understood that the moment influence lines are not additional influence lines that are used only for obtaining the other influence lines; on the contrary, they represent a set of influence lines necessary for the analysis of the structure, and in preliminary analysis offer the additional advantage of immediate study of the maximum member in the truss for the negative moment.

Derivation

In Fig. (1a) is shown a four-span continuous truss of unsymmetrical span lengths. First the structure is rendered statically determinate by releasing the continuities at supports (a), (b) and (c). To these hinged determinate structures a unit moment is applied successively at supports (a), (b) and (c). The resulting rotations and deflections of the hinged structures due to the unit moments are as shown in Fig. (1c), (1d) and (1e). Rotations are shown as the angle to the vertical from the line normal to the tangent of the elastic line. Let the following notations be used:

X = Unknown Moment
θ = Angular Rotation
Δ = Deflection
p = Any Panel Point

Subscripts for θ and Δ :

First subscript denotes the point where the rotation or deflection occurs and second subscript, the point where the unit load or moment is applied. For instance,

θ_{aa} = Angular rotation at point a due to a unit moment applied at point a,

4. For example, See Shedd & Vawter, 'Theory of Simple Structures,' 2nd Edition pp. 473-481.

COMPUTATION 1

Illustrative Example (Cont'd)

Member	ℓ	A	$\frac{\ell}{A}$	h	$\cos\alpha$	S_a	$E\delta\ell_a = \frac{S_a\ell}{A}$	$E_{W_a} = \frac{E\delta\ell_a}{h\cos\alpha}$	S_b	$E\delta\ell_b = \frac{S_b\ell}{A}$	$E_{W_b} = \frac{E\delta\ell_b}{h\cos\alpha}$	S_c	$E\delta\ell_c = \frac{S_c\ell}{A}$	$E_{W_c} = \frac{E\delta\ell_c}{h\cos\alpha}$
U_0U_1	16.00	-	-	16	1.00	0	0	$W_0 = 0$	0	0	0	0	0	0
U_1U_3	32.00	13.7	2.339	16	1.00	-125	-292.4	$W_2 = -18.28$	0	0	0	0	0	0
U_3U_5	32.00	42.0	0.761	16	1.00	-250	-190.3	$W_4 = -11.89$	0	0	0	0	0	0
U_5U_7	32.00	32.2	0.994	16	1.00	-375	-372.8	$W_6 = -23.30$	0	0	0	0	0	0
U_7U_9	32.00	30.0	1.067	16	1.00	-500	-533.5	$W_8 = -33.34$	0	0	0	0	0	0
U_9U_{11}	36.00	56.0	0.643	20	1.00	-500	-321.5	$W_{10} = -16.08$	0	0	0	0	0	0
$U_{11}U_{13}$	40.00	29.3	1.365	20	1.00	-400	-546.0	$W_{12} = -27.30$	-100	-136.5	= -6.83	0	0	0
$U_{13}U_{15}$	40.00	32.9	1.216	20	1.00	-300	-364.8	$W_{14} = -18.24$	-200	-243.2	= -12.16	0	0	0
$U_{15}U_{17}$	40.00	32.9	1.216	20	1.00	-200	-243.2	$W_{16} = -12.16$	-300	-364.8	= -18.24	0	0	0
$U_{17}U_{19}$	40.00	12.4	3.226	20	1.00	-100	-322.6	$W_{18} = -16.13$	-400	-1290.4	= -64.52	0	0	0
$U_{19}U_{21}$	40.00	58.2	0.687	20	1.00	0	0	$W_{20} = 0$	-500	-343.5	= -17.18	0	0	0
$U_{21}U_{23}$	40.00	12.8	3.117	20	1.00	0	0	$W_{22} = 0$	-400	-1246.8	= -62.34	-100	-311.7	= -15.59
$U_{23}U_{25}$	40.00	32.7	1.223	20	1.00	0	0	$W_{24} = 0$	-300	-366.9	= -18.35	-200	-244.6	= -12.23
$U_{25}U_{27}$	40.00	32.0	1.242	20	1.00	0	0	$W_{26} = 0$	-200	-248.4	= -12.42	-300	-372.6	= -18.63
$U_{27}U_{29}$	40.00	11.0	3.636	20	1.00	0	0	$W_{28} = 0$	-100	-363.6	= -18.18	-400	-1454.4	= -72.72
$U_{29}U_{31}$	40.00	56.5	0.708	20	1.00	0	0	$W_{30} = 0$	0	0	0	-500	-354.0	= -17.70
$U_{31}U_{33}$	40.00	16.6	2.424	20	1.00	0	0	$W_{32} = 0$	0	0	0	-375	-909.0	= -45.45
$U_{33}U_{35}$	40.00	33.4	1.196	20	1.00	0	0	$W_{34} = 0$	0	0	0	-250	-299.0	= -14.95
$U_{35}U_{37}$	40.00	30.1	1.329	20	1.00	0	0	$W_{36} = 0$	0	0	0	-125	-166.1	= -8.30
$U_{37}U_{38}$	20.00	-	-	32	1.00	0	0	$W_{38} = 0$	0	0	0	0	0	0

θ_{ap} = Angular rotation at point a due to unit load applied at panel point p and

Δ_{pa} = Deflection at panel point p due to unit moment applied at point a.

S_a, S_b, Etc. = Stresses in members of truss in basic determinate structure due to unit moment at points a, b, etc.

Assume a load P is applied at any panel point p. By the simple principle that the angular rotations over the supports due to the external loads on the simple spans must be restored by the moments existing over the supports in the continuous structure, the following equations are evident:

$$X_a\theta_{aa} + X_b\theta_{ab} + X_c\theta_{ac} + P\theta_{ap} = 0 \quad (1)$$
$$X_a\theta_{ba} + X_b\theta_{bb} + X_c\theta_{bc} + P\theta_{bp} = 0 \quad (2)$$
$$X_a\theta_{ca} + X_b\theta_{cb} + X_c\theta_{cc} + P\theta_{cp} = 0 \quad (3)$$

From the equations above, in order to find the influence line for the moment it is necessary to find the values θ_{ap}, θ_{bp} and θ_{cp} by moving the load P from one panel point to the other throughout the entire length of the bridge. It is obvious that the computation would be lengthy and prohibitive in actual practice. A modified Maxwell's principle of reciprocal relation is applied: it states that the rotation at a due to unit load applied at p is equal to the deflection at p due to unit moment applied at support a. Hence,

$$\theta_{ap} = \Delta_{pa} \quad (4)$$
$$\theta_{bp} = \Delta_{pb} \quad (5)$$
$$\theta_{cp} = \Delta_{pc} \quad (6)$$

By substituting P = 1 and Equ. (4), (5) and (6), Equ. (1), (2) and (3) become

$$X_a\theta_{aa} + X_b\theta_{ab} + X_c\theta_{ac} + \Delta_{pa} = 0 \quad (7)$$
$$X_a\theta_{ba} + X_b\theta_{bb} + X_c\theta_{bc} + \Delta_{pb} = 0 \quad (8)$$
$$X_a\theta_{ca} + X_b\theta_{cb} + X_c\theta_{cc} + \Delta_{pc} = 0 \quad (9)$$

Equating $\theta_{ab} = \theta_{ba}$, $\theta_{bc} = \theta_{cb}$, $\theta_{ac} = \theta_{ca} = 0$

and solving,

$$X_a = \frac{1}{Y}\left[-\Delta_{pa}(\theta_{bb}\theta_{cc} - \theta_{\overline{bc}^2}) + \Delta_{pb}(\theta_{ab}\theta_{cc}) - \Delta_{pc}(\theta_{ab}\theta_{bc})\right] \quad (10)$$

$$X_b = \frac{1}{Y}\left[\Delta_{pa}(\theta_{ab}\theta_{cc}) - \Delta_{pb}(\theta_{aa}\theta_{cc}) + \Delta_{pc}(\theta_{aa}\theta_{bc})\right] \quad (11)$$

$$X_c = \frac{1}{Y}\left[-\Delta_{pa}(\theta_{ab}\theta_{bc}) + \Delta_{pb}(\theta_{aa}\theta_{bc}) - \Delta_{pc}(\theta_{aa}\theta_{bb} - \theta_{\overline{ab}^2})\right] \quad (12)$$

Where

$$Y = \theta_{aa}(\theta_{bb}\theta_{cc} - \theta_{b\bar{c}}^2) - \theta_{\bar{a}b}^2\theta_{cc} \qquad (13)$$

The solution of the influence ordinates for moments X_a, X_b and X_c is now reduced to finding the rotations at points a, b and c and the deflections at all the panel points due to three unit loading conditions: (1) unit moment applied at support a, (2) unit moment at support b and (3) unit moment at support c. The rotations (θ) are constants and the deflections (Δ) vary at each panel point, which correspond to the varying values of influence ordinates of the influence line.

If the outline and span lengths of the four-span truss shown in Fig. (1a) are symmetrical with respect to the center support, the following equalities would apply:

$$\theta_{aa} = \theta_{cc}\ ,\ \theta_{bc} = \theta_{ab}\ ,$$
$$\Delta_{pa} = \Delta_{pb} \quad \text{and} \quad X_a = X_c$$

By substituting in Equ. (10), (11) and (12) above, one obtains

$$X_a = \frac{-\Delta_{pa}(\theta_{bb}) + \Delta_{pb}(\theta_{ab})}{\theta_{aa}\theta_{bb} - 2\theta_{\bar{a}b}^2} \qquad (14)$$

$$X_b = \frac{2\Delta_{pa}(\theta_{ab}) - \Delta_{pb}(\theta_{aa})}{\theta_{aa}\theta_{bb} - 2\theta_{\bar{a}b}^2} \qquad (15)$$

In a similar fashion expressions for moments X_a, X_b etc. could be derived for a multiple-span continuous truss with any number of spans.

Procedure of Analysis

Elastic Weights: To obtain the rotations (θ) and deflections (Δ) required for the solution of Equ. (10), (11) and (12), the simplest analytical method is by elastic weights. In Fig. (2a) is shown a portion of a continuous truss over an intermediate support. It has been shown elsewhere[5] that the elastic weights (w) for the chord and diagonals at panel point 11 in Fig. (2a) are:

For the chord,

$$w_k = \frac{\delta_k}{r_k} = \frac{\delta_k}{h\cos\alpha_k} \qquad (16)$$

5. See, for instance, D. B. Steinman's article 'Continuous Bridges' in 'Movable and Long-span Steel Bridges' by Hool and Kinne.

COMPUTATION 2

Member	ℓ	A	$\frac{\ell}{A}$	h	cos α	S_a	$E\delta\ell_a = \frac{S_a\ell}{A}$	$EW_a = \frac{E\delta\ell_a}{h\cos\alpha}$	S_b	$E\delta\ell_b = \frac{S_b\ell}{A}$	$EW_b = \frac{E\delta\ell_b}{h\cos\alpha}$	S_c	$E\delta\ell_c = \frac{S_c\ell}{A}$	$EW_c = \frac{E\delta\ell_c}{h\cos\alpha}$
L_0L_2	32.00	26.2	1.223	16	1.00	62.5	76.4	$W_1 = -4.78$	0	0	0	0	0	0
L_2L_4	32.00	39.3	0.814	16	1.00	187.5	152.6	$W_3 = -9.54$	0	0	0	0	0	0
L_4L_6	32.00	39.3	0.814	16	1.00	312.5	254.4	$W_5 = -15.90$	0	0	0	0	0	0
L_6L_8	32.00	24.9	1.285	16	1.00	437.5	562.2	$W_7 = -35.14$	0	0	0	0	0	0
L_8L_{10}	32.24	34.7	0.930	18	0.992	503.8	468.6	$W_9 = -26.24$	0	0	0	0	0	0
$L_{10}L_{12}$	40.00	26.7	1.498	20	1.00	450	674.1	$W_{11} = -33.71$	50	74.9	$= -3.75$	0	0	0
$L_{12}L_{14}$	40.00	26.5	1.509	20	1.00	350	528.2	$W_{13} = -26.41$	150	226.4	$= -11.32$	0	0	0
$L_{14}L_{16}$	40.00	35.4	1.130	20	1.00	250	282.5	$W_{15} = -14.13$	250	282.5	$= -14.13$	0	0	0
$L_{16}L_{18}$	40.00	26.5	1.509	20	1.00	150	226.4	$W_{17} = -11.32$	350	528.2	$= -26.41$	0	0	0
$L_{18}L_{20}$	40.00	27.9	1.437	20	1.00	50	71.9	$W_{19} = -3.60$	450	646.7	$= -32.34$	0	0	0
$L_{20}L_{22}$	40.00	28.9	1.384	20	1.00	0	0	$W_{21} = 0$	450	622.8	$= -31.14$	50	69.2	$= -3.46$
$L_{22}L_{24}$	40.00	26.0	1.538	20	1.00	0	0	$W_{23} = 0$	350	538.3	$= -26.92$	150	230.7	$= -11.54$
$L_{24}L_{26}$	40.00	35.9	1.114	20	1.00	0	0	$W_{25} = 0$	250	278.5	$= -13.93$	250	278.5	$= -13.93$
$L_{26}L_{28}$	40.00	25.2	1.587	20	1.00	0	0	$W_{27} = 0$	150	238.1	$= -11.90$	350	555.5	$= -27.78$
$L_{28}L_{30}$	40.00	26.5	1.509	20	1.00	0	0	$W_{29} = 0$	50	75.5	$= -3.78$	450	679.1	$= -33.96$
$L_{30}L_{32}$	40.00	27.8	1.439	20	1.00	0	0	$W_{31} = 0$	0	0	0	437.5	629.6	$= -31.48$
$L_{32}L_{34}$	40.00	26.7	1.498	20	1.00	0	0	$W_{33} = 0$	0	0	0	312.5	468.1	$= -23.40$
$L_{34}L_{36}$	40.00	35.4	1.130	20	1.00	0	0	$W_{35} = 0$	0	0	0	187.5	211.9	$= -10.60$
$L_{36}L_{38}$	41.76	25.0	1.670	26	0.958	0	0	$W_{37} = 0$	0	0	0	50.2	83.8	$= -3.36$

For the diagonals,

$$w_m = \frac{\delta_m}{r_m} = \frac{\delta_m}{h \cos \alpha_m} \qquad (17)$$

$$w_n = \frac{\delta_n}{r_n} = \frac{\delta_n}{h \cos \alpha_n} \qquad (18)$$

Where δ is the elongation or shortening of the member,
α, the angle of inclination of each member with the horizontal
and h, the height of the panel in question.

The total elastic weight acting at each panel point is therefore a combination of weights contributed by the chords and the diagonal members. In this paper the following system of denoting the direction of the elastic weights is employed to facilitate the summation of the individual weights; for top chords in tension or bottom chords in compression, the elastic weight is assumed to act upward, whereas for diagonals in tension, a pair of elastic weights in the form of a couple is assumed to act in the same general direction as the tensile forces acting at the ends of the diagonal member. Fig. (2b) illustrates the use of the system as described.

A convenient tabulation for finding the elastic weights due to unit moments applied at intermediate supports is as shown in Fig. (3). Note that there is a separate column for the area of each member to provide for any revision of areas during the various stages of design.

Rotations (θ) and Deflections (Δ): After the elastic weights have been determined and tabulated for the various unit loading conditions, it is a simple matter to obtain the rotations and the deflections for the solution of Equ. (10), (11) and (12). The rotations at the ends of each span are computed as the shears at the ends, and the deflections at various panel points are equal to the moments at those corresponding points for the simply-supported span subjected to the elastic weights. The computation of shear and moment on a simply-supported span under numerous concentrated loads can be accomplished by any conventional means; however, for purposes of simplicity and the ease of computation by an ordinary calculating machine, the writer favors Newmark's method.[6] In the example a detailed computation is carried out using Newmark's method. Note that in the example the sign convention is such that downward elastic weights have negative signs and downward deflections have positive signs. The total angular rotation over the intermediate supports (θ_{aa}, θ_{bb} and θ_{cc}) is computed as the combined reaction of the two adjacent hinged determinate spans, and hence is equal to the summation of shear and the elastic weight at the support as illustrated in the example.

Example

To illustrate the procedure outlined above, a numerical example for finding

6. N. M. Newmark, 'Numerical Procedure for Computing Deflections, Moments and Buckling Loads,' Trans. ASCE Vol. 108, 1943 p. 1163.

COMPUTATION 3

Member	ℓ	A	$\frac{\ell}{A}$	h	$\cos\alpha$	S_a	$E\delta\ell_a=\frac{S_a\ell}{A}$	$Ew_a=\frac{E\delta\ell_a}{h\cos\alpha}$	S_b	$E\delta\ell_b=\frac{S_b\ell}{A}$	$Ew_b=\frac{E\delta\ell_b}{h\cos\alpha}$	S_c	$E\delta\ell_c=\frac{S_c\ell}{A}$	$Ew_c=\frac{E\delta\ell_c}{h\cos\alpha}$
L_0U_1	22.62	32.4	0.698	16	0.707	-88.4	-61.7	$w_1^0=\pm5.45$	0	0	0	0	0	0
U_1L_2	22.62	21.3	1.064	16	0.707	+88.4	+94.1	$w_2^1=\pm8.32$	0	0	0	0	0	0
L_2U_3	22.62	18.8	1.203	16	0.707	-88.4	-106.3	$w_3^2=\pm9.40$	0	0	0	0	0	0
U_3L_4	22.62	15.9	1.426	16	0.707	+88.4	+126.1	$w_4^3=\pm11.14$	0	0	0	0	0	0
L_4U_5	22.62	11.8	1.922	16	0.707	-88.4	-169.9	$w_5^4=\pm15.02$	0	0	0	0	0	0
U_5L_6	22.62	20.5	1.103	16	0.707	+88.4	+97.5	$w_6^5=\pm8.62$	0	0	0	0	0	0
L_6U_7	22.62	23.9	0.946	16	0.707	-88.4	-83.6	$w_7^6=\pm7.39$	0	0	0	0	0	0
U_7L_8	22.62	34.7	0.652	16	0.707	+88.4	+57.6	$w_8^7=\pm5.09$	0	0	0	0	0	0
L_8U_9	22.62	33.2	0.681	16 / 18	0.707	- 0.1	0	$w_9^8=0$	0	0	0	0	0	0
U_9L_{10}	25.61	43.3	0.591	18 / 20	0.625	+ 0.1	0	$w_{10}^9=0$	0	0	0	0	0	0
$L_{10}U_{11}$	28.28	46.2	0.612	20	0.707	+70.7	+43.3	$w_{11}^{10}=\mp3.06$	-70.7	-43.3	$=\pm3.06$	0	0	0
$U_{11}L_{12}$	28.28	35.1	0.806	20	0.707	-70.7	-57.0	$w_{12}^{11}=\mp4.03$	+70.7	+57.0	$=\pm4.03$	0	0	0
$L_{12}U_{13}$	28.28	30.7	0.921	20	0.707	+70.7	+65.1	$w_{13}^{12}=\mp4.60$	-70.7	-65.1	$=\pm4.60$	0	0	0
$U_{13}L_{14}$	28.28	18.3	1.545	20	0.707	-70.7	-109.2	$w_{14}^{13}=\mp7.72$	+70.7	+109.2	$=\pm7.72$	0	0	0
$L_{14}U_{15}$	28.28	25.9	1.093	20	0.707	+70.7	+77.3	$w_{15}^{14}=\mp5.47$	-70.7	-77.3	$=\pm5.47$	0	0	0
$U_{15}L_{16}$	28.28	25.9	1.093	20	0.707	-70.7	-77.3	$w_{16}^{15}=\mp5.47$	+70.7	+77.3	$=\pm5.47$	0	0	0
$L_{16}U_{17}$	28.28	20.9	1.353	20	0.707	+7.07	+95.7	$w_{17}^{16}=\mp6.77$	-70.7	-95.7	$=\pm6.77$	0	0	0
$U_{17}L_{18}$	28.28	31.3	0.904	20	0.707	-7.07	-63.9	$w_{18}^{17}=\mp4.52$	+70.7	+63.9	$=\pm4.52$	0	0	0
$L_{18}U_{19}$	28.28	36.3	0.779	20	0.707	+7.07	+55.1	$w_{19}^{18}=\mp3.90$	-70.7	-55.1	$=\pm3.90$	0	0	0
$U_{19}L_{20}$	28.28	48.0	0.589	20	0.707	-7.07	-41.6	$w_{20}^{19}=\mp2.94$	+70.7	+41.6	$=\pm2.94$	0	0	0

the moment influence lines for a four-span continuous deck truss is shown in Fig. (4). The truss consists of 160-200-200-160 ft. spans, and is unsymmetrical in that the number and the height of panels in the two end spans are different. The tabulation of elastic weights and the computation of rotation and deflection follow the general procedure outlined previously; therefore no further explanation would be necessary. Note however that for convenience of handling the decimal place of the computed values a unit moment equal to 10,000 is applied. Furthermore, this moment is applied in a positive direction in order to take care of the signs of the moment influence ordinates automatically. It must be emphasized that the computation of elastic weights and constants (rotations and deflections) and the solution of simultaneous equations are so arranged that they can be quickly and conveniently evaluated by a conventional calculating machine. Note also that for clarity the modulus of elasticity (E) is shown as a constant in the example wherever it appears. Unless one is interested in the absolute values of the rotation or deflection, it is not essential to include (E) in the tabulation since in the final solution of X_a, X_b and X_c, the term E vanishes.

CONCLUSION

This paper has presented a simplified method of analyzing continuous trusses by the use of the moment influence line. The basic principle of rendering the structure statically determinate and restoring the continuity by applying moments at the supports is used to set up the simultaneous equations. The method of computing elastic weights and the determination of their directions are summarized. Elastic weights and the constants (rotations and deflections) for the solution of simultaneous equations are presented in tabular form for purposes of simplicity and ease of calculation. In conclusion, the method of the moment influence line has been found to be a practical means of analyzing continuous trusses because it simplifies the whole process of computation, and hence reduces considerably the chance of error in the solution of the basic set of influence lines to be used in the design of the structure.

ACKNOWLEDGMENTS

The principal part of the derivation and formulation of the method was made during the years from 1953 to 1956, while the writer was on the staff of D. B. Steinman, M. ASCE, in New York, N. Y., and was engaged in design of bridges. To the fellow members of the design staff and to the staff supervisor, C. H. Gronquist, M. ASCE, who gave the writer advice and encouragement, grateful acknowledgment is made.

COMPUTATION 4

Member	ℓ	A	$\frac{\ell}{A}$	h	cos α	S_a	$E\delta\ell_a = \frac{S_a \ell}{A}$	$Ew_a = \frac{E\delta\ell_a}{h\cos\alpha}$	S_b	$E\delta\ell_b = \frac{S_b \ell}{A}$	$Ew_b = \frac{E\delta\ell_b}{h\cos\alpha}$	S_c	$E\delta\ell_c = \frac{S_c \ell}{A}$	$Ew_c = \frac{E\delta\ell_c}{h\cos\alpha}$
$L_{20}U_{21}$	28.28	48.4	0.584	20	0.707	0	0	$w_{21}^{20} = 0$	+70.7	+41.3	$= \mp 2.92$	-70.7	-41.3	$= \pm 2.92$
$U_{21}L_{22}$	28.28	36.7	0.771	20	0.707	0	0	$w_{22}^{21} = 0$	-70.7	-54.5	$= \mp 3.85$	+70.7	+54.5	$= \pm 3.85$
$L_{22}U_{23}$	28.28	31.9	0.887	20	0.707	0	0	$w_{23}^{22} = 0$	+70.7	+62.7	$= \mp 4.43$	-70.7	-62.7	$= \pm 4.43$
$U_{23}L_{24}$	28.28	19.8	1.432	20	0.707	0	0	$w_{24}^{23} = 0$	-70.7	-101.2	$= \mp 7.16$	+70.7	+101.2	$= \pm 7.16$
$L_{24}U_{25}$	28.28	25.9	1.093	20	0.707	0	0	$w_{25}^{24} = 0$	+70.7	+77.3	$= \mp 5.47$	-70.7	-77.3	$= \pm 5.47$
$U_{25}L_{26}$	28.28	25.9	1.093	20	0.707	0	0	$w_{26}^{25} = 0$	-70.7	-77.3	$= \mp 5.47$	+70.7	+77.3	$= \pm 5.47$
$L_{26}U_{27}$	28.28	19.5	1.450	20	0.707	0	0	$w_{27}^{26} = 0$	+70.7	+102.5	$= \mp 7.25$	-70.7	-102.5	$= \pm 7.25$
$U_{27}L_{28}$	28.28	31.7	0.892	20	0.707	0	0	$w_{28}^{27} = 0$	-70.7	-63.1	$= \mp 4.46$	+70.7	+63.1	$= \pm 4.46$
$L_{28}U_{29}$	28.28	36.4	0.777	20	0.707	0	0	$w_{29}^{28} = 0$	+70.7	+54.9	$= \mp 3.88$	-70.7	-54.9	$= \pm 3.88$
$U_{29}L_{30}$	28.28	48.2	0.587	20	0.707	0	0	$w_{30}^{29} = 0$	-70.7	-41.5	$= \mp 2.93$	+70.7	+41.5	$= \pm 2.93$
$L_{30}U_{31}$	28.28	48.0	0.589	20	0.707	0	0	$w_{31}^{30} = 0$	0	0	0	+88.4	+52.1	$= \mp 3.68$
$U_{31}L_{32}$	28.28	36.0	0.786	20	0.707	0	0	$w_{32}^{31} = 0$	0	0	0	-88.4	-69.5	$= \mp 4.91$
$L_{32}U_{33}$	28.28	31.2	0.906	20	0.707	0	0	$w_{33}^{32} = 0$	0	0	0	+88.4	+80.1	$= \mp 5.66$
$U_{33}L_{34}$	28.28	18.8	1.504	20	0.707	0	0	$w_{34}^{33} = 0$	0	0	0	-88.4	-132.9	$= \mp 9.40$
$L_{34}U_{35}$	28.28	25.9	1.093	20	0.707	0	0	$w_{35}^{34} = 0$	0	0	0	+88.4	+96.6	$= \mp 6.83$
$U_{35}L_{36}$	28.28	25.9	1.093	20	0.707	0	0	$w_{36}^{35} = 0$	0	0	0	-88.4	-96.6	$= \mp 6.83$
$L_{36}U_{37}$	28.28	11.8	2.403	20 / 26	0.707	0	0	$w_{37}^{36} = 0$	0	0	0	+108.8	+261.4	$= \mp \frac{18.49}{14.22}$
$U_{37}L_{38}$	37.74	25.9	1.455	26 / 32	0.530	0	0	$w_{38}^{37} = 0$	0	0	0	-90.6	-132.2	$= \mp \frac{9.59}{7.79}$

COMPUTATION 5

For Δ_{pa}, θ_{aa} and θ_{ba}, (Unit Moment = 10,000 @ Pt a)

	0	1	2	3	4	5	6	7	8	9	a → 10	Common Factor
Elastic Wt	+5.45	-1.91	-17.20	-7.80	-8.01	-22.30	-24.53	-37.44	-38.43	-26.24	-8.04	$\frac{1}{E}$
Assumed Shear	34.92	33.01	15.81	8.01	0	-22.30	-46.83	-84.27	-122.70	-148.94		" $\frac{\lambda}{E}$
Trial Mom.	0	34.92	67.93	83.74	91.75	91.75	69.45	22.62	-61.65	-184.35	-333.29	"
Lin. Correction	0	33.33	66.66	99.99	133.32	166.65	199.97	233.30	266.63	299.96	333.29	"
Moment	0	68.25	134.59	183.73	225.07	258.40	269.42	255.92	204.98	115.61	0	"
(λ = Panel Length = 16'-0")												
$M = \Delta_{pa}$	0	1092	2153	2940	3601	4134	4311	4095	3280	1850	0	$\frac{1}{E}$

	a → 10	11	12	13	14	15	16	17	18	19	b → 20	
Elastic Wt	-11.10	-34.68	-27.87	-29.53	-15.99	-14.13	-13.46	-9.07	-15.51	-2.64	+2.94	$\frac{1}{E}$
Assumed Shear	92.08	57.40	29.53	0	-15.99	-30.12	-43.58	-52.65	-68.16	-70.80		" $\frac{\lambda}{E}$
Trial Mom.	0	92.08	149.48	179.01	179.01	163.02	132.90	89.32	36.67	-31.49	-102.29	"
Lin. Correction	0	10.23	20.46	30.69	40.92	51.15	61.37	71.60	81.83	92.06	102.29	"
Moment	0	102.31	169.94	209.70	219.93	214.17	194.27	160.92	118.50	60.57	0	"
(λ = 20'-0")												
$M = \Delta_{pa}$	0	2046	3399	4194	4399	4283	3885	3218	2370	1211	0	$\frac{1}{E}$

$E\theta_{aa}$ = 115.61 + 102.31 + 8.04 + 11.10 = 237.06 $E\theta_{ba}$ = 60.57 - 2.94 = 57.63

COMPUTATION 6

For Δ_{pb}, θ_{bb} and θ_{cb} (Unit Moment = 10,000 @ Pt. b) $\theta_{ab} = \theta_{ba}$

	a									b		Common Factor
	10	11	12	13	14	15	16	17	18	19	20	
Elastic Wt.	+3.06	-2.78	-6.26	-8.20	-14.41	-14.13	-16.94	-28.66	-65.14	-33.30	-11.53	$\frac{1}{E}$
Assumed Shear	91.38	88.60	82.34	74.14	59.73	45.60	28.66	0	-65.14	-98.44		"
Trial Mom.	0	91.38	179.98	262.32	336.46	396.19	441.79	470.45	470.45	405.31	306.87	$\frac{\lambda}{E}$
Lin. Correction	0	-30.69	-61.37	-92.06	-122.75	-153.44	-184.12	-214.81	-245.50	-276.18	-306.87	"
Moment	0	60.69	118.61	170.26	213.71	242.75	257.67	255.64	224.95	129.13	0	$\frac{\lambda}{E}$
					(λ = 20'-0")							
M = Δ_{pb}	0	1214	2372	3405	4274	4855	5153	5113	4499	2583	0	$\frac{1}{E}$

	b									C		
	20	21	22	23	24	25	26	27	28	29	30	
Elastic Wt.	-11.51	-32.07	-62.92	-29.65	-16.66	-13.93	-14.20	-9.11	-17.60	-2.83	+2.93	$\frac{1}{E}$
Assumed Shear	124.64	92.57	29.65	0	-16.66	-30.59	-44.79	-53.90	-71.50	-74.33		"
Trial Mom.	0	124.64	217.21	246.86	246.86	230.20	199.61	154.82	100.92	29.42	-44.91	$\frac{\lambda}{E}$
Lin. Correction	0	4.49	8.98	13.47	17.96	22.46	26.95	31.44	35.93	40.42	44.91	"
Moment	0	129.13	226.19	260.33	264.82	252.66	226.56	186.26	136.85	69.84	0	$\frac{\lambda}{E}$
					(λ = 20'-0")							
M = Δ_{pb}	0	2583	4524	5207	5296	5053	4531	3725	2737	1397	0	$\frac{1}{E}$

$E\theta_{bb}$ = 129.13 + 129.13 + 11.53 + 11.51 = <u>281.30</u> $E\theta_{cb}$ = 69.84 - 2.93 = <u>66.91</u>

COMPUTATION 7

For Δ_{pc} and θ_{cc} (Unit Moment = 10,000 @ Pt. c) $\theta_{bc} = \theta_{cb}$

b — c

	20	21	22	23	24	25	26	27	28	29	30	Common Factor
Elastic Wt.	+2.92	-2.53	-15.01	-8.81	-13.92	-13.93	-16.85	-30.57	-73.30	-34.91	-11.78	$\frac{1}{E}$
Assumed Shear	101.62	99.09	84.08	75.27	61.35	47.42	30.57	0	-73.30	-108.21		"
Trial Mom.	0	101.62	200.71	284.79	360.06	421.41	468.83	499.40	499.40	426.10	317.89	$\frac{1}{E}$
Lin. Correction	0	-31.79	-63.58	-95.37	-127.16	-158.95	-190.73	-222.52	-254.31	-286.10	-317.89	"
Moment	0	69.83	137.13	189.42	232.90	262.46	278.10	276.88	245.09	140.00	0	$\frac{1}{E}$
					(λ = 20'-0")							
$M = \Delta_{pc}$	0	1397	2743	3788	4658	5249	5562	5538	4902	2800	0	$\frac{1}{E}$

c

	30	31	32	33	34	35	36	37	38	
Elastic Wt.	-12.53	-32.71	-46.20	-27.14	-12.38	-10.60	-19.96	1.27	7.79	$\frac{1}{E}$
Assumed Shear	106.05	73.34	27.14	0	-12.38	-22.98	-42.94	-41.67		"
Trial Mom.	0	106.05	179.39	206.53	206.53	194.15	171.17	128.25	86.58	$\frac{1}{E}$
Lin. Correction	0	-10.82	-21.65	-32.47	-43.29	-54.11	-64.94	-79.76	-86.58	"
Moment	0	95.23	157.74	174.06	163.24	140.04	106.23	52.49	0	$\frac{1}{E}$
				(λ = 20'-0")						
$M = \Delta_{pc}$	0	1905	3155	3481	3265	2801	2125	1050	0	$\frac{1}{E}$

$E\theta_{cc}$ = 140.00 + 95.23 + 11.78 + 12.53 = 259.54

COMPUTATION 8

$$X_a = \frac{1}{Y}\left[-\Delta_{Pa}(\theta_{bb}\theta_{cc} - \theta_{\bar{bc}}^{-2}) + \Delta_{Pb}(\theta_{ab}\theta_{cc}) - \Delta_{Pc}(\theta_{ab}\theta_{bc})\right]$$

$$Y = \theta_{aa}(\theta_{bb}\theta_{cc} - \theta_{\bar{bc}}^{-2}) - \theta_{\bar{ab}}^{2}\theta_{cc}$$

$$\frac{1}{Y} = 0.0065 \times 10^{-5} \times E^{3}$$

$$\theta_{bb}\theta_{cc} - \theta_{\bar{bc}}^{2} = 68522 \times E^{-2}$$
$$\theta_{ab}\theta_{cc} = 14954 \times E^{-2}$$
$$\theta_{ab}\theta_{bc} = 3855 \times E^{-2}$$

Col. / Point	(1) $E\,\Delta_{Pa}$	(2) $E\,\Delta_{Pb}$	(3) $E\,\Delta_{Pc}$	(4) $-\Delta_{Pa}(\theta_{bb}\theta_{cc}-\theta_{\bar{bc}}^{-2})E^{-2}\cdot 10^{5}$	(5) $\Delta_{Pb}(\theta_{ab}\theta_{cc})E^{-2}\cdot 10^{5}$	(6) $-\Delta_{Pc}(\theta_{ab}\theta_{bc})E^{-2}\cdot 10^{5}$	(7) Col's (4)+(5)+(6)	(8) X_a
1	1092	0	0	-748	0	0	-748	-4.86
2	2153	0	0	-1475	0	0	-1475	-9.59
3	2940	0	0	-2015	0	0	-2015	-13.10
4	3601	0	0	-2468	0	0	-2468	-16.04
5	4134	0	0	-2833	0	0	-2833	-18.42
6	4311	0	0	-2954	0	0	-2954	-19.21
7	4095	0	0	-2806	0	0	-2806	-18.24
8	3280	0	0	-2248	0	0	-2248	-14.61
9	1850	0	0	-1268	0	0	-1268	-8.24
10	0	0	0	0	0	0	0	0
11	2046	1214	0	-1402	182	0	-1220	-7.94
12	3399	2372	0	-2329	355	0	-1974	-12.84
13	4194	3405	0	-2874	509	0	-2365	-15.37
14	4399	4274	0	-3014	639	0	-2375	-15.44
15	4283	4855	0	-2935	726	0	-2209	-14.36
16	3885	5153	0	-2662	771	0	-1891	-12.30
17	3218	5113	0	-2205	765	0	-1440	-9.36
18	2370	4499	0	-1624	673	0	-951	-6.18
19	1211	2583	0	-830	386	0	-444	-2.88
20	0	0	0	0	0	0	0	0
21	0	2583	1397	0	386	-54	332	2.16
22	0	4524	2743	0	677	-106	571	3.71
23	0	5207	3788	0	779	-146	633	4.11
24	0	5296	4658	0	792	-180	612	3.98
25	0	5053	5249	0	756	-202	554	3.60
26	0	4531	5562	0	678	-214	464	3.01
27	0	3725	5538	0	557	-214	343	2.23
28	0	2737	4902	0	409	-189	220	1.43
29	0	1397	2800	0	209	-108	101	0.66
30	0	0	0	0	0	0	0	0
31	0	0	1905	0	0	-73	-73	-0.48
32	0	0	3155	0	0	-122	-122	-0.79
33	0	0	3481	0	0	-134	-134	-0.87
34	0	0	3265	0	0	-126	-126	-0.82
35	0	0	2801	0	0	-108	-108	-0.70
36	0	0	2125	0	0	-82	-82	-0.53
37	0	0	1050	0	0	-41	-41	-0.26

COMPUTATION 9

$$X_b = \frac{1}{Y}\left[\Delta_{Pa}(\theta_{ab}\theta_{cc}) - \Delta_{Pb}(\theta_{aa}\theta_{cc}) + \Delta_{Pc}(\theta_{aa}\theta_{bc})\right]$$

$$\frac{1}{Y} = 0.0065 \times 10^{-5} \times E^{3}$$

$\theta_{ab}\theta_{cc} = 14954 \times E^{-2}$

$\theta_{aa}\theta_{cc} = 61518 \times E^{-2}$

$\theta_{aa}\theta_{bc} = 15859 \times E^{-2}$

Col. / Point	(1) $E\,\Delta_{Pa}$	(2) $E\,\Delta_{Pb}$	(3) $E\,\Delta_{Pc}$	(4) $\Delta_{Pa}(\theta_{ab}\theta_{cc})$ $E^{-3}\cdot 10^{5}$	(5) $-\Delta_{Pb}(\theta_{aa}\theta_{cc})$ $E^{-3}\cdot 10^{5}$	(6) $\Delta_{Pc}(\theta_{aa}\theta_{bc})$ $E^{-3}\cdot 10^{5}$	(7) Col's (4)+(5)+(6)	(8) X_b
1	1092	0	0	163	0	0	163	1.06
2	2153	0	0	322	0	0	322	2.09
3	2940	0	0	440	0	0	440	2.86
4	3601	0	0	539	0	0	539	3.50
5	4134	0	0	618	0	0	618	4.02
6	4311	0	0	645	0	0	645	4.19
7	4095	0	0	612	0	0	612	3.98
8	3280	0	0	491	0	0	491	3.19
9	1850	0	0	277	0	0	277	1.80
10	0	0	0	0	0	0	0	0
11	2046	1214	0	306	-747	0	-441	-2.87
12	3399	2372	0	508	-1459	0	-951	-6.18
13	4194	3405	0	627	-2095	0	-1468	-9.54
14	4399	4274	0	658	-2629	0	-1971	-12.82
15	4283	4855	0	641	-2987	0	-2346	-15.25
16	3885	5153	0	581	-3170	0	-2589	-16.83
17	3218	5113	0	481	-3145	0	-2664	-17.32
18	2370	4499	0	354	-2768	0	-2414	-15.69
19	1211	2583	0	181	-1589	0	-1408	-9.15
20	0	0	0	0	0	0	0	0
21	0	2583	1397	0	-1589	222	-1367	-8.89
22	0	4524	2743	0	-2783	435	-2348	-15.27
23	0	5207	3788	0	-3203	601	-2602	-16.92
24	0	5296	4658	0	-3258	739	-2519	-16.38
25	0	5053	5249	0	-3109	832	-2277	-14.80
26	0	4531	5562	0	-2787	882	-1905	-12.39
27	0	3725	5538	0	-2292	878	-1414	-9.19
28	0	2737	4902	0	-1684	777	-907	-5.89
29	0	1397	2800	0	-859	444	-415	-2.70
30	0	0	0	0	0	0	0	0
31	0	0	1905	0	0	302	302	1.96
32	0	0	3155	0	0	500	500	3.25
33	0	0	3481	0	0	552	552	3.59
34	0	0	3265	0	0	518	518	3.37
35	0	0	2801	0	0	444	444	2.89
36	0	0	2125	0	0	337	337	2.19
37	0	0	1050	0	0	167	167	1.08

COMPUTATION 10

$$X_c = \frac{1}{Y}\left[-\Delta_{Pa}(\theta_{ab}\theta_{bc}) + \Delta_{Pb}(\theta_{aa}\theta_{bc}) - \Delta_{Pc}(\theta_{aa}\theta_{bb} - \theta_{\bar{ab}}^{2})\right]$$

$$\frac{1}{Y} = 0.0065 \times 10^{-5} \times E^{3}$$

$$\theta_{ab}\theta_{bc} = 3855 \times E^{-2}$$
$$\theta_{aa}\theta_{bc} = 15859 \times E^{-2}$$
$$\theta_{aa}\theta_{bb} - \theta_{\bar{ab}}^{2} = 63355 \times E^{-2}$$

Col. / Point	(1) $E\,\Delta_{Pa}$	(2) $E\,\Delta_{Pb}$	(3) $E\,\Delta_{Pc}$	(4) $\frac{-\Delta_{Pa}(\theta_{ab}\theta_{bc})}{E^{-3}\cdot 10^{5}}$	(5) $\frac{\Delta_{Pb}(\theta_{aa}\theta_{bc})}{E^{-3}\cdot 10^{5}}$	(6) $\frac{-\Delta_{Pc}(\theta_{aa}\theta_{bb}-\theta_{\bar{ab}}^{2})}{E^{-3}\cdot 10^{5}}$	(7) Col's (4)+(5)+(6)	(8) X_c
1	1092	0	0	- 42	0	0	- 42	- 0.27
2	2153	0	0	- 83	0	0	- 83	- 0.54
3	2940	0	0	- 113	0	0	- 113	- 0.74
4	3601	0	0	- 139	0	0	- 139	- 0.90
5	4134	0	0	- 159	0	0	- 159	- 1.04
6	4311	0	0	- 166	0	0	- 166	- 1.08
7	4095	0	0	- 158	0	0	- 158	- 1.03
8	3280	0	0	- 126	0	0	- 126	- 0.82
9	1850	0	0	- 71	0	0	- 71	- 0.46
10	0	0	0	0	0	0	0	0
11	2046	1214	0	- 79	193	0	114	0.74
12	3399	2372	0	- 131	376	0	245	1.59
13	4194	3405	0	- 162	540	0	378	2.46
14	4399	4274	0	- 170	678	0	508	3.30
15	4283	4855	0	- 165	770	0	605	3.93
16	3885	5153	0	- 150	817	0	667	4.34
17	3218	5113	0	- 124	811	0	687	4.47
18	2370	4498	0	- 91	714	0	623	4.04
19	1211	2583	0	- 47	410	0	363	2.36
20	0	0	0	0	0	0	0	0
21	0	2583	1397	0	410	- 885	- 475	- 3.09
22	0	4524	2743	0	718	- 1739	- 1021	- 6.63
23	0	5207	3788	0	826	- 2400	- 1574	- 10.23
24	0	5296	4658	0	840	- 2951	- 2111	- 13.73
25	0	5053	5249	0	801	- 3326	- 2525	- 16.41
26	0	4531	5562	0	719	- 3524	- 2805	- 18.24
27	0	3725	5538	0	591	- 3509	- 2918	- 18.97
28	0	2737	4902	0	434	- 3106	- 2672	- 17.37
29	0	1397	2800	0	222	- 1774	- 1552	- 10.09
30	0	0	0	0	0	0	0	0
31	0	0	1905	0	0	- 1207	- 1207	- 7.85
32	0	0	3155	0	0	- 1989	- 1989	- 13.00
33	0	0	3481	0	0	- 2205	- 2205	- 14.34
34	0	0	3265	0	0	- 2069	- 2069	- 13.45
35	0	0	2801	0	0	- 1775	- 1775	- 11.54
36	0	0	2125	0	0	- 1346	- 1346	- 8.75
37	0	0	1050	0	0	- 665	- 665	- 4.32

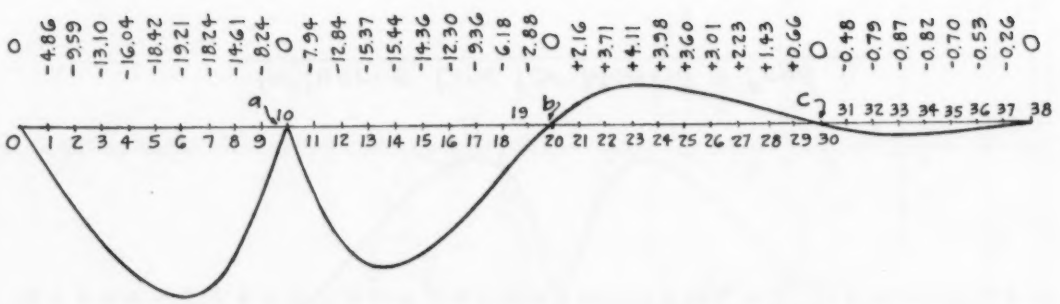

Influence Line for Moment @ Point a

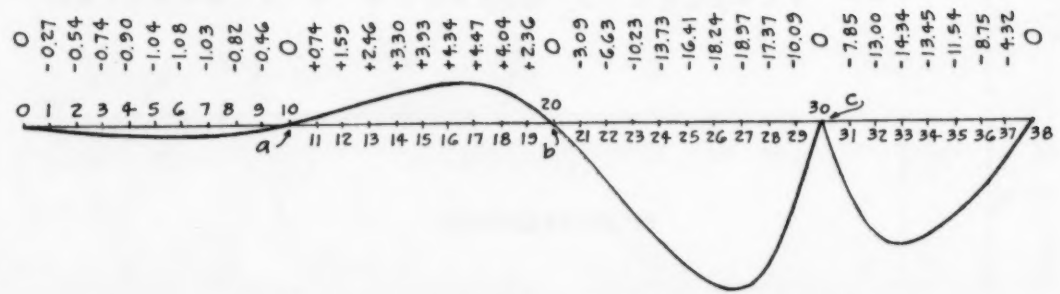

Influence Line for Moment @ Point c

COMPUTATION 12

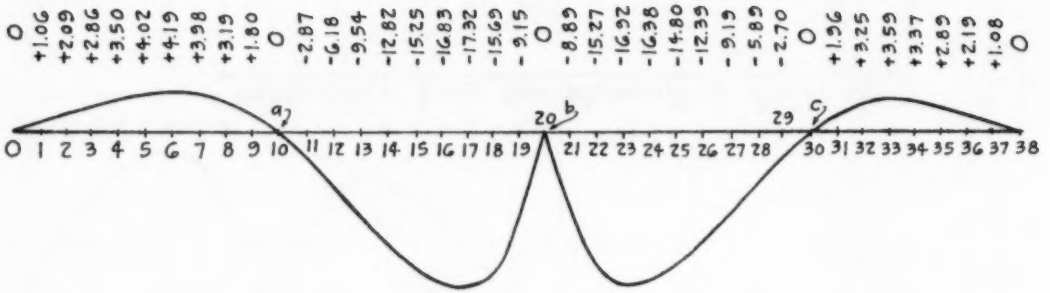

Influence Line for Moment @ Point b

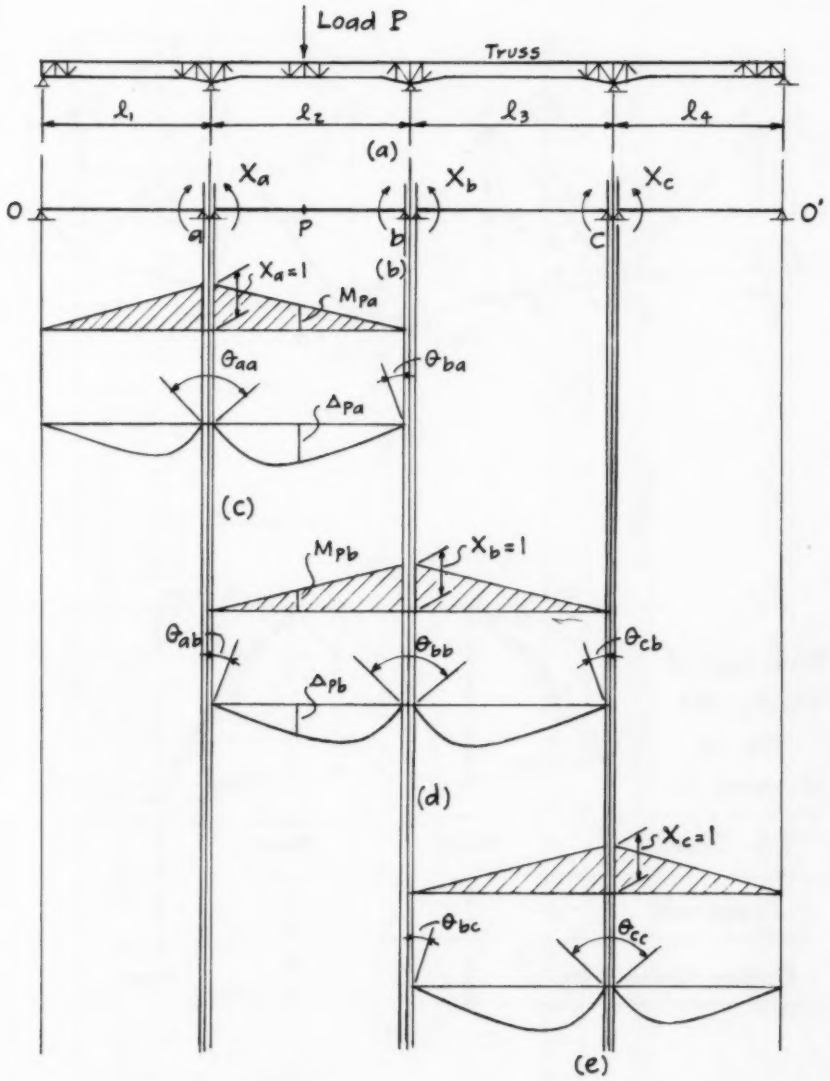

Fig.(1) Moments, Rotations & Deflections in Basic Systems Due to Unit Moments

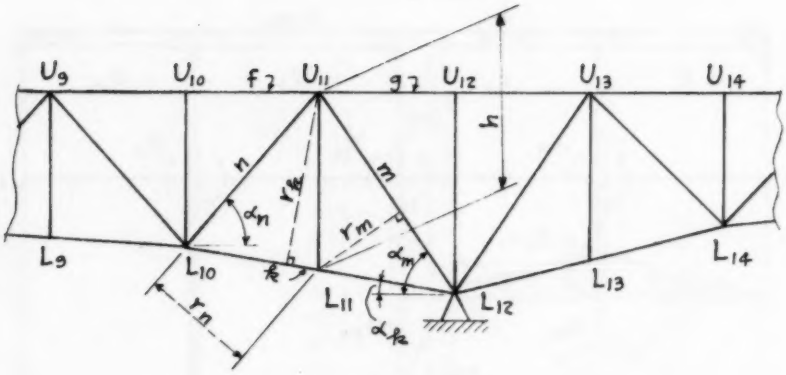

(a)

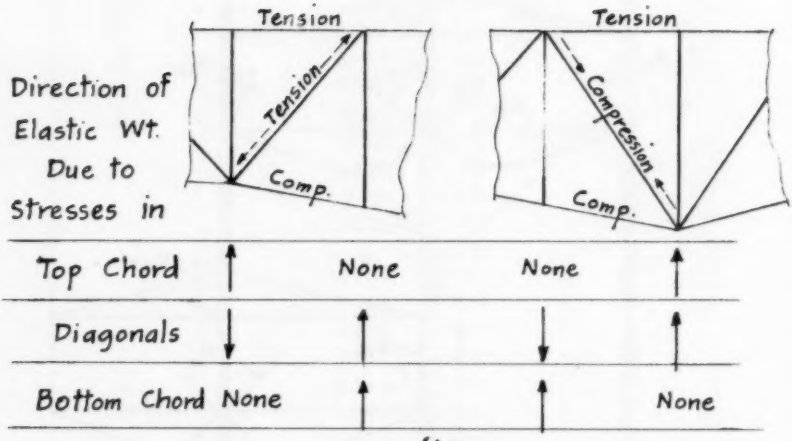

(b)

Fig. (2) Elastic Weights & Their Directions

Member	Length ℓ	Area A	$\frac{\ell}{A}$	Height h	Cosine of Inclin. $\cos\alpha$	Basic Stress S_a	Deformation $\delta\ell_a = \frac{S_a \ell}{AE}$	Elastic Wt. $w_a = \frac{\delta\ell_a}{h\cos\alpha}$	S_b	$\delta\ell_b = \frac{S_b \ell}{AE}$	$w_b = \frac{\delta\ell_b}{h\cos\alpha}$
Top Chords Bottom Chords Diagonals											

Fig (3) Table for Computing Elastic Weights

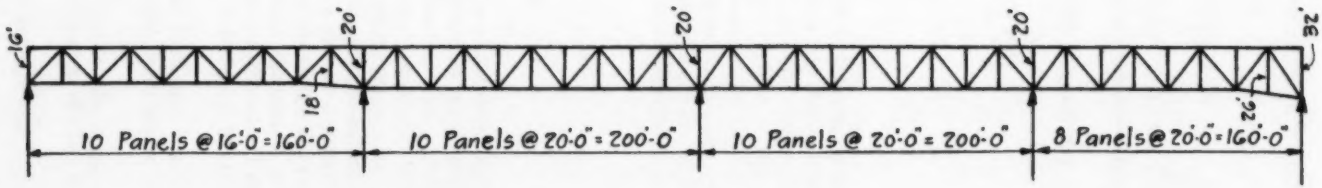

Fig. (4) Outline of Truss for Illustrative Example

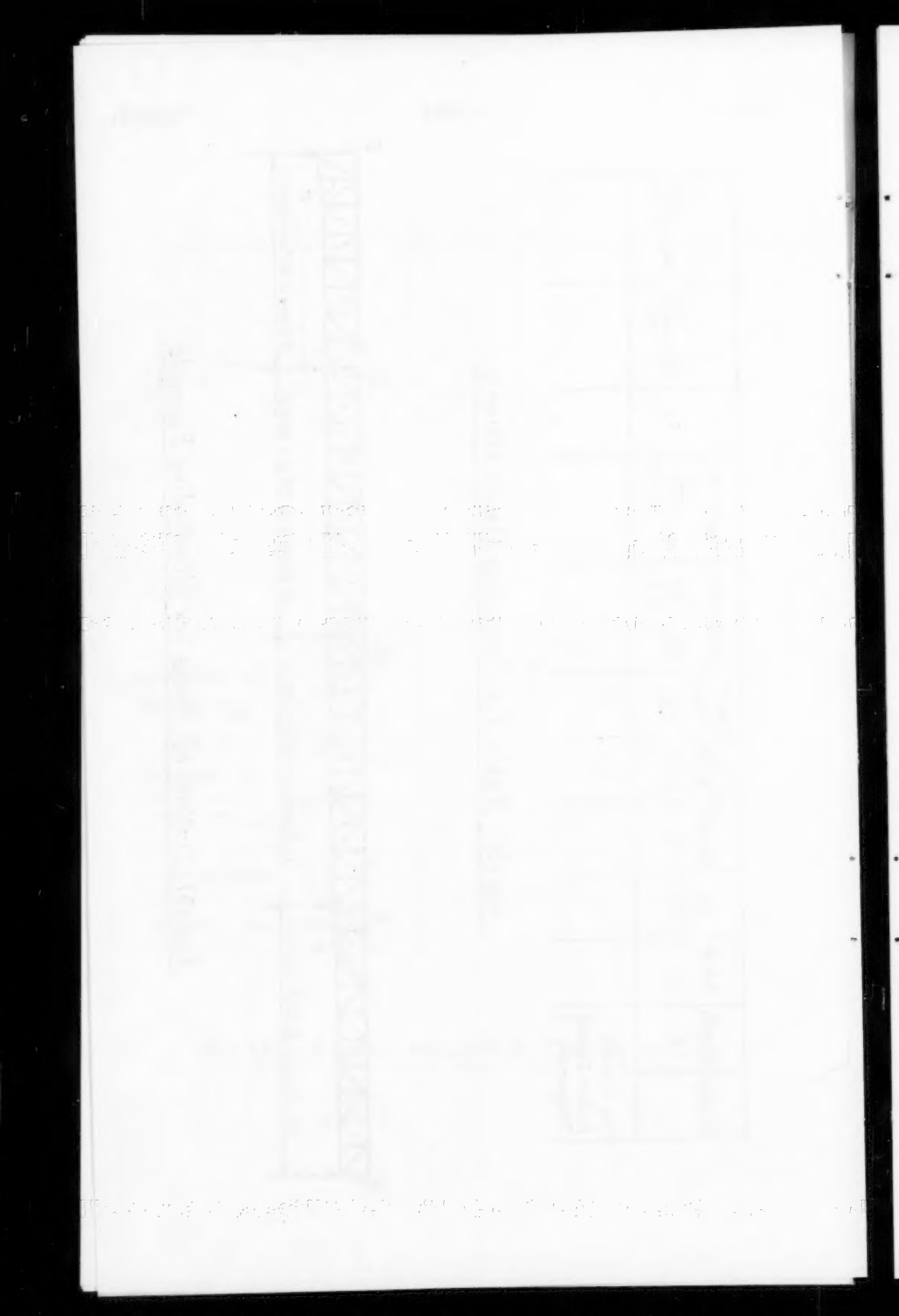

Paper 1188 ST 2

Journal of the
STRUCTURAL DIVISION
Proceedings of the American Society of Civil Engineers

RESISTANCE TO OVERTURNING OF SINGLE, SHORT PILES

E. Czerniak,* A.M., ASCE
(Proc. Paper 1188)

SYNOPSIS

This paper has been prepared with the object of furnishing structural engineers with practical aids, for the stress analysis and lateral force design of short piles, that will effectively reduce the tedious and time consuming labor, ordinarily required in their solution. More specifically, it was prepared for those concerned with foundation design in refineries and chemical plants, where short bored piles have been successfully used, to transmit to the ground all forces and couples acting on the supports for elevated horizontal vessels, heat exchanger equipment, pipe supports (overhead and sleepers) and miscellaneous light structures.

INTRODUCTION

Every structure standing above the ground is affected by lateral forces, which similarly to vertical loads, must be resisted at the ground. In some instances, it becomes desirable to depend on the resistance of the earth against lateral displacement of an imbedded pile. Analytical studies of certain refinery type structures, supported on concrete piles, cast in place against earth in drilled holes, showed that for some application the provisions for the vertical load (bearing or friction) gave a pile of proportions adequate to resist lateral loads as well. However, for many cases the resistance was well below what may be acceptable, and it became necessary, in the interest of economy and rational design, to establish the mathematical expressions that relate the pile proportions to the loads it is designed to transmit to the ground.

The problem itself is not new, and during the past fifty years a wide variety of methods and pile formulas were proposed, with the so called "flag

Note: Discussion open until August 1, 1957. Paper 1188 is part of the copyrighted Journal of the Structural Division of the American Society of Civil Engineers, Vol. 83, No. ST 2, March, 1957.

*Design Eng. Superv., The Fluor Corp., Los Angeles, Calif.

pole" formulas being, probably, most commonly used by practicing engineers. The simplifying assumption is that the pile would pivot about a point somewhere along its length as if it were absolutely rigid. C. C. Williams[1] presented a mathematical solution to the pivot point theory. In the sacred name of experimentation, some formulas were further modified, and though simple in form, were incompatible with static equilibrium.

As a result of tests of North Carolina Poles for Electric Distribution lines[3] some empirical formulas became available.[4] Other tests were described in the technical literature[5] and contributed valuable information to our knowledge of the subject, but most of all re-emphasized the danger of generalization based on rather limited experience, and the urgent need for additional quantitative and qualitative studies. Building Codes, in general, require that the allowable lateral loads on piles be determined by an "approved" formula (or by load tests). In some communities (e.g., Los Angeles City) the building officials will accept designs based on the Griffith[6] formula,

$$L = 3.81\sqrt{\frac{M_T}{dg}}$$

where L = Depth of pole setting, ft.

d = Diameter of pole foundation, ft.

$M_T = HE$ = Total moment at ground line, ft. lb.

g = Maximum allowable soil resistance, lb. per sq. ft.

It is generally recognized that a mathematical expression for the depth of piles subjected to lateral forces and moments should include the physical characteristics of the pile, such as E and I, the elastic modulus of the soil, the magnitude and direction of the applied forces and moments, as well as the lateral movement at the ground level that can be tolerated. However, because of the unavoidable uncertainties involved in the fundamental assumptions and the numerical values of the soil constants, simplicity is deemed to be of an utmost importance in obtaining practical solutions to the short pile problem.

The purpose of this paper is not to advance a new theory or method of analysis, but to present the necessary qualitative information, augmented by charts, to aid the designer in the solution of the single, short pile problem.

Short Piles

A short pile will be referred to as one whose imbedded depth does not exceed ten times its least lateral dimension.

The structural function of the short, single pile is to resist vertical as well as lateral loads and overturning moments, the successful accomplishment of which depends on the sufficient imbedment depth and capacity to sustain the axial loads, shears and bending moments.

(1) Numbers in parenthesis refer to references at the end of the paper.

For the purpose of analysis to resist lateral loads and moments, it is assumed that the pile is absolutely rigid with respect to the surrounding soil, and under the action of applied forces would rotate about a point somewhere along its length. It is correctly argued that absolute rigidity does not exist and bending stresses are always associated with deflections of the pile axis. However, the effect of such deflections on the soil pressure decreases, as the rigidity of the pile increases. For the short pile their effect may be neglected, and the expressions for depth of imbedment and maximum bending moment be derived by the principles of statics.

Soil Resistance

The resistance of the earth against lateral displacement of the pile is basically a stability problem, the solution to which is obtained by comparing the forces that tend to produce a failure to those that tend to prevent it. Although the soil in its physical behaviour under stress follows the same natural laws as do all other materials, the relationship is much more complex and obscure, and only certain aspects of the soil phenomena at the approaching failure condition can be predicted from the laboratory shearing test results. Let AB (Fig. 1), the axis of the pile, be vertical before the lateral loads and moments are applied. As the pile is moved into position A' B', the soil in front of A' O and in back of OB' becomes compressed, and the horizontal pressure against the pile increases until it reaches the limiting value, known as the passive earth pressure. Further displacement of the pile does not significantly change the pressure. Before the passive pressure is reached the body of the earth is in a state of elastic equilibrium and the magnitude of the pressure is related to the amount of pile movement. The movement, at the ground level, required to develop the passive pressure may be as high as 1/32 inch per foot of pile imbedment. In sandy soils full elasticity may not be realized even at low loads since the sand may fill the space left as the pile was moved, thereby preventing its return to the vertical position upon removal of the overturning forces. The result is more deflection for repeated loads. When the ultimate soil resistance is reached, the body of soil is in a state of plastic equilibrium and is on the verge of failure. The calculated value of this resistance, or passive pressure, when divided by a proper

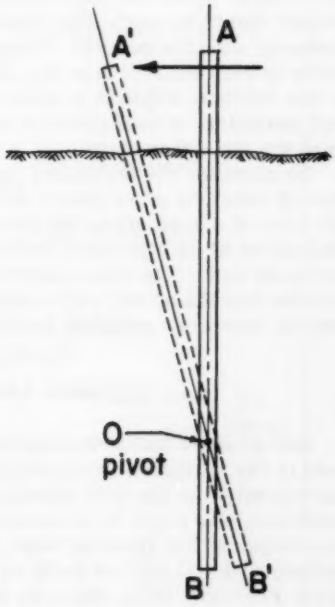

FIG. 1

factor of safety may be used in establishing the allowable lateral bearing pressure for design purposes. The general formula for estimating the passive pressure is:

$$p_h = k\gamma h \tan^2(45° + \phi/2) + 2c \tan(45° + \phi/2)$$

where γ = unit weight of soil, pounds per cu. ft.

h = depth, ft.

c = cohesion, pounds per sq. ft.

ϕ = angle of internal friction, degrees

k = efficiency factor

p_h = horizontal pressure against vertical plane, psf.

The unit weight is usually between 90 to 120 pcf, with 100 pcf being used for design. When the water table is within the pile depth the submerged unit weight should be used. The water pressure acts around the pile with equal intensity and thus cancels. Cohesion is very significant in clayey soils, but there is very little of it in dry sand and gravel. In contrast, the angle of internal friction, which is a measure of the frictional resistance between the soil particles, is negligible for some cohesive soils and may assume to be zero for the softer clays.

To allow for the additional resistance due to roughness of the contact surface of concrete piles poured in bored holes, or the naturally compact soil in the case of driven piles, the frictional portion of the passive pressure in multiplied by an efficiency factor, which for round bored foundations may be assumed as 2. The semi-empirical nature of the subject makes it very desirable that the actual soil resistance and the magnitude of the deflection should, wherever possible, be tested by experiment.

Allowable Lateral Soil Bearing Values

Just as there are several formulas and methods for computing the magnitude of the maximum pressure against the pile, so there is also no universal agreement as to the safe values that may be used for design. Previously, reference was made to the formula that is acceptable to the officials of the Los Angeles City Building Dept. The allowable unit lateral bearing values on undisturbed soil are set forth in Table I. These values are allowed in the city since February 1953. Prior to that date, the allowable pressures averaged about a third less. Figure 2 shows the formulas that the City uses for the determination of actual soil pressures. The Griffith formula (p^3) may be written as $L = 3.81\sqrt{\frac{HE}{dg}}$ and squared, $L^2 = 14.52\frac{HE}{dg}$ whence, $g = \frac{14.52\,HE}{dL^2} = S$, which is the formula given for a round section.

Los Angeles County discards the first foot of imbedment and for the remainder allows 400 psf/ft. depth.

When using the expressions and charts for depth of penetration, given in the next paragraph, it is assumed that the magnitude of the pressures

FIG. 2 (Los Angeles City)

LATERAL BEARING ON SOILS

DETERMINATION OF ACTUAL SOIL PRESSURES

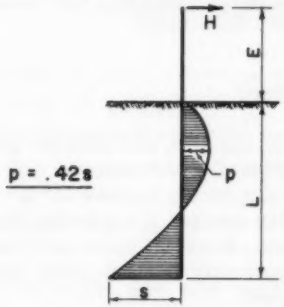

RECTANGULAR SECTION

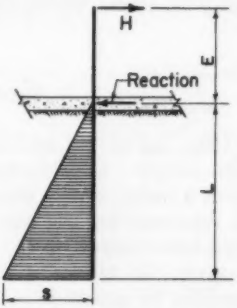

RECTANGULAR SECTION

d = Width of Face

$$s = \frac{9.36\,H\,E}{d\,L^2}$$

ROUND SECTION

$$s = \frac{14.52\,H\,E}{d\,L^2}$$

$$s = \frac{3\,H\,E}{d\,L^2}$$

ROUND SECTION

d = Diameter of Pile

$$s = \frac{4.68\,H\,E}{d\,L^2}$$

TABLE NO. 1

ALLOWABLE LATERAL SOIL BEARING VALUES

pounds per sq. ft. per foot depth

Soil Type	Description	Present Values —used since 1953	Old Values
B-1	Compact gravel with or without coarse sand	310	205
B-2	Compact coarse sand, loose sand and gravel mixtures	265	176
B-3	Loose coarse sand, compact fine sand	215	142
B-4	Loose fine sand	180	119
C-1	Hard clay	400	266
C-2	Medium clay	310	205
C-3	Soft clay	250	165
C-4	Adobe	190	128
D-1	Compact inorganic loam	215	142
D-2	Inorganic silt, loose inorganic loam, compact organic loam	180	119
D-3	Muck or loose organic loam	0	0

mobilized in front of the pile, and in the opposite direction at the bottom, will maintain equilibrium without excessive deflection at the ground level. The procurement of site and soil data is of paramount importance, and the design pressures should be determined from these data. After the adequacy and class of soil is determined, the allowable pressures as set forth in Table 2 may be used. These values may be modified through a soil investigation.

Fundamental Equations

Let H (Fig. 3a) be the applied lateral load on the pile, and take the ground level as the origin. Assume that under the action of this force, the pile pivots about a point, whose distance from the supporting surface is "a" (Fig. 3b). In order for the pile to behave in this manner it has to be absolutely rigid with respect to the surrounding soil. Since all piles are flexible to some extent, the following analysis shall apply only to short piles, which can reasonably be assumed to act as rigid bodies.

The overturning moment may be due to a lateral force, or an eccentrically applied vertical load or a combination of both. Hence, it is more convenient to have the formulas in terms of a lateral force, H_o, and moment, M_o, both applied at the ground level (Fig. 3d).

The soil resistance is assumed to increase lineally with the depth. Fig. 3c shows the resistance per unit of deformation, or soil modulus. Fig. 3d shows the pressure that must be developed, against the pile, to maintain equilibrium. The pressure is the product of the soil modulus by the deformation.

Let the pressure for any point distant x along the pile be p_x. At distance a/2 and L let the pressure against the pile be p and s respectively. Also, let the respective deformations be t and u, and the deflection for x = 0 be Δ.

Now, at distance x the unit resistance $= \omega \frac{x}{L}$

the deflection $= \Delta \frac{(a-x)}{a}$

and the pressure, $p_x = \frac{\omega x}{L} \times \frac{\Delta}{a}(a-x) = \frac{\omega \Delta}{La}(a-x)x$ (1.01)

at $x = a/2$ $\left(\frac{\delta p}{\delta x} = 0\right)$ $p_x = \frac{\omega \Delta a}{4L} = p$ (2.01)

at $x = L$ $p_x = \frac{\omega \Delta (-b)}{a} = s$ (3.01)

from (2.01) $\omega \Delta = \frac{4Lp}{a}$

from (3.01) $\omega \Delta = \frac{as}{b}$

TABLE NO. 2

RECOMMENDED LATERAL SOIL PRESSURE
pounds per sq. ft. per foot depth.

Class of Material	Value
Rock in natural beds — limited by the stress in the pile	
Medium hard caliche	500
Fine caliche with sand layers	400
Compact well graded gravel	400
Hard dense clay	400
Compact coarse sand	350
Compact coarse and fine sand	300
Medium stiff clay	300
Compact fine sand	250
Ordinary silt	200
Sandy clay	200
Adobe	200
Compact inorganic sand and silt mixtures	200
Soft clay	100
Loose organic sand and silt mixtures and muck or bay mud	0

FIG. 3

APPLIED LOAD AND RESISTANCE OF PILE

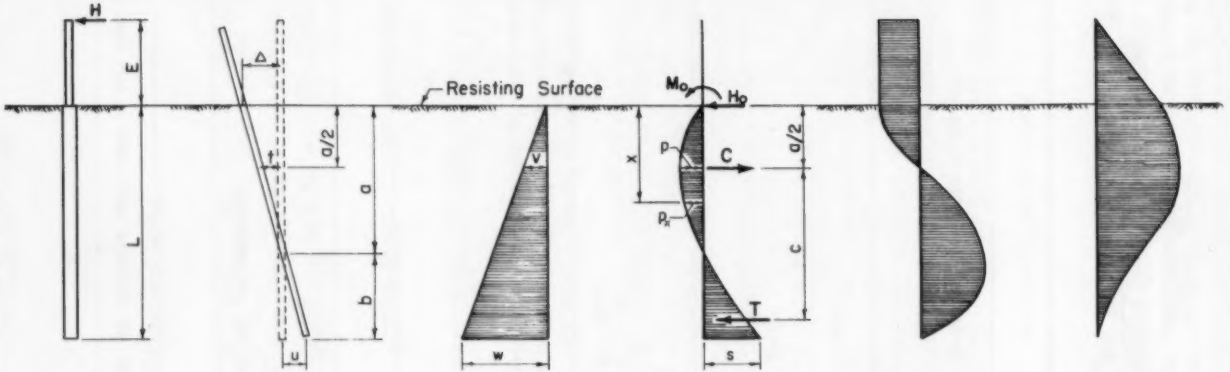

FIG. 3 (a) Applied Load

FIG. 3 (b) Pile Rotation

FIG. 3 (c) Unit Resistance

FIG. 3 (d) Pressure Diagram

FIG. 3 (e) Shear Diagram

FIG. 3 (f) Moment Diagram

substituting in (1.01) $$p_x = \frac{4p}{a^2}(a-x)x \tag{1.02}$$

substituting in (2.01) $$p = \frac{a^2 s}{4bL} = \frac{a^2 s}{4L(L-a)} = \frac{(a/L)^2 s}{4(1-a/L)} \tag{2.02}$$

The two independent statical equations for the equilibrium of a rigid body are

$$\Sigma F = 0 \quad \text{and} \quad \Sigma M = 0$$

to satisfy $\Sigma F = 0$

$$H_o = C - T = \int_o^L p_x dx = \frac{4p}{a^2}\int_o^L (ax - x^2)dx =$$

$$= \frac{4p}{a^2}\left[\frac{ax^2}{2} - \frac{x^3}{3}\right]_o^L = \frac{2pL^2}{3a^2}(3a - 2L) \tag{4.01}$$

Where C = total pressure acting on the pile in front

T = total pressure acting on the pile in back

Also, $$C = \int_o^a p_x dx = \frac{2}{3}pa \tag{4.02}$$

and $$T = \int_L^a p_x dx = \frac{2}{3}pa - \frac{2}{3}\frac{pL^2}{a^2}(3a - 2L) \tag{4.03}$$

and from $\Sigma M = 0$

taking moments about the ground line

$$M_o = -\int_o^L p_x x\,dx = -\frac{4p}{a^2}\int_o^L (ax^2 - x^3)dx = -\frac{4p}{a^2}\left[ax^3/3 - x^4/4\right]_o^L$$

$$= -\frac{pL^3(4a - 3L)}{3a^2} \tag{4.04}$$

Now, let $E = \frac{M_o}{H_o}$ multiplying (4.01) by E and equating to (4.04)

$$\frac{2}{3}p\frac{L^2}{a^2}E(3a - 2L) = -\frac{pL^3(4a - 3L)}{3a^2}$$

from which $$a = \frac{4EL + 3L^2}{6E + 4L}. \tag{7a}$$

multiplying the numerator and denominator by H_o

and substituting M_o for $H_o E$ $$a = \frac{4M_oL + 3H_oL^2}{6M_o + 4H_oL} \tag{7}$$

$$b = L - a = \frac{2EL + L^2}{6E + 4L} \tag{7b}$$

from equations 4.01 and 7

$$p = \frac{3(4M_o + 3H_oL)^2}{4L^2(3M_o + 2H_oL)} \tag{2.1}$$

substituting in (2.02) and re-writing

$$s = \frac{6H_o}{L} + \frac{12M_o}{L^2} \tag{3.1}$$

The pressure diagram is shown in Fig. 3(d). The general equation for the pressure along the pile is obtained by substituting in equation (1.02) the values derived for p and a, and reversing the sign.

$$p_x = \frac{6H_o}{L}\left[\left(6\frac{E}{L} + 4\right)\left(\frac{X}{L}\right)^2 - \left(4\frac{E}{L} + 3\right)\left(\frac{X}{L}\right)\right] \tag{1.1}$$

The solution can now be obtained by comparing the calculated maximum pressures p and s with the allowable earth pressures at distances a/2 and L respectively. Let R be the allowable earth pressure in pounds per sq. ft. per foot depth.

At a/2, allowable pressure = $R\frac{a}{2} = \frac{RL(4M_o + 3H_oL)}{4(3M_o + 2H_oL)} \geq p$

from which $$L^3 - 9H_oL/R - 12M_o/R = 0 \tag{4.1}$$

at depth L, allowable pressure = $RL \geq s = \frac{12M_o + 6H_oL}{L^2}$

from which $$L^3 - 6H_oL/R - 12M_o/R = 0 \tag{4.2}$$

It is apparent by comparing the two equations that the pressure at distance a/2 will govern design of unrestrained piles. For the particular case when $H_o = 0$ ($\frac{E}{L} \to \infty$) an identical solution is obtained by using the allowable pressure either at a/2 or L ($L^3 = \frac{12M_o}{R}$).

Now let $RL = g$ = allowable earth pressure at the base

for $H_o = 0$ $$L = 2.29\sqrt[3]{\frac{M_o}{R}} = 3.46\sqrt{\frac{M_o}{g}} \tag{5.1}$$

for $M_o = 0$ $$L = 3.0\sqrt{\frac{H_o}{R}} = 9.0\frac{H_o}{g} \tag{6.1}$$

Pivot Point

The mathematical expression for the location of the pivot point is given by equation 7. Rewriting it to the more convenient form, in terms of ratios of the pile depth, the hyperbolic function is written as follows:

$$\frac{a}{L} = \frac{4\frac{E}{L} + 3}{6\frac{E}{L} + 4} \qquad (7.01)$$

The function is plotted in Fig. 4. Its mathematical significance is in the rather general solution, applicable to all ratios of moment to lateral load, including partial or full restraint. Some of the cases are illustrated in Fig. 5. The following comments refer to the correspondingly lettered sketches:

(a) Increasing the arm of the lateral force, raises the pivot point. For the limiting case, where there is only an overturning moment ($H_o = 0$) the ratio of a/L is equal to 2/3. It is also seen from the graph, that as the ratio of E/L approaches infinity ($\pm$) the ratio of a/L approaches the asympotic constant value of 2/3.

(b) When E/L is zero, a/L becomes 3/4. This is the case when the lateral load is applied at the ground line ($M_o = 0$).

(c) a/L varies between 2/3 and 3/4, for all combinations of M_o and H_o that act on the pile in the same direction.

(d) When the moment and lateral force at the ground line act on the pile in an opposing sense, E/L will obviously reverse its sign. Such may be the case when there is an initially applied eccentric vertical loading, due to partial or full restraint offered by concrete paving, grade beams, tie rod anchoring, applied couple, etc. Thus, as E/L varies from zero to -0.50, a/L increases from 3/4 to 1.0. For the particular solution when E/L equal -0.50, the assumed point of rotation coincides with the bottom of the pile (a/L = 1.0).

For values of E/L between (-0.50) and (-0.667) a/L will exceed unity. At E/L = -2/3, the value of a/L approaches infinity and the pressure curve becomes a straight line (pressure diagram is triangular). Since there is no tendency for rotation, the pile is maintained in its vertical position and can move with translation only.

(e) An important solution is obtained when a/L equals zero (E/L = 3/4), indicating the lateral resistance of a pile restrained against translation. A concrete floor poured around the pile, may be proportioned to provide the necessary reaction force. For this case, H_o is resisted directly by the slab and does not effect the pile length. The resultant earth pressure, T, acting at a distance 0.75 L, together with the slab reaction, form the necessary resisting couple, equal in magnitude to the applied moment, M_o. Now, substituting M_o/E for H_o in equation 4.2

$$L^3 - \frac{6M_o}{R\,E/L} - \frac{12M_o}{R} = 0$$

and when E/L = -0.75

$$L^3 + \frac{8M_o}{R} - \frac{12M_o}{R} = 0$$

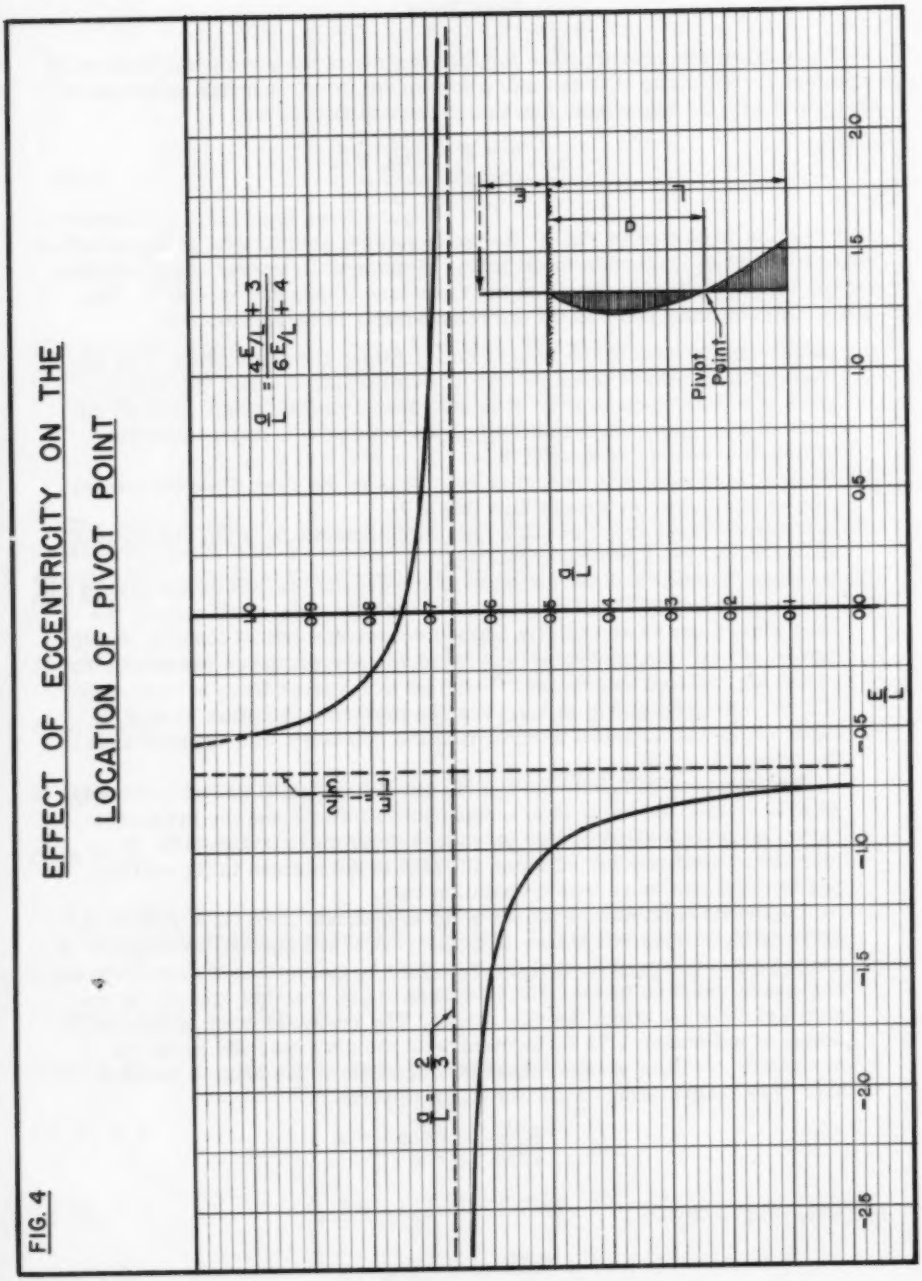
EFFECT OF ECCENTRICITY ON THE
LOCATION OF PIVOT POINT
FIG. 4
$\frac{a}{L} = \frac{4\frac{E}{L} + 3}{6\frac{E}{L} + 4}$
$\frac{a}{L} = \frac{2}{3}$
$\frac{a}{L} = \frac{1}{2}\left(1 - \frac{E}{L}\right)$
Pivot Point
a
D
L
$\frac{a}{L}$
$\frac{E}{L}$
1.0
0.9
0.8
0.7
0.6
0.5
0.4
0.3
0.2
0.1
0.0
.05
-.10
-.15
-.20
-.25
2.0
1.5
1.0
0.5

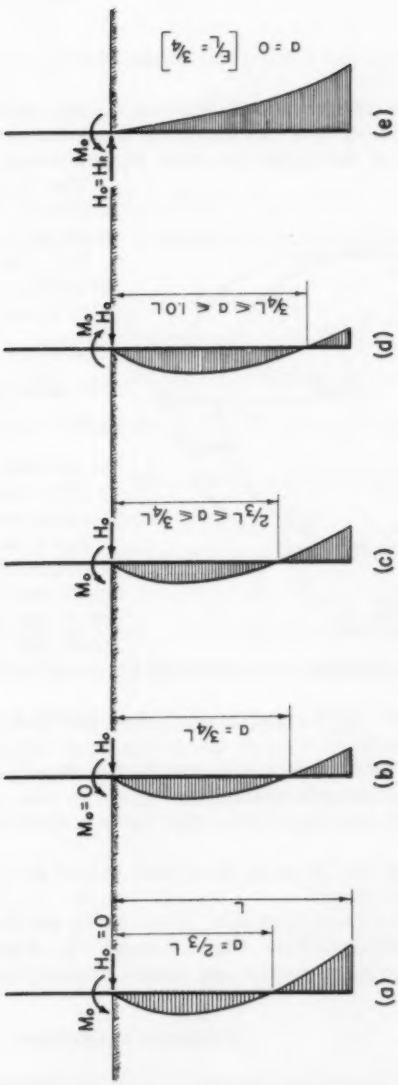

EFFECT OF EXTERNAL FORCES ON DEPTH OF PIVOT POINT

FIG. 5

from which $$L = 1.59\sqrt[3]{\frac{M_o}{R}} \qquad (14.1)$$

Round Piles

The previously developed expressions are applicable to flat surfaces. Since a curved surface can penetrate the earth easier than a flat surface, the effectiveness of the round pile must be decreased.

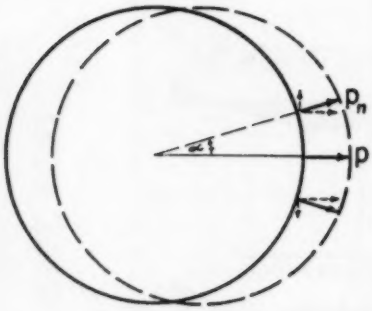

FIG. 6

The pressure is normal to the surface of the displaced pile, and is proportional to the displacement.

Let p be the maximum pressure at the middle element, Fig. 6. Then p_n is equal to p cos α. Average pressure = $\frac{1}{\pi} 2 \int_0^{\frac{\pi}{2}} p \cos\alpha = 0.636p$

The maximum pressure against the middle element is $\frac{\pi}{2}$ or 1.57 times the average on the projected area, or on a flat surface equal in width to the pile diameter.

Let R be the allowable lateral soil pressure on a flat surface, in lbs. per sq. ft. per foot depth. Then, from above the maximum pressure on the round pile should not exceed .636 R.

Rewriting equation 4.1 to be used for round piles.

$$L^3 - 14.14\, H_o L/R - 18.85\, M_o/R = 0 \qquad (4)$$

The relation between R, L, M_O and H_O for round piles is represented graphically in the alignment chart Fig. 7.

In the chart any four values that lie in a straight line will satisfy equation 4.

Hence when any three of these four values are given, the fourth can be found from the chart.

The values of soil pressure, shear force and bending moment along the pile may be obtained from Fig. 8 through 10. Finally, Fig. 11 is presented for the case of piles restrained against translation.

Rectangular Sections

To find the necessary embedment for members having rectangular sections, multiply the width by 1.57 before entering Fig. 7 or Fig. 11.

EXAMPLE 1

Given:

24" dia. x 12' long pile, required for vertical load.
Assume the supporting surface to start 2'-0" below present ground surface.

Lateral force of 1000 lbs. applied 15'-6" above ground surface. Allowable soil resistance = 300 psf./ft. depth.

Solution:

$H_o = \frac{1000}{2} = 500$ lbs $\qquad M_o = 500\ (15.5 + 2.0) = 8{,}750$ lb-ft.

$L = 12.0 - 2.0 = 10.0$ ft. $\qquad E = \frac{8{,}750}{500} = 17.5$ ft.

$E/L = 17.5/10 = 1.75$

On Fig. 7 draw a line from $M_o = 8.75$ to $H_o = 0.5$.

At intersection with R = 300, proceed vertically to horizontal scale and read

$L = 9.2$ ft. $<$ 10.0 ft. ok.

from Fig. 4 for $E/L = 1.75$ $\quad a/L = 0.69$

from Fig. 8, at $X/L = .345$ $c_p = 1.74$, at $X/L = 1.0$ $c_p = 4.5$

hence $r = 1.57 \times \frac{6 \times 500}{10} \times 1.74 = 810$ psf

$s = 1.57 \times 300 \times 4.5 = 2{,}120$ psf

from Fig. 9, at $X/L = 0.69$ $\quad c_s = -3.8$

max. shear force $V = 500 \times 2.0 \times (-3.8) = -3{,}800$ lbs.

from Fig. 10 at $X/L = 0.20$ $\quad (V_x = 0)$ $\quad c_m = 1.88$

max. bending moment $M = 500 \times 2.0 \times 10.0 \times 1.88 = 18{,}800$ lb-ft.

EXAMPLE 2:

Augers of the following shaft diameter are available at the site: 16", 22", 26", 30", and 36". Select a pile to resist a total moment of 30,000 lb. ft. and a horizontal force of 500 lbs. applied at the supporting surface. Use R = 300 psf/ft. depth. Min. bearing area to resist vertical loads is 3.0 sq. ft. at 7.0 ft. depth.

Solution:

diameter	area (sq. ft.)	M_o	H_o kips	L-ft.	V (cu ft.)
16 in 1.33 ft.	1.39			from Fig. 7	
22 1.83	2.63				
26 2.17	3.70 > 3.0	13.8	0.23	use → 9.7	36.0
30 2.50	4.91	12.0	0.20	9.2	45.2
36 3.00	7.07	10.0	0.17	8.8	62.3

Piles of minimum diameter prove usually most economical.

EXAMPLE 3:

What are the required depth and the reaction force if the pile of example 2 is restrained against translation.

Solution:

From Fig. 11 for $M_o = 13.8^{1k}$ and R = 300 L = 6.6 use 7.0 ft.

(Equation 16) $P_R = 230 + \frac{1.33 \times 13,800}{7.0} = 2850$ #/1

Reaction force = 2,850 x 2.17 = 6,200 #

EXAMPLE 4:

A rectangular section 26" wide is used to resist the loads of example 2. What is the required depth if R = 300.

Solution:

$$M_o = \frac{30.0}{2.17 \times 1.57} = 8.8^{1k} \qquad H_o = \frac{0.500}{2.17 \times 1.57} = 0.146^{k}$$

From Fig. 7 L = 8.5 ft.

NOMENCLATURE

a = distance from resisting surface to pivot point, ft.

b = distance from pivot point to bottom of pile, ft.

c = cohesion, pounds, per sq. ft.

c_m = moment coefficient

c_p = average soil pressure coefficient

c_s = shear coefficient

C = total earth pressure in front of pile pounds per ft. diameter.

d = diameter of pile, ft.

E = distance from lateral load to resisting surface, ft. (M_o/H_o)

g = allowable lateral soil bearing at depth L, psf.

h = depth, ft.

H = applied lateral force on pile, pounds

H_o = lateral force per foot of pile diameter, applied at the resisting surface, pounds per ft. diameter.

H_R = restraining reaction due to M_o, pounds per ft. diameter

k = efficiency factor, used in the passive pressure formula.

L = depth of pile, measured from the resisting surface, ft.

M_o = moment per foot of pile diameter, applied at the resisting surface, ft.-pounds per ft. diameter.

M_t = applied moment on pile, ft-pounds.

M_x = bending moment at distance x from resisting surface, ft-pounds per ft. diameter.

p = earth pressure against pile at distance a/2 from resisting surface, psf.

p_h = passive pressure against vertical plane, psf.

p_x = earth pressure against pile, at distance x from resisting surface, psf.

Pr = restraining reaction, pounds per ft. diameter.

R = allowable lateral soil pressure on flat surface, pounds per square ft. per ft. depth.

s = earth pressure against pile at distance L, psf.

t = deflection at distance a/2, ft.

T = total earth pressure in back of pile, pounds per ft. diameter.

u = deflection at distance L, ft.

v = unit resistance at distance a/2, pounds per $(ft.)^3$

Vx = shearing force at distance x from resisting surface, pounds per ft. diameter.

w = unit resistance at distance L, pounds per $(ft.)^3$

x = distance along pile, measured from resisting surface, ft.

γ = unit weight of soil, pounds per cu. ft.

Δ = deflection at the resisting surface, ft.

ϕ = angle of internal friction, degrees.

REFERENCES

1. The Design of Masonry Structures and Foundations, by C. C. Williams. 2nd Edition 1930, Page 479.

2. Civil Engineering Handbook, 2nd Edition, 1940, page 644, by L. C. Urquhart.

3. Bulletin No. 3 Engineering Experiment Station. North Carolina State College, August 1929.

4. Embedment of Poles, Sheeting and Anchor Piles, by M. A. Drucker, Vol. 4, No. 12 Civil Engineering for December 1934.

5. Lateral Pile Loading Tests by L. B. Feagin, with discussion by A. E. Cummings, J. C. Meen, T. Keinnard Thomson, August E. Niederhoff, Lazarus White, Y. L. Chang, D. P. Krynine. Paper No. 1959, Vol. 102, 1937 Transactions of ASCE.

6. Construction Design Charts, by James R. Griffith. Page 135. Published by Western Construction News, San Francisco, Calif. 1943.

7. Theory of Lateral Bearings Capacity of Piles, by Paul E. Raes. Paper H-1 Proceedings, International Conference on Soil Mechanics and Foundation Engineering (1936) Vol. 1.

SUMMARY OF EQUATIONS

A. DETERMINATION OF ACTUAL SOIL PRESSURES

ROUND SECTION (Max. at middle element)

$$p_x = 9.425 \frac{H_o}{L}\left[-(4\frac{E}{L}+3)(\frac{X}{L}) + 2(3\frac{E}{L}+2)(\frac{X}{L})^2\right] \quad \text{.....(1)}$$

$\underline{X=\frac{a}{2}}$ $$p = \frac{1.178\ (4M_o+3H_oL)^2}{L^2\ (3M_o+2H_oL)} \quad \text{.....(2)}$$

$$p = \frac{1.178\ H_o\ (4\frac{E}{L}+3)^2}{L\ (3\frac{E}{L}+2)} \quad \text{.....(2a)}$$

$\underline{X=L}$ $$s = \frac{9.425\ (2M_o+H_oL)}{L^2} \quad \text{.....(3)}$$

$$s = \frac{9.425\ H_o\ (2\frac{E}{L}+1)}{L} \quad \text{.....(3a)}$$

RECTANGULAR SECTION

$$p_x = 6\frac{H_o}{L}\left[-(4\frac{E}{L}+3)(\frac{X}{L}) + 2(3\frac{E}{L}+2)(\frac{X}{L})^2\right] \quad \text{.....(1.1)}$$

$\underline{X=\frac{a}{2}}$ $$p = \frac{0.75\ (4M_o+3H_oL)^2}{L^2\ (3M_o+2H_oL)} \quad \text{.....(2.1)}$$

$$p = \frac{0.75\ H_o\ (4\frac{E}{L}+3)^2}{L\ (3\frac{E}{L}+2)} \quad \text{.....(2.1a)}$$

$\underline{X=L}$ $$s = \frac{6\ (2M_o+H_oL)}{L^2} \quad \text{.....(3.1)}$$

$$s = \frac{6\ H_o\ (2\frac{E}{L}+1)}{L} \quad \text{.....(3.1a)}$$

B. EQUATIONS FOR REQUIRED PILE EMBEDMENT

	ROUND SECTION		RECTANGULAR SECTION	
(4)	$L^3 - 14.14\frac{H_oL}{R} - 18.85\frac{M_o}{R} = 0$		$L^3 - 9\frac{H_oL}{R} - 12\frac{M_o}{R} = 0$	(4.1)
(5)	$L = 2.66\sqrt[3]{\frac{M_o}{R}}$	$H_o = 0$	$L = 2.29\sqrt[3]{\frac{M_o}{R}}$	(5.1)
(6)	$L = 3.76\sqrt{\frac{H_o}{R}}$	$M_o = 0$	$L = 3\sqrt{\frac{H_o}{R}}$	(6.1)

C. DISTANCE TO PIVOT POINT

$$a = \frac{4M_oL + 3H_oL^2}{6M_o + 4H_oL} \quad \text{.....(7)}$$

$$a = \frac{4EL + 3L^2}{6E + 4L} \quad \text{.....(7a)}$$

D. SHEAR FORCE

$$V_x = H_o\left[1 - 3\left(4\frac{E}{L}+3\right)\left(\frac{X}{L}\right)^2 + 4\left(3\frac{E}{L}+2\right)\left(\frac{X}{L}\right)^3\right] \quad \text{.....(8)}$$

$H_o=0$ $$V_x = 12\frac{M_o}{L}\left(\frac{X}{L}-1\right)\left(\frac{X}{L}\right)^2 \quad \text{.....(9)}$$

$M_o=0$ $$V_x = H_o\left[1 - 9\left(\frac{X}{L}\right)^2 + 8\left(\frac{X}{L}\right)^3\right] \quad \text{.....(10)}$$

E. BENDING MOMENT

$$M_x = H_oL\left[\left(\frac{E}{L}+\frac{X}{L}\right) - \left(4\frac{E}{L}+3\right)\left(\frac{X}{L}\right)^3 + \left(3\frac{E}{L}+2\right)\left(\frac{X}{L}\right)^4\right] \quad \text{.....(11)}$$

$H_o=0$ $$M_x = M_o\left[1 - 4\left(\frac{X}{L}\right)^3 + 3\left(\frac{X}{L}\right)^4\right] \quad \text{.....(12)}$$

$M_o=0$ $$M_x = H_oL\left[\frac{X}{L} - 3\left(\frac{X}{L}\right)^3 + 2\left(\frac{X}{L}\right)^4\right] \quad \text{.....(13)}$$

F. PILES RESTRAINED AGAINST TRANSLATION $\left(\frac{E}{L} = -\frac{3}{4}\right)$

ROUND SECTION	RECTANGULAR SECTION
(14) $L = 1.85\sqrt[3]{\frac{M_o}{R}}$	$L = 1.59\sqrt[3]{\frac{M_o}{R}}$ .....(14.1)
(15) $s = 6.28\frac{M_o}{L^2}$	$s = 4\frac{M_o}{L^2}$ .....(15.1)

$$P_R = H_o + 1.33\frac{M_o}{L} \quad \text{.....(16)}$$

G. PILES RESTRAINED AGAINST ROTATION $\left(\frac{E}{L} = -\frac{2}{3}\right)$

ROUND SECTION	RECTANGULAR SECTION
(17) $L = 1.68\sqrt[3]{\frac{M_o}{R}}$	$L = 1.44\sqrt[3]{\frac{M_o}{R}}$ .....(17.1)
(18) $s = 4.71\frac{M_o}{L^2}$	$s = 3\frac{M_o}{L^2}$ .....(18.1)

$$P_R = H_o + 1.5\frac{M_o}{L} \quad \text{.....(19)}$$

FIG. 7

RESISTANCE TO OVERTURNING OF ROUND, SHORT PILES

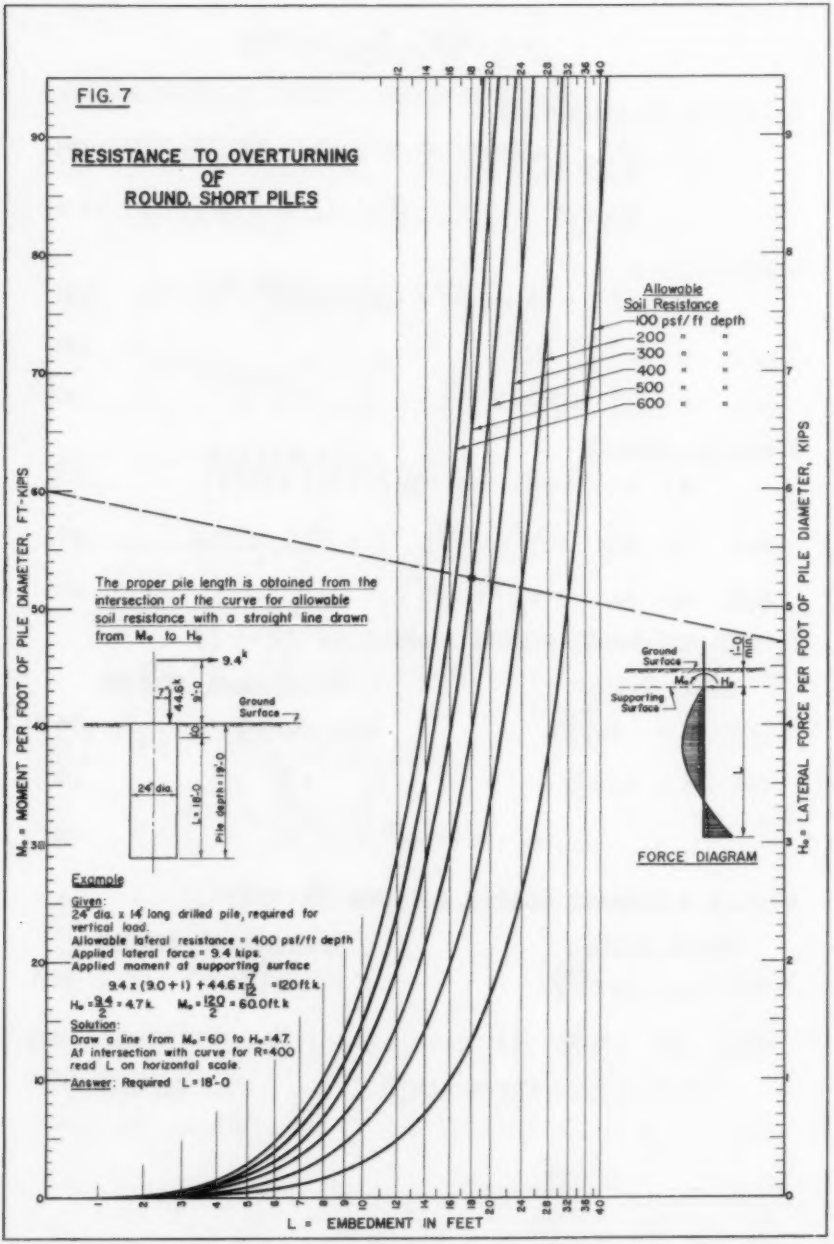

Example

Given:
24" dia. x 14' long drilled pile, required for vertical load.
Allowable lateral resistance = 400 psf/ft depth
Applied lateral force = 9.4 kips.
Applied moment at supporting surface

$$9.4 \times (9.0 + 1) + 44.6 \times \frac{7}{2} = 120 \text{ ft.k.}$$

$$H_o = \frac{9.4}{2} = 4.7 \text{ k.} \qquad M_o = \frac{120}{2} = 60.0 \text{ ft.k}$$

Solution:
Draw a line from $M_o = 60$ to $H_o = 4.7$.
At intersection with curve for R=400 read L on horizontal scale.

Answer: Required L = 18'-0

FIG. 8 SOIL PRESSURE COEFFICIENTS

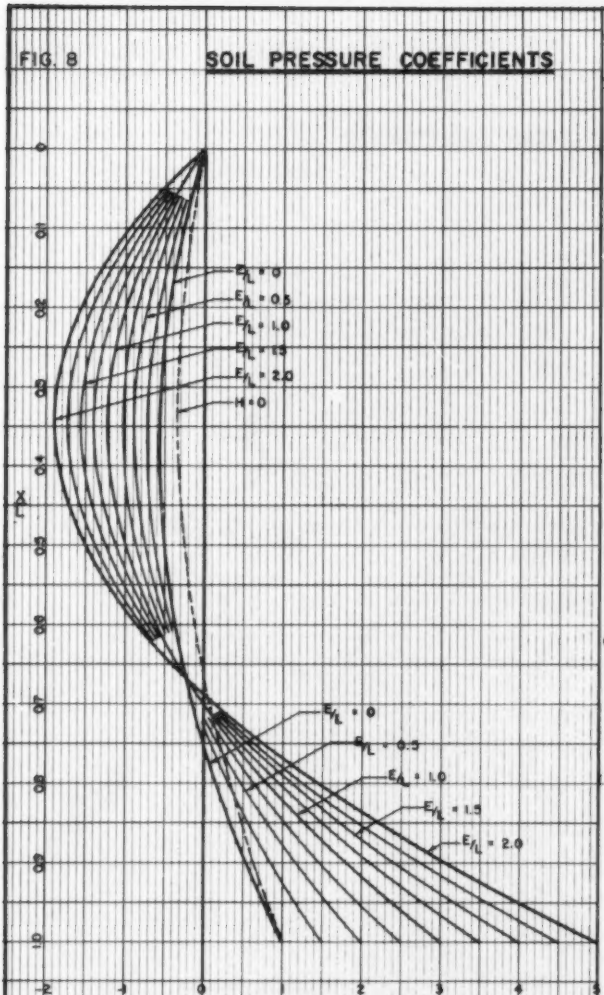

NOTE: The maximum pressure against the middle element of a round pile equals 1.57 multiplied by the average pressure

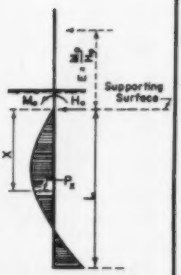

FORCE DIAGRAM

$$P_x = \frac{6H_o}{L} C_p$$

$$C_p = -(4\frac{E}{L}+3)(\frac{X}{L}) + 2(3\frac{E}{L}+2)(\frac{X}{L})^2$$

For $H_o = 0$ $(E/L \longrightarrow \infty)$

$$P_x = \frac{12M_o}{L^2} C_p$$

$$C_p = -2(\frac{X}{L}) + 3(\frac{X}{L})^2$$

FIG. 9 **SHEAR COEFFICIENTS**

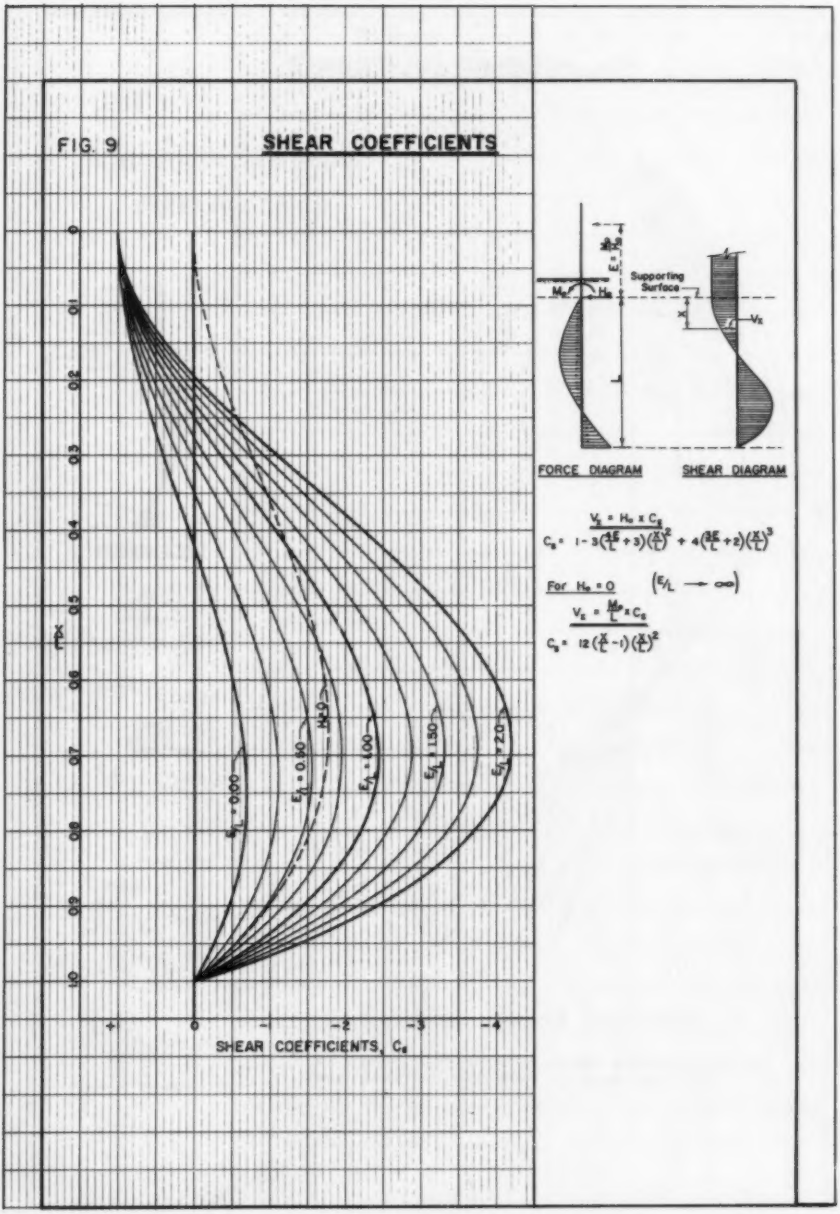

$$C_s = \frac{V_x = H_o \times C_s}{1 - 3\left(\frac{4E}{L} + 3\right)\left(\frac{x}{L}\right)^2 + 4\left(\frac{3E}{L} + 2\right)\left(\frac{x}{L}\right)^3}$$

For $H_o = 0$ $\left(E/L \rightarrow \infty\right)$

$$C_s = \frac{V_x = \frac{M_o}{L} \times C_s}{12\left(\frac{x}{L} - 1\right)\left(\frac{x}{L}\right)^2}$$

FIG. 10 **MOMENT COEFFICIENTS**

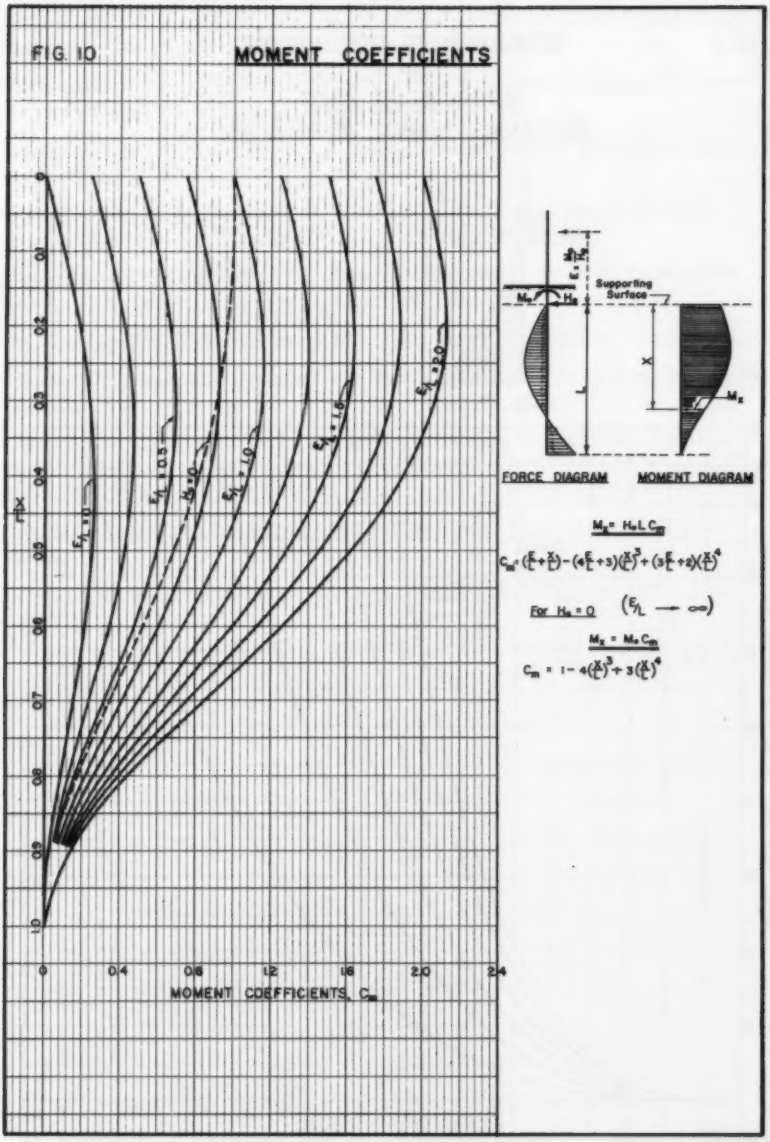

$$M_x = H_a L C_m$$

$$C_m = (\frac{E}{L} + \frac{X}{L}) - (4\frac{E}{L} + 3)(\frac{X}{L})^3 + (3\frac{E}{L} + 2)(\frac{X}{L})^4$$

For $H_a = 0$ $\quad (E/L \longrightarrow \infty)$

$$M_x = M_a C_m$$

$$C_m = 1 - 4(\frac{X}{L})^3 + 3(\frac{X}{L})^4$$

FIG. 11

RESISTANCE TO OVERTURNING OF ROUND, SHORT PILES RESTRAINED AGAINST TRANSLATION

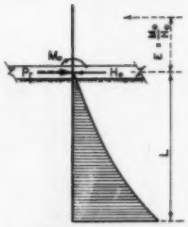

FORCE DIAGRAM

Reaction per foot of pile diameter

$P_f = H_o\left(1 + 1.33\frac{E}{L}\right)$

For $H_o = 0$

$P_f = 1.33\frac{M_o}{L}$

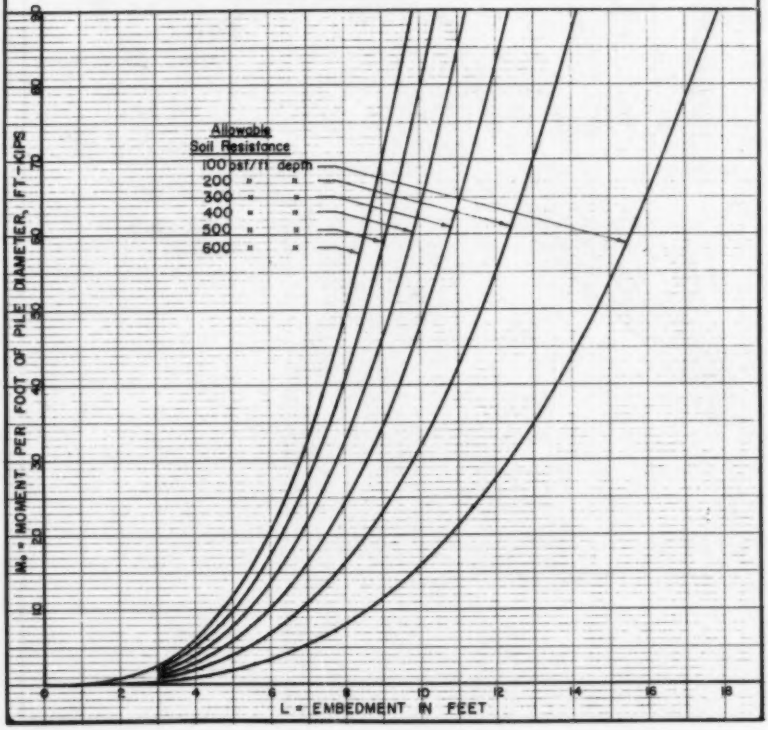

8. Discussion on the Lateral Resistance of Piles by P. Raes and A. E. Cummings. Paper H-11, Proceedings, International Conference on Soil Mechanics and Foundation Engineering (1936) Vol. 3.

9. Horizontal Forces Acting on Pile by L. C. Wilcoxen, Engineering News Record, December 17, 1931, Page 978.

10. Stanchions and Poles. Practical Design Handbook for Structural Engineers by Dr. Aldis Cibulka, Houston.

11. Experiments by D. P. Krynine, Vol. 98, 1933 Transactions of ASCE. P. 271-273.

12. Experiments by State Highway Board of Georgia. Wood Preservation News. November, 1932, Vol. 10, p. 156-158.

13. Proceeding ASCE, November 1935, Vol. 61. Page 1363 by Cummings.

14. The Short Bored Pile Foundation. Buildings Research Station Digest No. 42, May 1956.

15. Thrust Loadings on Piles by James F. McNutty. Paper 940, Journal of the Soil Mechanics and Foundations Division of American Society of Civil Engineers, Vol. 82, April, 1956.

16. Lateral Load Tests on Piles. ASTM Technical Publication STP 154 (1954).

17. Supplement to Symposium or Lateral Load Tests on Piles. STP 154-A (1955).

Journal of the
STRUCTURAL DIVISION
Proceedings of the American Society of Civil Engineers

CONFIRMATION OF INELASTIC STRESS DISTRIBUTION IN CONCRETE[a]

Eivind Hognestad,* A.M. ASCE
(Proc. Paper 1189)

SYNOPSIS

Studies reported in the literature regarding inelastic stress distribution in flexure of reinforced concrete members are reviewed, and the results obtained are compared to the recommendations of the Joint ASCE-ACI Committee on Ultimate Strength Design. Test results show that the inelastic concrete stress distribution consists of a rising curve from zero to the maximum stress and a descending curve beyond the maximum stress. A simplified rectangular distribution gives a satisfactory accuracy for the common practical design cases. The Joint Committee design coefficients are well substantiated by test results.

INTRODUCTION

Structural concrete and reinforcing steel both behave inelastically at high loads. In theories regarding the ultimate strength of reinforced concrete, therefore, inelastic behavior of both component materials is of fundamental importance and must be expressed in quantitative terms.

Most reinforcing steel used in this country has a distinct yield point. Inelastic behavior of reinforcement may then for most cases be expressed by a trapezoidal stress-strain diagram. For reinforcement without a yield point, such as prestressing steels, a stress-strain curve obtained in a simple tension test will usually give the necessary information.

Inelastic stress distribution in the concrete compression zone of flexural members is more difficult to measure and to express in mathematical terms.

Note: Discussion open until August 1, 1957. Paper 1189 is part of the copyrighted Journal of the Structural Division of the American Society of Civil Engineers, Vol. 83, No. ST 2, March, 1957.

a. Presented at ASCE Knoxville Convention, June 7, 1956, Knoxville, Tenn.

* Mgr., Structural Development Section, Research and Development Div., Portland Cement Assn., Chicago, Ill.

Discussions of this stress distribution, which is often referred to as the stress block, have appeared periodically in the reinforced concrete literature from the 1890's to the present day. It has been possible to gather information only slowly, principally because it is very difficult to measure stress in concrete although strain may be measured easily and accurately.

Studies of inelastic concrete stress distribution have taken two principal forms. In one group of investigations it has been attempted to arrive at the stress distribution by analysis of behavior and ultimate strength observed in tests of reinforced concrete columns and beams. In a second group of investigations, it has been attempted to measure the concrete stress distribution directly by various tests of plain concrete specimens. It is the principal object of this paper to describe the most important findings by these two approaches regarding inelastic stress distribution in structural concrete subject to flexure.

Historical Background

Studies of inelastic concrete stress distribution have been closely associated with the development of ultimate strength design theories as outlined in Fig. 1. The pioneers of reinforced concrete design defined the basic principles at the turn of the century. For instance, a theory based on a parabolic stress distribution was presented by W. Ritter in 1899, and studies of a rectangular distribution by von Emperger and E. Suenson followed.

This early emphasis on ultimate strength was discontinued when the elastic straight line theory and the concepts of safe loads and working stress became commonly used in design throughout the world. Since the elastic stress distribution at low loads is characterized by the modular ratio n, extensive researches were carried out regarding the modulus of elasticity of concrete. Effects of many variables were investigated in compression tests, and many expressions for the modulus of elasticity as a function of compressive strength and other variables were suggested. Only a few papers, such as those by Suenson, Mensch, and Kempton Dyson, and the experimental studies of Lyse, Slater, and Zipprodt, discussed inelastic stress distribution during the period between 1910 and 1930.

A renewal of interest and activity in ultimate strength studies began about 1930, initiated in this country by the ACI Column Investigation and in Europe by von Emperger's critical studies of the modular ratio and the allowable stress concepts of the straight-line theory. Some of the theories that resulted from experimental and analytical investigations are reviewed in Fig. 1. It is seen that the stress distributions chosen vary somewhat. In terms of predicted ultimate strength of reinforced concrete members, however, there is a relatively small difference between the various theories when the proper empirical parameters are used.

After about 1950, a consolidation of knowledge regarding ultimate strength design has been carried out. Theories have been extended to cover combined bending and axial load as well as prestressed reinforced concrete members. Important and extensive new test data have been reported. Ultimate strength design procedures have been put to practical use through introduction into building codes in several countries, and a change is being considered in other countries. Culminating more than ten years of thorough committee work, a final report of the ASCE-ACI Joint Committee on Ultimate Strength Design

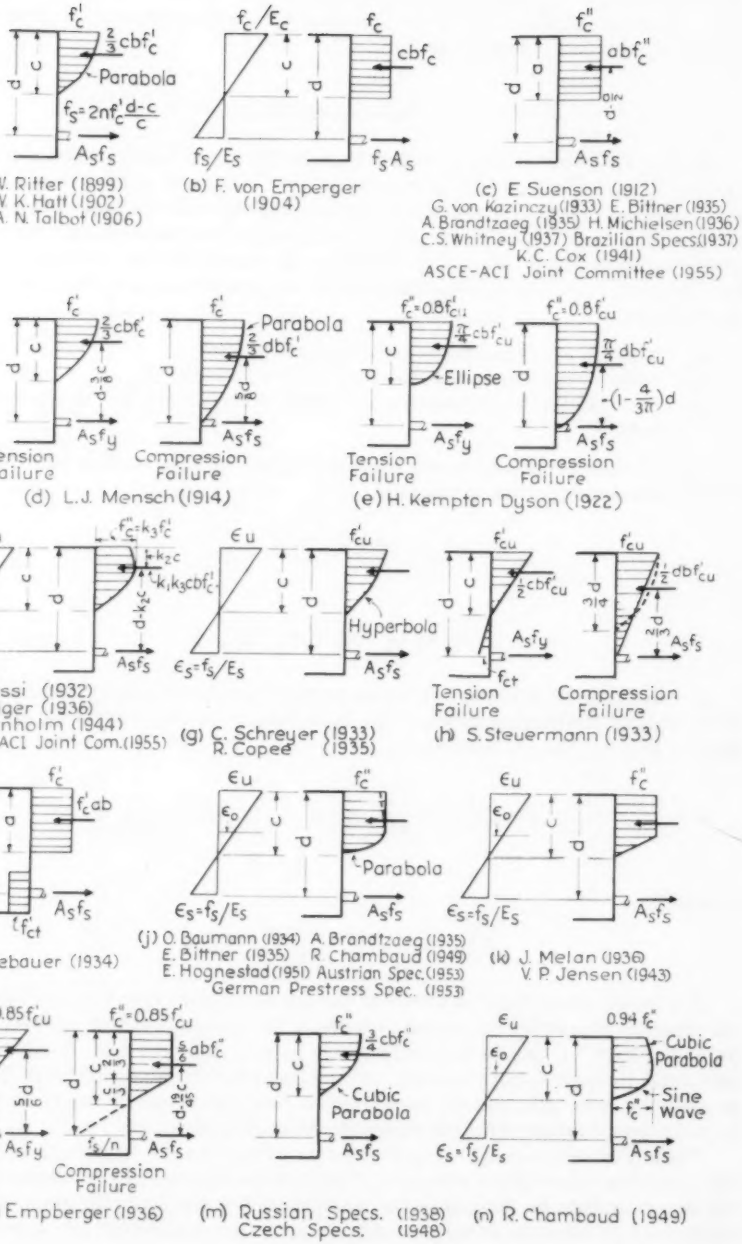

(a) W. Ritter (1899) W. K. Hatt (1902) A. N. Talbot (1906)

(b) F. von Emperger (1904)

(c) E. Suenson (1912) G. von Kazinczy (1933) E. Bittner (1935) A. Brandtzaeg (1935) H. Michielsen (1936) C.S. Whitney (1937) Brazilian Specs. (1937) K.C. Cox (1941) ASCE-ACI Joint Committee (1955)

(d) L.J. Mensch (1914)

(e) H. Kempton Dyson (1922)

(f) F. Stüssi (1932) R. Saliger (1936) H. Granholm (1944) ASCE-ACI Joint Com. (1955)

(g) C. Schreyer (1933) R. Copeé (1935)

(h) S. Steuermann (1933)

(i) F. Gebauer (1934)

(j) O. Baumann (1934) A. Brandtzaeg (1935) E. Bittner (1935) R. Chambaud (1949) E. Hognestad (1951) Austrian Spec. (1953) German Prestress Spec. (1953)

(k) J. Melan (1936) V. P. Jensen (1943)

(l) F. von Emperger (1936)

(m) Russian Specs. (1938) Czech Specs. (1948)

(n) R. Chambaud (1949)

FIG. 1 – DEVELOPMENT OF ULTIMATE STRENGTH FLEXURAL THEORIES

was published in October 1955,[1] and the recent revision of the ACI Building Code (ACI 318-56)[2] permits the ultimate strength method to be used for design of reinforced concrete members.

Ultimate Strength Equations for Flexure

To illustrate the extent to which quantitative expression of inelastic concrete stress distribution is of importance for practical design purposes, it is convenient to consider the basic equations for flexural strength of reinforced beams. It is assumed that tensile stress carried by the concrete may be neglected in sections subject to bending. As shown in Fig. 2, properties of the inelastic concrete stress distribution are represented by the following coefficients:

k_1 = ratio of average stress to maximum stress
k_3 = ratio of maximum stress to cylinder strength, f'_c
k_2 = ratio of depth to resultant of compressive stress and depth to neutral axis

Equilibrium of moments and forces for bending of a section with tension reinforcement only then gives (Fig. 2):

$$M_{ult} = A_s f_{su} (d - k_2 c) \tag{1}$$

$$k_1 k_3 f'_c \; bc = A_s \; f_{su} \tag{2}$$

In most practical cases, ultimate strength is controlled by tension. The steel stress at ultimate moment f_{su} then equals the yield point f_y, and we obtain by solving Eq. (1) and (2):

$$M_{ult} = bd^2 f'_c q \left(1 - \frac{k_2}{k_1 k_3} q\right) = A_s \; f_y \; d \left(1 - \frac{k_2}{k_1 k_3} q\right) \tag{3}$$

in which

$$q = p \; f_y / f'_c$$

It may be noted that the effect of the assumed concrete stress distribution on ultimate strength controlled by tension is completely represented by the ratio k_2/k_1k_3. It can be shown that this is also the case for combined bending and axial load when both tension and compression reinforcement is yielding at ultimate strength, and for prestressed concrete when the steel stress f_{su} is near the ultimate strength of the prestressing steel.

When ultimate strength is governed by compression, however, crushing of the concrete takes place without yielding of the tension reinforcement. Strains may then be considered in computing the stress in the tension reinforcement at ultimate strength. Assuming a linear distribution of strain, we obtain with the notation of Fig. 2:

$$k_u = \frac{c}{d} = \frac{\varepsilon_u}{\varepsilon_{su} + \varepsilon_u} \tag{4}$$

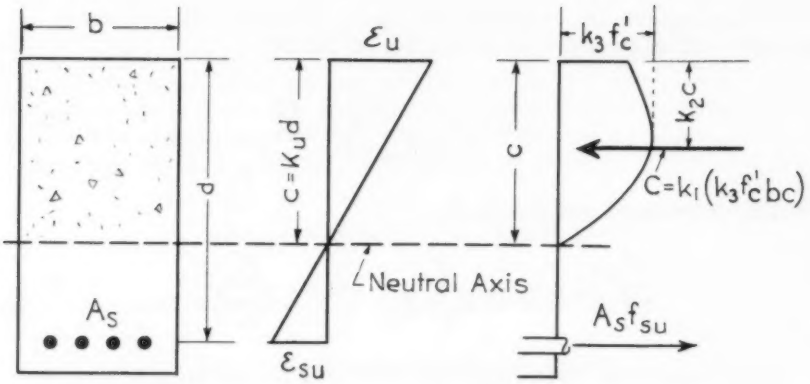

FIG. 2 - CONDITIONS AT ULTIMATE LOAD

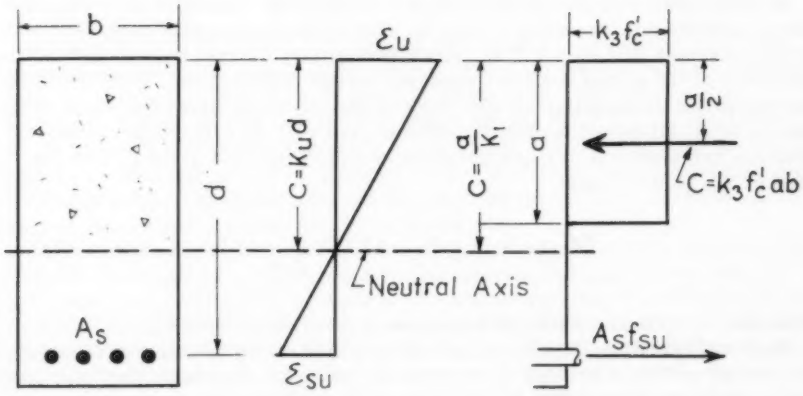

FIG. 3 - RECTANGULAR STRESS DISTRIBUTION

By combining Eq. (4) with Eq. (1) and (2), the stress f_{su} as well as the ultimate moment M_{ult} may be determined. It is then necessary to know ε_u and independent values of k_2 and k_1k_3, not only the ratio k_2/k_1k_3. To illustrate this, the balanced steel ratio p_b for which yielding of the steel and crushing of the compression zone concrete take place simultaneously at ultimate strength may be computed by solving Eq. (2) and (4):

$$p_b = k_1 k_3 \frac{\varepsilon_u}{\varepsilon_y + \varepsilon_u} \frac{f'_c}{f_y} \tag{5}$$

so that for balanced reinforcement:

$$\frac{M_{ult}}{bd^2 f'_c} = k_1 k_3 \frac{\varepsilon_u}{\varepsilon_y + \varepsilon_u} \left(1 - k_2 \frac{\varepsilon_u}{\varepsilon_y + \varepsilon_u}\right) \tag{6}$$

Similar equations cover compression failures for combined bending and axial load as well as for bonded prestressed concrete. Therefore, basic equations of this general nature are powerful design tools provided that reliable quantitative information regarding the stress distribution is available at least to the extent of k_2, k_1k_3, and ϵ_u. If the entire shape of the stress distribution is known, any shape of cross-section and nonsymmetrical bending can be analyzed.

Equivalent Rectangular Distribution

In many practical design cases it is convenient to consider a rectangular stress distribution as shown in Fig. 3. Use of the rectangular distribution tacitly assumes that $k_2 = 1/2\ k_1$, which fortunately corresponds closely to the geometry of the actual inelastic concrete stress distribution. If the depth of the equivalent rectangular stress block is chosen as k_1 times the depth to the neutral axis, all equations for the ultimate strength of rectangular cross-sections are identical to those obtained by Fig. 2 for $k_2 = 1/2\ k_1$. For instance, Eq. (3) becomes:

$$M_{ult} = A_s f_y d\left(1 - \frac{1}{2k_3} q\right) \tag{3a}$$

while Eq. (5) remains unchanged because it does not contain k_2.

Such mathematical identity is not obtained for nonrectangular sections and for nonsymmetrical bending of rectangular sections. In many practical cases and particularly when ultimate strength is controlled by tension, however, the errors associated with the use of the rectangular distribution are small. These mathematical errors are frequently less than the margin of experimental scatter in determination of design values for k_1, k_2, k_3, and ε_u.

An equivalent rectangular stress distribution was used to develop an ultimate strength theory for eccentrically loaded cylindrical columns.(3) Excellent agreement was obtained between theory and tests of 30 large columns.

Joint Committee Report

Numerical design values intended for practical use were suggested by the Joint Committee.[1] It was recommended that the maximum fiber stress in concrete should not exceed 0.85 f'_c, that is, k_3 should not exceed 0.85. A design value of $k_2 = 1/2\ k_1$ was suggested to permit use of the equivalent rectangular stress distribution. The committee recommended a value for k_1 of 0.85 reduced at the rate of 0.05 per 1000 psi concrete strength in excess of 5000 psi. Finally, it was suggested that the ultimate concrete strain ε_u should not be assumed greater than 0.003.

By letting $k_2 = 1/2\ k_1$ and $k_3 = 0.85$, Eq. (3) becomes:

$$M_{ult} = A_s f_y d(1-0.59q) \qquad (3b)$$

which is the equation suggested by C. S. Whitney in 1937.

Tests of Reinforced Columns and Beams

Analyses of Beam and Column Tests

Until recently, most of the available information regarding inelastic stress distribution in concrete was derived from tests of reinforced concrete members. In the early 1930's the extensive ACI column investigation[4] of concentrically loaded columns led to the addition law which states that the ultimate strength of a column equals 85% of the cylinder strength times the concrete area plus the yield stress of the longitudinal steel times its area. Thus, for concentrically loaded columns, the value $k_3 = 0.85$ was experimentally derived.

Several papers on stress distribution and ultimate strength design were published in Europe throughout the 1930's (Fig. 1), followed by the studies of ultimate strength in this country by C. S. Whitney.[5] His theoretical approach involved an equivalent rectangular stress block with a maximum stress of 0.85 f'_c so that his value of k_3 was 0.85, and Eq. (3b) was developed. Whitney avoided the use of an ultimate strain even for compression failures by linking design equations intended for specific practical cases directly to tests of reinforced concrete beams and columns.

V. P. Jensen then presented a study of the ultimate strength of beams in 1943.[6] He assumed a trapezoidal stress distribution and derived the properties of this trapezoid as a function of cylinder strength by analysis of the observed ultimate strength of reinforced beams. On this basis he found the values of k_1k_3 and k_2 shown in Fig. 4 as compared to the values recommended by the Joint Committee.

Another study of ultimate strength came from the University of Illinois in 1951.[3] To interpret the ultimate strengths observed in tests of 120 eccentrically loaded columns a stress distribution was used that consists of a rising parabola and a descending straight line after the maximum stress. From the results of concentrically loaded columns a maximum stress equal to 85% of the cylinder strength was chosen, that is, $k_3 = 0.85$. The slope of the descending straight line was then assumed at various values, and the corresponding theoretical strengths of all 120 eccentrically loaded columns were computed. A final slope of the straight line was then so chosen as to give the

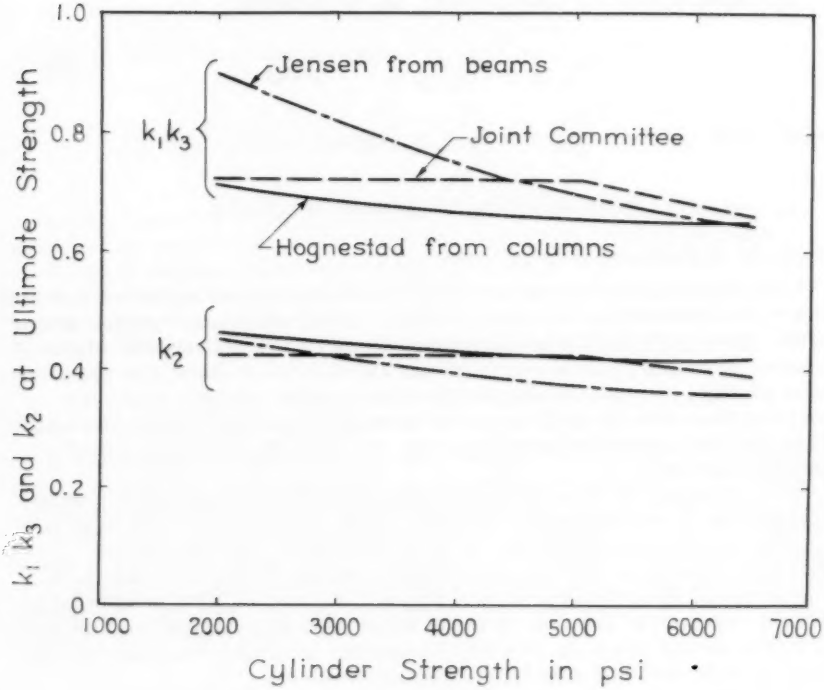

FIG. 4 - DESIGN VALUES FROM TESTS OF REINFORCED CONCRETE

best statistical agreement with the observed column strengths. The corresponding values of k_1k_3 and k_2 are given in Fig. 4. It is believed that the somewhat lower values of k_1k_3 as compared to Jensen's findings result from the fact that the test columns were cast in vertical position so that bleeding led to a weaker concrete near the top of the columns than near the bottom. Jensen's findings were based on tests of beams cast horizontally. To simplify the practical design methods without serious loss of accuracy, intermediate values applicable to both columns and beams were suggested by the Joint Committee.

In recent studies at the University of Illinois, k_1k_3 has been evaluated more directly from reinforced beam tests by measuring the depth c to the neutral axis at the ultimate moment. Eq. (1) and (2) may be expressed as:

$$\frac{M_{ult}}{d-k_2c} = k_1 k_3 f_c' bc \tag{7}$$

When M_{ult} and c are measured and a value of k_2 is assumed, k_1k_3 can be evaluated. In this manner Billet and Appleton[7] found:

$$k_1 k_3 = \frac{3000 + \frac{1}{2} f_c'}{1500 + f_c'} \tag{8}$$

Eq. (8) and other expressions developed in a similar manner tend to give values for k_1k_3 somewhat greater than those obtained by Jensen (Fig. 4). This may be a result of local stress disturbances in the immediate proximity of a flexural crack.

Under-Reinforced Beams

For the ultimate strength of beams as controlled by yielding of the tension reinforcement, the ratio k_2/k_1k_3 in Eq. (3) may be derived by statistical methods from tests of reinforced concrete beams. For this purpose Eq. (3) was expressed by R. C. Elstner as:

$$S = \sum \left[\frac{M_{ult}}{bd^2 f_c'} - q\left(1 - \frac{k_2}{k_1 k_3} q\right) \right]^2 \tag{9}$$

By differentiating S with respect to k_2/k_1k_3 and equating to zero, a least squares solution gives:

$$\frac{k_2}{k_1 k_3} = \frac{-\sum \frac{M_{ult}}{bd^2 f_c'} q^2 + \sum q^3}{\sum q^4} \tag{10}$$

By applying Eq. (10) to 364 beam tests carried out in this country or Canada,

a value $k_2/k_1k_3 = 0.59$ was found. This value is identical to, and therefore confirms, that obtained by C. S. Whitney almost 20 years ago as 0.50/0.85 in Eq. (3b), which value was also recommended for practical use by the Joint Committee. Elstner's findings, which have not been published previously, are summarized in Fig. 5.

Ultimate Concrete Strain

A large number of tests of reinforced concrete members have confirmed the hypothesis that the distribution of strain is essentially linear across a reinforced concrete cross-section even near ultimate strength. In this respect most investigators have agreed. However, values that have been suggested for the ultimate strain ε_u at the compression face vary considerably. For instance, R. Saliger and C. Schreyer indicated increasing values of ε_u with increasing compressive strength, while A. Brandtzaeg, M. Ros, and V. P. Jensen assumed a decrease of ε_u with increasing strength. It should be noted, on the other hand, that these conflicting opinions were expressed at a time when very few measurements carried to ultimate strength had been made.

Test results obtained at the University of Illinois after 1950[3,7] in tests of reinforced concrete columns and beams are plotted in Fig. 6. It is clearly seen that the ultimate strain of 0.003 recommended by the Joint Committee for practical design purposes is a conservative value.

Special Testing Techniques

Tests of plain concrete are a second and more direct approach to the study of inelastic concrete stress distribution. Three types of tests have been used, namely, concentric compression tests, direct stress measurement, and recently eccentric compression tests.

Concentric Compression Tests

Some information has been obtained by concentric compression tests of prisms and cylinders. In connection with establishing design values for the modular ratio as used in the straight-line theory, a great number of mathematical expressions were developed several decades ago for the stress-strain relationship of concentrically loaded prisms. Most of these expressions consider the range from zero to the maximum stress only. By using suitably stiff testing machines or by surrounding the concrete specimen with a system of steel springs, however, stress-strain relations have recently been observed beyond the maximum load and far into the inelastic range.[8-10] Though direct application of such stress-strain relations for concentric compression to the case of flexure has been vigorously challenged, concentric tests do, in the writer's opinion, give valuable qualitative information regarding the flexural stress distribution.

Direct Stress Measurement

Various special testing techniques have been developed to study the flexural stress distribution directly. A special testing machine was constructed at the Imperial College in London.[11,12] Photoelastic methods were tried at Ohio State University,[13] and various attempts have been made to develop

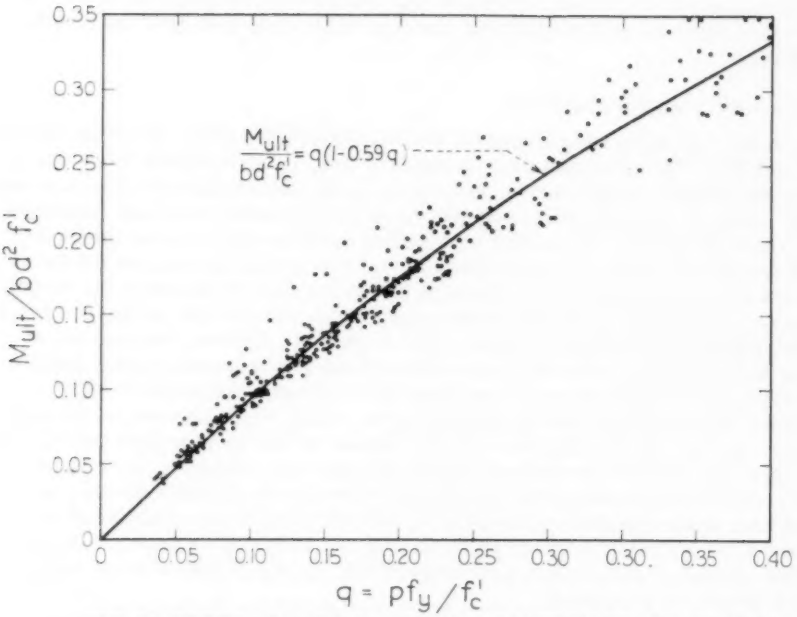

FIG. 5-TESTS OF 364 BEAMS CONTROLLED BY TENSION

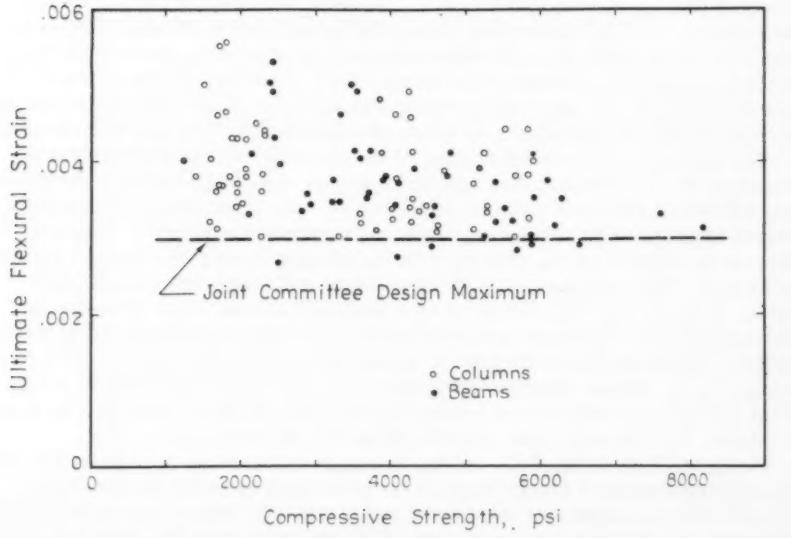

FIG. 6 - ULTIMATE STRAIN FROM TESTS OF REINFORCED MEMBERS

stress meters for measurements at high loads.(14) These methods involve serious experimental difficulties, and it is difficult to interpret the test data obtained.

Eccentric Compression Tests

A new special testing technique was recently developed at the PCA laboratories.(15) The specimen used is shown in Fig. 7. It should be noted that although suitable reinforcement was placed in the end brackets to accommodate the loads, no reinforcement was placed in the prismatic region at midheight. A major thrust P_1 was applied by a testing machine and a minor thrust P_2, which could be varied independently of P_1, was applied by a hydraulic jack and a tie-rod arrangement. Thereby, it was possible to maintain the neutral axis as observed by electric strain gages at the bottom face of the test specimen throughout the test from zero load to failure. Without assumptions of any kind it is then seen that, by equilibrium of external and internal axial forces, the average stress at any load level including ultimate strength equals the sum of P_1 and P_2 divided by the cross-sectional area of the specimen. By further dividing this average stress by the compressive strength of companion cylinder specimens, values of k_1k_3 were obtained. By considering equilibrium of moments, it is further possible to compute directly the position of the resultant internal compressive force in the concrete at any load level including ultimate strength, that is, values of k_2 were evaluated. This method of determining properties of the stress distribution was applied to a variety of concretes.

While this investigation was in progress, very similar work was being carried out independently at the Munich Institute of Technology by H. Rüsch.(16) Groups of about five identical specimens were tested with a different and constant eccentricity for each test. Typical eccentricities for a group of five specimens were 0, 0.2, 0.6, and 1.0 times the kern distance. By then plotting, for all specimens within one group, strain measured at an outside face at ultimate strength versus applied eccentricity, the eccentricity corresponding to a position of the neutral axis at an edge of the cross-section was determined. By applying suitable statistical methods, the magnitude and position of the internal concrete force at ultimate strength was determined.

The ultimate strength properties of the inelastic stress distribution obtained at the two laboratories are summarized and compared with the recommendations of the Joint Committee in Fig. 8. The PCA tests with sand and gravel aggregates have been reported in detail elsewhere;(15) a detailed report on the tests by J. A. Hanson with lightweight aggregates has not yet been published. The German tests(16) were made with sand and gravel aggregates. It is seen in Fig. 8 that an excellent agreement exists between the German and the American test results for sand and gravel concretes, and the radical change of aggregate type to lightweight materials caused only a minor change in the stress distribution properties. The recommendations of the Joint Committee, which were evolved before the test data given in Fig. 8 were available, are strongly confirmed by these recent findings.

From the data of the PCA eccentric compression tests it is possible, by simple mathematical means similar to those used by previous investigators(17-19) in analyses of reinforced beam tests, to derive the entire stress-strain curves for concrete in flexure.(15) This was done for sand and gravel concretes with five water-cement ratios tested at four different ages. The

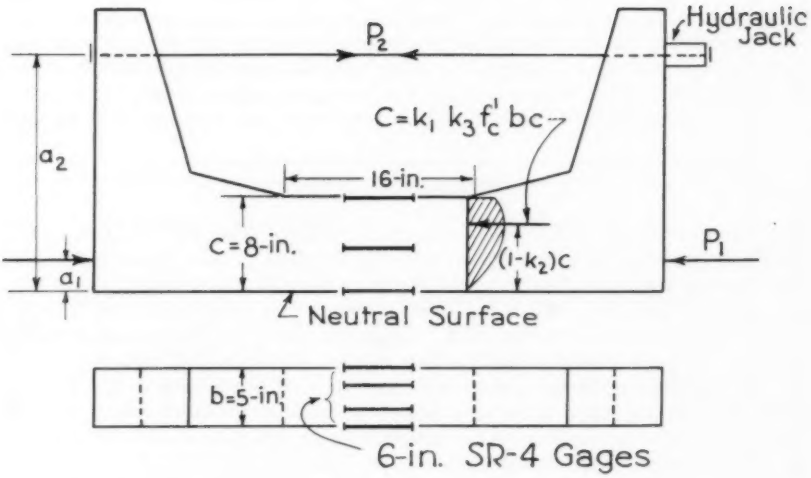

FIG. 7 - PCA ECCENTRIC LOAD SPECIMEN

3-25-55

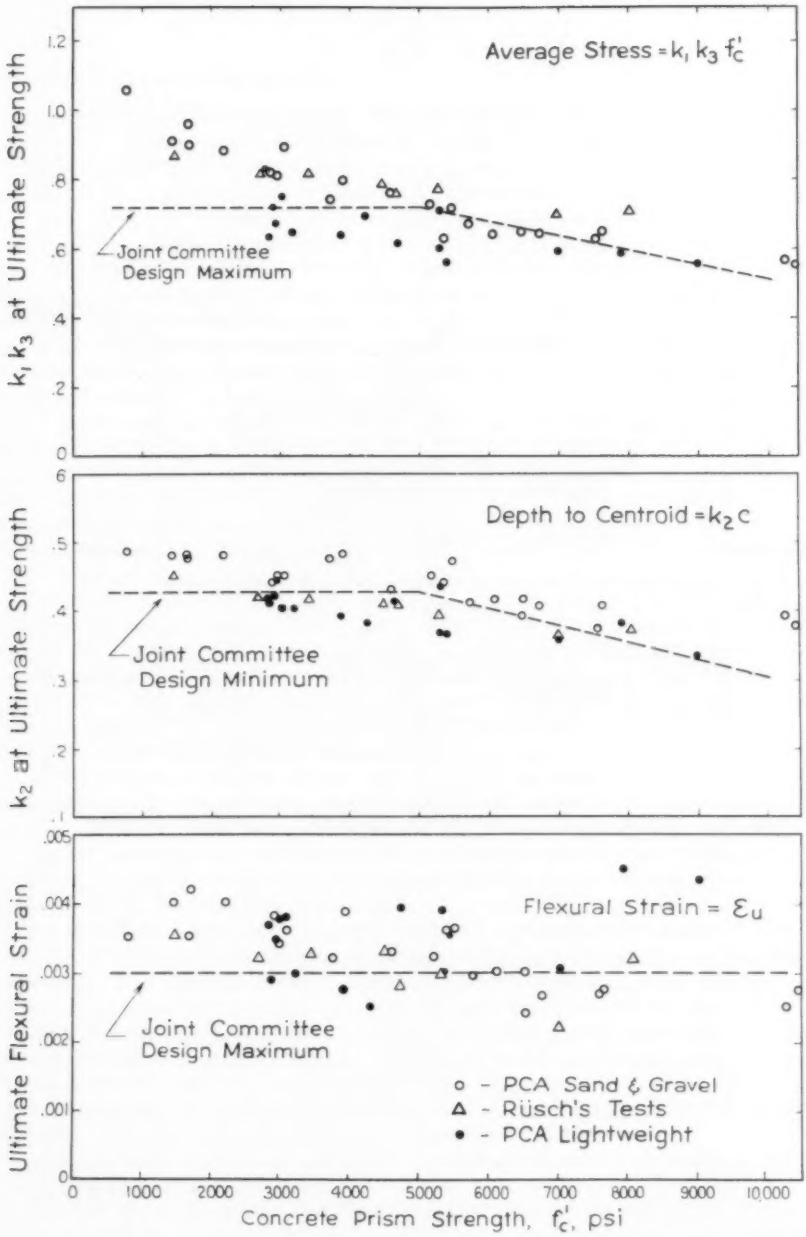
Average Stress = $k_1 k_3 f'_c$
k_1, k_3 at Ultimate Strength
Joint Committee Design Maximum
Depth to Centroid = $k_2 c$
k_2 at Ultimate Strength
Joint Committee Design Minimum
Flexural Strain = ε_u
Ultimate Flexural Strain
Joint Committee Design Maximum
○ - PCA Sand & Gravel
△ - Rüsch's Tests
● - PCA Lightweight
Concrete Prism Strength, f'_c, psi

FIG. 8 - ULTIMATE STRENGTH PROPERTIES OF STRESS DISTRIBUTION

shape of the curves was found to be primarily a function of concrete strength. The 28-day curves given in Fig. 9 are typical and consist of a rising curve from zero to the maximum stress followed by a descending curve beyond the maximum stress. This confirms previous indirect findings reached by analysis of reinforced beam and column tests.

The curves in Fig. 9 are also closely similar to those obtained in concentric compression tests. There is only one major difference between the behavior of a concrete specimen in concentric compression and that in eccentric compression. In concentric compression serious cracking of the test specimen often takes place at strains only slightly greater than those corresponding to maximum stress. In eccentric compression, however, the first visible cracking is usually observed practically at the ultimate load. This confirms previous findings in tests of reinforced members, namely, that when a stress gradient is present, first cracking takes place at strains considerably greater than those corresponding to first cracking in concentric compression tests of companion cylinder specimens. A redistribution of stress takes place; highly strained concrete close to a compression edge is aided by less strained material located closer to the neutral axis.

CONCLUDING REMARKS

The inelastic stress concepts used by the Joint ASCE-ACI Committee on Ultimate Strength Design to develop practical design procedures were essentially based on analyses of tests of reinforced concrete columns and beams. It was of primary importance to obtain a satisfactory agreement between calculated and measured ultimate strength of reinforced members and to obtain such agreement by reasonably simple routine calculations.

Eccentric compression test methods for plain concrete specimens have been developed recently by which ultimate strength properties of the inelastic concrete stress distribution may be measured accurately and directly. The results of such tests confirm the inelastic stress concepts used by the Joint Committee both qualitatively and quantitatively.

REFERENCES

1. "Report of ASCE-ACE Joint Committee on Ultimate Strength Design," Proceedings ASCE, Vol. 81, Paper No. 809, October 1955, 68 pp.
2. "Building Code Requirements for Reinforced Concrete (ACI 318-56)," ACI Journal May 1956, Proceedings Vol. 52, pp. 913-986.
3. Hognestad, E.: "A Study of Combined Bending and Axial Load in Reinforced Concrete Members," University of Illinois Engineering Experiment Station, Bulletin No. 399, November 1951, 128 pp.
4. Richart, F. E. and Brown, R. L.: "An Investigation of Reinforced Concrete Columns," University of Illinois Engineering Experiment Station, Bulletin No. 267, June 1934, 91 pp.
5. Whitney, C. S.: "Plastic Theory in Reinforced Concrete Design," Transactions ASCE, Vol. 107, 1942, pp. 251-326.

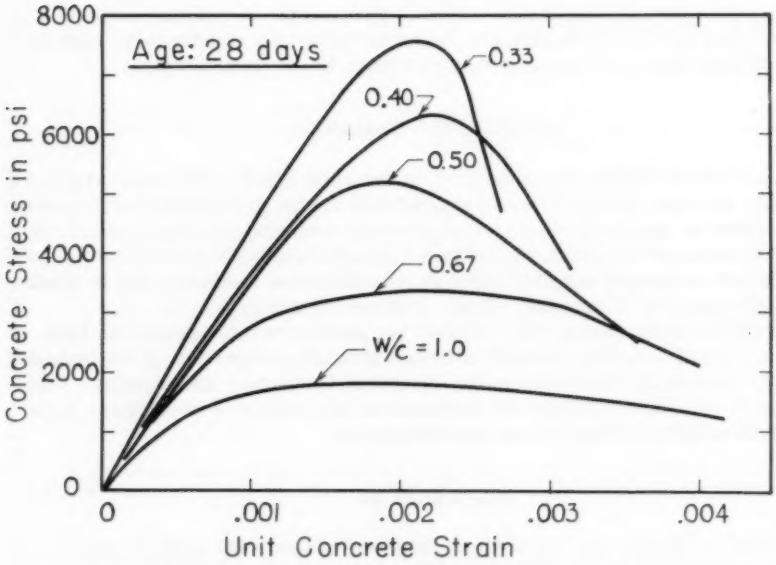

FIG. 9 - FLEXURAL STRESS-STRAIN CURVES

6. Jensen, V. P.: "Ultimate Strength of Reinforced Concrete Beams as Related to the Plasticity Ratio of Concrete," University of Illinois Engineering Experiment Station, Bulletin No. 345, June 1943, 60 pp.

7. Billet, D. F. and Appleton, J. H.: "Flexural Strength of Prestressed Concrete Beams," ACI Journal, June 1954, Proc. V. 50, pp. 837-854.

8. Kiendl, O. G. and Maldari, T. A.: "A Comparison of Physical Properties of Concrete Made of Three Varieties of Coarse Aggregate," Bachelor of Science Thesis, University of Wisconsin, 1938, 64 pp.

9. Ramaley, D. and McHenry, D.: "Stress-Strain Curves for Concrete Strained Beyond the Ultimate Load," Laboratory Report No. SP-12, U. S. Bureau of Reclamation, Mar. 1947, 23 pp.

10. Blanks, R. F. and McHenry, D.: "Plastic Flow of Concrete Relieves High-Load Stress Concentrations," Civil Engineering, V. 19, No. 5, May 1949, pp. 320-322.

11. Baker, A. L. L.: "Recent Research in Reinforced Concrete, and Its Application to Design," Journal of the Institution of Civil Engineers, London, V. 35, No. 4, Feb. 1941, pp. 262-298.

12. Baker, A. L. L.: "Further Research in Reinforced Concrete and Its Application to Ultimate Load Design," Proceedings, Institution of Civil Engineers, London, V. 2, Part III, Aug. 1953, pp. 269-310.

13. Herr, L. A. and Vandegrift, L. E.: "Studies of Compressive Stress Distribution in Simply Reinforced Concrete Near the Point of Failure," Proceedings, Highway Research Board, V. 30, 1950, pp. 114-125.

14. Parme, A. L.: Discussion of a paper by C. P. Siess: "Review of Research on Ultimate Strength of Reinforced Concrete Members," ACI Journal, June 1952, Proc. V. 48, pp. 862-864.

15. Hognestad, E.; Hanson, N. W.; and McHenry, D.: "Concrete Stress Distribution in Ultimate Strength Design," ACI Journal, December 1955, Proc. Vol. 52, pp. 455-479.

16. Rüsch, H.: "Versuche zur Festigkeit der Biegedruckzone," Deutscher Ausschuss für Stahlbeton, Berlin, Heft 120, 1955, 94 pp.

17. Prentis, J. M.: "The Distribution of Concrete Stress in Reinforced and Prestressed Concrete Beams When Tested to Destruction by a Pure Bending Moment," Magazine of Concrete Research, London, No. 5, Jan. 1951, pp. 73-77.

18. Hamann, H.: "Berechnung der Druckspannungs-Kurve im Stahlbeton-Biegequerschnitt," Schweizerische Bauzeitung, Zurich, V. 70, No. 44, Nov. 1, 1952, pp. 629-630.

19. Lee, L. H. N.: "Inelastic Behavior of Reinforced Concrete Members Subject to Short-Time Static Loads," Proceedings, ASCE, V. 79, Separate No. 286, Sept. 1953, 26 pp. Discussions: V. 80, Separates No. 429 and 530.

Paper 1190 ST 2

Journal of the
STRUCTURAL DIVISION
Proceedings of the American Society of Civil Engineers

DESIGN OF FLEXIBLE STEEL ARCHES BY INTERACTION DIAGRAMS

Haaren A. Miklofsky,[1] A.M. ASCE, and Omar J. Sotillo,[2] J.M. ASCE
(Proc. Paper 1190)

SYNOPSIS

This paper describes a direct method of structural design for all types of flexible steel arches by means of interaction diagrams. The interaction diagram developed gives the fiber stress and deflection of the arch cross-section as a function of its dimensions. This diagram is analogous to a structural interaction diagram for a statically determinate structure, the beam column. The design method is illustrated by the design of the quarter point sections of the following steel arch bridges: the two-hinged Rainbow, the Bayonne, and the hingeless Rainbow.

INTRODUCTION

In any type of arch, the rib or truss has two distinct functions: (1) to withstand direct compression, and (2) to furnish the flexural rigidity necessary to resist the bending moment created when the equilibrium polygon for the applied load system does not coincide with the position of the arch axis. The moment at any point of the arch axis, calculated by the usual elastic theory methods, is equal to the axial thrust at that point multiplied by the perpendicular distance from the funicular polygon for the applied load system to the unmoved arch axis. For long span arches, however, this common method of analysis is deficient because the arch axis does move considerably, and creates additional moments which in turn further increase the distance between the funicular polygon and the arch axis. This inevitable amplification of moment merits careful consideration by the designer.

Note: Discussion open until August 1, 1957. Paper 1190 is part of the copyrighted Journal of the Structural Division of the American Society of Civil Engineers, Vol. 83, No. ST 2, March, 1957.

1. Associate Prof., Dept. of Civ. Eng., Rensselaer Polytechnic Inst ., Troy, N. Y.
2. Technical Advisor, Oficina de Estudios Especiales de la Presidencia de la Republica, Miraflores, Caracas, Venezuela.

Several deflection theories,[3] developed in the past fifty years, are available to determine the additional stresses and deflections produced by the deflection of the arch axis under load. Either restrictive application or extensive computations, however, have prevented any of these methods from gaining universal acceptance. More important also is the fact that these are methods of analysis and not methods of design.

The interaction diagram—a set of curves describing the structural behavior of a member as a function of its dimensions—will enable the designer to visualize the entire design range in such a way that he can select a cross-section that will result in a desired fiber stress and radial deflection without trial or error.

In order to clarify the structural behaviour of the arch when the displacement of the arch axis is considered, a simple beam subjected to transverse bending and axial compression loads will be analyzed first. The bending interaction of this statically determinate structure will be proved analogous to that of the arch. The simple illustration for the beam will serve to explain to the reader what an interaction diagram is, and its function in design. Furthermore such a study based upon the interpretation of the physical behavior of the statically determinate structure, the beam, aids in understanding the physical behavior of the statically indeterminate structure, the arch. Later the bending interaction diagram for the stresses and deflections of the arch will be developed for its variable dimensions.

Interaction Diagram for a Beam Column

Consider a simply supported beam, Figure 1, which is subjected to an axial compression load P at its ends and the transverse load system w (x). The center deflection becomes:

$$v = \frac{kML^2}{EI} \tag{1}$$

where M is the bending moment at the center produced by the direct load P and the transverse load w (x). The term k is a constant depending on the distribution of the bending loads and the variation of the moment of inertia I along the beam.

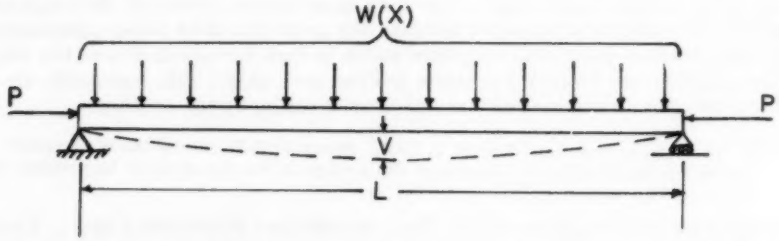

FIG. 1. SIMPLY SUPPORTED BEAM SUBJECTED TO TRANSVERSE BENDING AND AXIAL COMPRESSION LOADS.

3. Reference 7, pp. 128-132.

The maximum fiber stress f occurs at the outside top fiber of the beam at the midspan,

$$f = \frac{P}{A} + \frac{M_s c}{I} + \frac{Pvc}{I} \tag{2}$$

where A represents the cross-sectional area, M_s the bending moment at the center due to the transverse load only, and c half the beam depth. Combining equations (1) and (2):

$$f = \frac{P}{A} + \frac{M_s c}{I - \frac{kPL^2}{E}} \tag{3}$$

The term kPL^2/E has the same units as I. Its function in equation (3) is to reduce the flexural rigidity of the beam. Therefore it will be called the "reduction factor" and will be represented by I_r. Equation (3), therefore, can be written as,

$$f = \frac{P}{A} + \frac{M_s c}{I - I_r} \tag{4}$$

and since $M = M_s + Pv$, equation (1) becomes,

$$v = \frac{k M_s L^2}{E(I - I_r)} \tag{5}$$

The second part of equation (4) is a bending expression for the interaction of two separate bending effects: (1) the bending stress $M_s c/I$ induced by w(x), and (2) the bending stress Pvc/I induced by P acting on the sagged beam. Now the effect of each separate action on the structural behavior of the beam will be considered for varying beam depths and cross-sectional areas. The depth d shall be varied first, keeping the cross-sectional area A constant. The resulting curves will give stress and deflection values for the various depths. By changing the cross-sectional area later a family of curves will result.

If only the transverse load w(x) acts, then $P = 0$ and $I_r = 0$, and the bending stress in equation (4) becomes,

$$f' = \frac{M_s c}{I} = \frac{M_s d}{2KAd^2} \propto \frac{1}{Ad} \tag{6}$$

where K is a constant dependent on the distribution of the cross-sectional area. For a given A, equation (6) plots as a hyperbola (b) in Figure 2(b).

The effect of P alone is given by the second part of equation (4) when $I = 0$,

$$f'' = \frac{M_s c}{I_r} = \frac{M_s d}{I_r} \propto d \tag{7}$$

which plots as a straight line (c) in Figure 2(b).

The reciprocal of the bending stress in equation (4) is equal to the reciprocal of equation (6) minus the reciprocal of equation (7).

$$\frac{1}{f_b} = \frac{1}{f'} - \frac{1}{f''} \tag{8}$$

Equations (5) and (8) can be further simplified to:

$$v \propto \frac{1}{Ad^2 - 1} \qquad (9) \qquad f_b \propto \frac{d}{Ad^2 - 1} \qquad (10)$$

The relative bending stress f_b is plotted as curve (a) in Figure 2(b), and the relative deflection v is plotted as curve (d) in Figure 2(a).

The curve for f' is asymptotic to both the d abscissa and the f ordinate, while the bending stress f" is a linear function of d. The curve for the total bending stress f_b is asymptotic to two axes: the ordinate axis at $I = I_r$ and the d axis. At the d value where $I = I_r$, the influence of P acting on the sagged beam has become so great that the moment of inertia available to resist the bending action has been neutralized by the reduction factor I_r. When this occurs, the beam buckles in the vertical plane and $f_b \to \infty$. As the depth increases, the total bending stress f_b approaches the bending stress f' since the influence of the reduction factor I_r on the f_b curve diminishes as the depth d increases. Therefore, as I becomes much larger than the reduction factor I_r, the f_b curve practically coincides with the f' or bending stress due to simple beam action.

In the deflection diagram the same behavior is evident. Figure 2(a) shows the deflection curve asymptotic both to the ordinate at $I = I_r$ and to the depth axis. As the depth decreases, I decreases to the point where $I = I_r$, and then the beam buckles in the vertical plane as $v \to \infty$. If the depth increases very much, I will become greater thus producing an extremely high flexural rigidity; the deflection then tends towards zero.

Figure 3 is an extension of Figure 2, in which the effect of various relative areas upon the relative stress and deflection has been included. The solid curves of Figure 3(b) can be computed on a relative basis from the interaction expression for bending alone.[4] Once a scale for the relative unit coordinates for the graphs can be established for a given problem, the rest of the coordinates follow by proportion to Figure 3.

An interaction diagram, however, is not complete for this problem unless the effect of axial stress is included. Since the axial stress is dependent only upon the area and not the depth, it merely raises each bending interaction stress curve by an amount P/A. A sample set of final stress curves is shown dashed in Figure 3(b), and are dashed to indicate that relative values of P/A cannot be established for all problems on a proportional relative graph, but must be calculated individually for each problem.

Once scales have been established for the coordinates of the deflection and stress curves, and the effect of axial stress has been included to this scale, it is possible to directly determine the depth and area that will simultaneously satisfy a given stress and deflection. Only one such solution is possible that uses a minimum cross-sectional area. This will be illustrated in the use of the arch interaction diagram for design.

---

4. Sample calculations:
   Point (1), Figure 3(a). d = 1 and A = 2 in equation (9).
   $v = 1/((2)(1)^2 - 1) = 1.$
   Point (1), Figure 3(b). d = 1 and A = 2 in equation (10).
   $f_b = 1/((2)(1)^2 - 1) = 1.$

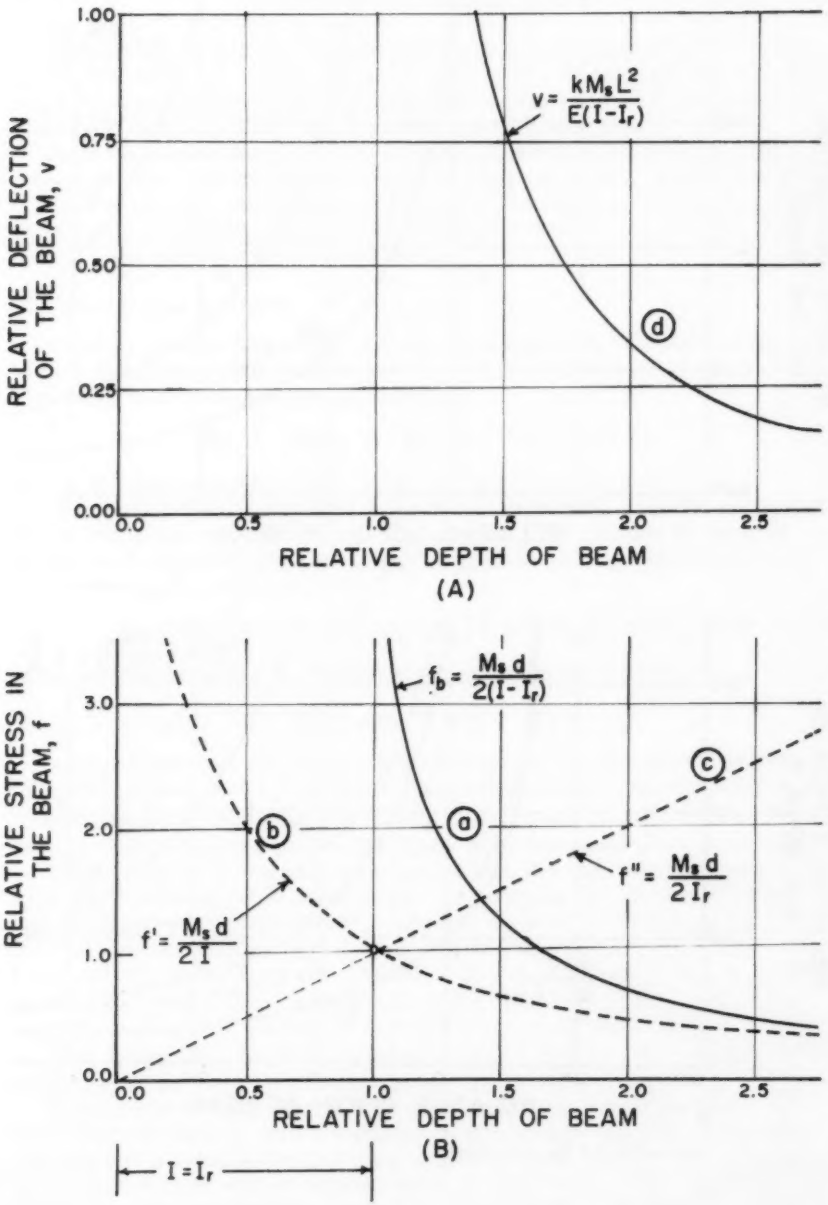

FIG. 2. DIAGRAM FOR STRESS AND DEFLECTION OF BEAM FOR A VARIABLE DEPTH AND A FIXED CROSS-SECTIONAL AREA.

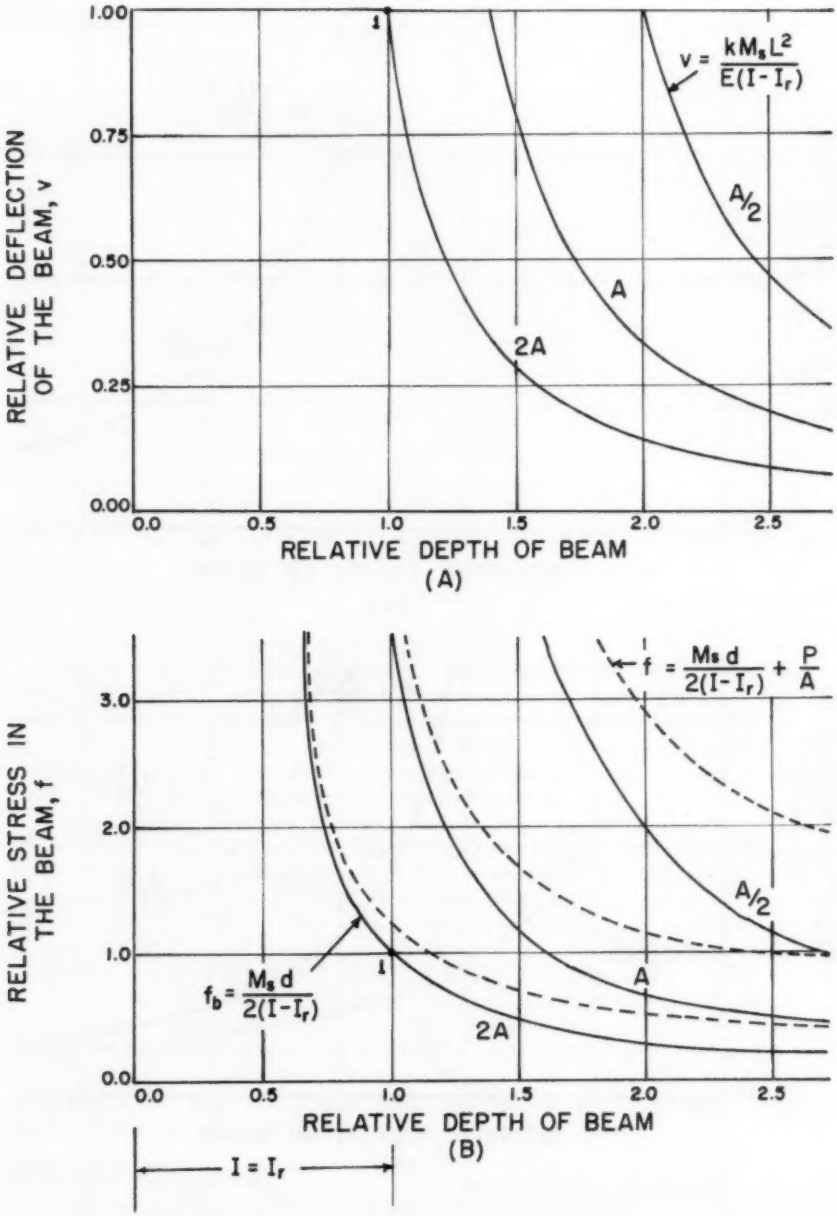

FIG. 3. INTERACTION DIAGRAM FOR A SIMPLY SUPPORTED BEAM SUBJECTED TO TRANSVERSE BENDING AND AXIAL COMPRESSION LOADS.

Interaction Diagram for Arches

The problem of the arch is very similar to the problem of the beam subjected to transverse and axial compressive loads. The arch problem is the beam problem with the following additional considerations: horizontal displacement, settlement of beam supports and axial distortion.

Since the elastic theory will be used for all derivations and solutions of the deflected arch, it would be inconsistent to refer to the usually accepted terms of "elastic theory" and "deflection theory." The authors consider more appropriate and descriptive the terms "rigid arch theory" and "flexible arch theory," and consequently will use them.

The Two-Hinged Rib Arch

Consider the two-hinged rib arch shown in Figure 4. The loading applied, w(x), critical for a point a, produces the shown displacement of the arch axis. The moment at point a in the rigid arch is:

$$M_r = V x_a - W(x_a - x_b) - H y_a \qquad (11)$$

where W = sum of all downward loads acting between A and a.

Assume that as the arch axis deflects, the value of H remains unchanged and b, where W is considered to act, does not move relative to the load points which also undergo a horizontal displacement. The moment at a in the flexible arch is expressed by:

$$M = V(x_a + n) - W\left[(x_a - x_b) + (n - n_b)\right] - H(y_a - m) \qquad (12)$$

which when combined with equation (11) reduces to the following:

$$M = M_r + Hm + Vn - W(n - n_b) \qquad (13)$$

A two-hinged arch rib must satisfy the equilibrium dictated by equation (13). The values of M_r, V, H and W can be determined from the rigid arch system, but three unknowns still appear in the equation: m, n and n_b. Therefore, in order to solve equation (13),three more equations must be introduced.

Figure 5 gives the moment diagram for both the rigid and the flexible arch for the loading being considered. The ordinate M, of course, is unknown. It has been assumed that point o is the point of zero moment for both the rigid and the flexible system. Assume that at any point of the arch $I = I_c \sec \theta$, where I_c is the moment of inertia at the crown and θ is the angle of inclination of the arch axis with the horizontal at that point. If the arch is cut at o, and a roller is inserted at the same point, an arch of span L_o with a rise differential h_o between supports will furnish two relations as a function of M. Such an arrangement is illustrated in Figure 6.

The purpose of the roller is to permit horizontal, but not vertical, translation of point o. From the shape of the moment diagram, it is evident that there is a relative displacement between points A and o. But since A is a hinged support with no displacement, point o must move horizontally to satisfy the flexural straining implied by the moment parabola with ordinate M. Once the horizontal displacement of o has taken place, the span Ao acts as an arch.

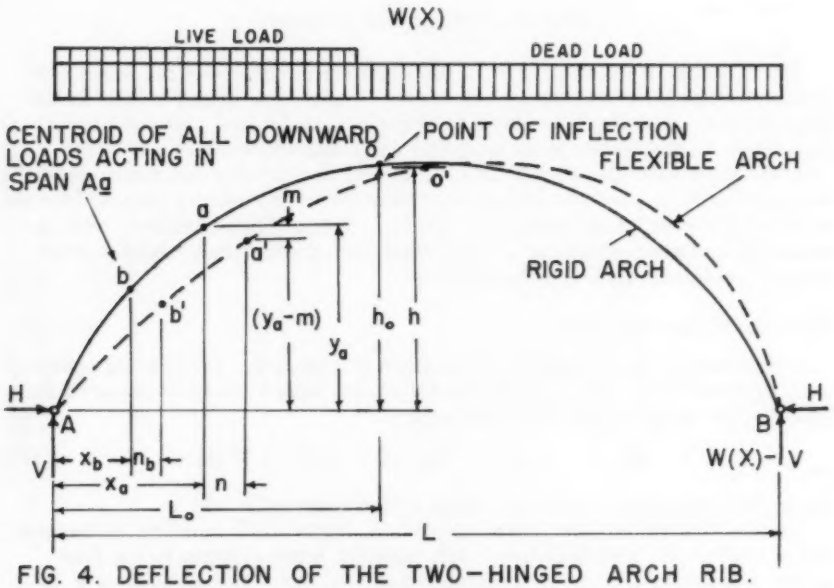

FIG. 4. DEFLECTION OF THE TWO-HINGED ARCH RIB.

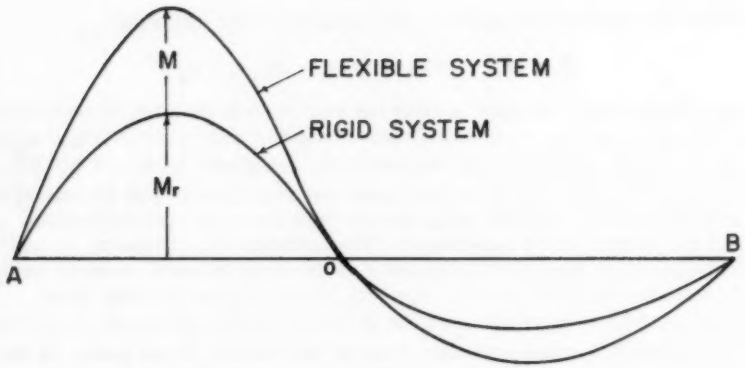

FIG. 5. MOMENT DIAGRAMS FOR RIGID AND FLEXIBLE ARCHES.

If the conjugate structure method[5] is employed, an equation for m and one for n as a function of M can be derived. Figure 7 shows the conjugate structure loaded with the elastic loads $M_x ds/EI$, where M_x is the moment at each ds segment along the conjugate structure, and EI is the flexural rigidity of each increment.

But since $I = I_c \sec\theta$ and $ds = dx \sec\theta$, the elastic load term becomes $M_x dx/EI_c$. If point o undergoes no vertical deflection (ie. $m_o = 0$), then the vertical deflection undergone by point a is equal to the bending moment at a, about the y-y axis, produced by the elastic loads which act on the conjugate structure lying on a horizontal plane:

$$m' = \frac{k_1 M L_o^2}{E I_c} \tag{14}$$

Taking moments about the x-x axis at a:

$$n' = \frac{k_2 M L_o h_o}{E I_c} \tag{15}$$

where k_1 and k_2 are constants depending on the section considered, the loading system and the distribution of I in the arch.

The values of k_1 and k_2 can be assumed to be 5/48 and 1/6 respectively without introducing much of an error. The calculations of these values is simple, however, and it is preferable to calculate them for the sake of precision.

Now the vertical deflection, m_o, in the arch at point o is not equal to zero. By the conjugate structure method, the initial deflection, m_{or}, at o can be calculated. If it is assumed that this initial displacement, as a result of the change in configuration of the arch axis, is amplified by the same proportion as the moment at a, then,

$$m_o = m_{or} \frac{M}{M_r} \tag{16}$$

Now let the additional vertical deflection at the quarter point a, due to the deflection of the inflection points (A and o) be equal to the average deflection of these. The vertical deflection at a in the flexible arch due to flexural strain only becomes:

$$m = \frac{k_1 M L_o^2}{E I_c} + \frac{M}{M_r} \sum \frac{m_{or}}{2} \tag{17}$$

It is also desirable to include the deflections due to secondary effects such as temperature, erection errors and rib shortening. These deflections increase the moment at a, but they are not subject to amplification themselves. The total vertical deflection at a then becomes:

$$m = \frac{k_1 M L_o^2}{E I_c} + \frac{M}{M_r} \sum \frac{m_{or}}{2} + m_2 \tag{18}$$

5. Reference 4.

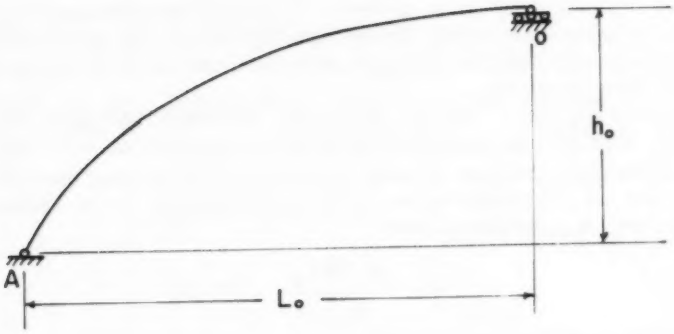

FIG. 6. THE SHORT ARCH AND THE ROLLER SUPPORT.

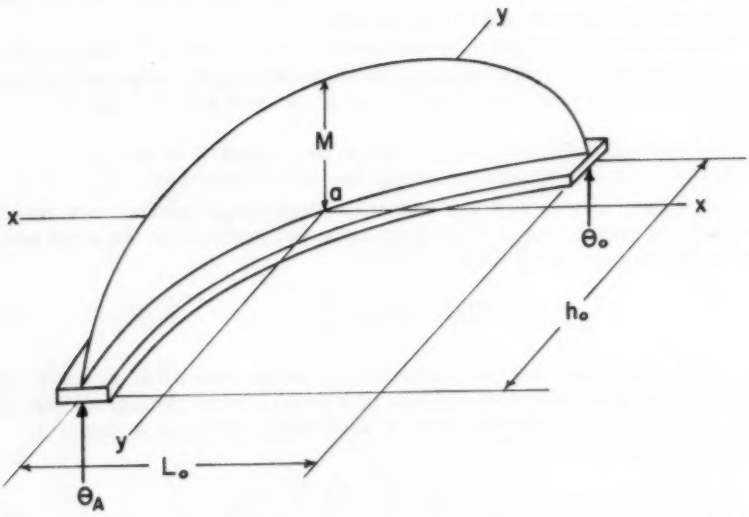

FIG. 7. THE CONJUGATE STRUCTURE FOR THE SHORT ARCH.

Likewise,

$$n = \frac{k_2 M L_o h_o}{E I_c} + n_2 \tag{19}$$

where m_2 and n_2 are the vertical and horizontal deflections respectively at a, due to axial distortion of the arch rib. Employing the same amplification factor used in equation (16),

$$(n - n_b) = \frac{M}{M_r}(n_r - n_{br}) + (n_2 - n_{b2}) \tag{20}$$

If equations (18), (19) and (20) are substituted in equation (13), then,

$$M = \frac{M_r + Hm_2 + Vn_2 - W(n_2 - n_{b2})}{1 - \frac{1}{E I_c}\left[k_1 H L_o^2 + k_2 V L_o h_o + \frac{H \Sigma E I_c m_{or} - 2WEI_c(n_r - n_{br})}{2M_r}\right]} \tag{21}$$

Since $I = I_c \sec\theta$ and $f = \frac{T}{A} + \frac{M_c}{I}$, and if c is taken as one half the depth d, then the total unit fiber stress at point a is:

$$f = \frac{T}{A} + \frac{[M_r + Hm_2 + Vn_2 - W(n_2 - n_{b2})]\, d/2}{I - \frac{\sec\theta}{E}\left[k_1 H L_o^2 + k_2 V L_o h_o + \frac{H \Sigma E I_c m_{or} - 2WEI_c(n_r - n_{br})}{2M_r}\right]} \tag{22}$$

Now the second part of the denominator in the bending expression has the same units as I. This term, as in the case of the simple beam, shall be called the "reduction factor" and be expressed by I_r.

Letting $M_1 = M_r + Hm_2 + Vn_2 - W(n_2 - n_{b2})$, equation (29) becomes:

$$f = \frac{T}{A} + \frac{M_1 d}{2(I - I_r)} \tag{23}$$

and the deflection expressions equation (18) and equation (19) become:

$$m = \frac{M_1 \sec\theta \left(k_1 L_o^2 + \frac{\Sigma E I_c m_{or}}{2M_r}\right)}{E(I - I_r)} + m_2 \tag{24}$$

$$n = \frac{M_1 \sec\theta\,(k_2 L_o h_o)}{E(I - I_r)} + n_2 \tag{25}$$

The form of equations (23), (24) and (25) is adequate for analysis work, but not for design because neither the shape nor the distribution of area in the cross-section is considered. Consequently, these three equations must undergo modification.

Let d = depth of rib, t = web thickness, I_w = moment of inertia of web about the bending axis, and I_f = moment of inertia of the flange about the

bending axis. Also let $K = \frac{I_f}{I_w}$ and $N = d/t$. The expression for the total area is,

$$A = d^2 \left(\frac{K+3}{3N}\right) \tag{26}$$

and for the total moment of inertia is,

$$I = d^4 \left(\frac{K+1}{12N}\right) \tag{27}$$

In order to account for bracing plates near the bending axis in box-type rib sections and for the cross-sectional area reduction due to rivet or template holes in plates, equation (26) should be modified to

$$A = g d^2 \left(\frac{K+3}{3N}\right) \tag{28}$$

where g is a factor varying from 0.95 to 1.15 in design work.[6]

Employing equation (27) and equation (28), the final expressions for f, m and n become:

$$f = \frac{T}{g d^2 \left(\frac{K+3}{3N}\right)} + \frac{M_1 d/2}{d^4 \left(\frac{K+1}{12N}\right) - I_r} \tag{29}$$

$$m = \frac{M_1 \frac{\sec \theta}{E} \left(k_1 L_o^2 + \frac{\Sigma E I_c m_{or}}{2M_r}\right)}{d^4 \left(\frac{K+1}{12N}\right) - I_r} + m_2 \tag{30}$$

$$n = \frac{M_1 \frac{\sec \theta}{E} \left(k_2 L_o h_o\right)}{d^4 \left(\frac{K+1}{12N}\right) - I_r} + n_2 \tag{31}$$

To construct the interaction diagram for design work, one would now proceed as follows: Guided by the specifications and past experience, select the value of N. The maximum allowable N depends on the specifications and the type of steel used, but under no circumstance is N greater than 170 so that the web is safe against buckling. The value of g the designer selects from experience and predesign calculations. The equations for f, m and n thus simplify to expressions involving two independent variables: d and K. Working with a value of K in table (1) and table (2) which are for N = 100,

6. If the designer assumes that 5% of the cross-sectional area for a box-type rib section will be removed for the riveting or welding operation, and that a transversal stiffening plate at the neutral axis will constitute 15% of the box-section area, then g = 1.00 - 0.05 = 1.10.

TABLE 1. VALUES OF CROSS-SECTIONAL AREA FOR THE RIB ARCH AS A FUNCTION OF THE SHAPE FACTOR AND THE DEPTH OF THE RIB. N = 100.

d, in. \ K	1	2	3	4	5	6	7	8	9	10
40	21	27	32	37	43	48	53	59	64	69
50	33	42	50	58	67	75	83	92	100	108
60	48	60	72	84	96	108	120	132	144	156
70	65	82	98	114	131	147	163	180	196	213
80	85	107	128	149	171	192	213	235	256	277
90	108	135	162	189	216	243	270	297	324	351
100	133	167	200	233	267	300	333	367	400	433
110	161	202	242	282	323	363	403	444	484	524
120	192	240	288	336	384	432	480	528	576	624
130	225	282	338	394	451	507	563	620	676	732
140	261	327	392	457	523	588	653	719	784	849
150	300	375	450	525	600	675	750	825	900	975
160	341	427	512	597	683	768	853	939	1024	1109
170	385	482	578	674	771	867	963	1060	1156	1252
180	432	540	648	756	864	972	1080	1188	1296	1404
190	481	602	722	842	963	1083	1203	1324	1444	1564
200	533	667	800	933	1067	1200	1333	1467	1600	1733
210	588	735	882	1029	1176	1323	1470	1617	1764	1911
220	645	807	968	1129	1291	1452	1613	1775	1936	2097
230	705	882	1058	1234	1411	1587	1763	1940	2116	2292
240	767	960	1152	1344	1536	1728	1920	2112	2304	2496
250	833	1042	1250	1458	1667	1875	2083	2292	2500	2708
260	901	1127	1352	1577	1803	2028	2253	2479	2704	2929
270	972	1215	1458	1701	1944	2187	2430	2673	2916	3159
280	1045	1307	1568	1829	2091	2352	2613	2875	3136	3397
290	1121	1402	1682	1962	2243	2523	2803	3084	3364	3644
300	1200	1500	1800	2100	2400	2700	3000	3300	3600	3900

Note. All tabular values are in inches^2.

TABLE 2. VALUES OF MOMENT OF INERTIA FOR THE RIB ARCH AS A FUNCTION OF THE SHAPE FACTOR AND THE DEPTH OF THE RIB. N = 100

d, in. \ K	1	2	3	4	5	6	7	8	9	10
40	4,267	6,400	8,533	10,667	12,800	14,933	17,067	19,200	21,333	23,467
50	10,417	15,625	20,833	26,042	31,250	36,458	41,667	46,875	52,083	57,292
60	21,600	32,400	43,200	54,000	64,800	75,600	86,400	97,200	108,000	118,800
70	40,017	60,025	80,033	100,000	120,050	140,058	160,065	180,075	200,083	220,092
80	68,267	102,400	136,533	170,668	204,800	238,933	273,068	307,200	341,332	375,467
90	109,350	164,025	218,700	273,375	328,050	382,725	437,400	492,075	546,750	601,425
100	166,667	250,000	333,333	416,667	500,000	583,333	666,667	750,000	833,333	916,667
110	244,017	366,025	488,033	610,042	732,050	854,058	976,067	1,098,075	1,220,078	1,342,092
120	345,100	517,650	690,199	862,750	1,035,300	1,207,849	1,380,400	1,552,950	1,725,500	1,898,050
130	476,017	714,025	952,033	1,190,043	1,428,050	1,666,058	1,904,066	2,142,075	2,380,083	2,618,092
140	640,268	960,400	1,280,533	1,600,067	1,920,800	2,240,933	2,561,067	2,881,200	3,201,321	3,521,479
150	843,750	1,265,625	1,687,500	2,109,377	2,531,250	2,953,125	3,375,000	3,796,875	4,218,750	4,640,627
160	1,092,267	1,638,400	2,184,531	2,730,667	3,276,800	3,822,931	4,369,067	4,915,200	5,461,333	6,007,467
170	1,392,017	2,088,025	2,784,033	3,480,070	4,176,050	4,872,056	5,568,067	6,264,075	6,960,080	7,656,092
180	1,749,600	2,624,400	3,499,200	4,373,999	5,248,800	6,123,600	6,998,400	7,873,200	8,747,997	9,622,800
190	2,172,017	3,258,025	4,344,033	5,430,085	6,516,050	7,602,058	8,688,071	9,774,075	10,860,083	11,946,096
200	2,666,667	4,000,000	5,333,333	6,666,667	8,000,000	9,333,333	10,666,667	12,000,000	13,333,333	14,666,667
210	3,241,350	4,862,025	6,482,700	8,103,376	9,724,050	11,344,724	12,965,400	14,586,075	16,206,749	17,823,425
220	3,904,267	5,856,400	7,808,526	9,760,745	11,712,800	13,664,933	15,617,067	17,569,200	19,521,333	21,473,467
230	4,664,018	6,996,025	9,328,024	11,660,134	13,992,050	16,324,049	18,656,067	20,988,075	23,320,074	25,652,092
240	5,529,601	8,294,400	11,059,199	13,824,110	16,588,800	19,353,589	22,118,400	24,883,200	27,647,989	30,412,801
250	6,510,418	9,765,625	13,020,832	16,276,043	19,531,250	22,786,445	26,041,667	29,296,875	32,552,082	35,807,304
260	7,616,267	11,424,400	15,232,381	19,040,667	22,848,800	26,656,932	30,465,068	34,273,200	38,081,331	41,889,619
270	8,857,352	13,286,025	17,714,700	22,143,376	26,572,050	31,000,707	35,429,418	39,858,075	44,286,732	48,715,602
280	11,550,956	17,326,400	23,101,864	28,877,335	34,652,800	40,428,243	46,203,756	51,979,200	57,754,667	63,530,133
290	11,928,186	17,892,275	23,856,367	29,820,482	35,784,555	41,748,639	47,712,736	53,676,825	59,640,893	65,605,032
300	13,500,000	20,250,000	27,000,000	33,750,000	40,500,000	47,250,000	54,000,000	60,750,000	67,500,000	74,250,000

Note. All tabular values are in inches^4.

for each d value the designer selects the values of $d^2(K + 3)/3N$ and $d^4(K + 1)/12N$ respectively. These different values he substitutes in equations (29), (30) and (31), obtaining values for f, m and n respectively. The m and n deflections are combined to determine the radial deflection $u = \sqrt{m^2 + n^2}$. Although the process appears long, the diagram plots rapidly by aid of tables (1) and (2). The interaction diagrams resulting then have f and u as the ordinate, d as the abscissa and a family of K curves. The interaction diagrams are analogous to those for the beam column, except K and u replace A and v respectively.

The Two-Hinged Truss Arch

The problem of the truss arch is solved by treating it basically as a rib arch. Let the dotted line in Figure 8 represent the arch axis which coincides with the desired force polygon.

The moment equation for point a in the arch axis for a specified loading condition, assuming $I = I_c \sec\theta$, is given by equation (21). The loading condition critical for member uc is shown in Figure 8. Since S_{uc}, the stress at uc, is equal to the moment at i divided by the radial depth d, and the moment at i is equal to $M_i = M \mp Hh$, then,

$$S_{uc} = \frac{M_i/d}{1 - \frac{\sec\theta}{EI}\left[k_1 H L_o^2 + k_2 V L_o h_o + \frac{H\Sigma EI_c m_{or} - 2WEI_c(n_r - n_{br})}{2M_{cr}}\right]} + \frac{Hh}{d} \qquad (32)$$

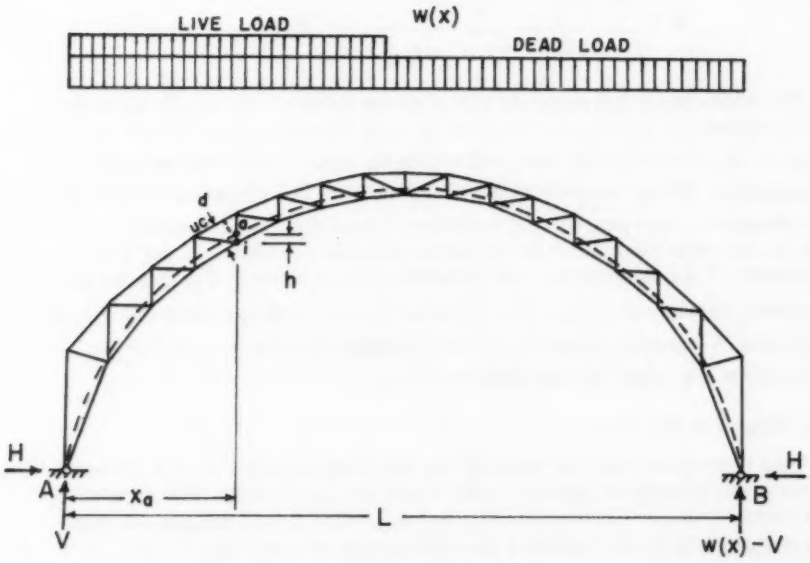

FIG. 8. THE TWO-HINGED TRUSS ARCH.

where M_1 is the same as in equation (23) and M_{cr} is the moment at a in the rigid arch system. The unit stress in member uc if $f = Suc/A_1$ where A_1 is the cross-sectional area of member uc. If d_1 and d_2 are the distances from the arch axis to the upper and lower chord respectively, and A_2 is the area of the lower chord, then the total moment of inertia about the arch axis is $I = A_1d_1^2 + A_2d_2^2$. Assume that the arch axis passes through the centroid of the chord areas (ie. $A_1d_1 = A_2d_2$); then the unit stress in the upper chord is,

$$f = \frac{M_1(d-d_2)}{A_1d(d-d_2) - \frac{\sec\Theta}{E}\left[k_1HL_o^2 + k_2VL_oh_o + \frac{H\Sigma EI_cm_{or} - 2WEI_c(n_r - n_{br})}{2M_{cr}}\right]} + \frac{Hh}{A_1d} \qquad (33)$$

But the second part of the denominator is equal to I_r, so equation (33) is simplified to:

$$f = \frac{M_1(d-d_2)}{A_1d(d-d_2) - I_r} + \frac{Hh}{A_1d} \qquad (34)$$

By making the same substitutions in equation (24) and equation (25):

$$m = \frac{M_1\frac{\sec\Theta}{E}\left(k_1L_o^2 + \frac{\Sigma EI_cm_{or}}{2M_{cr}}\right)}{A_1d(d-d_2) - I_r} \div m_2 \qquad (35)$$

$$n = \frac{M_1\frac{\sec\Theta}{E}(k_2L_oh_o)}{A_1d(d-d_2) - I_r} + n_2 \qquad (36)$$

The above three expressions will give the designer an ample description of the structural behavior of the section as a function of A_1, d and d_2. The value of d_2 is arbitrarily selected by the designer from architectural considerations. Then, for each value of A_1 in table (3), the desired A_1d values are obtained. Carrying out the indicated operations, and combining m and n into u, the resulting interaction diagrams would consist of f and u as ordinates, d as the abscissa and a family of A_1 curves. For the design of the lower chord, equations (34), (35) and (36) are employed with A_2 and d_1 replacing A_1 and d_2 respectively; the loading condition, of course, is critical for the lower chord member.

The Hingeless Rib Arch

This type of arch is the same as the two-hinged rib arch, with the additional consideration of the fixed end moments. In the following derivation, two more terms are included: M_{fr} and M_f, which represent the moment at the fixed end of the rigid and flexible arches respectively.

TABLE 3. VALUES OF THE PRODUCT OF CHORD AREA AND RADIAL DEPTH FOR THE TRUSS ARCH

d, in. \ A, in.^{2}	50	100	200	300	400	500	600	700	800	900	1000
50	2,500	5,000	10,000	15,000	20,000	25,000	30,000	35,000	40,000	45,000	50,000
100	5,000	10,000	20,000	30,000	40,000	50,000	60,000	70,000	80,000	90,000	100,000
150	7,500	15,000	30,000	45,000	60,000	75,000	90,000	105,000	120,000	135,000	150,000
200	10,000	20,000	40,000	60,000	80,000	100,000	120,000	140,000	160,000	180,000	200,000
250	12,500	25,000	50,000	75,000	100,000	125,000	150,000	175,000	200,000	225,000	250,000
300	15,000	30,000	60,000	90,000	120,000	150,000	180,000	210,000	240,000	270,000	300,000
350	17,500	35,000	70,000	105,000	140,000	175,000	210,000	245,000	280,000	315,000	350,000
400	20,000	40,000	80,000	120,000	160,000	200,000	240,000	280,000	320,000	360,000	400,000
450	22,500	45,000	90,000	135,000	180,000	225,000	270,000	315,000	360,000	405,000	450,000
500	25,000	50,000	100,000	150,000	200,000	250,000	300,000	350,000	400,000	450,000	500,000
550	27,000	55,000	110,000	165,000	220,000	275,000	330,000	385,000	440,000	495,000	550,000
600	30,000	60,000	120,000	180,000	240,000	300,000	360,000	420,000	480,000	540,000	600,000
650	32,500	65,000	130,000	195,000	260,000	325,000	390,000	455,000	520,000	585,000	650,000
700	35,000	70,000	140,000	210,000	280,000	350,000	420,000	490,000	560,000	630,000	700,000
750	37,500	75,000	150,000	225,000	300,000	375,000	450,000	525,000	600,000	675,000	750,000
800	40,000	80,000	160,000	240,000	320,000	400,000	480,000	560,000	640,000	720,000	800,000
850	42,500	85,000	170,000	255,000	340,000	425,000	510,000	595,000	680,000	765,000	850,000
900	45,000	90,000	180,000	270,000	360,000	450,000	540,000	630,000	720,000	810,000	900,000
950	47,500	95,000	190,000	285,000	380,000	475,000	570,000	665,000	760,000	855,000	950,000
1000	50,000	100,000	200,000	300,000	400,000	500,000	600,000	700,000	800,000	900,000	1,000,000

Point a, Figure 4, the critical point, is in equilibrium when the following equation is satisfied:

$$M + M_f = V(x_a - n) - H(y_a - m) - W\left[(x_a - x_b) + (n - n_b)\right] \quad (37)$$

The increase in positive moment at a introduced by the shifting of the arch axis, however, is approximately equal to the increase in negative moment at the fixed end.[7] Therefore, $M - M_r = M_f - M_{fr}$, and equation (37) becomes:

$$M = \frac{M_r + \frac{1}{2}\left[Hm_2 + Vn_2 - W(n_2 - n_{b2})\right]}{1 - \frac{\sec\theta}{2EI}\left[k_1 HL_o^2 + k_2 VL_o h_o + \frac{H\Sigma E I_c m_{or} - 2WEI_c(n_r - n_{br})}{2M_r}\right]} \quad (38)$$

Let

$$M_1 = M_r + \tfrac{1}{2}\left[Hm_2 + Vn_2 - W(n_2 - n_{b2})\right] \quad (39)$$

and

$$I_r = \frac{\sec\theta}{2E}\left[k_1 HL_o^2 + k_2 VL_o h_o + \frac{H\Sigma E I_c m_{or} - 2WEI_c(n_r - n_{br})}{2M_r}\right] \quad (40)$$

From this point on, the problem for analysis or design is identical to that of the two-hinged arch rib. Therefore, equations (23), (24) and (25) should be used for analysis, and equations (29), (30) and (31) for design.

The Hingeless Truss Arch

This type of arch combines the flexural rigidities developed by the absence of hinges and also by the depth of the truss. The problem can be solved by combining the derivations for the hingeless rib arch and the two-hinged truss arch. The unit stress at the lower chord and the vertical and horizontal deflections are given by equations (34), (35) and (36) respectively, where M_1 is given by equation (39) and I_r by equation (40).

The Tied Arch

The inward pull at each support is produced by the tie member connecting the hinges, and this internal pull enables the structure to be analyzed as an arch. A structure of this type should be designed as a two-hinged arch as previously considered.

Design Illustrations

The design procedure to be proposed will be accurate and simple for an experienced designer. After the designer has selected the type, span and rise of the arch, has designed the floor deck and established the geometry of the arch axis, the design of the arch rib or truss is undertaken. From this point on, five definite design steps are necessary.

7. Reference 2, p. 32.

(1) Assume that at any point of the arch rib $I = I_c \sec \theta$.[8] Compute the influence line for the redundant horizontal reaction H at the supports.

(2) Using the solved redundant information from the previous step, calculate the necessary influence lines for moment and axial thrust at the desired panel points. Use these influence lines to determine the critical location of the live load in each case.

(3) In the rigid arch system determine at each desired point the reactions due to dead load, critical live load, impact, wind, temperature and errors of erection. For the critical loading for each point, determine H, V, W, L_o and h_o.

(4) Determine for each critical loading condition the values of k_1 and k_2, and the deflection values of n_r, m_{or}, n_{or}, m_2, n_2 and n_{b2}.

(5) Substitute the necessary values in the interaction expressions for every point considered. The resulting fiber stresses and deflections are then plotted. The interaction diagrams then enable the designer to select an adequate cross-section for each point considered in the arch system.

Design of the Rib Section at the Quarter Point of the Two-Hinged Rainbow Bridge for D.L. + L.L. + I.

The two-hinged Rainbow Bridge, 950 feet in span, never advanced beyond the preliminary design stage because it lacked flexural rigidity. Instead, the hingeless Rainbow Bridge was designed and built in 1941 at the Niagara gorge.

The design procedure will be illustrated for the quarter-point of the two-hinged Rainbow for the condition of dead load, live load and impact. Temperature and erection errors, which make the loading condition more critical shall be neglected, for the sake of comparison with published design information by Hardesty.[9]

Step (1). To compute the influence line for the redundant horizontal reaction H at the supports, the following expression for H for any load on the arch is used:

$$H = \frac{\Sigma M_s y \, ds/EI}{\Sigma \, y^2 \, ds/EI} \tag{41}$$

8. This assumption for direct design will involve only negligible errors, and can safely be employed to solve for the external redundants. It is true that the external reactions in an indeterminate structure are influenced by the cross-sectional dimensions throughout the structure; but there is another factor which exercises far more influence on the magnitude of the external reactions: the location of the axis of the structure with respect to the force polygon. Therefore, if $I = I_c \sec \theta$, and the arch axis ordinates coincide with the desired force polygon, hardly any accuracy is sacrificed in the procedure. Furthermore, the relation $I = I_c \sec \theta$ somewhat approaches the variation in cross-sectional dimensions in most arches, whether two-hinged or hingeless.
9. Reference 2, p. 30.

where M_s = simple beam moment at each segment due to the loading system. Since $I = I_c \sec \theta$, $ds = \sec \theta \, dx$ and dx is the panel length, then

$$H = \frac{\Sigma M_s y}{\Sigma y^2} \tag{42}$$

Step (2). Using the solved redundant information from step (1), we now compute the influence lines for the reactions at the quarter point, which is point (7). The influence line for the moment at point (7) and AASHO specifications require that the uniform live load of 1.375 kips per foot be extended from the left support to x = 400 feet, and that the concentrated live load of 26.7 kips be placed at point (7). See Figure 9.

Step (3). For the loading shown the rigid arch analysis produces the following values: M_r = 24,877 ft-k., T = 7,534 k, H = 7,191 k, V = 4,921 k, W = 2,263 k, L_o = 438.2 ft. and h_o = 149.8 ft.

Step (4). The values of k_1 and k_2 are determined by loading with the elastic loads the conjugate structure of a short arch, which has a span L_o and a differential height of h_o between supports, and calculating the quantities $m'EI_c$ and $n'EI_c$ at point (7) of the short arch. Having these values, then

$$k_1 = \frac{m' E I_c}{M_r L_o^2} \tag{43}$$

and

$$k_2 = \frac{n' E I_c}{M_r L_o h_o} \tag{44}$$

where M_r is the moment at the quarter point of the rigid arch. Since the ordinates—but not the shape of the moment diagram—changes as the arch deflects, then the k values are the same for the flexible as for the rigid arch system. The elastic loads acting are $M_r \, ds/EI$ or $M_r \, dx/EI_c$, but since dx/EI_c is a constant the moment value M_r at each individual segment can be employed as the relative elastic load at the corresponding segment. Taking moments about an axis parallel to the y-y axis and passing through point o (see Figure 6), the reaction θ_A is 94,149 ft-k. Taking moments about the y-y axis and x-x axis at point a the values of $m'EI_c$ and $n'EI_c$ respectively are obtained and substituted in equations (43) and (44):

$$k_1 = \frac{491,198,614}{(24,877)\,(438.10)^2} = 0.1029$$

$$k_2 = \frac{270,429,667}{(24,877)\,(438.10)\,(149.62)} = 0.1657$$

In the above two equations the numerator represents the statical moment of the elastic loads on a conjugate structure, and includes the value of I_c as a component part. Hence the absolute value of I_c is not needed in calculation. Since the deflections resulting from axis distortion are being neglected, the terms m_2, n_2 and n_{b2} have a zero value. The terms n_r, m_{or} and n_{br} can be calculated by loading the conjugate structure of 950 ft. span and

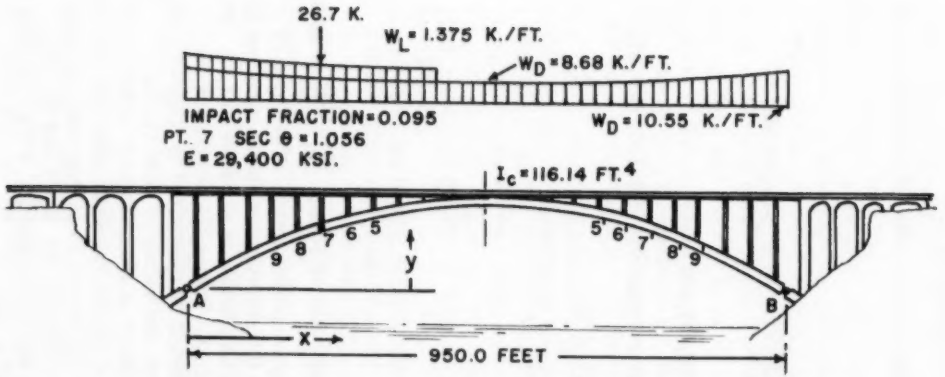

Col. Pt.	x, ft.	y, ft.	M_r, ft.-k. (12 - 1)	M_r, ft.-k. (12' - 1')
12	19.6	12.546	6,238	- 886
11	59.2	36.106	12,870	-6,280
10	98.8	57.302	18,221	-10,605
9	138.4	76.291	21,560	-14,584
8	178.0	92.972	24,011	-17,092
7	217.6	107.491	24,877	-18,825
6	257.2	119.863	23,251	-19,534
5	296.8	130.121	20,213	-19,296
4	336.4	138.294	15,907	-17,966
3	376.0	144.404	10,378	-15,502
2	415.0	148.468	3,534	-11,995
1	455.2	150.497	-2,597	-7,773
Crown	475.0	150.750		

FIG. 9. LOADING CONDITION CRITICAL FOR THE QUARTER POINT OF THE TWO-HINGED RAINBOW BRIDGE: D.L.+L.L.+ I.

150.75 ft. rise with the moment values appearing in Fig. 9. Taking moments about the necessary axes:

$$\Sigma EI_c\, m_{or} = 26{,}324{,}702 \text{ k-ft}^3$$

$$EI_c\, n_r = 270{,}907{,}243 \text{ k-ft}^3$$

$$EI_c\, (n_r - n_{br}) = 75{,}585{,}940 \text{ k-ft}^3$$

Step (5). Having available the necessary values, the following terms are calculated:

$$I_r = 995{,}119 \text{ in}^4$$

$$\frac{M_1 \sec \theta}{E} \left(k_1 L_o^2 + \frac{\Sigma EI_c\, m_{or}}{2\, M_r} \right) = 31{,}310{,}776 \text{ in}^5$$

$$\frac{M_1 \sec \theta}{E} \left(k_2\, L_o\, h_o \right) = 16{,}807{,}649 \text{ in}^5$$

Substituting these and previous values in equations (29), (30) and (31):

$$f = \frac{7534}{gd^2 \frac{(K+3)}{3N}} + \frac{298{,}524\ (d/2)}{d^4 \frac{(K+1)}{12N} - 995{,}119}$$

$$m = \frac{31{,}310{,}776}{d^4 \frac{(K+1)}{12N} - 995{,}119}$$

$$n = \frac{16{,}807{,}649}{d^4 \frac{(K+1)}{12N} - 995{,}119}$$

In the actual Two-Hinged Rainbow, the value of N was $\frac{(14)\ (12)}{(2)\ (5/16)} = 89.6$. The designer selects N = 90 for the quarter point section. The value of g, to account for a lateral bracing plate at the midheight of the section and also for area deductions due to rivet or template holes, is selected as 1.10. This value of g usually varies from 0.95 to 1.15. Tables (1) and (2) are for N = 100, so the values in those tables should be multiplied by (100/90). In the case of the axial unit stress, however, the values of table (1) for N = 100 can be used provided the axial thrust is modified to T = 7534 (1.00) (90) /1.10 (100) = 6164 k. The moment of inertia values in table (2), however, must still be multiplied individually by 100/N or 1.11 in this case. A sample calculation will illustrate this. For example, for K = 1 and d = 200, from table (1) $d^2\,(K+3)/3N = 533$ in.^{2}, and from table (2) $d^4\,(K+1)/12N = 2{,}666{,}667$ in.^{4}. The values for f, m and n are:

$$f = \frac{6146}{533} + \frac{298{,}524\ (200/2)}{(1.11)\ (2{,}666{,}667) - 989{,}051} = 26.75 \text{ ksi.}$$

$$m = \frac{31{,}310{,}776}{(1.11)\ (2{,}666{,}667) - 989{,}051} = 15.8 \text{ in.}$$

$$n = \frac{16,807,649}{(1.11)\,(2,666,667) - 989,051} = 8.5 \text{ in.}$$

$$u = \sqrt{(15.8)^2 + (8.5)^2} = 18.0 \text{ in.}$$

The above calculation is carried out for the values of K and d that interest the designer, and are plotted as shown in Figure 10.

The primary function of the interaction diagrams is to enable the designer to select a section that will be safe for the loading specified. Suppose that Hardesty's resulting quarter point values of f = 29.22 ksi, and u = 23.40 in. are specified as allowable for the quarter point.[10] This means that any section which lies below these two values will satisfy the requirement. It is evident that the most economical section is that one which meets both of these limiting conditions simultaneously. Only one section can do this because $29.22 = f_1(K,d)$ and $23.40 = f_2(K,d)$; these two equations involve two unknowns, K and d, which can describe only one section. This one section, though, can be easily located in the diagram; it is marked (1), and has a K = 2.30 and d = 168 in. Therefore, the section has the following dimensions: d = 168 in. = 14 ft. which is also Hardesty's value.[11]

$A = gd^2(K + 3)/3N = 1.10\,(168)^2\,(2.30 + 3)/270 = 609$ in.^{2}, which substantially checks Hardesty's value of 614 in.^{2}.

$I = d^4(K + 1)/12N = (168)^4(2.30 + 1)/12^4(1080) = 118$ ft.^{4}, which agrees closely with Hardesty's value of 120.24 ft.^{4}.

$t = d/N = 168/90 = 1.87$ in., but since a box-type section is used, each web plate must be 0.5(1.87) or 0.93 in. thick. Hardesty's value was 15/16 in. or 0.94 in.

The area of the flange, including the area of the flange angles, is: $A_f = Ktd/3 = 2.30(1.87)\,(1.68)/3 = 241$ in.^{2}.

It is interesting to note that if the arch were considered rigid, then the reduction factor $I_r = 0$ in the interaction expression; and the quarter point unit stress in the rigid arch is:

$$f = \frac{7534}{609} + \frac{(24,877)\,(12)\,(168/2)}{(118)\,(12)^4 - 0} = 22.55 \text{ ksi.}$$

Consequently the increase in stress brought about by the change in configuration of the arch axis is:

$$f = \frac{29.22 - 22.55}{22.55} = 29.6\%$$

Sometimes, however, architectural restrictions fix the depth, and then it is impossible to satisfy exactly the f, u and d requirement simultaneously. If the 29.22 ksi. and the 23.40 in. are retained, and d is fixed at 144 in., then point (3) with K = 5.2 and u = 23.4 in. and f = 25.8 ksi. would have to be selected; point (2) with K = 4.5 satisfies the stress requirement at f = 29.22 ksi., but exceeds the allowable deflection with u = 29 in.

The Two-Hinged Rainbow was a preliminary design and it was greatly overstressed as a result of the deflection stresses. Using the allowable unit

10. Reference 2, p. 24 and p. 31.
11. Reference 2, p. 24.

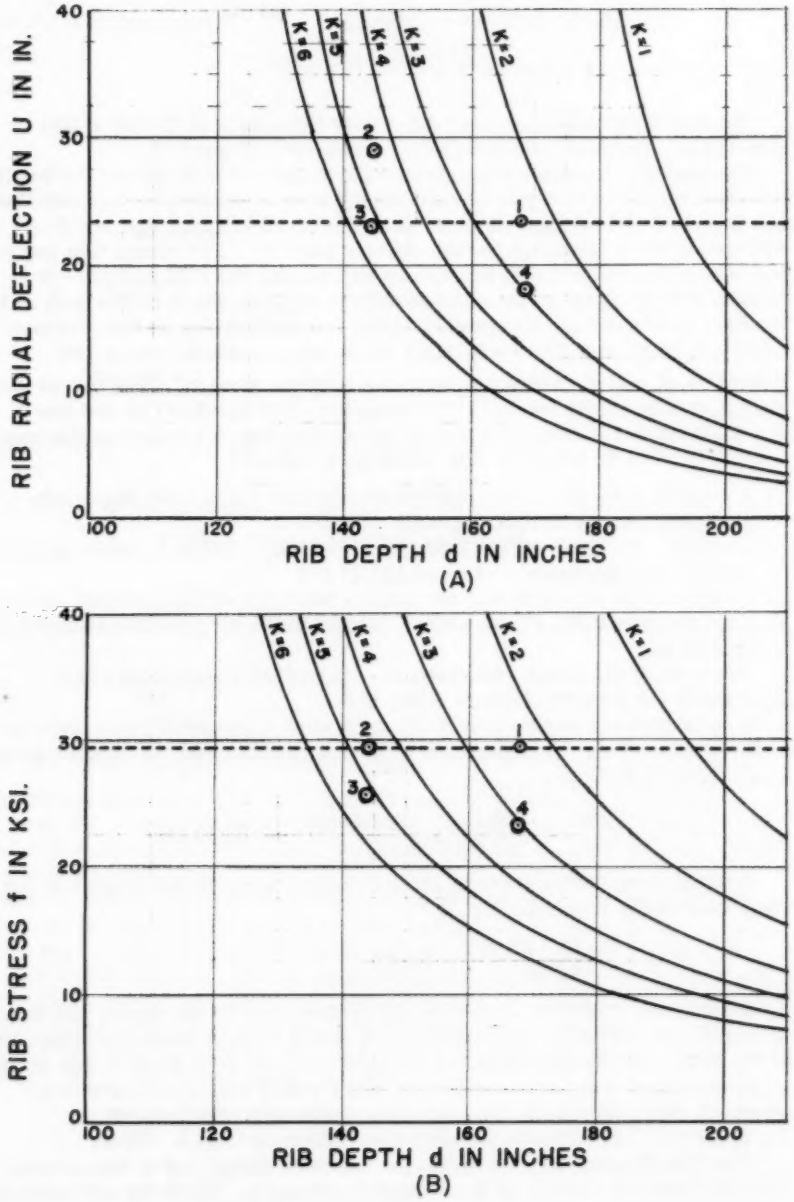

FIG. 10. INTERACTION DIAGRAM FOR THE QUARTER POINT OF THE TWO-HINGED RAINBOW BRIDGE: D.L.+L.L.+I.

stress for the silicon arch rib as 23.00 ksi. the importance of the deflection of the arch axis will become more evident. Suppose the designer had decided to keep the bridge as a two-hinged arch and wanted to retain the depth of 168 in. Then point (4), where K = 3, would satisfy the condition; but the properties of the cross-section would be:

$$A = gd^2 \frac{(K+3)}{3N} = (1.10)(168)^2 \frac{(3+3)}{270} = 687 \text{ in}^2.$$

$$I = d^4 \frac{(K+1)}{12N} = \left(\frac{168}{12}\right)^4 \left(\frac{3+1}{1080}\right) = 142.5 \text{ ft}^4.$$

The radial deflection for this section would have been only 18.0 in., but the rib section is considerably heavier than that which was employed in the hingeless bridge which was eventually built.

Design of the Upper Chord at the Quarter Point of the Bayonne Bridge for D.L. + L.L. + I. + T.

The Bayonne bridge was designed and built as a 1652 foot long two-hinged arch truss, so that the necessary flexural rigidity was obtained without introducing problems of design and construction. This part shall be concerned with the design of the upper chord at the quarter point for the condition of dead load, live load, impact and temperature drop. This is the same loading condition employed by the designer, O. H. Ammann.[12]

Assuming that the dead load panel concentrations are known, the dead load funicular polygon and arch axis are passed through the end pins and a crown point 275.342 feet above them. This was the case in the actual design.

The influence line for the horizontal reaction is determined in the design step (1). The second design step constitutes the determination of the influence line for the moment about the lower chord point L_{10}. (See Figure 11.) The lower chords of the arch truss, in order to satisfy the navigation clearance requirements, lie on a parabola that passes through the pins and a mid-span point 266.0 feet above the pins.

From the influence line for M_{L10}, the critical loading condition is that which has a uniform live load of 3.4535 kips per foot of truss extending over 44.4% of the span, or from point 0 to x = 734 feet.

Step (3). By the usual procedure: H = 18,216 k, V = 13,141 k, W = 6845 k, h = 9.278 ft., L_o = 826 ft., and h_o = 275 ft.

Step (4). Also by the conjugate structure method: $k_1 = 0.1038$, $k_2 = 0.1734$, $\Sigma EI_c m_{or} = -699{,}537{,}100$ k-ft.^{3}, $EI_c n_r = 6{,}384{,}868{,}291$ k-ft.^{3}, $EI_c n_{br} = 5{,}016{,}497{,}801$ k-ft.^{3}, $EI_c (n_r - n_{br}) = 1{,}368{,}370{,}500$ k-ft.^{3}, $m_2 = 0.566$ ft. = 6.8 in., $n_2 = 0.106$ ft. = 1.3 in., $n_{b2} = -0.087$ ft. = -1.0 in.

Step (5). Employing the above values, $M_1 = 2{,}336{,}599$ in.-k., $I_r = 8{,}860{,}576$ in.^{4}.

$$I_r = 8{,}860{,}576 \text{ in}^4.$$

12. Reference 6, Figure 16.

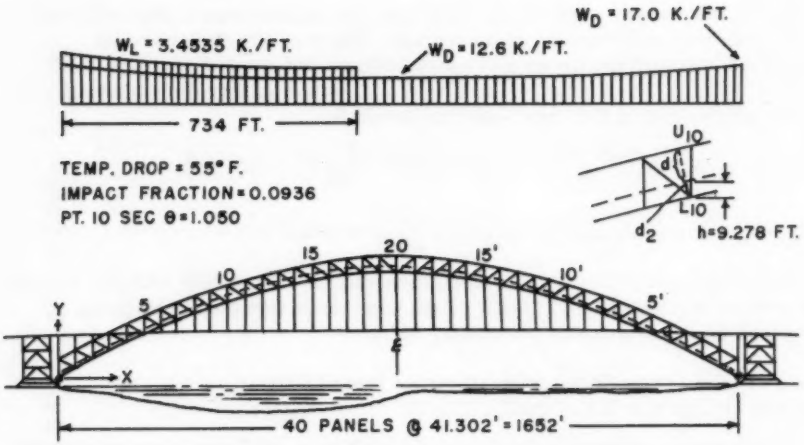

Panel Point	Arch Axis Ordinates x, ft.	y, ft.	Moments M_T in Arch Axis, Ft.-K. (0 - 20)	(20' - 0')
0	0	0	0	0
1	41.302	27.849	35,456	-25,024
2	82.604	54.012	67,426	-47,069
3	123.906	78.525	95,172	-66,922
4	165.208	101.692	119,528	-83,723
5	206.510	123.210	140,132	-97,835
6	247.812	143.294	157,042	-109,200
7	289.114	161.905	169,877	-118,226
8	330.416	178.984	178,829	-124,668
9	371.718	194.562	184,568	-127,882
10	413.020	208.778	185,669	-129,292
11	454.322	221.568	183,658	-127,374
12	495.624	232.949	177,273	-123,389
13	536.926	242.960	166,882	-116,969
14	578.228	251.595	152,808	-107,790
15	619.330	258.871	135,055	-95,850
16	660.832	264.810	113,084	-81,778
17	702.134	269.422	87,219	-64,977
18	743.436	272.710	55,712	-45,751
19	784.738	274.682	26,620	-24,112
20	826.042	275.342	-50	-50

Note: See references 1 and 6 for additional data.

FIG. 11. LOADING CONDITION FOR THE UPPER CHORD AT THE QUARTER POINT OF THE BAYONNE BRIDGE: D.L.+L.L.+I.+T.

$$\frac{M_1 \sec \theta}{E} \left(k_1 L_o^2 + \frac{\Sigma EI_c m_{or}}{2M_r}\right) = 628{,}319{,}793 \text{ in}^5.$$

$$\frac{M_1 \sec \theta}{E} \left(k_2 L_o h_o\right) = 301{,}278{,}207 \text{ in}^5.$$

$H h = 2{,}028{,}169$ in.-k.

The value of d_2, the radial distance from L_{10} to the arch axis, is 8.85 ft. or 106 in. Substituting the above values in equations (34), (35) and (36):

$$f = \frac{2{,}336{,}599 (d - 106)}{Ad (d - 106) - 8{,}860{,}576} + \frac{2{,}028{,}169}{Ad}$$

$$m = \frac{828{,}319{,}793}{Ad (d - 106) - 8{,}860{,}576} + 6.8$$

$$n = \frac{301{,}278{,}207}{Ad (d - 106) - 8{,}860{,}576} - 1.3$$

Substituting the various values of chord area and radial depth that interest the designer, the necessary values for the interaction diagrams are computed and plotted as shown in Figure 12.

The maximum compressive unit stress allowed in the silicon steel is 23.00 ksi. Since there is no deflection specification, any point at or below the 23.00 ksi. line will satisfy all safety requirements. If for this section a radial depth of 43 feet, or 516 in., is selected, as it was in O. H. Ammann's design, the most economical upper chord section is that indicated by point (1). This chord section has an approximate area of 390 in.^{2}, which is in substantial agreement with the 385 in.^{2} of the member U_9U_{10} in the actual design.[13] Furthermore, the radial displacement undergone by the quarter point, for the present loading, would be 22.8 in. Since all the upper chord panel points must form a smooth curve, there is not much chance of varying the radial depths. As a matter of fact, once two or three upper chords have been designed, the radial depth value is practically fixed for the rest of the points. Consequently the stress and deflection values thereafter become a function of A only, and not A and d. The use of a greater depth, for example 975 in., would have resulted in an upper chord area of 200 in.^{2}, but this selection would have involved much longer web members and further detraction from the esthetic element. This selection, indicated by point (2), would have meant a radial displacement of approximately 12.0 in.

It is interesting to note that the truss provides a high degree of flexural stiffness. The radial displacement of 22.8 in. would have been far greater had a box-type rib been selected as in the Rainbow Bridge. Furthermore, if the effect of deflections had been neglected, then $M_1 = M_r$ and $I_r = 0$, and $f = 21.15$ ksi. This is only an increase of 23.00 - 21.15 = 8.75%, as compared to the 29.6% increase in the two-hinged Rainbow. This increase of 8.75%, nevertheless, deserves the attention of the designer and should not be ignored under any circumstances.

13. Reference 6, Figure 16.

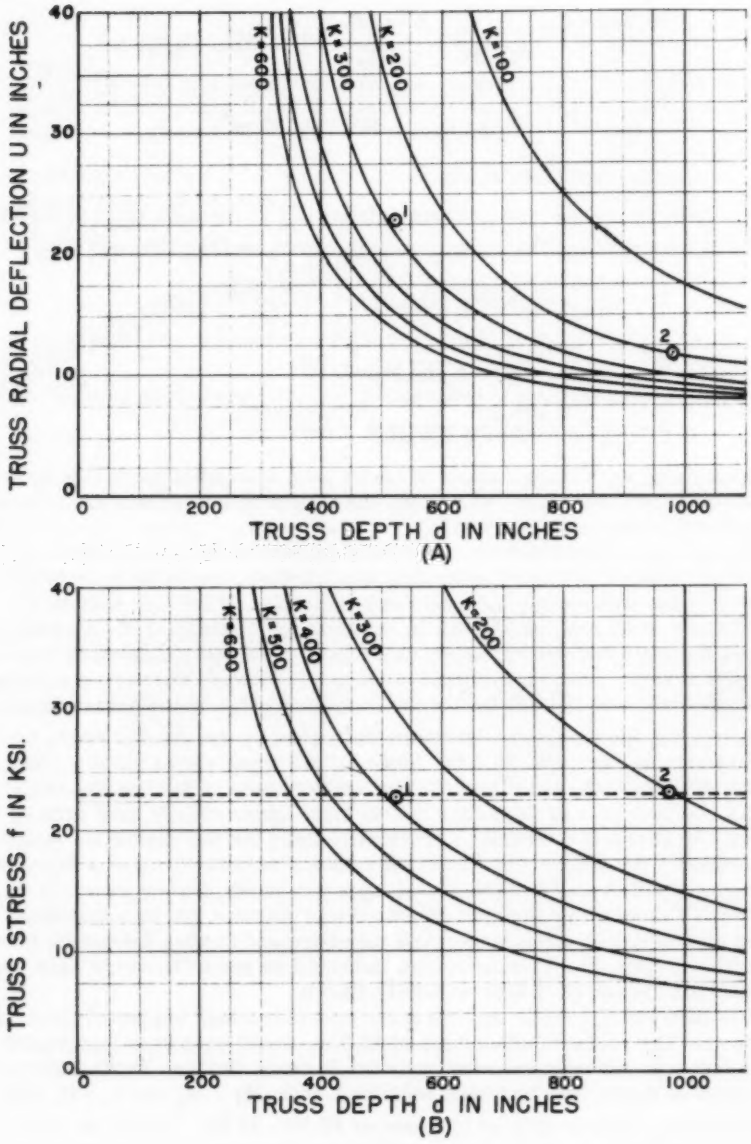

FIG. 12. INTERACTION DIAGRAM FOR THE UPPER CHORD OF THE QUARTER POINT OF THE BAYONNE BRIDGE: D.L.+L.L.+T.+I.

Design of the Rib Section at the Quarter Point of the Hingeless Rainbow Bridge for D.L. + L.L. + I. + T. + E.

As pointed out before, the two-hinged Rainbow Bridge was a preliminary design which was abandoned because it lacked the necessary flexural stiffness. Considerations of the esthetic element did not favor a truss arch, so the solution was a hingeless box-type rib arch 950 feet in span. The quarter point section shall be designed for the critical condition of dead load, live load, impact, temperature drop and errors of erection. All these effects contribute to the disfiguration of the arch axis and are consequently included in the design.

The fixed arch has three external reactions at each end, and is indeterminate to the third degree. One convenient solution is to employ the neutral point method to compute the influence lines for the external reactions and for the internal reactions at point f, the quarter point. (See Figure 13.)[14] In this method influence lines are first obtained for neutral point reactions which can be combined by statics to give the influence lines for any desired point. The Muller-Breslau principle states that "the shape of the deflected structure becomes an influence line for reaction when a simple unit movement in the nature of the reaction is produced at the reaction point." If the arch is cut at the crown as shown in Figure 12, then the total elastic weight of the arch produced by a unit load is A, and the moments of inertia of this total elastic weight about the x and y axis passing through the neutral point are given by I_{xx} and I_{yy} respectively.

Since I_{xx} is then the horizontal displacement of the neutral point caused by $H_n = 1$, then a force $1/I_{xx}$ would produce a unit horizontal deflection without an accompanying vertical displacement or rotation of the neutral point. The horizontal deflections of the arch axis produced by the neutral point force $1/I_{xx}$ would represent the influence ordinates for H_n to scale. The same pattern, of course, holds true for I_{yy} and A with respect to V_n and M_n. All the deflection values, or influence line ordinates for the neutral, are then readily calculated by the conjugate structure method.

The influence lines for the external reactions and for the reactions at the quarter point are first calculated as design steps (1) and (2). The influence line for the moment at point f and AASHO specifications require that the uniform live load of 1.375 kips per foot be extended from the left support to the point x = 409 feet., and that the concentrated load of 26.7 kips be placed at point f. As shown in Figure 14, a temperature drop of 60°F has been considered in addition to the following erection errors: the span is 1 inch too short and point f has deviated from the calculated position 1 inch in the horizontal and 1 inch in the vertical direction.

Step (3). From the analysis of the rigid arch, the following values are obtained: M_r = 17,524 ft.-k., H = 6186 k., T = 6,404 k., V = 4513 k., W = 2958 k., L_o = 336.2 ft., and h_o = 81.54 feet.

Step (4). Next the conjugate structures serve to determine the following values: $k_1 = 0.1032$, $k_2 = 0.1682$, and due to D.L. + L.L. + I.: $\Sigma EI_c m_{or} = -78{,}815{,}779$ k.-ft.^{3}, $EI_c n_r = 76{,}444{,}793$ k.-ft.^{3}, $EI_c n_{br} = 58{,}259{,}608$ k.-ft.^{3}, and $EI_c(n_r - n_{br}) = 18{,}185{,}185$ k.-ft.^{3}.

14. For a detailed description of the neutral point method see reference 3.

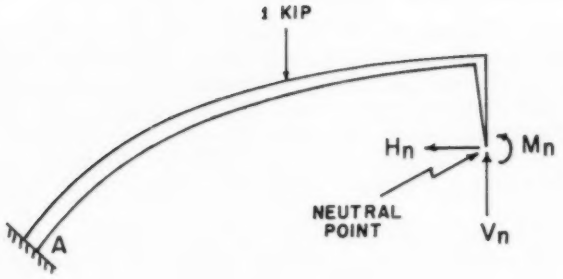

FIG. 13. THE HINGELESS ARCH WITH THE NEUTRAL POINT REACTIONS.

The point b is located at x = 135 feet.

It was pointed out that I_{xx} was equal to the horizontal displacement of the neutral point caused by a unit load at that point. Consequently, the neutral point thrust at the neutral point is:

$$H = \frac{\epsilon t L + \text{error}}{I_{xx}} \qquad (45)$$

If a temperature drop of 60° F and a shortness of 1 inch in span is assumed, then equation (45) becomes: $H = 1.0287\ I_c$, and if it is assumed that the crown section has already been designed and $I_c = 81.17$ ft.^{4}, then H = 83.5 kips.[15]

Using the conjugate structure method, the deflections at the desired points caused by the 60° F drop and 1 inch shortness in span are: $n_2 = -0.7$ in., $m_2 = 6.3$ in., and $n_{b2} = -0.3$ inches. But considering the displacements of point f due to erection errors, $n_2 = -0.7 + 1.0 = 0.3$ inches, and $m_2 = 6.3 + 1.0 = 7.3$ inches. (Negative signs mean that the deflection is either upward or to the left.)

Step (5). Since at point f $M_r = 17{,}524$ ft.-k., equation (39) becomes: $M_1 = 232{,}615$ in.-k.; and equation (40) becomes $I_r = 192{,}052$ in.^{4}. Also,

$$\frac{M_1 \sec\theta}{E}\left(k_1 L_o^2 + \frac{\Sigma E I_c m_{or}}{2 M_r}\right) = 11{,}074{,}392 \text{ in.}^5$$

and

$$\frac{M_1 \sec\theta}{E}\left(k_2 L_o h_o\right) = 5{,}422{,}436 \text{ in.}^5$$

15. From experience the designer must select a preliminary value of I_c that will approximate the final value. If these values are very different then the preliminary value is modified accordingly. This successive correction procedure is employed only for the design of the crown, which of course should be the first section to be designed.

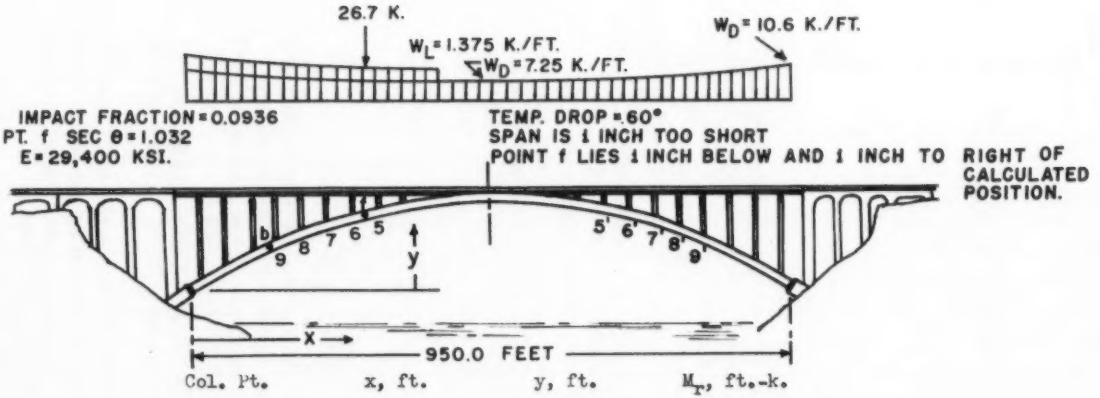
26.7 K.
W_L = 1.375 K./FT.
W_D = 7.25 K./FT.
W_D = 10.6 K./FT.
IMPACT FRACTION = 0.0936
PT. f SEC θ = 1.032
E = 29,400 KSI.
TEMP. DROP = 60°
SPAN IS 1 INCH TOO SHORT
POINT f LIES 1 INCH BELOW AND 1 INCH TO RIGHT OF CALCULATED POSITION.
b
9 8 7 6 5
y
5' 6' 7' 8' 9'
X
950.0 FEET

Col. Pt.	x, ft.	y, ft.	M_T, ft.-k.
12	22.307	14.394	-27,685
11	61.672	37.768	-15,940
10	101.036	58.698	-4,864
9	140.401	77.251	4,414
8	179.766	93.582	11,123
7	219.130	107.751	15,624
6	258.495	119.817	18,032
f	278.177	125.958	17,524
5	297.859	129.826	17,171
4	337.224	137.808	14,761
3	376.589	143.783	10,734
2	415.953	147.763	5,248
1	455.318	149.751	785
Crown	475.000	150.000	-2,324

FIG. 14. LOADING CONDITION CRITICAL FOR THE QUARTER POINT OF THE HINGELESS RAINBOW BRIDGE: D.L. + L.L. + I. + T. + E.

The above values are then substituted in equations (29), (30) and (31), using N = 90 and g = 1.10 which are the approximate values for the actual bridge.

$$f = \frac{6404}{\frac{gd^2(K+3)}{270}} + \frac{232{,}615\,(d/2)}{\frac{d^4\,(K+1)}{1080} - 192{,}052}$$

$$m = \frac{11{,}074{,}392}{\frac{d^4\,(K+1)}{1080} - 192{,}052} + 7.3$$

$$n = \frac{5{,}422{,}536}{\frac{d^4\,(K+1)}{1080} - 192{,}052} + 0.3$$

Varying d and K, with the help of tables (1) and (2), the values of f, m and n are computed and plotted to give the interaction diagrams of Figure 15. In the actual design, the quarter point section has a depth of 12 feet., a total moment of inertia of 88.2 ft.^{4} and each web plate is 13/16 in. thick.[16] The shape factor is then $K = I_f/I_w = ((88.2)\,(12)^4 - 404{,}352)/404{,}352 = 3.52$. Point (1) represents this section, and from the diagrams it is seen that the stress is approximately 22.00 ksi. and the total displacement is 14.7 inches. The section, stressed below the allowable 23.00 ksi. for the silicon steel, is safe and fairly economical for the given depth. Point (2) indicates a somewhat more economical section with a shape factor of approximately 3.3 and the same depth. This section would be stressed to the allowable 23.00 ksi. and would deflect radially 15.2 inches, and its dimensional properties would be:

$$I = \left(\frac{144}{12}\right)^4 \left(\frac{3.3+1}{1080}\right) = 82.5 \text{ ft.}^4$$

$$A = 1.10\,(144)^2 \left(\frac{3.3+3}{270}\right) = 556 \text{ in.}^2$$

The fact that the actual quarter point section is slightly understressed is not surprising, because the section was actually designed by the elastic theory with 20.00 ksi. as the allowable unit stress in the silicon steel rib.[17] In the rigid system, of course, $M_1 = M_r = 17{,}524$ ft.-k. and $I_r = 0$. Then, $f = 6404\,(270)/1.10\,(144)^2\,(6.52) + 17{,}524\,(12)\,(72)/1{,}830{,}000 = 19.98$ ksi. The change in geometry of the arch axis produces a $(22.00 - 19.98)/19.98 = 10.01\%$ increase in stress.

It is of interest to note that a section with a smaller depth could have been used without making the rib any heavier by increasing the shape factor. Point (3), for example, has a fiber stress of 23.00 ksi. and a radial displacement of 16.8 in. The K is equal to 6, so the effective area is $A = gd^2(K+3)/3N = 546$ in.^{2}, while the actual section has an A = 554 in.^{2}. Thus the interaction diagram illustrates its usefulness in design in being able to give the stress and deflection values for a great many combinations of dimensions of the cross section without extended or sometimes prohibitive computations.

16. Reference 2, p. 24, p. 32.
17. Reference 2, p. 9.

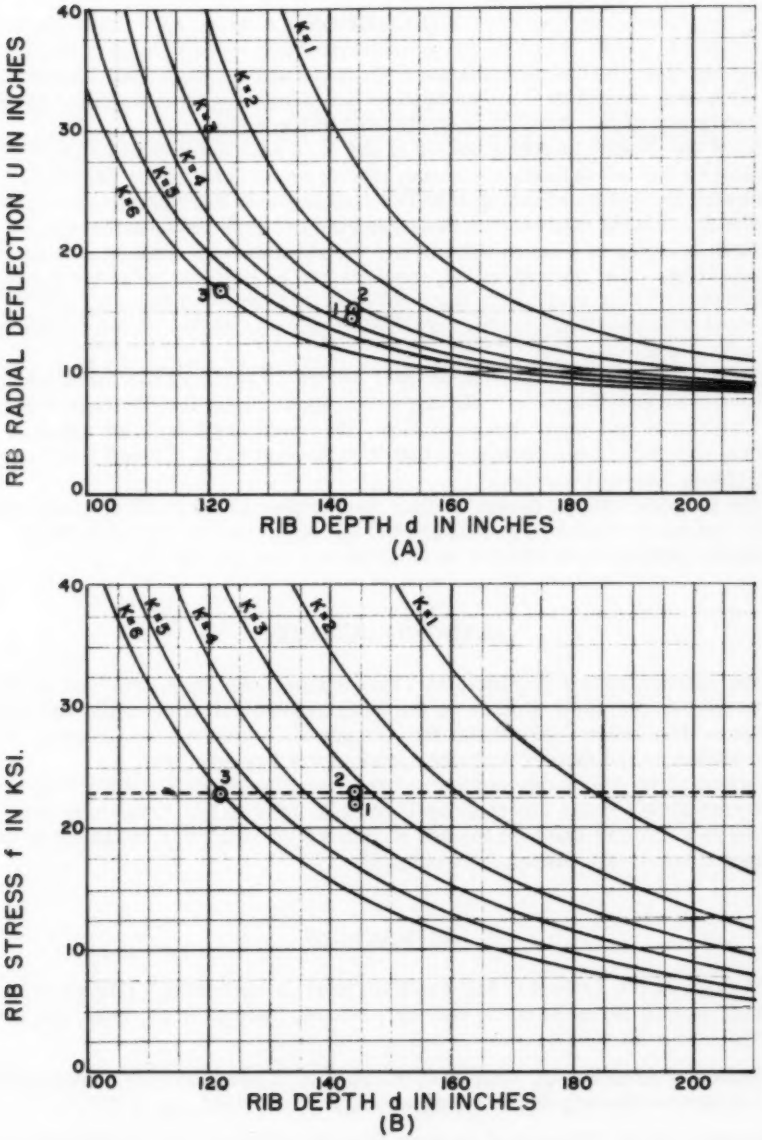

FIG. 15. INTERACTION DIAGRAM FOR THE QUARTER POINT OF THE HINGELESS RAINBOW BRIDGE: D.L.+L.L.+I.+T.+E.

CONCLUSION

In long span flexible arches, the neglect of the deformed configuration of the arch axis caused by the load system may introduce an intolerable degree of inaccuracy in the stability computations of the structure.

When the change in configuration of the arch axis is considered, it is mandatory that all deflection-causing effects be included in the problem. Otherwise the critical loading condition has not truly been produced.

The interaction expressions developed for the arch indicate that the flexible arch behaves as a beam column and the rigid arch is analogous to the simple beam. The interaction expressions can be of great value for purposes of analysis. Their application does not deal with involved concepts nor lengthy calculations beyond the rigid arch analysis, and the results obtained are highly accurate.

The interaction expressions, in their design form, facilitate the drawing of the interaction diagrams. Making use of these plots, the designer evades the usual trial and error design tactics. He visualizes the entire range of design, and selects his section so that it is stressed to a desired level and deflects an intended amount.

The proposed direct design method may further prove to be of great value in the not too distant future when the bridge design codes may specify an allowable deflection in addition to an allowable unit stress.

ACKNOWLEDGMENTS

The authors were indebted to Mr. Shortridge Hardesty for the use of his office data during their studies on the design characteristics of the Rainbow bridges. The authors also thank Mr. Othmar H. Ammann for supplying information on the design characteristics of the Bayonne arch.

Research for this publication was performed by Omar J. Sotillo[18] as a doctorate thesis under direction by Haaren A. Miklofsky. This study is a sequel to a similar study on the use of interaction diagrams in design of the stiffening truss of a suspension bridge.[19]

REFERENCES

1. "Design of the 1,675-Ft. Kill van Kull Steel-Arch Bridge," (Bayonne), Engineering News-Record, Vol. 101, No. 24, December 13, 1928, pp. 873-877.

2. "Rainbow Arch Bridge over Niagara Gorge: A Symposium," Transactions —American Society of Civil Engineers, No. 110, 1945, pp. 1-178.

3. Grinter, L. E. "Theory of Modern Steel Structures," Vol. II, Statically Indeterminate Structures and Space Frames, Revised Edition, Macmillan, New York, 1949, Chapter 8.

18. Reference 7.
19. Reference 5.

4. Kinney, J. S. "Analysis of Multi-Span Rigid Frames," in Steel Rigid Frames Manual, Design and Construction, by Martin P. Korn, published by J. W. Edwards, Inc., Ann Arbor, Michigan, 1953, pp. 50-66.

5. Miklofsky, H. A. "Bending Interaction in Suspension Bridges," Proceedings Separate No. 652—American Society of Civil Engineers, March 1955.

6. Moisseiff, L. S. "The Design, Materials and Erection of the Kill Van Kull (Bayonne) Arch," Journal of the Franklin Institute, Vol. 213, No. 5, May 1932.

7. Sotillo, O. J. "Design of Flexible Steel Arches by Interaction Diagrams," Thesis submitted to the Civil Engineering Department of Rensselaer Polytechnic Institute, Troy, New York, in candidacy for the degree of Doctor of Philosophy, June 1956.

Paper 1191 ST 2

Journal of the
STRUCTURAL DIVISION
Proceedings of the American Society of Civil Engineers

PRESTRESSED TRUSS-BEAMS

Ralph L. Barnett,[1] J.M. ASCE
(Proc. Paper 1191)

SYNOPSIS

The purpose of this paper is to present a design procedure for simply supported beams which makes possible the utilization of statically indeterminate composite action and favorable initial stress distribution to strengthen available beam sections. A variation of the Queen Post truss with a pretensioned tie rod is studied and weight savings of over thirty percent are demonstrated by example designs. The techniques used are based entirely on elastic considerations.

INTRODUCTION

Consider a simply supported beam with constant moment of inertia under an arbitrary downward acting load system. Impose the rather weak restriction on this beam, that the maximum moment, M_{max}, govern its design. If, for example, two negative end moments of magnitude $M_{max/2}$ were applied to this structure, the design moment would clearly be reduced to $|M_{max/2}|$. Since the external shear distribution remains unchanged, the possible lighter design might be governed by shear, web-crippling, deflection, or the moment $|M_{max/2}|$. Under rather special conditions of loading, continuous and overhanging beams may achieve a moment distribution similar to figure (1-b), in general however, a design based on these moments would be unrealistic. In an attempt to approach the condition illustrated in figure (1-a), examine the statically indeterminate structure formed by adding two similar rigid brackets and a tie rod to the beam shown. The resulting moment diagram differs from that of a simple beam by the constant negative moment $\underline{H}\ e$

Note: Discussion open until August 1, 1957. Paper 1191 is part of the copyrighted Journal of the Structural Division of the American Society of Civil Engineers, Vol. 83, No. ST 2, March, 1957.

1. Asst. Engr., Armour Research Foundation, Chicago, Ill.

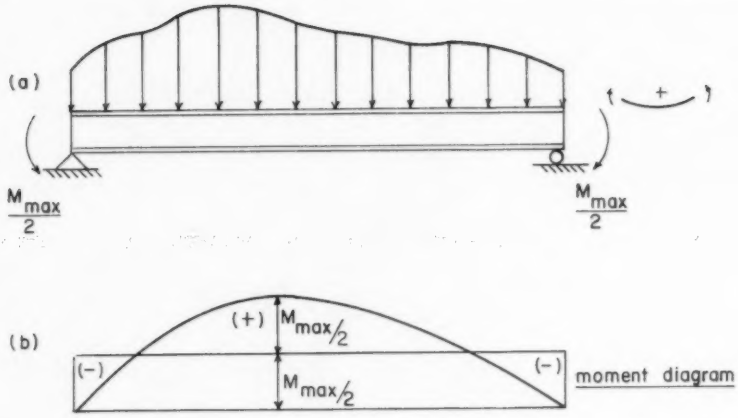

FIG. 1 LOADED BEAM WITH TERMINAL COUPLES

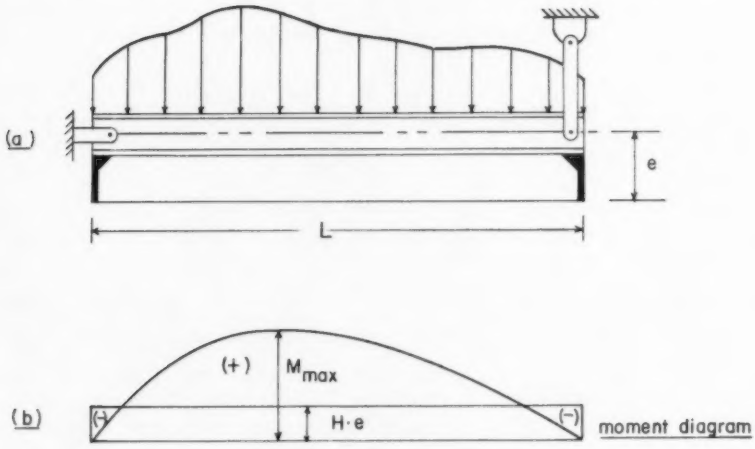

FIG. 2 TRUSSED BEAM

throughout L, where H is the tensile stress induced in the tie rod by the loads and e is the eccentricity of H with respect to the centroid of the beam. The moment H e will not reduce the design moment to $|M_{max/2}|$ unless e is unreasonably large compared to the beam depth or the tie area assumes massive proportions.

The stress in the tie rod can be increased by "pretensioning." To illustrate this procedure imagine the tie rod with a turnbuckle in the center. By tightening the turnbuckle a prestress force F can be added to H which will produce a total negative moment in the loaded beam, (F + H)e, equal to $M_{max/2}$. The beam design may then be based on the bending moment $|M_{max/2}|$ and the axial load (F + H). With e sufficiently large, the above technique will increase the load capacity of a given simply supported beam designed for M_{max}. Furthermore, if sufficient gradation exists in the available beams, a specified load may be carried on a lighter section than the corresponding simple beam.

A lower bound for e can be obtained by considering the states of stress in the beam shown in figure (2-a). Since the design of a combined stress member is sought, an interaction criterion must be assumed. Hence, require that a beam be proportioned to satisfy the straight line interaction formula:[2]

$$\frac{f_a}{F_a} + \frac{f_b}{F_b} \leq 1 \qquad (1)$$

where the terms are defined in appendix A.

To the simple beam bending stresses, add the stresses resulting from the indeterminacy and the prestressing:

$$f = \frac{P}{A} \pm \frac{My}{I} = \frac{F + H}{A} - \frac{(F + H)\,ey}{I} \qquad (2)$$

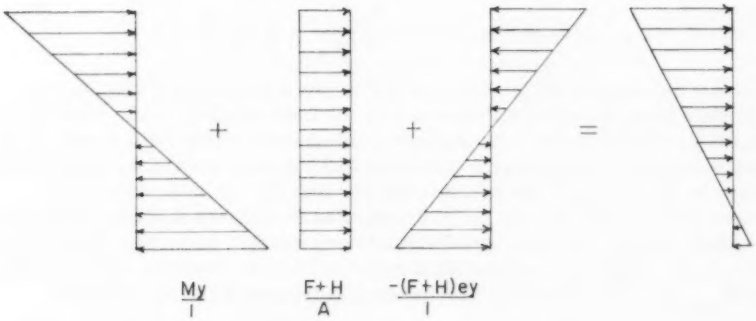

FIG. 3 STRESS DISTRIBUTION – PRESTRESSED BEAM

If a reduction of the simple beam design is to result from this addition:

$$\frac{F + H}{AF_a} - \frac{(F + H)\,e}{S_1 F_{b1}} < 0 \qquad (3)$$

2. See A.I.S.C. Specifications, section 12a, 1954.

from which,

$$e > \frac{S_1}{A} \frac{F_{b1}}{F_a}, \tag{4}$$

where the subscript (1) refers to the top fibers. For an I or WF section, an upper bound can be obtained for the expression $\frac{S_1}{A} \frac{F_{b1}}{F_a}$. The maximum possible ratio of section modulus to section area is obtained by neglecting the web.

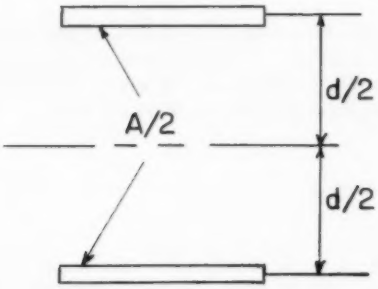

$$\frac{S'_1}{A} = \frac{I'}{Ac} = \frac{A(d/2)^2}{A(d/2)} = \frac{d}{2} \tag{5}$$

$$\frac{S}{A} < \frac{S'}{A} = \frac{d}{2} \tag{6}$$

From the A.I.S.C. specifications,

$$F_a \geq 10.02 \text{ ksi. for } (L/r) \leq 120 \text{ and}$$

$$F_{b1} \leq 20.00 \text{ ksi. Then, } \frac{S_1}{A} \frac{F_{b1}}{F_a} < \frac{d}{2} \frac{20.00}{10.02} < d \tag{7}$$

Hence, for any simply supported I or WF beam with $(L_u/r) \leq 120$, an $e \geq d$ will always make possible an increase in the load capacity while satisfying the A.I.S.C. requirements. To achieve a diminution in the total weight of a simply supported beam under a specified load, e must provide a reduction in the section that exceeds the bracket and tie weight. As e increases, the stresses in the beam and the tie rod decrease in a linear fashion. The corresponding weights of these members are accordingly reduced. When e becomes greater than d/2, a bracket is required to transmit the negative moment $M_{max/2}$. The weight of this bracket increases linearly with the eccentricity, and a value is reached after which the total weight economy diminishes.

Improved Design

The simple prestress design previously indicated can be substantially refined to permit greater savings in weight. In subsequent discussions, the following property of moment diagrams is assumed. Under a downward acting load system, the shape of a simple beam moment diagram may never be convex with respect to an interior point. This fact is assured by the fundamental relationship,

$$w = -\frac{d^2M}{dx^2} \quad \text{where } w \geq 0. \tag{8}$$

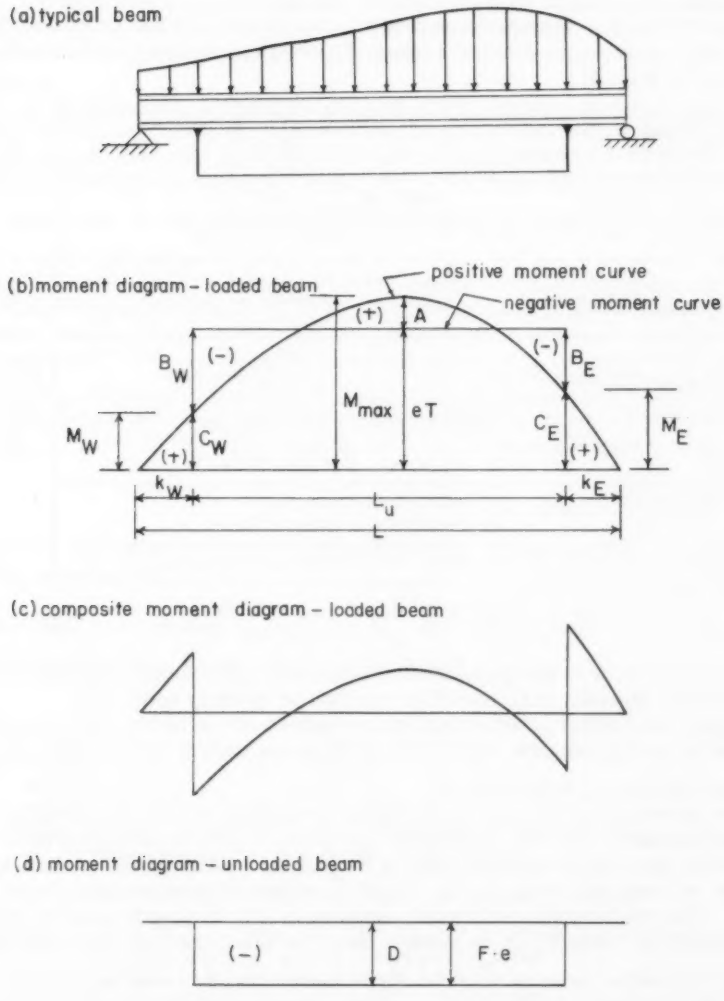

FIG. 4 TYPICAL PRESTRESSED TRUSS-BEAM

A unimodal shape is implied by this non-convexity requirement.

Consider the typical moment diagram shown in figure (4) for a prestressed trussed-beam whose maximum moment lies between the brackets and whose brackets lie within the span. The critical stress conditions are tabulated in table (1).

Points of Critical Stress Combinations	$\frac{f_b}{F_b} + \frac{f_a}{F_a}$	
A top fibers	$\frac{M_{max} - eT}{S_1 F_{b1}} + \frac{T}{AF_a}$	(9)
$B_{W,E}$ bottom fibers	$\frac{eT - M_{W,E}}{S_2 F_{b2}} + \frac{T}{AF_a}$	(10)
$C_{W,E}$ top and bottom fibers	$\frac{M_{W,E}}{S_{1,2} F_{b1,2}}$	(11)
D bottom fibers	$\frac{Fe}{S_2 F_{b2}} + \frac{F}{AF_a}$	(12)
Where subscripts (1) refer to the top fibers (2) refer to the bottom fibers W refer to the West end of the beam E refer to the East end of the beam		

TABLE I - POINTS OF CRITICAL STRESS

The problem is to design a trussed-beam which will render the values of expressions (9), (10), (11), and (12) less than or equal to unity.

Inspect the typical prestressed truss-beam shown in figure (4a). Assume that the allowable moment resistance of the beam section is less than M_{max} and that the loading is downward.

The beam section outside of the brackets must resist only the positive bending moment. The allowable moment on the section is given by SF_b. The abscissas associated with the ordinate SF_b on the positive moment diagram are the optimum positions for the brackets as noted in subsequent discussions. With the brackets so placed, expression (11) is clearly equal to unity. Because the moment M_{max} is greater than that which the beam section can resist, a negative moment must be superimposed on the beam section between the brackets to reduce M_{max}. This negative moment results from the induced force $\underline{H}$ and the prestress force $\underline{F}$ produced in the tie rod. Its magnitude is $\underline{(F + H)e}$ and it is transferred to the beam through the brackets. The net or design moment is lowered, but an axial stress, $\underline{F + H}$, is produced between the brackets. With $\underline{e}$ sufficiently large the combined effect of the axial stress and the negative moment reduces the stresses associated with M_{max} [See inequality (4)]. The lowest permissible value of $\underline{(F + H)}$, called $\underline{T}$, is found by equating expression (9) with unity and solving for this quantity.

The moment $\underline{eT}$ may be large enough to have produced negative resultant bending moments near the brackets as shown in figures (4b-c). Their

maximum values would occur at the brackets and the resulting stresses would add to the axial stresses also present. If the design is to satisfy equation (1), expression (10) must be verified to be less than or equal to unity. If this condition can be met, the possibility of producing a tie rod stress T must be investigated.

The prestress force F will be sustained in the unloaded structure in contrast to the induced force H. The unloaded beam is subjected to the negative moment eF and the axial force F. By equating expression (12) with unity the maximum allowable value of this force, F_{max}, is obtained. The induced force must be at least as great as the difference between T and F_{max} if critical point A is to be satisfied.

The minimum size brackets and tie rod can be designed using the force T. With the geometry and elastic properties of all structural elements known, the indeterminate stress H can be calculated using standard procedures. If H is less than $T - F_{max}$, it may be possible to increase this quantity by increasing the stiffness of the tie rod (See Design Procedure V-B). When H is greater than $T - F_{max}$, the prestress force is equal to $T - H$.

Design Procedures

I. Select a lighter section than the corresponding simply supported beam without prestressing.

II. Calculate the maximum k_W, k_E, and $M_{(x)}$ by equating expression (11) with unity. Calculate $L_u = L - k_W = k_E$. Calculate M_{max}.

$$\frac{M_{(x)}}{SF_b} = 1 \qquad (13)$$

where: (1) x is measured from the left and right ends of the beam when solving for k_W and k_E respectively.

(2) S and F_b are the smaller of the possible values.

note: (1) As L_u becomes smaller, F_a and H increase. Therefore use the maximum k_W and k_E when possible.

(2) If values of k_W and k_E are used which are less than the maximum allowable values, calculate $M_{(x)} \big| x = k_W, k_E$.

III. Method A

A. Select an e. (note: total depth $\approx e + \frac{\text{depth of conventional design}}{2}$)

B. Calculate minimum T by equating expression (9) with unity.

$$T = \frac{M_{max} - S_1 F_{b1}}{e - \frac{S_1 F_{b1}}{A F_a}} \qquad (14)$$

(1) $eT > M_{W,E}$ . . . . check B, i.e. [express. (10)] ≤ 1

If [express. (10)] > 1 { Try stronger section / Increase $\underline{e}$. (Method B) / (Try minimum L_u)

note: If $S_1 = S_2$, and $F_{b1} = F_{b2}$, a necessary and sufficient condition for $B_{W,E}$ to satisfy $\frac{f_a}{F_a} + \frac{f_b}{F_b} \leq 1$ is that:

$$M_{max} - eT \geq eT = M_{W,E} \tag{15}$$

(2) $eT \leq M_{W,E}$ . . . . . critical condition at $B_{W,E}$ does not exist.

Method B

Calculate the minimum $\underline{e}$ necessary for the stresses at A and $B_{W,E}$ to satisfy inequality (1). Also compute the associated T. [Set expressions (9) and (10) equal to unity and solve simultaneously for $\underline{e}$ and T.]

$$e = \frac{M_{W,E}S_1F_{b1} + M_{max}S_2F_{b2}}{AF_a(M_{W,E} - M_{max} + S_1F_{b1} + S_2F_{b2})} \tag{16}$$

note: use greater $\underline{e}$ when $M_W \neq M_E$

$$T = \frac{M_{W,E}S_1F_{b1} + M_{max}S_2F_{b2}}{e(S_1F_{b1} + S_2F_{b2})} \tag{17}$$

IV. Calculate the maximum allowable $\underline{F}$ by equating expression (12) with unity.

$$F_{max} = \frac{S_2F_{b2}}{e + \frac{S_2F_{b2}}{AF_a}} \tag{18}$$

note: If part of the dead load moment in the positive moment distribution acts on the beam without overstressing it before the pretensioning is applied, the prestress force $\underline{F}$ may be increased. The loads responsible for this dead load moment may not be used in the calculation of $\underline{H}$. F_{max} becomes,

$$F_{max} = \frac{S_2F_{b2} + M_{DL}(x)\big|_{x=k}}{e + \frac{S_2F_{b2}}{AF_a}} \tag{19}$$

where k gives the smaller value of $M_{DL}(x)$.

This can be seen by imposing a positive moment distribution on figure (4d) with the smaller amount over either bracket equal to $M_{DL}(x)$.

V. Calculate $\underline{H}$ (Virtual work). Design brackets using force T.

Use: $$A_c = T/f_c \tag{20}$$

$$H = \frac{\sum\int Mm\,\frac{ds}{EI}}{\sum\int m^2\,\frac{ds}{EI} + \sum\frac{u^2 L}{AE}} \tag{21}$$

where M is produced by the loads not acting when the prestressing was applied.

(A) $H + F_{max} \geq T$ . . . . Section O.K.

(B) $H + F_{max} < T$

(1) Increase A_c and hence $\underline{H}$. Set: $H = T - F_{max}$ and solve for A_c.

(a) $A_c > 0$ . . . section may be used with this A_c, however the total weight may be excessive.

(b) $A_c < 0$ . . . meaningless . . . . see (2) or (3) below -

(2) Increase $\underline{e}$ - return to III. - Method A. If $\underline{e}$ becomes too large see (3) below.

(3) Select a stronger section.

VI. Calculate prestressing force and check shear, deflection, etc.

$$F = T - H \tag{22}$$

Comments on the Design Procedure

I. The procedure herein is intended to increase the strength of available beams at the expense of depth. If a girder or truss is to be designed with a given depth, only small weight savings result from this technique. The design of a prestressed girder is considered in reference (4) by Professor Magnel.

II. The maximum values of k_W and k_E depend on the shape of the positive moment diagram. The design may therefore depend not only on the maximum moment but on the type of loading. A single concentrated load placed anywhere in the span produces the smallest L_u of all downward acting load systems with equal maximum moments. The values of $\underline{H}$ given in appendix B increase with diminishing L_u. With $k_W = k_E = 0$, $S_1 = S_2$, and $F_{b1} = F_{b2}$, the simple procedure suggested in the outset of this paper represents the optimum design which can be produced by the more detailed scheme.

III. Method A

If a prestressed member has the prestressing element attached to it in such a way that the distance between their centroids remains fixed regardless of any configuration entertained, the possibility of axial buckling as a result of the prestress force alone is eliminated. If a hinged strut is subjected to an axial load and a lateral force or initial crookedness provides some curvature in the strut, a moment is produced in the plane of the curvature

proportional to the distance from the centroid of the strut to the line of action of the axial force. The moment gives rise to more curvature and hence more moment, etc. When an axial force is produced by cables fixed to the edge of a strut, the line of action of the force remains at a fixed distance from the centroid and no moment due to curvature is realized. Consider a WF section with a hollow tube welded along the bottom flange. Pass a cable snugly through the tube and prestress the beam. Because the distance between the cable and the centroids of the bottom flange and entire section cannot vary, no axial buckling in the weak direction or lateral buckling of the bending compression flange can occur without external loading. When the structure is loaded as a beam lateral buckling is possible, however axial buckling remains unattainable. In the examples where such cable attachment was feasible, F_{b2} and F_a were valued at 20,000 psi. The following illustration attempts to indicate that an equivalent lateral load does not exist and hence no second order bending effects are produced when the cable is fixed to the section. It can be shown that the vanishing of the equivalent lateral loads establishes the first statement of this paragraph.

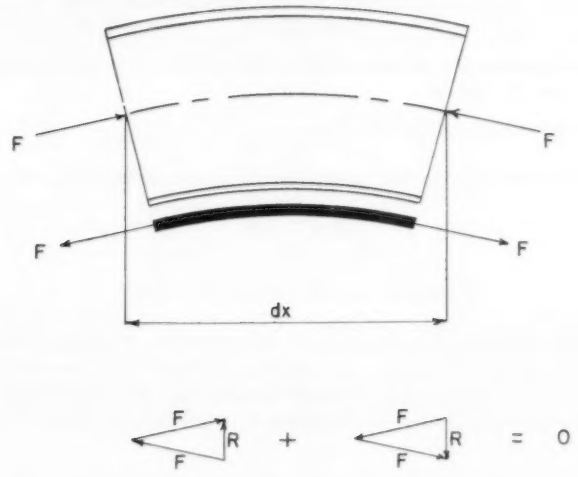

FIG. 5 VANISHING RESULTANT LOAD ON AN ELEMENT OF A PRESTRESSED BEAM

Method B

By placing brackets at the intersection of the positive moment curve and a horizontal line with ordinate $\frac{M_{max}}{3}$, and then applying a negative moment of $\frac{2M_{max}}{3}$, the design moment assumes a value of $\left|\frac{M_{max}}{3}\right|$. With the truss

configuration used, this is the smallest possible value. When designing rolled beams using Method B, trial sections can be obtained by entering the $\frac{Ld}{bt}$ table of the A.I.S.C. Manual with $\frac{M_{max}}{3}$ and L.

IV. The high strength steel used for prestressing may experience losses in stress due to creep or relaxation.[3] F_{max} as computed in IV. represents the maximum cable stress which can be applied to the unloaded section while satisfying the interaction formula, (1). If creep losses occur the remaining stress, F'_{max}, can be used in part V. It might be feasible to overstress [with respect to formula (1)] the structure initially such that the final prestress is equal to F_{max}.

V. The calculation of the induced force H in the prestressed structure is equivalent to the determination of H in the single redundant structure without prestressing. This follows directly from the principle of super-position. The prestressed structure will have an upward deflection when unloaded, a downward deflection when loaded. The difference represents the total live load deflection and can be calculated using the conjugate beam.

$$\Delta_{LL} = \delta_{LL}(x) - \frac{HeL_u\left(\frac{L_u}{2} + k_E\right)x}{LE_bI_b} \qquad 0 \le x \le k_W \qquad (23)$$

$$\Delta_{LL} = \delta_{LL}(x) - \frac{HeL_u\left(\frac{L_u}{2} + k_E\right)x}{LE_bI_b} + \frac{He(x - k_W)^2}{2E_bI_b} \qquad k_W \le x \le L - k_E \qquad (24)$$

where $\delta_{LL}(x)$ represents the deflection of the simply supported beam without prestressing.

The King Post truss and the conventional form of the Queen Post truss were compared to the trussed-beam studied in this paper. In general they were not as effective due to a smaller induced moment, i.e. the moment produced by the indeterminacy. Lower values of F_a in both trusses and the shape of the negative moment diagram for the King Post truss were contributing disadvantages.

VI. The cost of prestressing will dictate the usefulness of the technique herein described. Under average construction conditions, it requires approximately 0.4 man hours to prestress a single bar. The following procedure is commonly used for prestressing steel rods or cables with threaded ends:

(1) Place bar in position with washers and nuts on each end, completely seating the nut on the non-jacking end. Run nut down on the jacking end to provide room for an adapter.
(2) Screw on the adapter and position the jack.
(3) Jack to required pressure or bar elongation.
(4) Run nut home and seat moderately tight.
(5) Release pressure and remove jack.

3. "Method Presented for Computing Steel Prestress Losses," by H. K. Stephenson and T. R. Jones, Jr., Civil Engineering, Aug. 1955, Vol. P. 510.

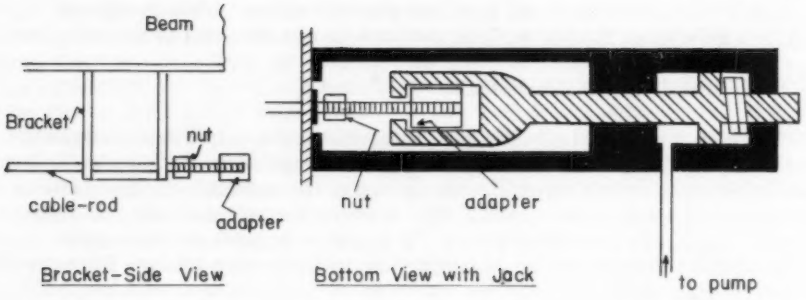

FIG. 6 PRESTRESSING BRACKET AND HYDRAULIC JACK

Many of the companies who supply prestressing steel rent the tensioning equipment and provide detailed instructions. The techniques being developed for prestressing high strength bolts may conceivably be utilized for tie rods and high strength cables.

Numerical Examples

Example 1.

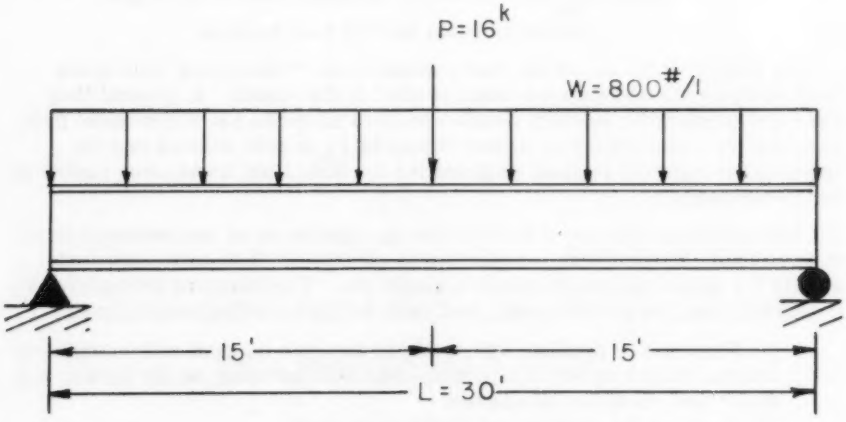

(1) Assume beam laterally supported at third points (both flanges).
(2) Neglect the dead load.
(3) Use a WF section - A.I.S.C. specifications for stresses.
(4) Allowable cable stress: f_c = 100,000 psi.
(5) Modulus of elasticity for all members: E = 30,000,000 psi.

Design Without Prestress:

$M_{max} = 210.0'^{-k}$; unsupported length, $L' = 10.0'$

Try 21WF62 $S = 126.4\ in^3$

$$S = \frac{M_{max}}{F_b} = \frac{210(12)}{20} = 126.0 < 126.4 \quad O.K.$$

Design Using Prestressed Trussed-Beam:

I. Try 16WF40: $A = 11.77\ in^2$, $S = 64.4\ in^3$, $I = 515.5\ in^4$,

$$r_{min} = 1.50\ in, \quad \frac{d}{bt} = 4.54\ in^{-1}$$

II. $M_{max} = 210.0'^{-k}$, $F_b = 20$ ksi.

$$\frac{M_{(x)}}{SF_b} = \frac{(20x - .4x^2)12}{64.4(20)} = 1, \qquad x = k_W = k_E = 6.11'$$

$$M = 107.33'^{-k}$$

$$L_u = L - k_W - k_E = 30 - 12.22 = 17.78'$$

III.-A Try $e = 24.0''$; $\frac{L''}{r} = \frac{10(12)}{1.5} = 80$, $F_a = 13.90$ ksi.

$$T = \frac{M_{max} - SF_b}{e - \frac{SF_b}{AF_a}} = \frac{2520 - 1288}{24 - 7.87} = 76.39^k$$

$eT = 2(76.39) = 152.78'^{-k} > M = 107.33'^{-k}$ .... check B

$M_{max} - eT = 210.00 - 152.78 = 57.22 > eT - M = 152.78 - 107.33$

$= 45.45$ .... B O.K.

IV. $$F_{max} = \frac{SF_b}{e + \frac{SF_b}{AF_a}} = \frac{1288}{24 + 7.87} = 40.41^k$$

V. Truss Bracket

$$B.F. = 2E_b I_b \sum \frac{u^2 L}{A_a E_a}$$

$$= \frac{2(515.5)}{144}\left[\frac{1^2(1.33)}{3.84} + \frac{(1.414)^2(1.89)}{6.50}\right]$$

$$= 6.64\ k\text{-}ft^3$$

$$Weight = 2(3.4)\left[1.33(3.84) + 1.89(6.50)\right]$$

$$= 118.27\#$$

$$A_c = \frac{T}{f_c} = \frac{76.39}{100} \doteq 0.764\ in^2$$

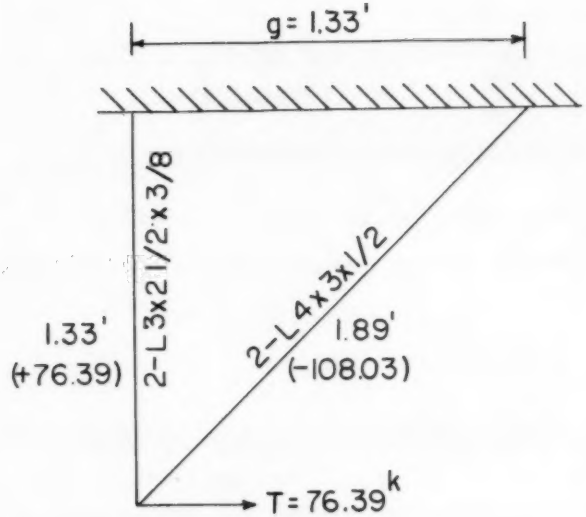

$$H = \frac{\frac{Pe}{2}\left(\frac{L^2}{4} - k^2\right) + \frac{we}{12}\left(L^3 - 6Lk^2 + 4k^3\right)}{L_u\left(e^2 + \frac{1}{A}\right) + (L_u + 2g)\frac{1}{A_c} + \text{Bracket Factor}}$$

$$= \frac{\frac{16(2)}{2}\left(\frac{30^2}{4} - 6.11^2\right) + \frac{.8(2)}{12}\left[30^3 - 6(30)(6.11)^2 + 4(6.11)^3\right]}{17.78\left[2^2 + \frac{515.5}{144(11.77)}\right] + (17.78 + 2.67)\frac{515.5}{144(.764)} + 6.64}$$

$$= \frac{5828.40}{179.00} = 32.56^k$$

note: bending between the legs of each bracket is ignored – the exact value is H = 33.26 kips.

$H + F_{max} = 32.56 + 40.41 = 72.97 < T = 76.39$ .... increase A_c

$H = T - F_{max} = 76.39 - 40.41 = 35.98^k$

$$H = \frac{5828.40}{76.53 + \frac{20.45(515.5)}{144(A_c)} + 6.64} = 35.98; \quad A_c = 0.929 \text{ in}^2$$

VI. $F = T - H = 76.39 - 35.98 = 40.41^k$

Weight Saved:

Cable	20.45(3.4)(.929) =	64.59	21WF62: 30(62) = 1860.00#
Bracket	..... =	118.27	
Beam section	30(40) =	1200.00	
		1382.86#	

$$\frac{1860.00 - 1382.86}{1860.00} \times 100 = \frac{477.14}{1860.00} \times 100 \approx 25.7\%$$

Example 2.

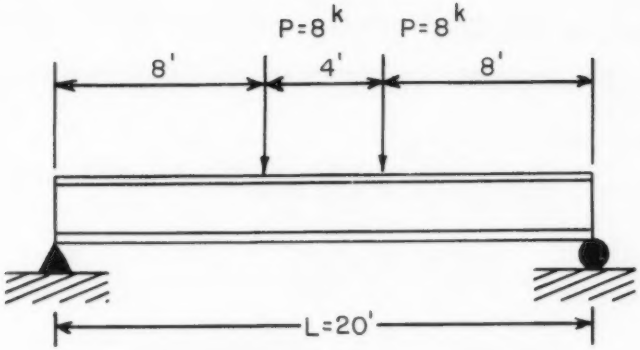

(1) Lateral support at center (both flanges).
(2) Use the specifications in the previous problem

Design Without Prestress: Use 14WF30

Design Using Prestressed Trussed-Beam:

I. Try 8WF20: $A = 5.88\ in^2$, $S = 17\ in^3$, $I = 69.2\ in^4$, $r_{min} = 1.2$ in

$$\frac{d}{bt} = 4.08\ in^{-1}$$

II. $M_{max} = 64.0'\text{-k}$; $F_b = 20$ ksi.; $k_W = k_E = 3.54'$; $M = 28.33'\text{-k}$;

$L_u = 12.92'$

III.-B $\frac{L''}{r} = \frac{(12.92/2)(12)}{1.2} \doteq 65$, $F_a = 14.95$ ksi.

$$e = \frac{(M + M_{max})\frac{SF_b}{AF_a}}{2SF_b + (M - M_{max})} = \frac{(28.33 + 64.00)\frac{17(20)}{5.88(14.95)}}{\frac{2(17)(20)}{12} + (28.33 - 64.00)}$$

$$= 17.0'' = 1.417'$$

$$T = \frac{M + M_{max}}{2e} = \frac{(28.33 + 64.00)12}{2(17)} = 32.59^k$$

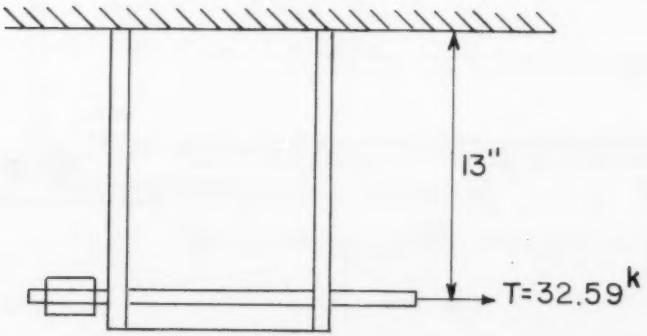

IV. $F_{max} = 16.29^{k}$

V. Cantilever Bracket

$$S = \frac{M}{f_c} = \frac{13(32.59)}{20} = 21.2 \text{ in}^3$$

Use: 12B19 ... 21.4 in^3

Shear: $\frac{32.59}{12.16(.24)} = 11.17 < 13$ O.K.

$$B.F. = 2E_b I_b \int \frac{m^2 ds}{E_a I_a} = \frac{2x^3}{3} \frac{I_b}{I_a} \int_0^{1.08}$$

$$= .667(1.08)^3 \frac{(69.2)}{(130.1)} = 0.447 \text{ insignificant}$$

Weight: $\frac{2(13)19}{12} = 41.17\#$

$$A_c = \frac{T}{f_c} = \frac{32.59}{100} = 0.326 \text{ in}^2$$

$$H = \frac{Pe(ab - k^2)}{L_u(e^2 + \frac{I}{A} + \frac{I}{A_c})} = \frac{8(1.417)\left[8(12) - (3.54)^2\right]}{12.92\left[(1.417)^2 + \frac{69.2}{144(5.88)} + \frac{69.2}{144(.326)}\right]} = 20.55^{k}$$

$H + F_{max} = 20.55 + 16.29 = 36.84 > T = 32.59$ ... O.K.

VI. $F = T - H = 32.59 - 20.55 = 12.04^{k}$

Weight Saved:

Cable $14.92(3.4)(.326)$ =	16.54	14WF30: $20(30) = 600.00\#$
Bracket ..... =	41.17	
Beam section... $20(20)$ =	400.00	
	457.71#	

$$\frac{600.00 - 457.71}{600.00} \times 100 = \frac{142.29}{600.00} \times 100 = 23.7\%$$

Example 3.

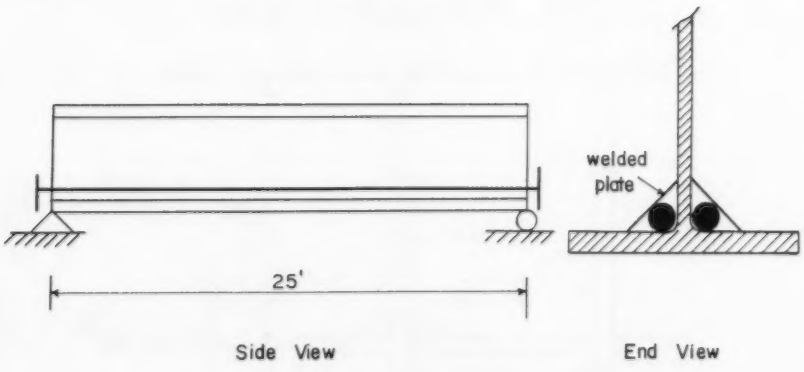

(1) Lateral support at center (both flanges).
(2) Cable attached to top of the lower flange.
(3) f_c = 100,000 psi.; Modulus of elasticity for all members: E = 30,000,000 psi.
(4) Examine a 24WF76 - A.I.S.C. specifications for stresses.
(5) $k_W = k_E = 0$

Moment-Weight Ratio ..... Without Prestressing:

24WF76: $A = 22.37\ in^2$, $S = 175.4\ in^3$, $\frac{d}{bt} = 3.90$, ... $F_b = 20$ ksi.

$$R \equiv \frac{M_{max}}{wt./ft.} = \frac{SF_b}{wt./ft.} = \frac{175.4(20)}{76} = 46.158\ \text{in.-k}/\frac{\#}{ft}$$

Moment-Weight Ratio ..... With Prestressing:

$F_a = 20$ ksi., $M_D = \frac{M_{max}}{2}$, $P_D = \frac{M_{max}}{2e}$, $e = \frac{23.91}{2} - .682 - .500 = 10.773"$

$$\frac{f_a}{F_a} + \frac{f_b}{F_b} = \frac{M_{max}}{2eAF_a} + \frac{M_{max}}{2SF_b} = 1; \quad M_{max} = \frac{2SF_bAF_ae}{eAF_a + SF_b}$$

$$M_{max} = \frac{2(175.4)(20)(22.37)(20)(10.773)}{10.773(22.37)(20) + 175.4(20)}$$

$$M_{max} = 4060.60\ \text{in-k}$$

$$P_D = \frac{M_{max}}{2e} = \frac{4060.60}{2(10.773)} = 188.46^k$$

$$A_c = \frac{P_D}{f_c} = \frac{188.46}{100} = 1.885\ in^2; \quad Wt./ft. = 76 + 3.4(1.885) = 82.409\ \#/ft.$$

$$R' \equiv \frac{M_{max}}{wt./ft.} = \frac{4060.60}{82.409} = 49.274\ \text{in-k}/\frac{\#}{ft}$$

Increase in R by Prestressing:

$$\frac{49.274 - 46.158}{46.158} \times 100 = 6.75\%$$

With cable attached to the bottom of the lower flange:

$e = 12.455"$; $M_{max} = 4305.52$ in-k; $P_D = 172.84^k$; $A_c = 1.728\ in^2$

$Wt./ft. = 76 + 3.4(1.728) = 81.875\ \#/ft.$

$R = 52.586\ \text{in-k}/\frac{\#}{ft.}$

Increase in R by Prestressing:

$$\frac{52.586 - 46.158}{46.158} \times 100 = 13.93\%$$

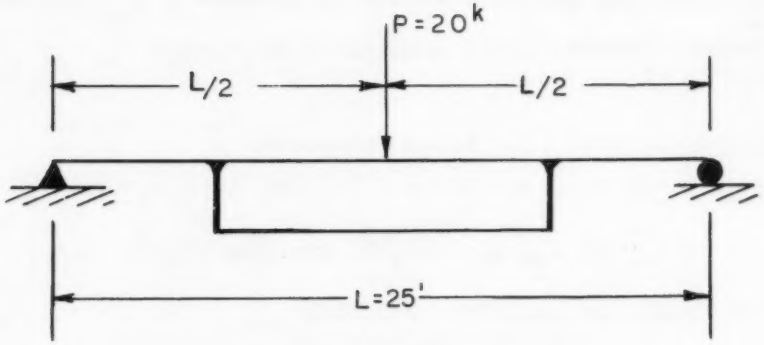

e	Beam Section	A_c in.^{2}	Equiv. Cable Wt. /Ft.	Equiv. Bracket Wt. /Ft.	Total Depth (e+d/2)	Percentage Wt. Saved	
8.0"	14WF48	3.48	4.20 #/Ft.	--------	15.0"	10.0%	Laterally Unsupported Conventional Design 12WF58
7.0	10WF49	1.73	1.60	--------	12.0	12.8%	
12.0	10WF45	0.79	0.96	1.26 #/Ft.	17.0	18.6%	
12.0	12WF45	1.22	1.67	1.00	18.0	17.8%	
18.0	10WF39	0.61	1.09	2.60	23.0	26.4%	
24.0	10WF39	0.42	0.75	3.30	29.0	25.8%	
33.05	8WF35	0.32	0.79	4.36	37.05	30.8%	
8.0	14WF38	4.81	4.45	--------	15.05	15.1%	Laterally Braced at the Center Conventional Design 16WF50
9.0	16WF40	0.97	0.80	--------	17.0	18.4%	
12.0	12WF40	0.76	0.80	1.00	18.0	16.4%	
12.0	14WF38	0.72	0.67	0.70	19.0	21.2%	
12.0	16WF36	4.15	6.11	0.51	20.0	14.8%	
12.0	12WF36	1.40	1.89	1.08	18.0	22.1%	
18.0	12WF31	0.59	0.95	2.40	24.0	31.3%	
24.0	12WF31	0.40	0.81	2.87	30.0	30.6%	
30.0	14WF30	0.47	1.14	3.69	37.0	30.4%	
8.5	16WF40	0.82	0.40	--------	16.5	19.2%	Laterally Braced Entire Length Conventional Design 16WF50
12.0	16WF36	0.61	0.52	0.37	20.0	26.2%	
12.0	14WF34	0.79	0.94	0.70	19.0	28.7%	
12.0	14WF30	2.20	3.30	0.73	19.0	31.9%	
18.14	12WF27	0.71	1.31	2.40	24.14	38.6%	
24.0	12WF27	0.43	0.97	4.58	30.0	34.9%	

TABLE 2 - TYPICAL DESIGNS OF PRESTRESSED TRUSS-BEAMS

CONCLUSION

The major disadvantage of the prestressed truss-beam is the depth required for it to be effective. Equation (5) indicates that no improvement results from prestressing an ideal bending member without increasing its total depth. The technique described herein essentially reinforces a given beam, therefore, an assortment of sections is required for designing. A "trial and error" method is used to select a beam from this assortment which produces the lightest structure. When designing with rolled sections substantial savings in weight are achieved by prestressing. This procedure is applicable where depth limitations are not severe or when it is possible to utilize the space between the lower flange and the tie rod for pipes, ducts, etc. Stresses produced by differential settlement and temperature changes in continuous beams are non-existent in the truss-beam. The laborious problem of influence calculations for continuous beams has a simple counterpart in the structure considered in this paper.

REFERENCES

1. Fritz, B., Prestressed Steel Structures (in German), Bauingenieur 27, 3, 99-100, March, 1952.
2. Magnel, G., Precompressed Steelwork (in French), Publ. Int. Assn. Bridge Struct. Engng. 11, 325-336, 1951.
3. Magnel, G., Prestressed Steel (new considerations) (in French), Ossature Metallique 15, 9, 428-435, Sept. 1950.
4. Magnel, G., Structures in Precompressed Steel (in French), Ossature Metallique 15, 6, 300-313, June, 1950.
5. Soete, W., Possibilities of the Prestressing of Metallic Constructions. Trans. of Inst. of Weld., vol. 14, Oct., 1951, pp. 161-167; disc. pp. 167-168.
6. American Institute of Steel Construction, Steel Construction Manual, 1954.

APPENDIX A - NOTATION

A_c	Cross section area of cable or tie rod
A	Area of beam section
b	Width of rolled section (compression flange)
c	Distance from the centroid of a beam to the extreme fibers
d	Depth of a beam section
e	Eccentricity of cable with respect to the centroid of a beam section
E	Modulus of elasticity
E_a	Modulus of elasticity of the brackets
E_b	Modulus of elasticity of the beam
E_c	Modulus of elasticity of the cable

f_a	Unit axial stress
f_b	Bending unit stress
f_c	Allowable cable stress
F	Force due to prestress
F_a	Axial unit stress permitted if axial stress alone existed
F_b	Bending unit stress permitted if bending stress alone existed
F_{max}	Maximum allowable prestress force
F'_{max}	Remaining maximum allowable prestress after creep losses
H	Tie rod stress produced by indeterminacy
I_a	Moment of inertia of the brackets
I, I_b	Maximum moment of inertia of a beam cross section
I'	I for an ideal bending member
$k_{W, E}$	Distances from the left and right ends of a beam to the nearest bracket
L	Length of span
L_u	Distance between brackets or unsupported length for bending
L''	Unsupported length for axial buckling
$M_{(x)}$	Bending moment at any point along a simple beam
M_{DL}	Bending moment due to dead load
M_{max}	Maximum bending moment in a simple beam
$M_{W, E}$	Positive bending moments at brackets
M_D	Design moment
m	Virtual bending moment at any cross section caused by a unit load
P_D	Axial design load
R & R'	Moment-weight ratios
r	Radius of gyration
S	Section modulus
S'	Section modulus of ideal bending member
T	Minimum permissible value of the quantity (F + H)
t	Thickness of the compression flange of a rolled section
u	Virtual axial stress caused by a unit load
$\delta_{LL}(x)$	Live load deflection of a simple beam
Δ LL	Live load deflection of a prestressed truss-beam

APPENDIX B - VALUES OF H

$$H = \frac{\frac{Pe}{2L}\left[abL - bk_W^2 - ak_E^2\right]}{(L - k_W - k_E)\left[e^2 + \frac{I}{A} + \frac{I}{A_c}\frac{E_b}{E_c}\right]} \qquad k_W \leq a \leq L - k_E$$

$$H = \frac{\frac{Pae}{2L}\left[(L - k_W)^2 - k_E^2\right]}{(L - k_W - k_E)\left[e^2 + \frac{I}{A} + \frac{I}{A_c}\frac{E_b}{E_c}\right]} \qquad 0 \leq a \leq k_W$$

$$H = \frac{\frac{we}{12}\left[L^3 - 3Lk_W^2 - 3Lk_E^2 + 2k_W^3 + 2k_E^3\right]}{(L - k_W - k_E)\left[e^2 + \frac{I}{A} + \frac{I}{A_c}\frac{E_b}{E_c}\right]}$$

$$H = \frac{\frac{We}{12L^2}\left[L^4 - 2L^2(k_W^2 + 2k_E^2) + 4Lk_E^3 - k_E^4 + k_W^4\right]}{(L - k_W - k_E)\left[e^2 + \frac{I}{A} + \frac{I}{A_c}\frac{E_b}{E_c}\right]}$$

W ... total load

$$H = \frac{\frac{We}{12L^2}\left[5L^4 - 12L^2(k_W^2 + k_E^2) + 8(k_W^4 + k_E^4)\right]}{(L - k_W - k_E)\left[e^2 + \frac{I}{A} + \frac{I}{A_c}\frac{E_b}{E_c}\right]}$$

W ... total load

Note: For brackets over twelve inches long add a bracket factor to the denominator.

$$\text{B.F.} = 2E_bI_b\left[\sum \frac{u^2L}{A_aE_a} + \int \frac{m^2ds}{E_aI_a}\right]$$

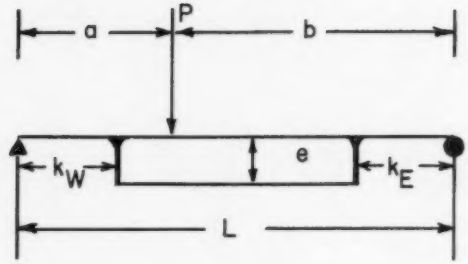
a
P
b
e
k_W
k_E
L

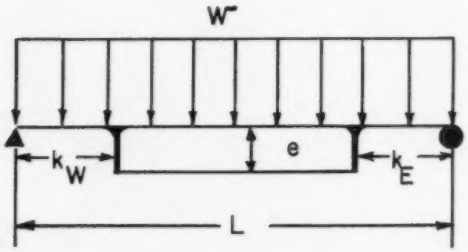
W
e
k_W
k_E
L

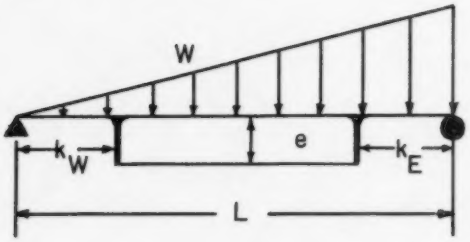
W
e
k_W
k_E
L

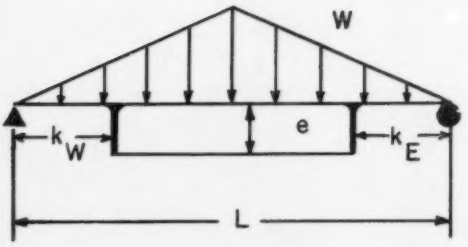
W
e
k_W
k_E
L

Journal of the
STRUCTURAL DIVISION
Proceedings of the American Society of Civil Engineers

CONTENTS

DISCUSSION
(Proc. Paper 1192)

Page

Plastic Strength of Steel Frames, by Lynn S. Beedle. (Proc. Paper 764. Prior discussion: 878, 924. Discussion closed.)
by Lynn S. Beedle (Closure) 1192-3

Determining Basic Wind Loads, by George F. Collins. (Proc. Paper 825. Prior discussion: 972. Discussion closed.)
by George F. Collins (Closure) 1192-7

Introduction to Semi-Rigid Determinate Polygonal Trusses, by Alexander H. Kenigsberg. (Proc. Paper 828. Prior discussion: 878, 972. Discussion closed.)
by Alexander H. Kenigsberg (Closure) 1192-9

Influence Lines for Reactions of Continuous Beams, by Andrew John Pyka. (Proc. Paper 914. Prior discussion: 1067, 1112. Discussion closed.)
by Andrew John Pyka (Closure) 1192-25

Tests on Bolted Connections in Light Gage Steel, by George Winter. (Proc. Paper 920. Prior discussion: 1112. Discussion closed.)
by George Winter (Closure) 1192-35

The Load Distribution in Highway Bridge Decks, by A. W. Hendry and L. G. Jaeger. (Proc. Paper 1023. Prior discussion: none. Discussion closed.)
by Pranab Kumar Chaudhuri 1192-37

(Over)

Note: Paper 1192 is part of the copyrighted Journal of the Structural Division of the American Society of Civil Engineers, Vol. 83, ST 2, March, 1957.

Page

Stresses in Pressure Pipelines and Protective Casing Pipes, by M. G. Spangler. (Proc. Paper 1054. Prior discussion: none. Discussion closed.)
by A. A. Eremin 1192-41
by C. Neufeld 1192-41
by E. A. Richardson 1192-43

Prestressed Continuous Beams and Frames, by P. B. Morice and H. E. Lewis. (Proc. Paper 1055. Prior discussion: none. Discussion closed.)
by E. L. Kemp and A. H. Mattock 1192-47
by Dean C. Kamaras 1192-54

Hyperbolic Paraboloids and Other Shells of Double Curvature, by Alfred L. Parme. (Proc. Paper 1057. Prior discussion: none. Discussion closed.)
by T. Au 1192-57
by W. Watters Pagon 1192-59
by Sandi Pado Bannerjee 1192-59
by M. G. Salvadori 1192-62

Moment Distribution Constants from Models, by Otakar Ondra. (Proc. Paper 1058. Prior discussion: none. Discussion closed.)
by John C. Murphy 1192-67
by Thomas D. Y. Fok 1192-69

The Painting of Structural Steel, by E. J. Ruble. (Proc. Paper 1100. Prior discussion: none. Discussion open until April 1, 1957.)
by Ludwig Adams 1192-77

Simplified Analysis of Rigid Frames, by Robert M. Barnoff. (Proc. Paper 1106. Prior discussion: none. Discussion open until April 1, 1957.)
by Thein Wah 1192-79

Discussion of
"PLASTIC STRENGTH OF STEEL FRAMES"

by Lynn S. Beedle
(Proc. Paper 764)

LYNN S. BEEDLE,[1] A.M. ASCE. — Mr. Benjamin has brought up a number of topics which are important but which could not be covered in a brief article designed to document the applicability of plastic analysis to structural design. Concerning joint details, the discusser correctly points out that much of the information developed could be applied in elastic design. Figs. 5, 12, and 13 in the paper are cases in point, and further information with regard to such details may be found in Refs. 12, 13, and in chapter 10 of Ref. 14.

The author intended to leave the impression that the profession could safely adopt plastic design for certain steel structures. Of course, it will not replace all other design procedures; sometimes the design criterion will be fatigue, or buckling, or notch toughness. But in ordinary building construction such limitations are the exception. Already in England, plastic design has been used on a considerable number of structures(15) and one building was erected in Canada according to a design based on the plastic method.

Mr. Benjamin mentions the lack of information on members where a considerable length is in the plastic region. On the contrary, most of the tests have been conducted on members with one-third or more of the span was under pure bending or in a condition approaching it. This is true of the examples shown in Fig. 2, 3, 14b, 15 all of the "Lehigh tests" of Fig. 22, and all of the tests of Fig. 23. Since this "pure bending" condition is not ordinarily found in practice, the typical behavior will usually be better than that evidenced by most of these tests.

The other type of member mentioned is the tapered beam. It is true that studies of such beams have not been completed (although tests of their lateral buckling characteristics are underway at Columbia University). However, plastic design achieves its economy without the necessity for tapering the members. On the other hand, if there are instances where tapering might be desirable for other reasons, then such a beam can be analysed without difficulty by the plastic methods. This is illustrated by the following example in which a comparison is made on the basis of a uniformly-loaded, fixed-ended beam of forty-foot span. Two possible solutions will be examined; the load may be supported by a uniform member or by one tapered from the ends to midspan. In the first instance, a 30 WF 108 beam ($S = 299.2$ in^3, $Z = 340$ in^3) on a 40-ft. span will support a total distributed load of 375 kips according to Eq. (3),

$$\frac{P_u L}{8} = 2 M_p \qquad (3)$$

1. Assoc. Prof. and Chairman of Structural Eng. Div., Fritz Eng. Lab., Lehigh University, Bethlehem, Pa.

How will a tapered beam compare? In analysing the tapered member, equilibrium of moment requires that

$$\frac{P_u L}{8} = M_{p1} + M_{p2} = 2M_{p(WF)}$$

where M_{p1} and M_{p2} are plastic moments at the ends and center, respectively, and $M_{p(WF)}$ is the plastic modulus of the 30 WF 108 member. It is assumed that the member has a uniform taper, smaller at the center, and symmetrical about the center line. The ratio of M_{p1} and M_{p2} can be selected as any reasonable value, say $M_{p1} = 3\ M_{p2}$. Since the plastic modulus, Z, bears a linear relationship to M_p (Eq. 1), then $Z_1 = 3Z_2 = \frac{3}{2}\ Z_{WF}$.

For a built-up member the value of Z may be determined from

$$Z = 2 \int_0^{d/2} y\, dA$$

$$Z = bt(d-t) + \frac{w}{4}(d-2t)^2 \qquad (8)$$

where Z is the required plastic modulus, b the flange width, t the flange thickness, w the web thickness, and d the depth of the member. If the flange dimensions and the web thickness are selected to be about what would be found for such members (b = 11.0", t = .75", w = .625"), then the only unknown in Eq. (8) is the depth, d, which may be obtained by solving the following quadratic (solution of Eq. (8)):

$$\frac{w}{4}d^2 + dt(b-w) - (Z + t^2(b-w)) = 0 \qquad (9)$$

For $Z_1 = \frac{3}{2} Z_{WF} = 510\ in^3$ and $Z_2 = \frac{1}{2} Z_{WF} = 170\ in^3$, the required depth at the ends is 38-in. and that at the center is 16.8-in.

Comparing the weight of the two beams, the uniform member, according to the plastic design, weighs 4320#. The weight of the plastically designed tapered beam is 4440#. Thus the two designs end up at about the same weight with a slight advantage (3%) for the uniform member. Of course there would have to be added to this the additional fabrication cost for the tapered member. Incidentally, conventional elastic design of the uniform beam would have required a section modulus of 429 in^3. A 33 WF 141 section would have been used, the total weight being 5640# or an increase of 31% over the similar plastic design. In addition to showing the economy of material of plastic over elastic design, this example demonstrates that plastic design achieves economy without the necessity of tapering the members.

A discussion of load factors was particularly avoided in the paper. While studies of the maximum strength of structures will be helpful in arriving at a rational load factor, many other factors also enter into the problem. Rather than confuse the presentation of plastic behavior of structures with a discussion of the factor of safety—a discussion, incidentally, which is equally applicable to conventional elastic design—the factor of safety was selected in the paper on the basis that "ultimate load as the design criterion provides at least the same margin of reserve strength as is presently afforded in the

conventional design of simple beams." Depending on the shape factor selected, this value could vary from 1.75 to 2.03; the former was chosen in the paper for illustration.

Concerning "office design costs," the techniques are relatively simple and are being learned by many practicing engineers. But the task of instruction and education belongs with the colleges and universities, and many now include the subject in their curricula.

The matter of code revisions comes up frequently. What form should a code or specification for plastic design take? A complete revision may not be necessary. In England and in Australia, specifications now permit use of the method, and this was done simply by adoption of an "enabling clause." A similar approach might be used in this country. Of course such a provision would be preceded by surveys and evaluations. Refs. 4, 8, 10, 14, and 16 are examples. Two other documents eventually are required and work is underway on each:

1) Rules of practice (with commentary) for plastic design
2) A manual of design examples.

The former will include a justification of provisions, a documentation by the inclusion of test results, and a summary of procedures. Ref 4 constituted a first step in the completion of the task of formulating such "rules of practice." It has now been taken on as a joint project of the ASCE (Committee on Plasticity Related to Design) and the Welding Research Council (Structural Steel Committee, Lehigh Project Subcommittee). The report is now being drafted. Work on the Manual of Design Examples is currently under way in the offices of the American Institute of Steel Construction of which T. R. Higgins is Director of Engineering and Research. Documents such as these should go far towards speeding the day when plastic design will be more frequently used by engineers.

Mr. Sobotka's discussion unfortunately contains an error in the formulation of equilibrium equations (1), (2), (7), and (8). All of the forces acting on the "free bodies" were not included in the moment calculation. In general, a vertical shear force is present at section C whenever the member is tapered. Of course, if the member AB had been of uniform strength in the examples, then the shear force would truly have been zero at section C even if the moments at A and B were dissimilar. In the tapered beam example cited earlier, the plastic hinge forms at the point of maximum moment (and zero shear) only because of the particular symmetrical arrangement chosen. Had the beam been tapered in the other direction (deeper at center than at ends) the hinge would not have formed at the center. Instead, two hinges would have formed simultaneously to left and right of center at those points where the moment capacity of the beam was just equal to the required statical moment of the member. The shear is of course not zero at those points. This simply underscores that the variation in moment capacity with distance along the beam must be considered in determining the location of plastic hinges therein.

Mr. Sobotka's "method of forces" is the same as the "semi-graphical equilibrium method" noted on page 764-26, described in detail by Ref 5, and used to solve the fixed-ended beam problem (See Eq. (3)).

In closing, the author would like to thank Mr. Benjamin and Mr. Sobotka for the interesting points they have raised.

REFERENCES

13. Toprac, A.A., Johnston, B.G. Beedle, L.S. "CONNECTIONS FOR WELDED CONTINUOUS PORTAL FRAMES," Weld. Jour. 30(7), 30(8), and 31(11), 1951 and 1952.

14. Beedle, L.S. Thurlimann, B. Ketter, R.L. "PLASTIC DESIGN IN STRUCTURAL STEEL," Lecture Notes, AISC-Lehigh Univ., Sept. 1955.

15. Little, D.H. Smith, A.A. "SOME STEEL STRUCTURAL FRAMES DESIGNED ON PLASTIC THEORY" Proc. Instn. Civ. Engrs., Paper #44, May, 1955.

16. A.I.S.C. "PLASTIC DESIGN IN STEEL" Proc. Nat'l Engr. Conf. AISC, April, 1956.

Discussion of
"DETERMINING BASIC WIND LOADS"

by George F. Collins
(Proc. Paper 825)

GEORGE F. COLLINS.[2] — The writer did not mean to imply in his paper that the only difficulty in designing for wind loads has been the correct evaluation of the precise wind velocities. He agrees with Mr. Hainlin that assigning the proper "form factor" is also very difficult. The writer did state, however, that his study was restricted to the first step—the determination of wind-load variation with elevation.

The writer also agrees with Mr. Hainlin's second point that the worst winds are often accompanied by heavy rain and hence the impact load is greater than if the wind occurred without rain. Dr. H. E. Landsberg, Chief, Climatological Services Division, U.S. Weather Bureau, has made this same point.

Mr. Rathbone has extrapolated the writer's Figure 5 to much higher wind speeds than ordinarily observed. It is unlikely that a sustained wind of 120 miles per hour at 30 ft. elevation would ever be encountered except possibly at sea. The writer's curve can be said to fit the storms studied with a high degree of reliability at the elevations of most structures. They may not apply to extremely high television and radio towers. Here it is possible that the velocity profile might, on occasion, reverse and decrease with elevation. It is agreed that Figure 5 will not cover all cases and many more actual field observations should be made on tall towers, preferably with pressure-tube type anemometers. The 1500 to 2000 ft. level is usually considered by meteorologists to be the "gradient wind level" or the point at which surface friction largely disappears and the wind speed and direction is dependent entirely on the horizontal atmospheric pressure gradient.

There have been several theoretical formulas proposed which give a very good fit to actually observed wind profiles (References 2-11, Paper 825). These techniques take into account the stability of the atmosphere and therefore require knowledge of the vertical temperature distribution. Unfortunately, information of this type is not readily available. Perhaps the best approach would be to take the highest wind on record for a location and assume a pseudo-adiabatic lapse rate and apply to one of the aforementioned formulas such as that proposed by Deacon. (A pseudo-adiabatic lapse rate is a vertical temperature distribution such as found in stormy areas where a rising air parcel experiences a temperature decrease with increase in elevation at a dry adiabatic rate until the dew point is reached. At this point the heat of condensation is added to the rising column of air and the decrease is at a lower rate.)

The writer agrees wholeheartedly that the case is far from "closed."

---

2. Eng. Dept., E.I. duPont de Nemours & Co., Inc., Wilmington, Del.

Discussion of
"INTRODUCTION TO SEMI-RIGID DETERMINATE POLYGONAL TRUSSES"

by Alexander H. Kenigsberg
(Proc. Paper 828)

ALEXANDER H. KENIGSBERG,[3] M. ASCE. — The writer wishes to express his appreciation to Messrs. Berg, Lane and Prof. Scordelis for their interest in his polygonal web trusses. Their comments have been interesting, instructive and stimulating. He is particularly grateful to Mr. Lane for the opening remark to his extensive comments that "the new and untried must go through the objection and obstruction stage of criticism prior to its turning into beneficial development for the betterment of those concerned" — for this has been the primary object of the basic presentation and the present closure.

Mr. Berg is right, of course, in pointing out that, in the paper's example, the moment at the M-joint of M10L10 becomes +826 in-kips, in place of the stated -3,053 in-kips, under the combination of partial live load on the left portion of the span and concentrated live load at the L8 joint. While the reversal in the direction of the moment would still be of no significance in the design of the bars of segment YM10, in the sense that reversal from tensile to compressive stress affects the design of members of axially stressed conventional trusses, the error is regretted, nevertheless, especially since it is inconsistent with the subsequent statement in the paper that "steps represented by diagram (d) for partial loading and diagram (e) for concentrated loads. . . . may have to be employed to establish critical design conditions."

In view of Mr. Berg's doubts as to the validity of the claim in the paper that "both initial and reserve strengths (of polygonal trusses) virtually eliminate the possibility of structural failure under any conceivable conditions of loading" the statement is here substantiated by an examination of the stresses in the simple hypothetical truss dealt with in the paper, and would certainly be enhanced in actual all-rigid construction. Thus, the live load stresses in any of the members of the semi-rigid truss are not over one-third of the 18,000 psi allowable under AASHO Specifications. If loaded, at any point and any time to 33,000 psi., just under the yield point and theoretical plastic hinge stress for ordinary steels, the additional uniform live load, still "safely" to be carried by the bridge, would amount to (33,000-18,000) divided by 6,000, or 2.5 times the design live load. Further, since maximum stress conditions are not concurrent in any group of adjoining members, redistribution of stress, when yielding is reached in any member, would increase the group resistance to structural failure well above the indicated 250% conceivable increase in loading. Further, Mr. Berg is right in observing that "the top chord could be removed completely without impairing the

3. Civ. and Structural Engr., Nashville Dist., Corps of Engrs., U.S. Dept. of the Army, Nashville, Tenn. (Retired)

stability of the structure if the web members were of sufficient strength and rigidity." While such construction would not be considered for practical reasons, the observation is viewed as another and direct confirmation of the validity of the claim which he seems to doubt, since it affirms "the fundamental concept of the rigid frame that distress in any of its members, (such as buckling in the said top chord) is instantly relieved by the other members."

The consideration by Mr. Berg of a plastic hinge at an M-joint is not germane to the case at hand for several reasons:

1) As already indicated, its formation can occur only after the stress had passed the elastic limit of the material, that is, beyond the implied limitation of "conceivable conditions of loading."

2) The hypothetical hinged truss of the paper obviously has no stability, whether the added hinge at an M-joint is plastic, as indicated by him in his Fig. 11, or real.

3) Formation of plastic hinges under critical loading implies a time element which, in general, is not present in truss structures subject to moving live loads.

4) It is felt that, with due respect to modern analytical approach, there is as yet a dearth of knowledge as to the actual behavior of polygonal trusses under load within the range of elastic limits.

5) While the plastic hinge is a convenient and useful concept in the analysis of structural behavior of rigid frames, its formation at an M-joint of a polygonal truss does not appear to be a realistic approach. It is believed that, under critical stress conditions, the formation of a collapse mechanism at an M-joint would be preceded by a tendency to form a series of plastic hinges all around the joint, and these, in turn, would likely be preceded by buckling failure of the compression flanges.[4] Similar developments would be anticipated also at the chord joints of the truss, when restrained, since the stiffness of a truss joint is necessarily much greater than that of its entering members. And, finally,

6) While it is confidently expected that the novel trusses would reveal exceptional reserve strength beyond the elastic limit of the material, the technique of plastic hinges has not been adequately extended to be applied with certainty to complex rigid frames, such as long polygonal trusses.

Messrs. Berg and Scordelis dwelt at length on the writer's omission of the deflections due to bending in the web system of the hypothetical truss of the paper. In compliance with Mr. Berg's indicated desire, these deflections are now furnished in detail in Table 5. It can be observed that the 5.45 inch theoretical moment deflection is only 1.77 times the 3.08 inch deflection (Table 2 of the paper) induced in the same truss by the axial stresses alone, although it is several times as great as applied to the web system, as correctly anticipated by Mr. Berg.

It is significant, however, that on the same basis, the hypothetical shallow truss, Fig 5(c) in the basic paper, would be deflected only 4.4 inches by the bending stresses in its web members and 3.38 inches by the axial stresses. Thus, while its height at the center is reduced to 28 ft. versus 44 ft. for the high truss of Fig. 5(a), its total theoretical deflection is actually less, namely: 7.78 inches for the former vs. 8.53 inches for the latter.

4. "Elastic-Plastic Design of Single-Span Beams and Frames," H.A. Sawyer, Jr., M. ASCE, Sep. No. 851, p.2, Failure Source (c).

TABLE 5

DEAD LOAD DEFLECTION AT L10 DUE TO MOMENTS

Bar	L inches	D.L. Moments in-kips	Mean I in.	$\frac{LM}{31}$	m10 in-lbs	$\frac{LM}{31}$ m10
1	2	3	4	5	6	7
U1U1'	-	0	-	-	-	-
L0L0'	-	0	-	-	-	-
M2L2	210	49,959	31,925	109.6	83.8	9,180
M4L4	210	29,216	19,700	103.9	67.2	6,975
M6L6	222	18,186	10,040	134.0	65.0	8,710
M8L8	228	9,846	6,500	115.2	66.8	7,690
M10L10	240	3,053	2,800	87.3	1.9	165
M10'L10'	240	3,053	2,800	87.3	63.6	5,550
M8'L8'	228	9,846	6,500	115.2	56.1	6,460
M6'L6'	222	18,186	10,040	134.0	54.4	7,285
M4'L4'	210	29,216	19,700	103.9	56.1	5,830
M2'L2'	210	49,959	31,925	109.6	70.0	7,665
U1M2	216	29,946	19,700	109.5	50.3	5,510
M2U3	261	20,013	12,700	137.0	33.5	4,585
U3M4	261	16,690	10,570	137.4	38.4	5,275
M4U5	302	12,526	7,475	168.5	28.8	4,850
U5M6	292	10,101	4,758	206.5	36.1	7,450
M6U7	322	8,086	4,758	182.5	28.9	5,270
U7M8	317	5,368	3,100	183.0	36.4	6,660
M8U9	336	4,477	2,500	200.5	30.4	6,090
U9M10	325.5	1,600	1,300	133.5	1.0	134
M10U11	332.4	1,453	1,300	123.8	0.9	111
U11M10'	332.4	1,453	1,300	123.8	30.3	3,750
M10'U9'	325.5	1,600	1,300	133.5	33.3	4,450
U9'M8'	336	4,477	2,500	200.5	25.5	5,110
M8'U7'	317	5,368	3,100	183.0	30.6	5,600
U7'M6'	322	8,086	4,758	182.5	24.2	4,420
M6'U5'	292	10,101	4,758	206.5	30.2	6,230
U5'M4'	302	12,526	7,475	168.5	24.1	4,060
M4'U3'	261	16,690	10,570	137.4	32.0	4,400
U3'M2'	261	20,013	12,700	137.0	28.0	3,835
M2'U1'	216	29,946	19,700	109.5	42.0	4,600
Total	-	-	-	-	-	157,900

At L10, deflection $D = \frac{157,900 \times 1,000}{29,000,000} = 5.45$ in.

Notes: 1. For deflection at L10 due to axial stresses see Table 2.

2. The bending stresses m10 due to unit load at L10 are obtained in the same manner as actual bending stresses in the truss members.

In passing, it seems worth noting that, in an actual pentagonal truss having restrained joints throughout, the values of L, A, I, M and m10 would be materially different from those given in Tables 2 and 5 and would have relatively large influence in reducing the magnitude of the deflections due to bending. An estimate of the resulting deflections of an all-rigid truss indicates that the corresponding theoretical values by elastic analysis would be approximately: $d_{m10} = 2.4$ in., $d_{u10} = 2.5$ in. and total $D_{L10} = 4.9$ in.

Evidently truss deflections, per se, would actually be of small concern and can be readily provided for in fabrication, similarly to the camber provisions for girders and conventional trusses.

In his Figs. 1, 2 and 3 and Tables 1 and 2 Prof. Scordelis investigated a polygonal and an equivalent Warren type truss for the purpose of comparing their relative deflections and stress distributions, using for the polygonal truss both "exact and approximate methods of analysis. In the belief that "they would not change the conclusions," he assigned identical A and I values to each and every member of the two trusses. Unfortunately, the arbitrary figures actually result in disproportionate and misleading values with respect to the relative magnitudes of the deflections and in addition, reveal unorthodox distribution of the stresses. First, the stated magnitudes are overrated for the pentagonal truss and underrated for the Warren truss. This can be readily established by inspection of the pertinent data in his tables in which, under comparable stresses, the axial deflections alone are considerably larger for the polygonal than the Warren truss in spite of the appreciably shorter web system of the former.

In order to obtain more representative values for this comparison, there is compiled Table 6 which is, in fact, a recapitulation of his Tables 1 and 2, but having A and I values for the web members that are reasonably compatible with the types of stresses for the trusses under consideration. It can be observed from this table that the increase in the theoretical deflection of the polygonal truss over that of the Warren type is only about 14%, instead of the more than 100% increase indicated in his Tables 1 and 2. For the short, stiff trusses of comparison, the nominal 14% increase is evidently in line with their actual deformations. Since the total moment in the frames is a constant under the given loading condition, it seems more than a coincidence that the magnitudes of the deflections in the polygonal truss examples of Prof. Scordelis are essentially identical, (Tables 1 and 2) even though there is a marked difference in the stress patterns of its members (Figs 1 and 3) as obtained by him by the "exact" and approximate analyses.

In winding up the discussion of relative deflections it seems appropriate to invite attention to Mr. Morris Ojalvo's recent paper[5] in which are given the deflections of two identically loaded comparable trusses, 60 ft. span by 15 ft. center height, one a Vierendeel type and the other the writer's rigid pentagonal type. For the Vierendeel he determined the center deflection to be 1.48 in., 95% of which is due to bending, while for the pentagonal truss it is only 0.60 in., 85% due to bending. These figures are theoretical values and do not include deflections due to shear, which are relatively substantial in Vierendeel frames since normal truss shears are carried by them in flexure across the chord systems. Shear deflections are negligible in poly-

5. "Internal Ties in Slope Deflection and Moment Distribution," ASCE No. 1096, Tables 4 and 8.

TABLE 6

DEFLECTION OF POINT B IN POLYGONAL TRUSS, FIG. 3,

AND WARREN TRUSS, FIG. 2

Bar	L inches	A in^2	I in^4	Polygonal Truss Fig. 3				Warren Truss Fig. 2	
				S and u: kips	$\frac{uSL}{A}$	M and m: in-kips	$\int \frac{mMds}{I}$	S and u: kips	$\frac{uSL}{A}$
AB	96	1	40	.333	10.7	0	0	.333	10.7
BC	96	1	40	.500	24.0	0	0	.500	24.0
CD	96	1	40	.166	2.7	0	0	.166	2.7
AE	107	1	40	-.746	60.0	0	0	-.746	60.0
EF	96	1	40	-.916	80.6	0	0	-.666	42.7
FG	96	1	40	-.333	10.7	0	0	-.333	10.7
GD	107	1	40	-.373	15.0	0	0	-.373	15.0
BH	48	3	160	1.000	16.0	8.0	6.4	-	-
EH	68	2	80	.884	26.6	4.0	4.5	-	-
FH	68	2	80	.530	9.6	4.0	4.5	-	-
CI	48	3	160	0	0	16.0	25.6	-	-
FI	68	2	80	-.354	4.3	8.0	18.1	-	-
GI	68	2	80	.354	4.3	8.0	18.1	-	-
EB	107	1	40	-	-	-	-	.746	60.0
FB	107	0.5	25	-	-	-	-	.373	30.0
FC	107	0.5	25	-	-	-	-	-.373	30.0
GC	107	1	40	-	-	-	-	.373	15.0
Totals		-	-	-	264.5	-	77.2	-	300.8

Polygonal $D_p = (264.5 + 77.2)/E = 341.7/E$

Warren $D_w = 300.8/E$

Increase $D_p/D_w = (341.7 - 300.8)/300.8 = 13.6\%$

gonal trusses, in which the vertical shears are carried axially by the diagonals of the web system.

As to stress distribution, both Mr. Lane and Prof. Scordelis rightly call attention to the need of considering also the secondary stresses developed in the bars of the truss as a result of the deformations and joint rotations. Mr. Lane's concern that "the top chord shortening will induce unduly heavy secondary stresses in the upper arms of the wyes. . . and that increasing their section modulus would accentuate a vicious cycle (underscoring supplied) by means of which a part of top chord compression would be carried in uneconomical manner through the upper arms" seems to imply the inability of the frame to readjust itself to its internal stresses. This approach is untenable, as already indicated in the basic paper, (Truss Characteristics, item 2), since it is axiomatic that any Y-segment, properly designed to resist the primary stresses due to applied loads, will perform its function in such a manner that the total strain energy in the frame is a minimum. Contrarywise, it would imply that the strain energy, due to the secondary stresses in the frame is greater than that due to the external loads causing the deformations.

Examinations of stress distribution in polygonal trusses, particularly such as shown for the Y-segment EFHB of Prof. Scordelis' Fig. 1, reveal maldistribution due to such adjustment and/or the difficulties of "exact" analyses based on compatibility of deformations. Thus, since both arms of the Y are in tension under the given loading and their $K = I/L$ values are identical, it is inadmissible, on the basis of the theory of moment distribution at a joint, that one arm carry 5 times as large a portion of the total moment as the adjacent arm, namely: 6.67 in-kips in member HE versus only 1.33 in-kips in member HF. Only a small portion of the difference in these moments is chargeable to direct stresses which are of the same sense and constitute but a minor fraction of the total stress in members of the web system. Since the two conditions, moment distribution and compatibility of deformations at a joint, are fundamental to structural analysis, the imbalance in Prof. Scordelis' examples seems to point to a different analytical approach for polygonal web trusses, whose M-joints are unique, if the resulting data are to conform with the accepted concepts. Unquestionably, the actual effects of the deformations on the stress pattern present a difficult analytical problem for which the writer has no answer. However, a possible clue may be found in the statement of Mr. Lynn S. Beedle:[6] "It has been often demonstrated that elastic stress analysis cannot predict the real stress distribution in a building frame with anything like the degree of accuracy that is assumed in the design. The work done in England by Professor Baker[7] and his associates as a forerunner to their ultimate strength studies clearly indicates this in his paper 'Shortcomings of Structural Analysis'."

An increase in allowable stresses due to bending at rigid joints, as is done in bridge and building codes, obviously is not an answer to the problem at hand. Since stress distribution and deformation values of analyses by the elastic theory are known to be too severe as compared to those observed in test and actual structures, it is held that, pending the development of realistic analytical procedures for complex rigid frames, greater reliance will have to be placed on test data obtained from model studies of the polygonal structures.

---

6. "Plastic Strength of Steel Frames" Separate No. 764, p.2.
7. J.F. Baker, Trans. N.E. Coast Inst. Eng. Ship., Vol. 68 p. 31, 1951.

Of course, it is presumed such data, too, would be interpreted in the light of engineering experience, design assumptions, imperfections of materials and workmanship and other contingencies of fabrication, assembly and erection.

Mr. Lane's extensive observations are extremely interesting, encouraging and thought provoking. Some of them are well beyond the scope of the introductory paper, particularly those pertaining to Figs. 1(b), 2(b), 3(a) and (b) and 4, since they were introduced merely to illustrate a few simple embodiments of the novel type trusses; others, notably his suggestions and projections of hexagonal web trusses for double deck bridges, are indeed unique and are gratefully being added to the writer's own diversified conceptions for their applications; still others, as his thoughts about field applications for portable bridges by the military forces, have been receiving detailed study by the writer and are well taken. The following, as all these comments, are confined only to remarks pertaining to the pentagonal type trusses dealt with in the paper.

With respect to Mr. Lane's varied observations regarding the special treatment of the end panels, shown in Fig. 6 of the paper, it may be helpful to suggest that this is an optional arrangement, somewhat analogous to the midspan panels of Pratt type trusses in which it is economically advantageous to provide them with X-bracing in place of stiff single diagonals. However, in polygonal trusses there is the added significant advantage of virtual assurance against collapse of the structure from critical damage to the end posts by wayward vehicles.

Mr. Lane's several references, direct and indirect, to the economic aspects of the polygonal trusses are interesting. However, most of them are not concurred in, largely because the conjectures appear premature for the state of knowledge regarding the behavior of these trusses under load and their latent reserve strength and seem to ignore some salient facts. Thus:

1) It is true that the numbers of members and joints in polygonal trusses are larger than those of the main members and joints of ordinary span conventional trusses. However, these are all the members and joints required since polygonal trusses do not need secondary members that "stay" the main members of longer spans and subdivided panel Baltimore, Pettit and Warren type trusses in which these extra members were evidently omitted from Mr. Lane's summations of joints and bars.

2) The aggregate length of the members of the polygonal web systems is materially less. Thus the lengths of the web members of the high and shallow pentagonal trusses of the paper are only 80% and 60%, respectively, of the length of the web system in the prototype conventional truss.

3) The 90^{o} hanger joints to the bottom chords are materially simpler in fabrication and erection than the web-to-chord joints of conventional trusses.

4) Vierendeel trusses are not noted for their economy or simplicity of fabrication in spite of fewer members, yet their use is steadily growing.

5) Since Y-frames of polygonal web trusses can be assembled from continuous bent elements, their M-joints should be exceptionally economical. Thus, the shop joint M4 of Fig. 8, already relatively simply, when formed by continuous sections, would involve no excessive use of material, labor or number of parts that would render its cost prohibitive or even critical.

6) It is true that flexural members are heavier and more costly than axially stressed types. However, rigid frames have been displacing axially stressed frames, including trusses, in bridge and building construction, in

spite of their higher cost. Evidently, this must be attributed to their proven superiority structurally and esthetically. Further, rigidity of modern riveted bridge trusses is also accomplished at considerable expense over that of the prototype pin-connected trusses of but a generation or two ago.

7) The excessive weights of the pentagonal trusses given in Table 4 of the paper should not be viewed as a guide for actual designs for the following reasons:

a) In the hypothetical semi-rigid truss of the paper the moments induced by the horizontal shears are carried by the web members alone. When a portion of these moments, estimated to be about a third at each Y, is transferred to the chords in rigid trusses, the substantial weight of the web system would be reduced accordingly, without a correspondingly large increase in the weights of the chords, especially when the effects of gussets at the joints would likely be considered in the all-rigid structures. Fig. 13 and the section on Model Studies following these comments clearly indicate this to be the case. And,

b) Considerably larger unit stresses would undoubtedly be employed in rigid designs than the 18,000 psi allowable under AASHO Specifications and used in the paper truss.

8) When trusses are preassembled at the site and hoisted in toto into final position, the erection procedure for polygonal trusses would obviously be the same as for conventional types. In cantilever construction, when the bar-by-bar erection procedure is employed, it is questioned whether "the two members forming the triangular web frames of Warren, Pratt or Howe Trusses" are sufficiently self-supporting as an assembly, without the aid of temporary bracing, as would be the case with preassembled rigid Y-segments of polygonal trusses. It is also doubtful if the same two-member groups "would have a definite edge in time, labor and amount of scaffolding" since capacity of lifting equipment would not be a limiting factor and the auxiliary stiffening arrangements, usually required in conventional truss erection on account of stress reversals in their members, would not be needed in the case of polygonal trusses.

9) Since the strength of the materials is seldom developed in the usual compression members, the effectual elimination, in polygonal web trusses, of the problem of columns and their concomitant limitations in the design of conventional trusses,[8,9] permits a flexibility of panel spacing, truss heights and spans that may result in more economical rigid frame structures than indicated in the introductory paper. And,

10) As to Mr. Lane's general doubts whether "the writer's trusses could ever be competitive with long span tied arches or trusses requiring subdivided panels," it may be helpful to remember the historical fact that the ingenuity and skill of structural engineers have always asserted themselves heretofore in adapting novel ideas and are certain to reassert themselves in developing analytically and structurally sound and economically competitive polygonal trusses when their true merits are established, as confidently anticipated,

---

8. "Buckling of Trusses and Rigid Frames" by G. Winter, P.T. Hsu, B. Koo and M.H. Loh, Bulletin No. 36, Engineering Experiment Station, Cornell University, Ithaca, N.Y.
9. "A Survey of Progress 1944-1951" by Bruce G. Johnston, Bulletin No. 1, January, 1952, Column Research Council of Engineering Foundation.

by test data of large scale models, as also suggested by Mr. Lane.

In view of several allegations by the discussers which indicate undesirable misconceptions with respect to the true character of the trusses and design procedures, it is deemed proper to add here a few pertinent general clarifications to the purely technical aspects of the paper and the discussions:

1) In conventional frames, designations such as K-type, Warren or Vierendeel truss convey finite ideas as to their geometric configurations and corollary stress patterns. It is thought that the generic term "polygonal truss," or "polygonal web truss," as introduced in the paper, is completely descriptive in that, at the outset, it is shown to imply, basically, a serial combination of triangular frames with five- or six-sided polygons resulting in an intrinsically rigid truss structure by virtue of primary fixed joints midheight between its chords.

Accordingly, it is felt that labeling the new trusses in terms of semi-existing types tends to obscure, rather than contribute to, either the concept of their geometric formations or functional characteristics. It is conceivable that one may transform a Warren or Vierendeel type into a semblance of simple pentagonal truss by imaging their alternate chord joints moved up or down to a midheight position without, however, supplying any particular structural conception. It would be embarassing indeed to try to extend such a procedure to obtain the trusses of Figs. 2, 3 and 4 which picture, respectively, hexagonal, subdivided panel and double stem pentagonal trusses, or to any other derivations from the basic polygonal web types, let alone trusses with bent frames. From the engineer's standpoint it would seem simpler and more useful to think of the new structures as a distinct type of trusses, just as the familiar types of triangular web conventional and quadrangular frame Vierendeel trusses, each type having its characteristics, its merits and its applications.

2) Another source of confusion seems to arise from the indiscriminate use of the terms "stiff" and "rigid." Thus, to Mr. Berg the "claims concerning rigidity (evidently implying stiffness) seemed premature" and Prof. Scordelis "felt that the author leaves an erroneous impression that the polygonal truss is stiffer than a conventional truss. . . ." These misconceptions are deeply regretted since the writer meticulously avoided the employment of the term "stiffness" with respect to his trusses anywhere in the paper. In view of such misinterpretations it is hoped that the following venture into engineering semantics may prove beneficial.

We have stiff beams, girders and columns, if their I values are large relative to their lengths, and stiff trusses if their heights are large relative to their spans, even though they are pin-jointed. Conventional trusses are often spoken of as "rigid" if their joints are riveted or welded. This nomenclature is not applicable nowadays since, basically, they are axially stressed structures and unlike the modern true rigid frames and the Vierendeel trusses whose stresses are predominantly flexural. It should be clear that only the latter types are rigid frames even when they are too flexible to be labeled stiff frames, since their stability is dependent entirely on the rigidity of their members and joints, in full conformity with the concept of rigid frames.

Accordingly, it is maintained that the claims to rigidity of the polygonal trusses are as indicated throughout the paper.

3) Lastly, Mr. Lane directly, and Prof. Scordelis by implication, refer to the "author's method of designing the wyes as pin-ended and detailing simple connections. . . ." In spite of repeated statements in the paper and indication

in its heading that the semi-rigid hinged-chord arrangement was a hypothetical frame chosen for its simplicity in introducing and developing fundamentals of the novel type trusses and, by inference, to avoid involvement in the intricacies and controversies that would accompany the treatment of a complex all-rigid polygonal truss and defeat the primary object of the paper. For this reason it is emphasized here again that the analytical procedure of the paper for an idealized hinged truss is not proposed by the writer as a design procedure for actual rigid polygonal trusses. Instead, in view of the limitations of elastic analysis, it is advocated that reliable values of stress distribution and deflections in the untried structures be established first from adequate experimental data and then utilized to develop acceptable analytical procedures. Results of limited tests to data are given in the next section.

Model Studies

Since it may be of general interest and may help allay implied concern of the discussers regarding the behavior of the novel trusses, it seems relevant to refer now very briefly to exploratory studies that were carried out in 1954 on two models, as theses assignments, by two students at Massachusetts Institute of Technology under the general supervision of Dr. C. H. Norris, head of the Structural Laboratories.

The first, a celluloid model of a 5-panel all-rigid pentagonal truss, 9 in. high by 36 in. long, was tested by the Beggs deformation method for the general determination of stress patterns in the truss under different panel loadings. The results of the tests were reported by Mr. D. P. Sullivan in his unpublished thesis[10] for the degree of B.S.

The second model, an all-rigid welded structural steel frame, 52.5 in. high by 86.64 in. long, comprising a single Y-segment and designed for determining the stress distribution in its members and the ultimate capacity of its M-joint, was tested by means of a Riehle loading mechanism and Baldwin SR-4 type strain gages. The results of these tests and pertinent discussions of both model studies are contained in the unpublished thesis[11] for M.S. degree by Mr. C. K. Myers.

The Beggs method, used on the celluloid model, involved cutting a dozen members at midlength, applying distortions and, through micrometer microscope readings and calibration constants, obtaining the axial, shearing and bending stresses at the cut sections. Then, using the method of moment distribution, the stresses in all the truss members were obtained by an exact analytical procedure and the results compared with the applicable stresses obtained by measurements on the model. For his conclusions it should suffice to quote here from Mr. Myers' thesis:

"It can be seen that the values for thrust (axial stress) in the members agree quite well for the two solutions, whereas shear and moment seem to be violently in error. These differences can best be explained by the fact that the values for moment and shear were quite small and did not give good readings by the Beggs method. It was unfortunate that the moment had to be

10. "Celluloid Model Analysis of a Polygonal Truss," Massachusetts Institute of Technology, 1954.
11. "Analysis of a Polygonal Truss," Massachusetts Institute of Technology, 1954.

measured at the center of the members near the point of inflection where the moment was small. This was necessary, however, in order to fit the Beggs gage to the model. With this in mind it is safe to say that the best comparison is between values of thrust, and the close agreement of these values may be said to verify the exact solution."

Fig. 12 shows the physical features of the large scale model and the locations and numbers of the SR-4 strain gages. Fig. 13 is a compilation of the computed and experimental stress data and shows graphically the loading arrangement and the scalar relation of computed and test moments, of which the test moments are extrapolated along a straight line from the gage stations to the joint intersections. Fig. 14 is a photograph of the model frame and a detailed view of most of the SR-4 gages in the test position.

The model was designed to begin to yield at a load of 110 kips at the M-joint. To obtain moment in the single segment frame it was loaded eccentrically through two rollers bearing on the top panel points, as indicated in Fig. 13. The gages were placed so as to obtain a complete determination of all moments, shears and axial forces in the frame and located to be one or one and one-half times the depth of the member away from gusset plates or other inconsistencies. The testing procedure involved a series of loadings within the elastic range and another beyond the proportional limit. In the former series the test loads were brought by increments up to 100 kips. Three sets of test data in this range, plotted as strain versus load, show a rather consistent behavior of the frame under load and indicate that the first yield was probably at about 120 kips.

In the first attempt to reach the ultimate load, the loading beam failed in web crippling under a load of 180 kips, the error in choosing the beam being attributed to a poor approximation of the ultimate load of the frame. Upon replacement with a much heavier loading beam, the test was completed when, at 243 kips, the end post U3L4 reached yield point and began to buckle just below joint U3, which had been permanently strained by the eccentricity of the previous loading. An initial contributory cause of eccentric loading at the four support joints, L0, U1, U3, and L4, was lack of true parallelism between the top plane of the top chord and the bottom plane of the bottom chord, which could not be easily remedied in the test set-up. While the frame was carefully fabricated, errors were found in the lengths and depths of the members and others irregularities in dimensions. Among the other errors, thought as having appreciable effects on the test results, there were the eccentricities developed in the joints; distributed loads at bearing plates where point loads were assumed; effects of joints near the gages; friction of the rollers causing horizontal forces at the reactions; and, of course, errors inherent in the experimental methods, which amounted as high as 10%.

The frame was also subjected to an exact analytical treatment taking into consideration the taper of its web members. A comparison of the experimental and analytical stresses shows the differences to be rather large: thrust varies by an average of 17.5%, shear by an average of 35.1%, and moment by an average of 40.4% (Fig. 13).

An analysis of the plots of the test readings indicates that members began to yield at the joint, at which point more of the load had to be taken by the gage section which gave the indication. Further, the entire structure began to yield at one load due to the large degree of interaction of the members and the small size of the frame. It must be noted that the first yield did not cause the structure to fail. A plastic hinge was formed and the reserve strength of the structure in bending carried the load. The load might then have been in-

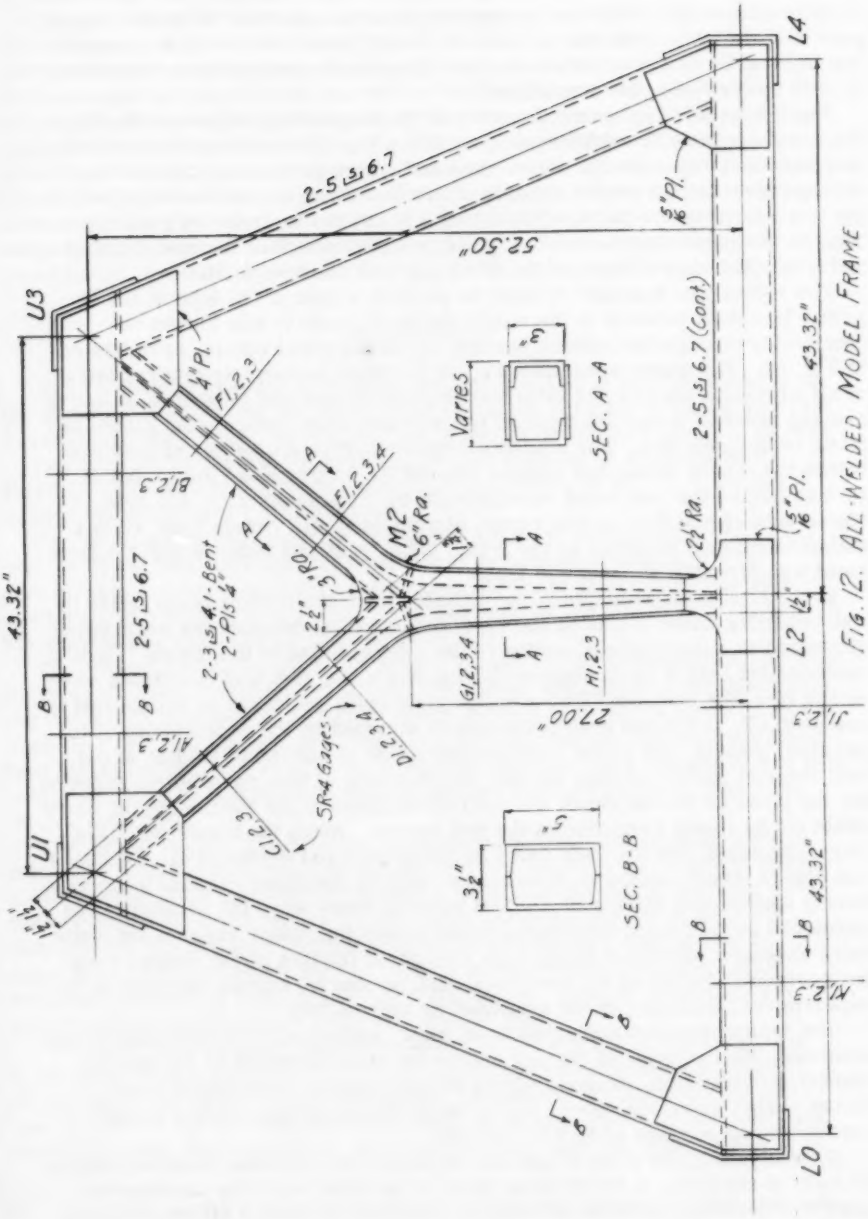

FIG. 12. ALL-WELDED MODEL FRAME

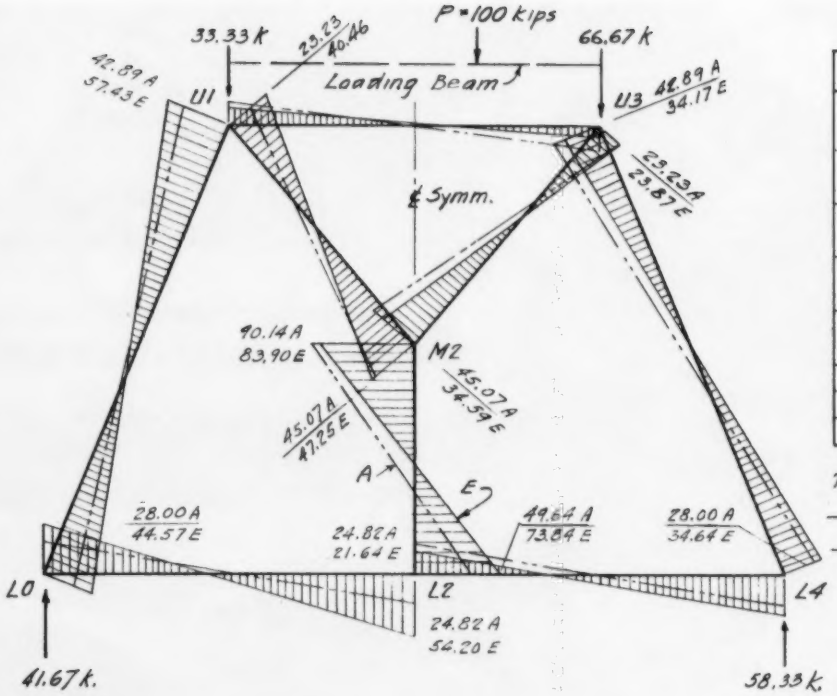

STRESS TABLE

BAR	A-KIPS	E-KIPS	TYPE
L0L2	18.04	16.67	T
	1.22	2.28	S
U1U3	20.62	18.65	C
	0.91	0.61	S
U1M2	6.42	4.32	T
	2.04	2.62	S
M2U3	6.42	7.73	C
	2.04	1.75	S
M2L2	0	2.58	C
	5.18	5.85	S
L2L4	All Stresses		
L0U1	from Statics		
U3L4			

T-C-S - Ten., Comp., Shear.
A - Analytical.
E - Experimental.
Moments - Ft.-Kips.

FIG. 13.- MODEL FRAME STRESS AND LOADING DATA.

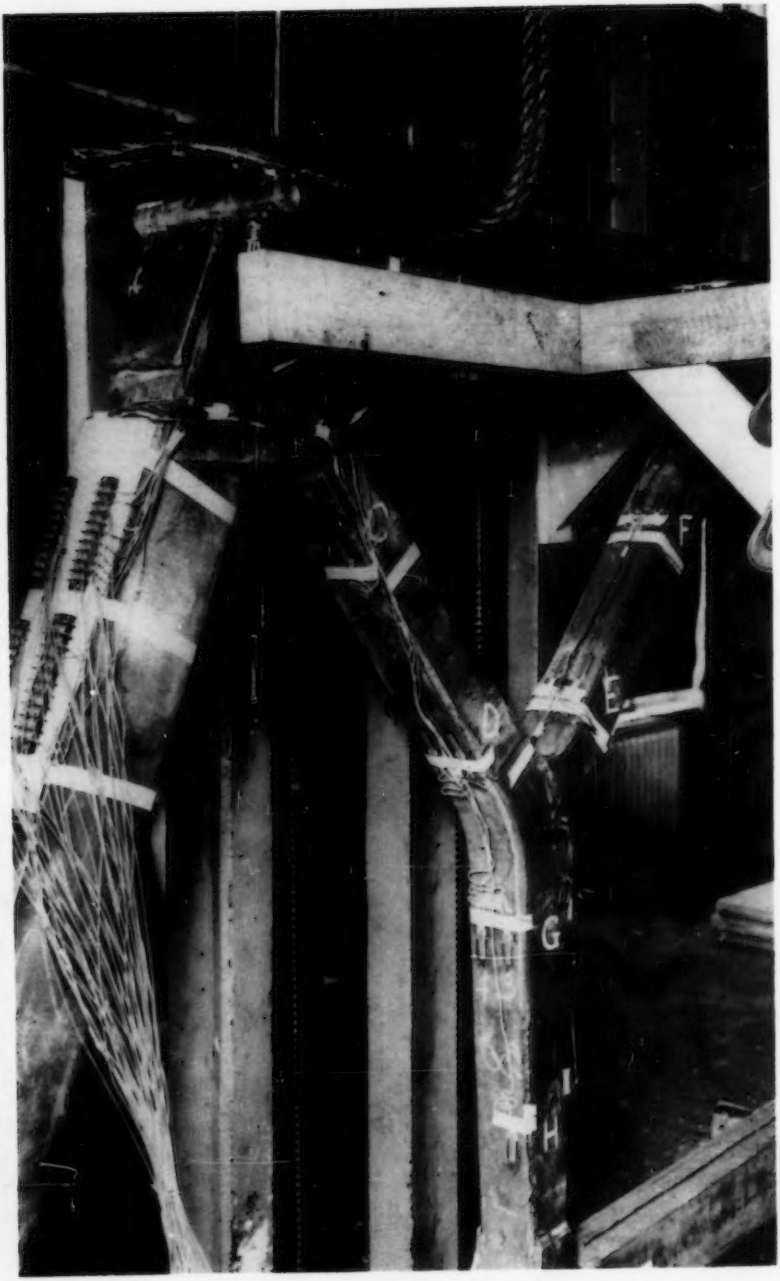

Fig. 14 - Model Frame in Test Position.

creased until a second plastic hinge was formed, and so on until the structure deformed intolerably or the stability requirements were no longer satisfied. In this case, however, the second hinge did not form because of the failure of the end post.

It is to be noted that the above recitation with respect to the description of the models, test and analytical results and conclusions is essentially a series of verbatim statements—without comments by the writer—taken from Mr. Myers' thesis and, for brevity, condensed and assembled in this presentation.

In commenting now on the model studies, the writer wishes to call attention to a few significant aspects of the test data which, in his opinion, are relevant to the discussion and closing remarks as to stress distribution in the members of polygonal trusses. Thus:

1) The moments in the identical Y arms at the M2 joint are reasonably in balance, since a large part of the difference may be ascribed to the opposite sense of their axial stresses.
2) The relatively large moments at the outer ends of the Y members are evidently a result of the highly stiff chord members and gusset joints.
3) The substantial compressive stress in bar M2L2, although zero theoretically, is evidently due to the unorthodox loading of the frame. And,
4) Joint M2 had yet to fail, as it should have in buckling, at a load 120% above that computed for the elastic limit of the material.

CONCLUSION

Mr. Lane might as well have included in his opening sentence that "the new and untried" must also go through the process of weeding out the "bugs," hidden and apparent. In a broader participation the writer would have been elated by the lack of serious challenge to the premises underlying the novel trusses or their distinguishing characteristics listed in the paper, which, so far, necessarily are based on rudimentary engineering conceptions and intuition alone. It is hoped that the actual stress patterns, deformations and general behavior of the polygonal trusses will ultimately be established on a solid foundation of extensive experimental data.

In closing, the writer would like to state that the paper would have been quite incomplete without a grateful acknowledgement to Mr. Albert E. Dykes[12] for his unstinted help and constructive criticism in the editing of the basic paper and the closure comments.

12. Chief, Planning and Report Branch, Nashville District, Corps of Engineers, Nashville, Tennessee.

Discussion of
"INFLUENCE LINES FOR REACTIONS OF CONTINUOUS TRUSSES"

by Andrew John Pyka
(Proc. Paper 914)

ANDREW JOHN PYKA,[13] M. ASCE. — The author wishes to thank Professor A. C. Scordelis for a presentation verifying the validity of the procedure as presented by the author in his paper. However, he wants to take exception to some of the comments and to clarify the misunderstanding as indicated in the Professor's discussion.

In the first place, it was not deemed necessary to provide any proof of the procedure in that, basically, the presentation is a mere tabulation form for the components of the fundamental deflection equations derived from the theory of virtual work, i.e., $1 \times \Delta = \sum \frac{PUL}{A}$; the external virtual work done by an external one pound force acting on the structure equated to the internal virtual work performed by all the truss members. This is elementary.

For instance, take the example of the 5 panel Warren type truss (see Fig. No. A) similar to the one given by Professor Scordelis in his discussion. The deflection at any point "C" is equal to the $\sum \frac{PUL}{A}$ of all the members to the left of line 1-1 plus the $\sum \frac{PU'L}{A}$ of all the members to the right of line 2-2 where P represents the stress in the respective truss members due to the external load and U and U' represent the virtual stresses in the members to the left of 1-1 to the right of 2-2 respectively. In other words

$$\Delta C = \sum \frac{PUL}{A} + \sum \frac{PU'L}{A} \quad (1)$$

where the effect of any one member is not repeated. Since the reactions at A and F (Fig. A) are taken as unity in the analogous cantilevered trusses, figures "B" and "C", the following alterations to equation (1) must obviously be made:

$$\Delta C = \frac{T-N}{T} \times \sum \frac{PUL}{A} + \frac{N}{T} \times \sum \frac{PU'L}{A}$$

$$= \frac{T-N}{T} \left\{ \sum \frac{PUL}{A} + \frac{N}{T-N} \times \sum \frac{PU'L}{A} \right\} \quad (2)$$

Where T equals the total number of panels and N equals panel point location counting from left to right, i.e., N is equal to one at point B, two at point C, etc.

It should be noted that equation (2) above is the same as the $\left(\frac{T-N}{T}\right)$(13) values of Column 14 of the table as shown on page 914-4 of the Proceedings.

---

13. Consultant, Technical Staff, Consolidated Western Steel Div., U.S. Steel Corp., Maywood, Calif.

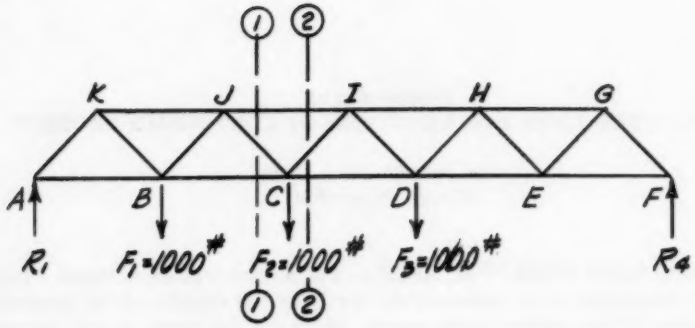

Fig. "A"

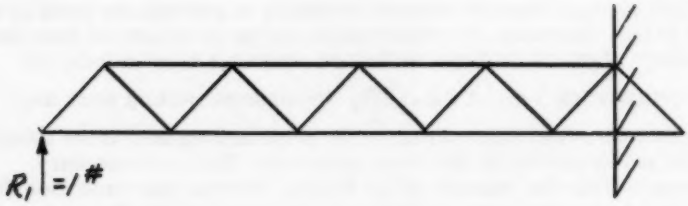

Fig. "B"

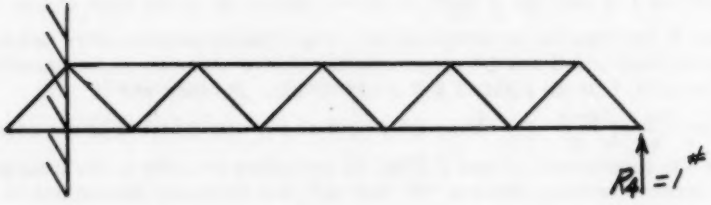

Fig. "C"

The author disagrees with Professor Scordelis in regard to the necessity for making certain corrections to the virtual stresses; namely, in member JC of the Warren truss shown in Figure A when calculating the vertical displacement at "C". The impression may be that the analogous cantilevered truss method applies only to those trusses which have vertical members in their makeup. This is erroneous. The method applies to all trusses without exception.

Table 1 below has been set up for Professor Scordelis' truss (Figure A) with the following assumed conditions for convenience:

$F_1 = F_2 = F_3 = 1{,}000$ lbs.
All members are 100 in. in length.
All areas have 10 square inches.

	1	2	3	4	5	6	7	8	9	10	11	12	13	14
Member	L Length (in.)	Area Sq.In.	$\frac{L}{A}$	U $R_1 = 1\#$	$\frac{UL}{A}$	P Stresses	$\frac{Pul}{A}$	$\Sigma\frac{Pul}{A}$	$\frac{U'L}{A}$	$\frac{Pu'l}{A}$	$\Sigma\frac{Pu'l}{A}$	$\frac{N}{T\text{-}N} \times$ (11)	(8)(12)	$\frac{T\text{-}N}{T} \times$ (13)
AK	100	10	10	-1.15	-11.5	-2.08	+23.92							
AB	100	10	10	+ .575	+ 5.75	+1.04	+ 5.98		+52.	+54.08				
KB	100	10	10	+1.15	+11.5	+2.08	+23.92		-11.5	-23.92				
KJ	100	10	10	-1.15	-11.5	-2.08	+23.92		-46.0	+95.68				
Joint B								+77.74			+456.48	+114.12	191.86	153.48
BJ	100	10	10	-1.15	-11.5	- .921	+10.59		+11.5	-10.59				
BC	100	10	10	+1.73	+17.3	+2.54	+43.94		+40.4	+102.62				
JC	100	10	10	+1.15	+11.5	+ .921	+10.59		-11.5	-10.59				
JI	100	10	10	-2.30	-23.0	-3.0	+69.0		-34.5	+103.5				
Joint C								+211.86			+271.54	+181.01	392.87	235.72
CI	100	10	10	-1.15	-11.5	+ .23	- 2.64		+11.5	+ 2.65				
CD	100	10	10	+2.88	+28.8	+2.89	+83.23		+28.8	+ 83.23				
ID	100	10	10	+1.15	+11.5	- .23	- 2.64		-11.5	+ 2.65				
IH	100	10	10	-3.45	+34.5	-2.77	+95.57		-23.0	+ 63.71				
Joint D								+385.38			+119.30	+178.95	564.33	225.73
DH	100	10	10	-1.15	-11.5	+1.38	-15.87		+11.5	+ 15.87				
DE	100	10	10	+4.04	+40.4	+2.08	+84.03		+17.3	+ 35.98				
HE	100	10	10	+1.15	+11.5	-1.38	-15.87		-11.5	+ 15.87				
HG	100	10	10	-4.60	-46.0	-1.38	+63.48		-11.5	+ 15.87				
Joint E								+501.15			+ 35.71	+142.84	643.99	128.80
EG	100	10	10	-1.15	-11.5	+1.38	-15.87		+11.5	+ 15.87				
EF	100	10	10	+5.20	+52.0	+ .69	+35.88		+ 5.75	+ 3.97				
GF	100	10	10	-	-	-1.38	-		-11.5	+ 15.87				

Note: Col. 5 is always the same as Col. 9, except in reverse order.
Col. 14 = relative deflections; when divided by E, they become actual deflections.

TABLE I

Column No. 14 gives the relative vertical deflections for the ordinates of the deflection curve due to the external loading. It should be noted that no correction is necessary. As a matter of fact, a correction is rarely required and then only for those members in the truss which are directly affected by localized loading and which also have "P" stresses which are not 0. Figure D is presented in hopes that it may clarify this particular phase of the operation. The members of truss No. 1 of Figure D may be listed in a systematic manner as indicated in the author's original paper and the deflections automatically obtained by going through the arithmetical computations. Corrections should then be made for all the verticals at the load line since they will be affected by the unit load as it moves from panel point to panel point. For example, members cd, ef, etc. will change an amount equal to plus-unity from the respective U and U' quantities. Therefore, the correction at panel points b, d, f, g, f', d', b' along the bottom chord should be P X (+1) $\times \frac{L}{A}$ which is algebraically added to the respective values in Column No. 14 (see Figure 4 page 914-4 in the Proceedings).

It is interesting to note that had the Mississippi River bridge at Dubuque, Iowa been made up at joints L9 and L'9 as shown in Figure D (2), no correction would have been required.

Figure D (3) indicates a sub-panel truss where no correction would be required for the loading "P". However, with a load "P_1" (the P load removed) a correction of P_1 x "Change in Stress" x $\frac{L}{A}$ is required for members ab, ac, bc, and dc and should be algebraically added to the summation values at joint "a" in Column 14. This correction quantity is very small in most cases and may be neglected unless a precise solution is desired.

It is recognized that the definition of "T", page 914-4 of the Proceedings, should be amended to read as follows:

"T = number of panels (in Figure No. 1 there are 14 panels)."

The author was pleased to know that someone has made a comparison between the analogous cantilevered truss method and the elastic weights method. The elastic weights method (more accurately described as the angle weights method) is in some cases, particularly in parallel chord continuous trusses, a simple tool for determining deflections of all panel points on a truss. It was gratifying to note that Mr. Robert R. Dickey had found the analogous cantilevered truss method comparable to the angle weights method, even though he was more familiar with the latter. This certainly would indicate that designers not versed or familiar with either method would find the author's method simpler and more automatic. The analogous cantilevered truss method lends itself to automation whereas other methods do not. Once a table has been set up (similar to the one on page 914-4 of the Proceedings) and Columns 1, 2, 4 and 6 determined, any non-technical employee can complete the work and thus relieve design personnel to do other design tasks. On the other hand, in the case of the angle weights method, the analysis will require supervisory attention more so than in the case of the author's method.

The author contends that computational errors are more easily detected and corrected in the case of the analogous cantilevered truss method. A tabulation setup as that given for the method lends itself to a scrutiny in which sudden variations in the normal differences of numbers can be detected and corrections made accordingly. The author is very familiar with the

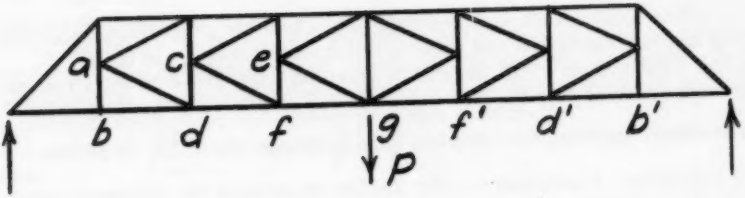

(1)

(2)

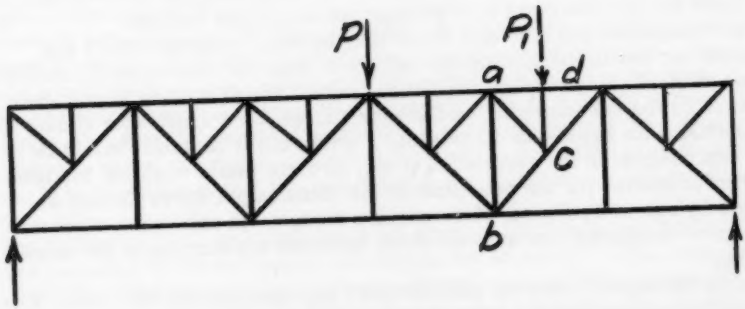

(3)

Fig. "D"

angle weights method and has found that the analogous cantilevered truss method is more adaptable in setting a design procedure routine for the drafting room.

The author does not quite understand Mr. Dickey's suggestion regarding changing the nomenclature and pattern for the tabulations. In the first place, the definition of a "P" stress as given on page 914-4 of the Proceedings is correct as it stands. The stresses for members to the left of R_2 are still determined by the formula. $\frac{(L-L_1)}{(L)}$ U and not $\frac{(-L_1)}{(L)}$ U as Mr. Dickey indicated. Furthermore, Mr. Dickey suggested the following changes to the author's columns No. 11, 12, 13, and 14:

11	12	13	14
$\frac{\Sigma PU'L}{A}$	$\frac{N}{T} \times (11)$	$\frac{T-N}{T} \times (8)$	$(12) + (13)$

Column No. 11 as given above is obviously incorrect for $\sum \frac{PU'L}{A} \neq \frac{\Sigma PU'L}{A}$

Changes as indicated in 12, 13 and 14 are inconsequential. These are relatively the same as the author's and do give the same results. In a comparable situation in the product equation A x B = B x A, it is obvious that the left side of the equation offers no more clarification than does the right side. The author recommends that the columns 11, 12, 13 and 14 remain as originally given. However, it should be understood that "T" = the number of panels in the bridge structure and not the number of intermediate panel points.

It is recommended that Mr. Dickey read the discussion on the subject as presented by Professor Scordelis on page 1007-11 in the discussions of the Proceedings. The theoretical basis for the headings for columns 12, 13, and 14 in Figure 4 is an obvious arithmetical conclusion and has been clarified and verified by Professor Scordelis in his discussion.

The author is pleased to learn that Mr. A. A. Eremin, Bridge Engineer of the California Division of State Highways, has found the analogous cantilevered truss method to be a simplified procedure for computing deflections and influence lines for the reactions of statically indeterminate trusses.

It is recognized and true that there may be other methods which are adaptable for use in calculating the influence lines for reactions of continuous trusses without going through the tedious procedure of solving simultaneous equations as the designers of the Dubuque Bridge have done. The author is not familiar with Professor Krivoshein's work, but it certainly would be a great contribution to the profession if Mr. Eremin would work out the influence line ordinates for the reactions of the Mississippi River Bridge at Dubuque by use of Professor Krivoshein's method. In any event, it would give a good comparison of at least three different approaches to the same problem.

It is of the utmost interest and certainly appropriate that Mr. Jacob Karol was able to comment on the author's method for determining influence lines for reactions of statically indeterminate trusses, particularly so since Mr. Karol calculated the influence line ordinates for the reactions of the Mississippi River Bridge.

It is true that a change in the section of a single chord or diagonal member subsequent to the original analysis will change the deflections of every panel point determined by any method of analysis. It is also true that these deflection changes depend in some direct proportion upon the amount of change in

the area of the member, considering the geometry to be fixed. It is believed that Mr. Karol has missed the point here. The analogous cantilevered truss method as presented depicts a mathematical tally of the computations and results thereof on one large sheet. The effect of changes on area or lengths of members can be readily noticed or results predicted and corrections made accordingly with a minimum amount of waste of previous work. It is, in effect, a simplified tabulation of procedure and results.

In the case of Mr. Karol's method, the general equations used are as follows:

$$\left.\begin{aligned} R_1 \Sigma va + H \Sigma ua + R_4 \Sigma vd + \Sigma a &= 0 \\ R_1 \Sigma ua + H \Sigma ub + R_4 \Sigma ua + \Sigma b &= 0 \\ R_1 \Sigma vd + H \Sigma ua + R_4 \Sigma va + \Sigma d &= 0 \end{aligned}\right\} \quad A$$

Where (Σva, Σub, Σua, Σvd, and Σa, Σb, Σd) B are variables which will be effected by a change in area or length of a member.

Calculations for the "B" portions within themselves involve tabulations at least of the same amount as the author's complete tables on pages 914-8, 914-9, 914-10.

After determining the values for "B", a substitution in "A" will result in equations similar to those used by Mr. Karol in his fi m's presentation on page 1283 of Paper No. 2387 of the transactions; namely:

$$\left.\begin{aligned} 0.0002538867 R_1 - 0.000106734 H + 0.000143508 R_4 + \Sigma a &= 0 \\ -0.000106734 R_1 + 0.0000730703 H - 0.000106734 R_4 + \Sigma b &= 0 \\ 0.000143508 R_1 - 0.000106734 H + 0.0002538867 R_4 + \Sigma d &= 0 \end{aligned}\right\} \quad (C)$$

These equations (C) are ridiculous in the sense that the average experienced bridge designer would not take time out to solve them. Certainly those who continually have occasion to work on indeterminate truss structures would be inclined to deviate from this cumbersome algebraic manipulation. The author's own mathematical background indicates to him the numerous pitfalls in solving such equations having coefficients of 9 digits in back of the decimal. Mr. Karol's comment regarding his procedure that "the detailed calculations cover two pages of the final design" is certainly an understatement. It is more likely that the results of these calculations will cover two pages.

The author, in his own calculations all through his tabulation, had noticed a little variation of the ordinates between points 13 and 13' when compared with Mr. Karol's influence line ordinates between these same points. Since the author happened to have the final influence line ordinates for the reactions of the Mississippi River Bridge, he has taken particular notice and made special independent checks on various points between joints 13 and 13'. The results were the same as shown by the analogous cantilevered truss method. Therefore, it is his conclusion that either Mr. Karol's results were slightly in error, and this can be reasonably so since solutions for algebraic equations as given in "C" above would lend themselves to an indeterminate amount of error, or areas of members as given by the author were not those used by Mr. Karol in his final analysis.

It is known and certainly understandable that a preliminary design and analysis is required prior to final design. This is basic and it was not the intention of the author to intimate that the analogous cantilevered truss method is the most convenient approach for determining preliminary or approximate solutions. It is a rapid solution for an exact analysis. There are numerous ways of determining preliminary areas for truss members of continuous trusses and this was thought to be superfluous and not pertinent to the problem. Mr. Karol has gone to a great deal of trouble to explain preliminary approaches which, in this case, are irrelevant to the immediate subject. Preliminary influence line ordinates for a three-span continuous truss structure, using a constant I, can be obtained directly from such books as "Movable and Long Span Steel Bridges" by Hool and Kinne without doing any of the calculations as shown by Mr. Karol in Table D-1.

For a symmetrical five-span structure only one additional "P" stress analysis is required. The following additional columns should be added to the table on page 914-4 of the Proceedings:

15	16	17	18	19	20	21	22
P_1	$\frac{P_1UL}{A}$	$\Sigma\frac{P_1UL}{A}$	$\frac{P_1U'L}{A}$	$\Sigma\frac{P_1U'L}{A}$	$\left(\frac{N}{T-N}\right)\times$(19)	(17) + (20)	$\left(\frac{T-N}{T}\right)\times$(21)

Columns 15 through 22 are similar to columns 8, 10, 11, 12, 13, and 14 of the author's tabulation Table No. 4. "P" values in column 6 of the table on Figure 4 page 914-4 of the Proceedings are stresses due to a unit load at R2, and P_1 in the above are the stresses in the truss due to a unit load at R3. These "P" and "P_1" stresses can be obtained directly by proportion from the U and U' stresses of the analogous truss. Columns No. 14 and 22 will give the relative deflection ordinates for the elastic curve when a unit load is placed at R2 and R3 respectively. Since the five-span truss is symmetrical, deflection curves with unit loads at R4 and R5 are opposite hand to those determined for R3 and R2 respectively.

A close study of the author's method should make it evident that the procedure lends itself very readily for use in determining elastic curves that are required in calculating the reactions of continuous trusses with even more than five spans.

Mr. Karol indicated that computations would be required for deflections due to unit vertical loads at R1, R2, and R3, extending over the entire length of the structure. It is evident here that Mr. Karol does not have a thorough understanding of the author's method. Deflections are never required for either the first nor the last reaction. The analogous cantilevered truss method is developed around the fact that influence lines are obtained for the inner supports only; the ordinates for the external reactions are obtained by statics. Evaluations of influence line ordinates do not involve small differences of large numbers, whereas such would be the case when utilizing algebraic equations.

Mr. Howard H. Mullins should be commended for his effort and wonderful dissertation on the analysis of indeterminate framed structures. The method of least work is undoubtedly invaluable in its application of analysis for indeterminate structures. However, it should be emphasized that any one method of stress analysis is only as good as the user's knowledge of its application.

Basically, there are three fundamental procedures for stress analysis of truss structures; namely, Least Work, Virtual Work and the Theory of Redundant Members—anyone of which has a direct relationship to the others. It is desirable that the bridge designers have information in regard to, and be able to apply, these classical methods of analysis. Nevertheless, it is most desirable that the short cuts, "tools" or a simple presentation be recognized as being essential in stress analysis.

It is for this reason that the author has sought ways and means of simplifying procedures. His presentation is no novel theoretical approach, but a simple tabulating procedure based upon certain relative facts and readily lending itself to simple arithmetical computations. It is with this in mind that the author has presented his paper.

Mr. Mullins' dissertation on the subject approaches the author's presentation which can also be made applicable to the various types of bridge trusses. However, upon making a close comparison of the two methods, it can be seen that Mr. Mullins' approach involves a few more calculation procedures, more columns in the tables, and additional basic calculations for determining unit stresses such as S_a, S_e, S_c, r_1, r_2. For a long bridge this would involve considerably more work. In any event, Mr. Mullins' method certainly would eliminate the nine digit decimal coefficients in the algebraic expressions or equations as presented in the original design analysis by the designers of the Mississippi River bridge.

In closing the author wishes to take this opportunity to express his appreciation to those participating in the discussion of his paper.

Discussion of
"TESTS ON BOLTED CONNECTIONS IN LIGHT GAGE STEEL"

by George Winter
(Proc. Paper 920)

GEORGE WINTER,[14] M. ASCE. — The evidence presented by the contributors to the effect that the performances and relationships observed in the tests on bolted light-gage steel connections are similar to those which have been observed in aluminum riveted joints, is interesting and gratifying. At the same time it is difficult to see any advantage in the use of the contributors' Eqs. (A) and (B) and it is believed, on the contrary, that they becloud the physical picture.

By simple transformation, Eq. (A) takes the altogether not surprising form

$$\sigma_n(s-d)t = \sigma_b dt \qquad (A,1)$$

The left side represents the bolt load if one chooses to express it in terms of the nominal stress on the net section, the right side expresses it in terms of the nominal bearing stress, and the two are equal by definition. The equation by itself contributes nothing to the explanation or description of failure. This is illustrated by the fact that the contributors have to resort to the writer's test result, i.e. to his Eq. 4, in order to determine their empirical coefficient 3.6 which alone makes their Eq. (A) reasonably applicable over a limited range of the present, relevant tests. There seems to be little promise, then, in trying to apply a bearing stress concept to those specimens which obviously failed in tension (Fig. 3, III) and vice versa (Fig. 3, II).

As regards Eq. (B), a similar simple transformation gives, no more surprisingly,

$$\sigma_n(s-d)t = k\tau_b(\pi d^2/4) \qquad (B,1)$$

The left side, as before, represents the bolt load if one chooses to express it in terms of the net stress, the right side that same load if one chooses to express it in terms of an effective bolt shear stress, $k\tau_b$, the two sides being equal by definition. The above discussion of Eq. (A,1) applies identically to Eq. (B,1) if the term "bolt shear" is substituted for "bearing stress" and Fig. 3,IV for Fig. 3,II.

In particular, Eq. (B) gives no information on the value of the ratio τ_b/σ_{tb}, the bolt shear at failure to the ultimate strength of the bolt material. The contributors, in Eq. (B), tacitly assume that the tensile strength of the sheet, σ_t, is equal to that of the bolt (the writer's σ_{tb}). Otherwise an attempt to relate the shear strength of the bolt to the tensile strength of the sheet rather than that of the bolt, as in Eq. (B), makes no physical sense. The tensile strengths of the bolt and sheet materials may be equal in the contributors' aluminum connections. They definitely were not equal in the

14. Prof., Head, Dept. of Structural Eng., Cornell University, Ithaca, N.Y.

writer's steel connections so that his results cannot possibly be represented by Eq. (B). This will be evident from the following information:

Since the time of publication of the subject paper the writer and his collaborators have carried out 476 additional, similar tests, but with high-strength steel bolts. His Eqs. 1 to 8 were found applicable to these additional tests without any change. (A paper describing these tests was presented at the Lisbon Congress of the Int. Assoc. for Bridge & Structural Engineering in June 1956 and is in process of publication of that Association's Publications, Vol. 16, 1956). In the totality of these more-than-one-thousand tests, the tensile strengths of the sheets, σ_t, ranged from 41,000 to 77,000 psi while that of the bolts, σ_{tb}, ranged from 63,000 to 171,000 psi. It is seen that an expression for the shear strength of bolts, such as Eq. (B), which contains the evidently extraneous tensile strength of the sheet, σ_t, but does not contain the basically relevant tensile strength of the bolts, σ_{tb}, is undoubtedly inapplicable except for the case when $\sigma_t = \sigma_{tb}$.

In both papers it has been the writer's aim to refer the strength properties of the connections to those dimensional parameters and materials properties which seemed relevant to the actually observed modes of failure (Fig. 3) while maintaining maximum simplicity at the expense of some scatter. While Eqs. (A) and (B) do not seem to contribute to a better analytical representation of the test results, the information presented by Messrs. Matthiesen and Moore which shows that relationships similar to the writer's are in agreement with tests on aluminum connections, is interesting and gratifying.

Discussion of
"THE LOAD DISTRIBUTION IN HIGHWAY BRIDGE DECKS"

by A.W. Hendry and L.G. Jaeger
(Proc. Paper 1023)

PRANAB KUMAR CHAUDHURI [15]. — The problem of assessing accurately how a concentrated load or a system of concentrated loads applied on a bridge deck is distributed among the main longitudinal girders which are interconnected by transverse girders and/or the deck slab has assumed a great importance today. However since the interconnected structure is highly redundant an exact elastic analysis normally becomes extremely cumbersome and during recent years a number of ingenious methods has been advanced for tackling the problem. The authors of the paper under consideration must be congratulated for adding a new method to the list. Apart from being fairly simple, their method has the added virtue of being complete; that is to say, it is directly applicable to all kinds of interconnected bridge girders with any degree of torsional stiffness and with any variation in the relative sizes of the girders composing the grid. This, of course, is the chief merit of the author's method. However the following points arising out of the paper may deserve some consideration.

It will be realised very easily that unless a bridge structure has a high torsional rigidity, the significance of a transverse girder helping in the distribution of load among the various longitudinals will diminish gradually as the said transversal is located further and further away from the center of the span. It follows directly, therefore, that in an ordinary steel bridge system where the longitudinals have low torsional stiffness, the use of a large number of transverse girders does not contribute to an economic distribution of the superimposed load. Leonhardt(15) holds that the lateral distribution of a concentrated load among the longitudinals of an interconnected bridge system of low torsional stiffness remains the same for more than five transverse girders as for five and consequently in his approximate solution he uses the same equivalent single cross girder at the middle to replace five or more transversals. Secondly, to a designer, the interconnected bridge girder will have little appeal for long spans as, then, the dead weight of the structure will be too high for the consideration of an interconnected design for the distribution of heavy concentrated loads to be worthwhile. A third point for the designer's consideration will be the added cost by way of formwork in concrete and of extra welding and manipulation in steel for a bridge system with a large number of interconnection points between girders in two directions. On the other hand, for very small span bridges the load distribution problem is not of such a great importance. It can be contended therefore that the design of a grid for the effective distribution of heavy concentrated

15. Structural Designer, Hind Consts. Ltd., Calcutta, India; (temporarily) research student, Dept. of Civ. Eng., Imperial College of Science and Technology, London, England.

loads acting on a bridge (steel or concrete) is economical, in general, only in the case of medium-span (say 100' to 200') structures. As a matter of fact, bridges designed and constructed consciously as grids rarely go beyond the medium-span limit suggested above.

The practical usefulness of the authors' method—as that of any other method—to a designer must be assessed in the light of his practical design requirements. If, as shown above, he has to design an economical medium-span steel bridge he will rarely need to exceed 6 longitudinals x 3 (intermediate) transversals for his purpose. The authors have pointed out that their assumption of a continuous transverse medium holds for as few as three cross girders. While this may very will be true, the point remains whether the elaborate analysis of the authors is really a simplification of the designer's job for most practical steel bridge cases. Even if one is not satisfied with Leonhardt's formulae for such cases, one can precisely analyze such a "negligible-torsional stiffness" case without undue difficulty. Coming to practical concrete bridges, the formulae and especially the curves given by the authors for use in the case of a five-or more longitudinal bridge are very handy but similar curves must also be provided for three- and four longitudinal bridges before the authors' method, in general, competes on equal terms with the Massonet solution the fruits of which are now available to designers in a nicely produced design-folder issued by the Cement and Concrete Association, England. Basically the authors' method is certainly simpler, and easier to understand, but Massonnet's curves are very easy to use in a design office.

However, talking of methods like the authors' or Massonnet's where the torsional stiffness of the grid can be taken into account if required one is inevitably led to a study of the importance of torsion in the analyses of practical bridge grids. Experiments have been conducted by Massonnet in Europe and Naruoka in Japan, among others, on actual bridge grids. It is premature to come to a definite conclusion yet but the present contributor has a feeling that the effect of torsion in a practical bridge case has often been over emphasized. Thus the cautious designer spending a lot of time and energy on an "exact" analysis probably does not realise that more concrete grids than he suspects could be analysed on the perfectly justified simple assumption of negligible torsional stiffness in Leonhardt's method. This is not to say that the effect of torsion is always negligible but that the designers should develop that practical structural sense which alone can guide him in the selection of a method of analysis.

The results included in the paper seem to be drawn entirely from tests carried out on bridges where the transverse distribution is effected only with the help of slabs or jack arches but not by discrete cross girders. This is interesting, as it is appreciated that in such structures the elegance of the authors' method is fully evident. There are, of course, other methods available, notably the numerical procedure developed by Newmark and the conventional orthotropic plate analysis and its variants 3, 13, 16, 17, 18 but the authors' solution is definitely a neat, general approach for these structures. The fact that the difficulty in computing the effective second moments of area, torsion constants etc., of the bridge elements and the consequent wide variations in the assumed properties of the elements result in relatively small variations of the distribution coefficients lends special weight to the claim of advantage put forward by the authors in favour of their method applied to slab-bridges. If in most of the discussion above an attempt has been made

to gauge the practical utility of the authors' method to designers, this is not to detract from its merits which are acknowledged and pointed out. One last point may perhaps be made to tie up the above remarks. By virtue of its "completeness," explained before, the authors' method is probably the most convenient for analysing existing bridges of all kinds which were not designed consciously as grids but which, nevertheless, act as such. A knowledge of the load distribution in such structures is of enormous importance, as,on it alone will depend whether the existing bridge can be expected to respond satisfactorily to the ever increasing demands of the present and the future.

Note: There seems to be a typing error in equation (14) in the paper. The first term in the numerator should be π^2 in place of π.

BIBLIOGRAPHICAL REFERENCES

1 - 14 — As in the original paper.

15. F. Leonhardt and W. Andra: Die vereinfachte Trägerostberechnung— Stuttgart, 1950.

16. W. Cornelius: Die Berechnung der ebenen Flächentragwerke mit Helfe der Theorie der orthogonal-anisotropen Platten. — Der Stahlbau, 1952.

17. M. Naruoka and I. Hirai: A study of composite grillage girder bridge— Technical Report No. 30. Engineering Research Institute, Kyoto, Japan, 1956.

18. N. Naruoka and H. Yonezawa: On the application of the theory of the orthotropic plate to the continuous beam bridge. — Proceedings of the 5th Japan National Congress for Appl. Mech., 1955.

Discussion of
"STRESSES IN PRESSURE PIPELINES AND PROTECTIVE CASING PIPES"

by M. G. Spangler
(Proc. Paper 1054)

A. A. EREMIN,[16] A.M. ASCE.—By presenting a development of Marston's method of computation of stresses in rigid and flexible pipes, the author has made a valuable contribution to theory of stress distribution in the pipes. It is true that, at present, long pipe lines are widely used. Therefore, greater accuracy in design and analysis are needed.

In addition to a transverse loading, the pipes are often highly stressed due to variation in loading along the pipe axis. With the lack of an exact method of computation of longitudinal stresses in pipes, long pipes are generally constructed in sections broken by the transverse construction or expansion joints which accomodate a free displacement. Of course, the transverse expansion joints are not an ideal solution and a greater study for their ellimination is highly desirable.

During construction of flexible pipes temporary vertical struts are often installed along the vertical pipe axis to take a direct load from fill. After completing the fill the struts are removed. Obviously, the effect of struts may be considered as a method of prestressing of the pipe. Therefore, introduction of the struts in the pipe may affect the computation of the reaction forces which was not considered by the author.

Continued study of distribution of stresses in rigid and flexible pipes is highly desirable. Therefore, the author's analysis of the Marston's theory is quite timely and should be highly complimented.

C. NEUFELD,[17] A.M. ASCE.—The method of determining stresses in pressure pipe lines and casing pipes, as presented by Professor Spangler, will be a very useful starting point in arriving at adequate installations which must safely convey materials possessing a degree of hazard and must also safely support heavy dynamic loads transferred through soil.

The application of the design procedure for pipe lines under railways and highways involves certain practical considerations which should be drawn to the attention of the readers. Professor Spangler has assumed that the concentrated loads are distributed by the rails, ties and ballast to such an extent that the weight of a locomotive can be considered as a uniformly distributed load over the entire length of the locomotive. Figure 1 has been drawn to scale to illustrate the loading conditions for a typical pipe installation under a railway track. It is obvious that the effect of axles Nos. 1 and 6 to 9 inclusive on the pipe line is negligible and it would be interesting to have Professor Spangler's assumption as to the distribution of load if the tender were removed entirely. It should be borne in mind that the track structure

17. Eng. of Bridges, Canadian Pacific Railway Co., Montreal, Que., Canada.

is relatively flexible and on this basis if is difficult to understand how the weight from the drivers could be distributed over the length of the entire wheelbase of the engine and tender. A more logical assumption would be that for a pipe line located as shown on Figure 1, the load at the base of the ties in the vicinity of the drivers is equal to the weight of one axle distributed over an area of 5' x 8'. On this basis, the unit pressure at the base of the ties including impact is approximately 3,060 lbs. per sq. ft. instead of 2,090 lbs. per sq. ft., used in Example 1 by Professor Spangler.

The paper illustrates the method of determining pipe wall thicknesses based on deflections but does not indicate the maximum permissible deflection for this type of installation. A recent pipe line undercrossing a railway consisted of a 30" O.D. carrier pipe in a 34" O.D. casing pipe with 3/8" wall thickness. This provides a clear space around the carrier pipe of only 1.625" whereas the usual assumption that a deflection equal to 5% of the diameter is safe, would permit a deflection of 1.7". For the installation in question, this would result in the casing pipe contacting the top of the carrier pipe which is not satisfactory. If deflection is considered a criterion for design, it should be strictly limited and in the writer's opinion should not exceed 2.5% of the diameter of the pipe.

Pipe line installations frequently involve a large number of crossings over a vast territory in which conditions can vary considerably. The passive resistance of the soil may be unknown so that the designer must consider that an installation may occur where passive resistance can be considerably less than the 30 psi assumed in the example illustrated by Professor Spangler. The reader has been cautioned that the numerical values were chosen arbitrarily but he may have difficulty in arriving at the correct value for a particular installation. It would be useful to have factual data on the range of passive resistances which can be encountered in natural ground but in the absence of such information, it would be prudent to assume a value not exceeding 20 psi and possibly 15 psi would be justified.

A pipe line undercrossing from a structural standpoint is an unsatisfactory type of installation because on completion, the structure is literally buried and cannot be inspected or maintained without complete removal of the carrier pipe. This procedure is impractical and is not contemplated so that some provision must be made to ensure a safe structure for an unknown period of time. In addition, the usual method of installation by boring and following with the casing pipe precludes the use of protective coatings. The steel or wrought iron casing is therefore immediately subject to corrosive elements in the soil which are also unknown and may be very severe in certain locations.

Consideration must also be given to the effect of stress corrosion on the casing pipe. It has been assumed by certain authorities that a stress level of 30,000 psi is acceptable but it is not known whether this is consistent with the criterion that a maximum deflection of 5% of the diameter can be tolerated. It should be realized that the rate of corrosion is a function of the stress level and will be accelerated by high internal or external stresses. Such stresses are produced by methods of manufacture, such as cold-forming which is used in making the pipe, or by methods of assembly such as welding. The weld metal itself can be a stress raiser and there is no assurance that the line of weld will not be located at the point of maximum stress when the pipe is installed. Corrosion fatigue will also be present where stresses are fluctuating or cyclic in nature which corresponds to the stress pattern resulting

from railway loading. It has also been demonstrated that planes of slip induced by cold-working may be the cause of susceptibility to stress-corrosion cracking. With these factors in mind, it is the writer's opinion that the stress level should not be permitted to exceed 20,000 psi for steel irrespective of the yield point strength and, as a protection against corrosion, at least 1/16" thickness of metal should be provided in addition to the theoretical thickness obtained on the basis outlined above.

E. A. RICHARDSON [18].—The paper under discussion presents quite well the mathematical theory of buried-pipe behavior as that theory has been built up, together with important additions. The author's analysis would appear to yield conservative results in most cases. However, in the light of modern soil mechanics, the theory seems inadequate in some respects. Without in any way intending to detract from the author's work on this subject, the following comments are an attempt to point out some deficiencies in present theory and to suggest a way toward future and more precise development.

To clear up a few minor corrections to the paper as it stands: Equation (25) should have $\Delta X'$, not ΔX, in the second term, right hand member. Also, according to line 2, page 1054-27, W_c as used in equation (25) is derived from equation (3). But the latter is in pounds per lineal foot. The notation governing the section, given on page 1054-20, requires W_c to be in pounds per lineal inch. A similar confusion could apply to equations (19) and (20), for which W should be in pounds per lineal inch.

Equation (25) is based upon a pipe-laying procedure which does not appear to correspond to preferred practice, particularly for large pipe. It is assumed, (a) that a pipe of circular cross-section is placed in the trench, (b) that the trench is then backfilled with no pressure in the pipe, whereupon the horizontal diameter increases and the vertical diameter decreases under the earth load, (c) that the application of internal pressure (i) increases the vertical diameter and reduces the horizontal diameter, (ii) the pressure on top of the pipe is not increased by the rise of the top surface, (iii) the pressure on the pipe sides is not decreased by the decrease in horizontal diameter, and (iv) the expansion of the pipe does not set up outside earth pressure reducing the expected tensile stresses.

If equation (25) applies measurably, the rise of the top of the pipe may increase W_c materially. In general the value of W_c can exceed the pressure due to the full head of earth through reversing the direction of shears on the fill at the sides of the trench. Such action tends to reduce the change in ΔX. Furthermore, any reduction in lateral diameter may remove a large proportion of the lateral pressure supporting the pipe. It seems improbable that this equation (25) is typical of the phenomena involved.

In practice the pipe placed in the trench may not be circular. If it is relatively thin, its horizontal diameter tends to increase at the expense of the vertical diameter through vibrations in transit, handling operations, and settlement under its own weight. When placed in the trench, the pipe is rotated about its axis through 90° so that the long axis is vertical. Tamping and back-filling is then carried out. The aim is to have the horizontal and vertical diameters substantially equal after the earth load is applied. In such a case equation (25) is unnecessary, for the application of internal

18. Engr., Publications Dept., Bethlehem Steel Co., Bethlehem, Pa.

pressure may expand the pipe but it will not tend to raise the fill or draw the pipe away from the passive pressure of the side fill. Likewise equation (23) is not fully applicable, for the expansion of the pipe tends to compress the earth outside and produce an external pressure limiting the amount of expansion and the tensile stresses.

The methods which have been used for estimating ring stresses due to earth loads, and the deflections to be expected, suffer from several departures from assumptions. The ring theory as applied in this paper assumes that ring deformations have no effect upon the outside pressure distribution. It also assumes that the required deflections may occur freely without restraint. Neither assumption agrees with practice. Hence equations such as (21) and (30) must be regarded as essentially empirical and may well be of very narrow range in agreeing with practice. For example, factor "e" is used for any and all soils, even though K is closely related to the type of soil. Nor does this factor take into account wide variations in lateral pressure due to large vertical heads of earth, or the rise in such pressure with the application of compressive forces to a body such as dense sand or gravel. In the case of jacking up the pipe, it should be possible to estimate stress distributions quite closely. But those due to earth pressure are difficult to estimate due to the departures of the deformations from those assumed. Local bending stresses would remain, but the bulk of the load would be taken by arch action, with the earth so limiting deformation that this would be true. It is believed that the formulas (21), (23) and (30) do give adequately conservative results. Lacking better methods of calculation, their use should continue.

Suppose that a pipe has been designed and installed. Time passes. Another pipe is to be laid close to the first. A trench is opened, whereby the vertical shears partially supporting the old fill are removed. The new trench is now filled. According to theory, the loads on the first pipe will be very materially increased, since the shear of the new fill is now downwards on the old. The first pipe should be taking loads in excess of the full head of earth on top of it. In practice, it is found that such apparent overloading has no tendency to collapse a flexible pipe. It is said that pipes buried some time have been evacuated, giving rise to apparently enormous stresses, without any sign of collapse. Such examples tend to show that the formulas may give conservative pipe proportions, but they most assuredly give no real information concerning the true behavior of pipes. It is said that no buried steel pipe once installed has ever failed.

If pipe is installed in earth supported at no great depth on limestone, it would appear that adequate attention should be given to providing strength in bending to permit a pipe to sustain safely the stresses arising from the development of a sink hole around it. Similarly, if pipe should be installed where the sand can become quick (as fine sand, through which water may move upwards or downwards with considerable speed), external fluid pressure and loss of support may occur with upwards flow, while subsequent downwards water flow may impose nearly full vertical loads on the pipe but destroy any appreciable lateral support. In general pipes would be given special attention in the latter case and protected from such soil behavior. In the former case no special attention might be given. Even then, steel pipe tends to carry the loads without failure.

It is not the purpose of this discussion to develop better formulas. More information is required on the pressure of, and resistance of earth for small deformations. Then equations for ring behavior fitting the pressures and

deflections must be set up. From such equations it may be possible to derive simplified equations adequate for a reasonable analysis of the stresses and deflections to be expected. Tests of formulas so derived are then required. It is sufficient for the present to take note of the weaknesses of present-day analysis.

It should be noted that where "steel pipe" appears herein, the wording "flexible pipe" may be substituted.

In conclusion: It has been suggested that the method for estimating stress and moment distribution circumferentially of a buried pipe through use of the combined ring-theory, load-distribution method leads to uncertainties. It would seem well to check buried pipe behavior through observing the strains both inside and outside the pipe at a large number of points circumferentially. This should be done throughout the period from placing the pipe in the trench to the completion of the back-fill and for as long afterwards as may be practicable. It should cover particularly the steps of elongating the vertical diameter, the tamping of fill about the pipe, and the placing of several levels of back-fill. In this manner it should be possible to estimate moment distribution and direct stress distribution circumferentially. The discusser is aware of pressure cell measurements, but so far no references available to him suggest the employment of this strain method. Obviously much information regarding the actual behavior of different soils with respect both to active and passive pressure could be obtained through a sufficiently extended test program, and the effectiveness of the preferred method for installing pipe could be evaluated.

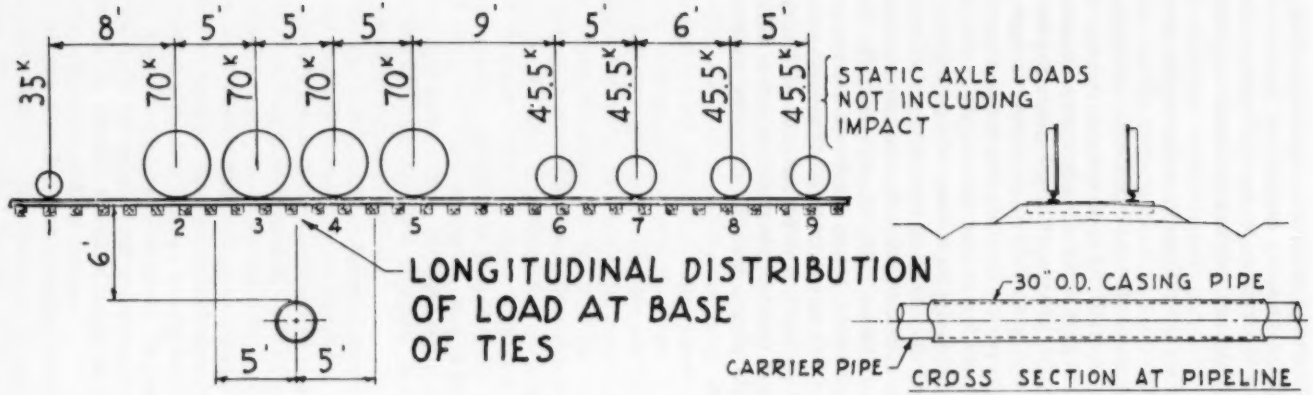

FIG. 1
COOPER'S E-70 LOCOMOTIVE
LOCATED FOR MAXIMUM
LOAD ON PIPELINE

Discussion of
"PRESTRESSED CONTINUOUS BEAMS AND FRAMES"

by P. B. Morice and H. E. Lewis
(Proc. Paper 1055)

E. L. KEMP,[19] J.M. ASCE, and A. H. MATTOCK[20].—The authors have dealt with the question of transformation of tendon profiles at some length. Although satisfied as to the effect of transformation of tendon profiles at the working load stage, when the behaviour of prestressed structures is elastic, many engineers have expressed doubts about the safety of structures incorporating transformed tendons. With the object of checking the influence of transformation of tendon profile on the ultimate load-carrying capacity of prestressed concrete portals, two tests were recently carried out at Imperial College. In the first test a prestressed concrete portal with a concordant tendon profile was loaded to destruction. In the second test a portal identical with the first in all respects, except that the tendon profile was given the maximum possible transformation, was loaded to destruction using the same loading system. The details of the two portals are set out in Fig. 1.

Two equal vertical point loads "P" were applied at the third points of the transom of the portal, and a third load equal to "0.2P" was applied at one corner, acting diagonally inwards. The purpose of the third load was to simulate the effect of wind loads on a portal, and to induce maximum moment in the structure at a corner instead of in the transom. Under this loading arrangement, and with the cable transformed downwards in the transom, a plastic hinge must first form at the corner subject to maximum moment, when the frame is overloaded. Considerable rotation of this hinge must occur to permit full redistribution of bending moments in order that the second critical section, (i.e. at the third point of the transom remote from the hinging corner,) can reach its ultimate moment of resistance before collapse of the hinging section. All previous tests known to the writers have produced hinges in the transom and not at a corner.

The working load design for both portals was carried out as if the sway load could be applied at either corner. A symmetric parabolic profile was used in the transom, and linear profiles in the legs of the portals. The tendon profile in the second portal was transformed downwards in the transom as far as possible, whilst still providing adequate cover for the tendon at midspan. The leg tendons were rotated inwards so as to produce the same moment change at the top of the legs as the transom profile transformation produced at the ends of the transom. Both the portals were post-tensioned with 3/4" Lee-McCall (Stressteel) bars in the columns and pairs of 1/2" Lee-McCall bars in the transoms. The tendon ducts were injected with cement grout after the bars were tensioned.

---

19. Research Student, Dept. of Civ. Eng., Imperial College of Science and Technology, Univ. of London, England.
20. Lecturer, Dept. of Civ. Eng., Imperial College of Science and Technology, Univ. of London, England.

Fig. 2 shows the second portal in position in the testing machine after completion of the test. The vertical loads were applied to the transom by a 200 Kip Riehle testing machine, and were measured by a proving ring placed between the crosshead of the testing machine and the load distribution beam. The sway load was applied by a turnbuckle, and measured using an electrical resistance gauge dynamometer. Both the vertical and horizontal reactions were measured using electrical resistance gauge dynamometers. Concrete strains were measured at both critical sections, using an eight inch gauge length demountable mechanical strain gauge.

Full redistribution of bending moments was attained before failure in both cases, even though very considerable redistribution was required in the portal with transformed tendon profile. The hinging corner of this portal after complete redistribution is shown in Fig. 3.

It can be seen in Fig. 2 that the transom critical section was able to reach its failure moment whilst the corner was still maintaining its hinging moment.

The variation of moments at the two critical sections in each portal is shown in Figs. 4 and 5. In the case of the portal with transformed tendon profile, the immediate effect of cracking at the corner was to reduce the parasitic moment produced at the time of prestress. This reduction must have been caused by the change in stiffness of the corner produced by the cracking. The reduction of the parasitic moment has the effect of causing the actual moment acting on the corner to increase more rapidly than was the case prior to cracking. When the parasitic moment had entirely disappeared, plasticity at the corner reduced the rate of increase of moment at this section, and eventually halted increase altogether. Almost constant moment was maintained at the corner of the transformed tendon portal whilst the vertical load increased from 22 kips to 30 kips, (with proportionate increase of the sway loading.) The variation of moment at the transom critical section was regulated by the behaviour of the corner, the two being connected by the moment relationship for the portal made statically determinate by a hinge at the corner.

The total loads carried by each of the portals at failure were almost identical, i.e. transformation of the concordant tendon profile did not reduce the ultimate load carrying capacity of the portal in the case considered.

The measured moment rotation curves for the corners of the portals are shown in Fig. 6. These resemble closely the curves for a simple prestressed beam referred to by Dr. Morice in a recent paper.(1) The presence of the prestressing anchorages at the corner did not appear to affect the behaviour of the corner when acting as a plastic hinge.

It should be noted that the plastic hinges which formed at the critical sections were of the compression type, (i.e. the concrete crushed whilst the steel strain was only slightly plastic,) and that therefore adequate rotation depended entirely on achieving high concrete compressive strains. The corners reached their maximum moments at about 0.2% maximum concrete compressive strain, and continued to hold almost constant maximum moment for concrete compressive strains in excess of 0.45%. The large strains achieved resulted in sufficient rotation of the hinging section being available to permit full redistribution of bending moments to take place before complete failure of the portals. The maximum concrete compressive strain at the transom critical sections at failure was in both cases approximately 0.2%.

The attainment of concrete compressive strains at hinging sections greatly

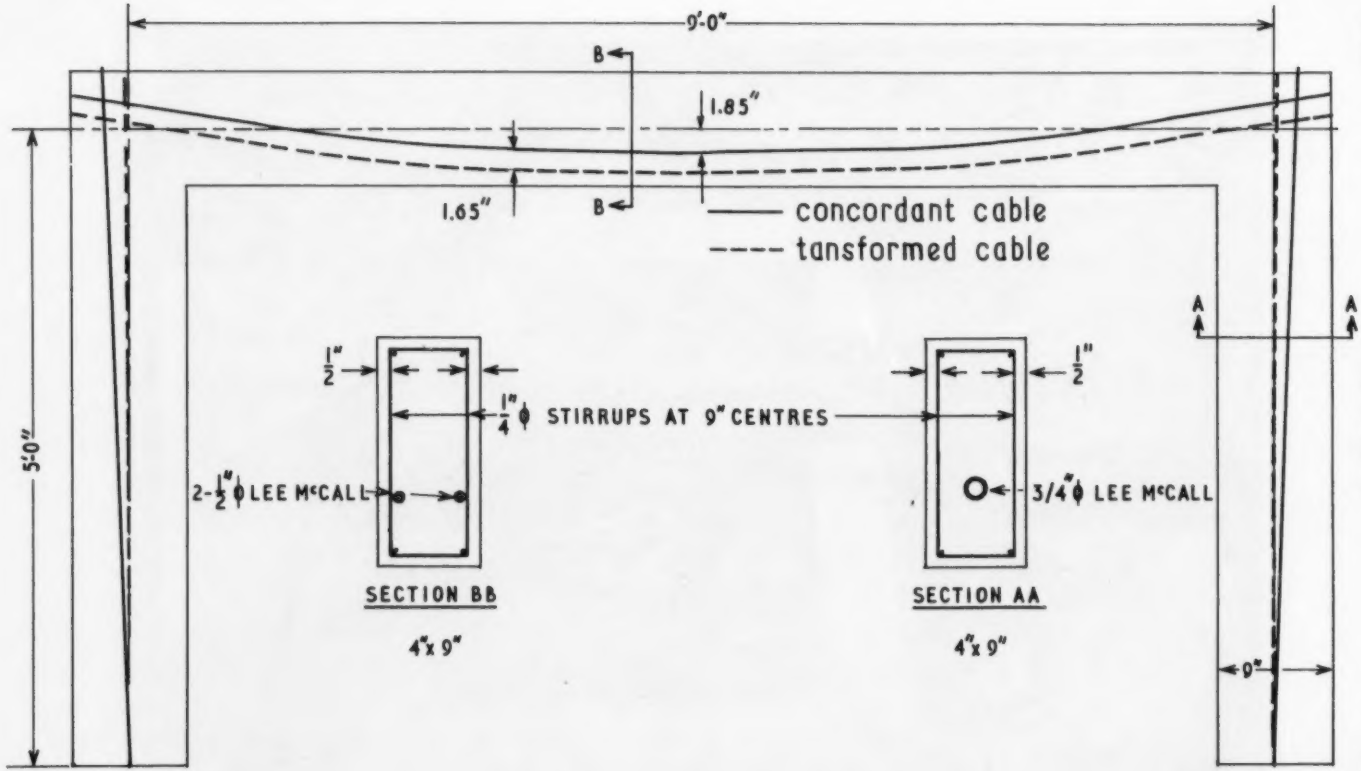

FIG. 1 PRESTRESSED CONCRETE PORTAL ELEVATION

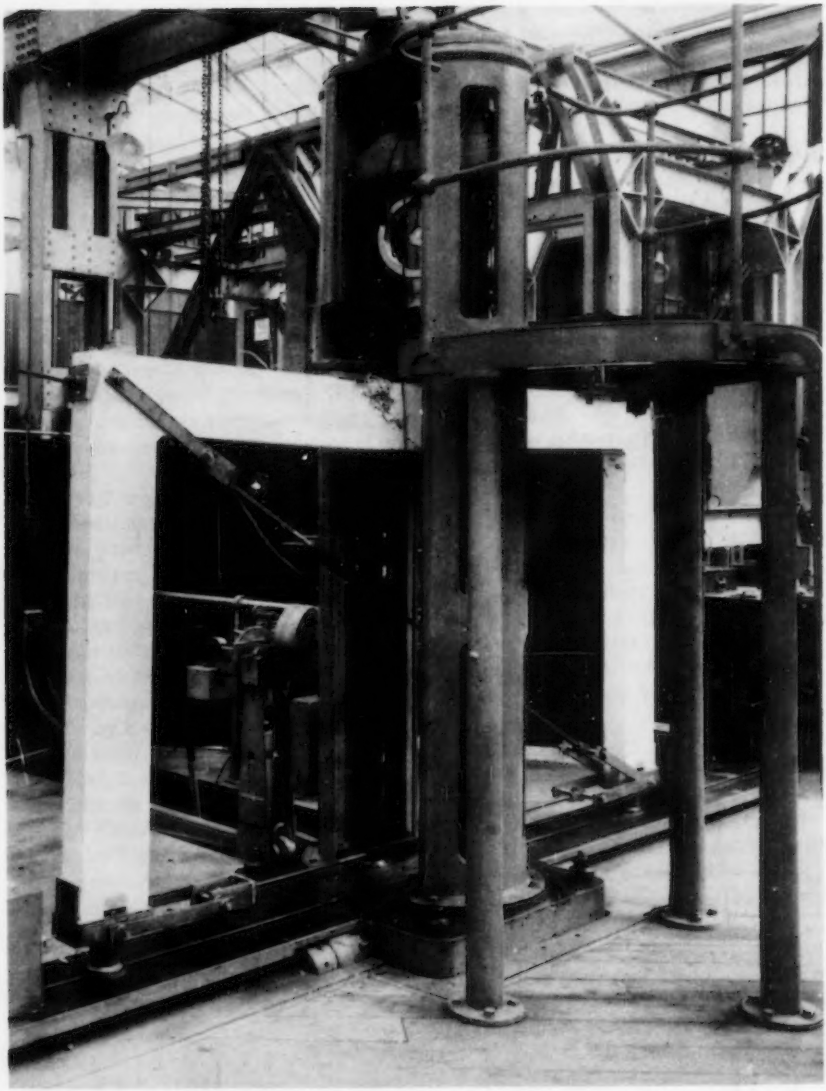

Fig. 2. Portal with transformed tendon profile after test.

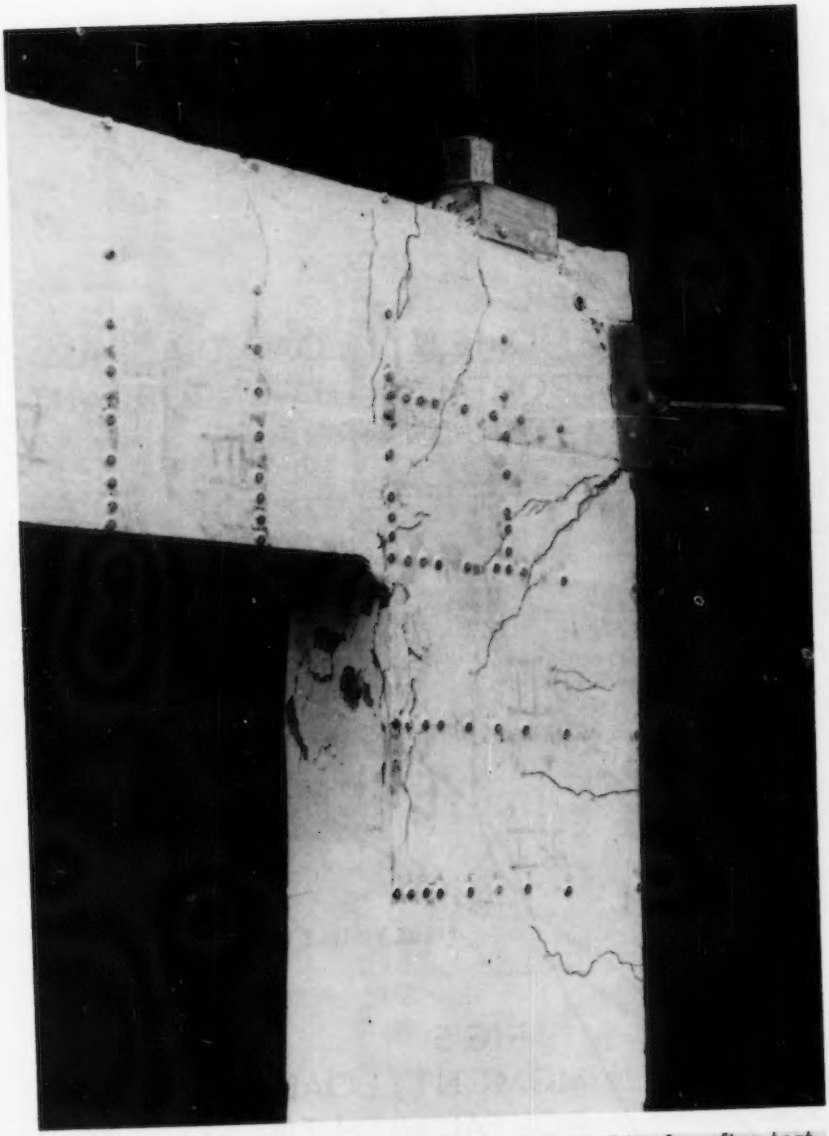

Fig. 3. Hinging corner of portal with transformed tendon after test.

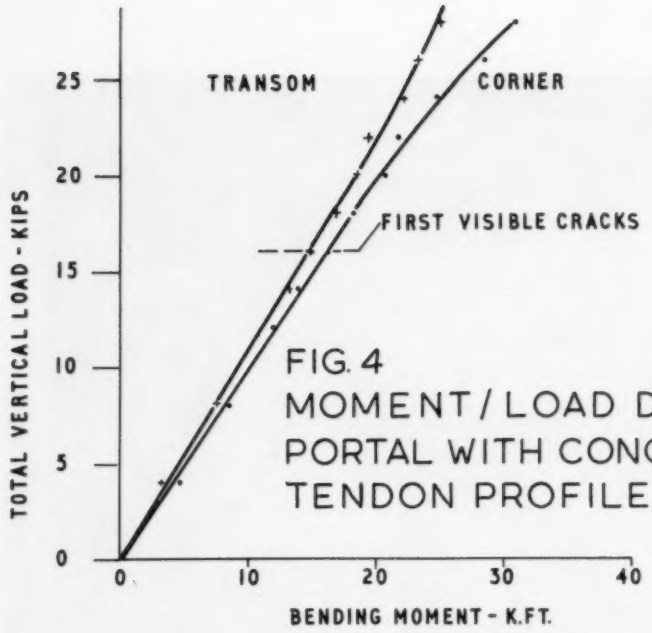

FIG. 4
MOMENT / LOAD DIAGRAM,
PORTAL WITH CONCORDANT
TENDON PROFILE.

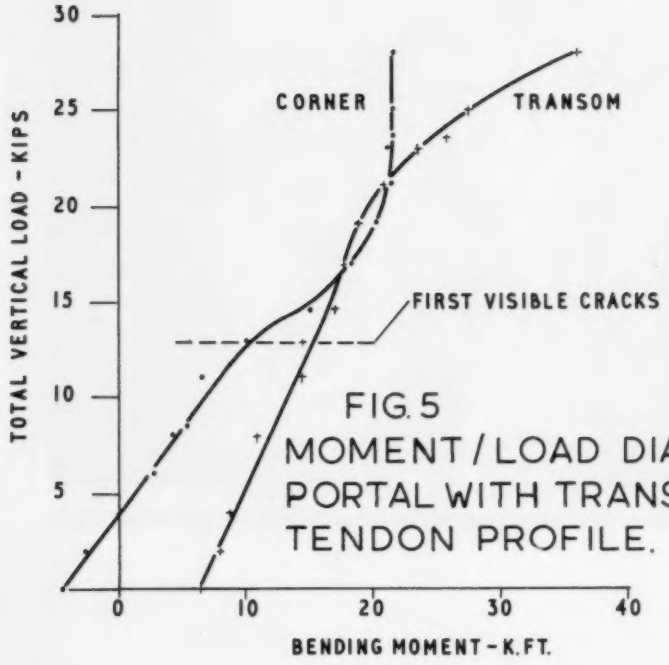

FIG. 5
MOMENT / LOAD DIAGRAM,
PORTAL WITH TRANSFORMED
TENDON PROFILE.

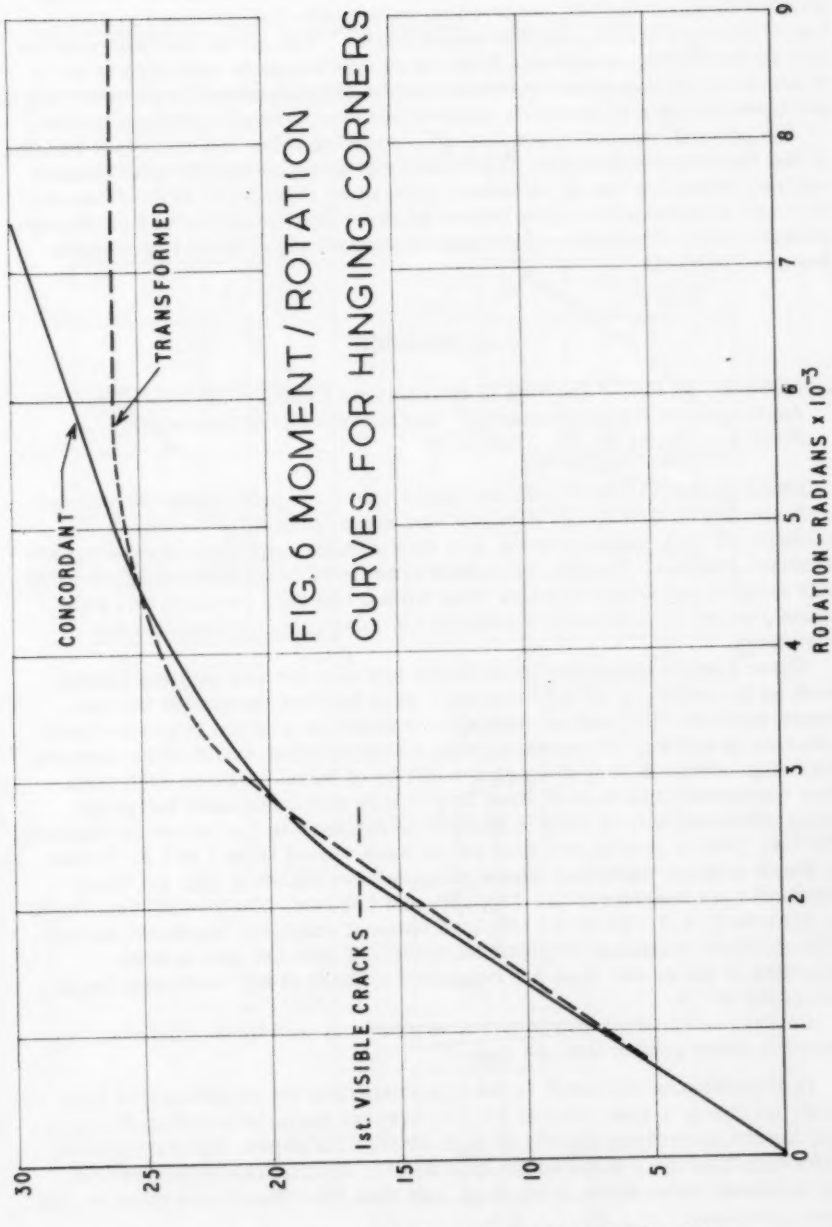

FIG. 6 MOMENT / ROTATION CURVES FOR HINGING CORNERS

in excess of those which occur at failure sections in statically determinate structures, has also been observed in many tests of prestressed and reinforced concrete frames and continuous beams. The actual available rotation at a section acting as a plastic hinge in an indeterminate structure is much in excess of the calculated available rotation, if parameters used in calculation are based on tests of statically determinate structures, i.e. simple beams.

The general conclusion reached after studying these and other test results, is that the ultimate load carrying capacity of an indeterminate prestressed concrete structure can be estimated reasonably if complete redistribution of moments is assumed to occur before failure. The validity of this conclusion depends on the elimination of premature bond or shear failure by suitable design of sections.

REFERENCE

1. MORICE, P. B. — "Analysis of Prestressed Concrete Structures and the Application of Recent Research." Institution of Civil Engineers, Structural Paper No. 51, 1956.

DEAN C. KAMARAS,[21].—In this paper under the subheading "The Effects of Continuity on Live Load Moments" the authors consider the effect of variation of span length upon the live load moment conditions in prestressed continuous beams. Using a three span symetrical beam under uniform load, with ratio of end spans to center span from 0 to 1 they conclude that equal spans give the best moment conditions i.e. minimum live load moment variations.

These results raised the question—Is this true for non uniform loading such as the AASHO H 20-S 16 loading? It is felt that because of the continued steel shortage and increasingly competetive position of prestressed concrete in highway bridge design that a study similar to that of the authors, but using AASHO H 20 S 16 loading would be of value. A three span structure was selected as typical since this type is commonly used for grade separations and will be used in increasing numbers in the Interstate Highway System. Center span to end span ratios were varied from 1 to 1.5. Points at which moment variations where computed are shown in Fig. 1. Total length of span considered are 120, 150, and 180 feet. The results are shown in Figures 2, 3, 4. M1 is the live load moment range i.e. algebraic sum of maximum and minimum live load moments. In addition simple beam moments of the center span are compared to those of the continuous beam; see curve No. 5.

General conclusions should not be drawn from only three examples; however the above graphs indicate that:

1) If horizontal clearance is not a problem then the minimum live load range occurs at a span ratio of 1:1,3:1; however there is less than 4% variation for the controlling section at span ratios considered. Furthermore the difference between a three equal span staticly determinate structure and the minimum value above is equal or less than 7%. These minimums do not

---

21. Structural Engr., Gannett, Gleming, Corddry & Carpenter, Inc., Pittsburgh, Pa.

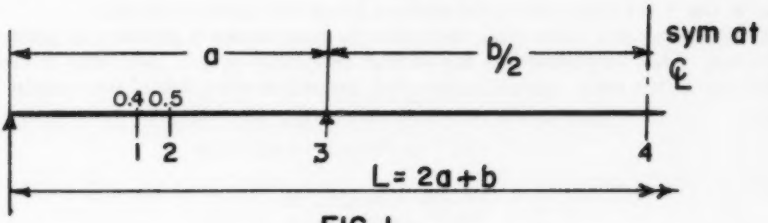
a
b/2
sym at
℄
0.4 0.5
1 2
3
4
L = 2a + b

FIG. 1

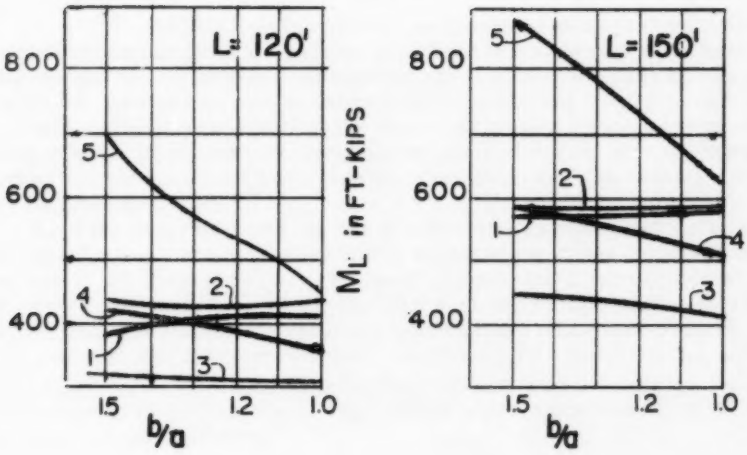
L = 120'
800
600
400
5
4
2
1
3
1.5
1.2
1.0
b/a
ML in FT-KIPS
L = 150'
800
600
400
5
2
1
4
3
1.5
1.2
1.0
b/a

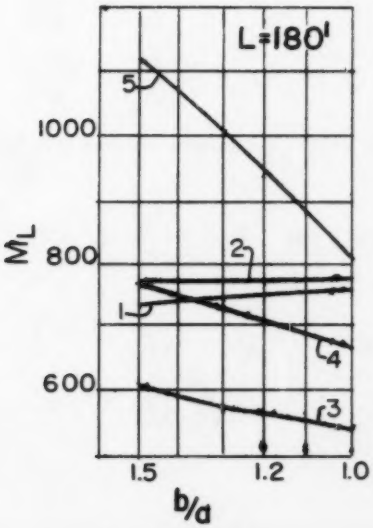
L = 180'
1000
800
600
ML
5
2
1
4
3
1.5
1.2
1.0
b/a

FIG. 2

occur at the 1:1:1 ratio which the authors found for uniform loading.

2) However since horizontal clearance is many times a problem in grade crossings. This data indicates substantial reduction in L.L. moments at the 1:1.5 ratio which show approximately 30% reduction over that of the simple beam.

Discussion of
"HYPERBOLIC PARABOLOIDS AND OTHER SHELLS OF DOUBLE CURVATURE"

by Alfred L. Parme
(Proc. Paper 1057)

T. AU,[22] A.M. ASCE.—The author has presented in a systematic and logical order the general equations for shells of double curvature based on membrane theory, with special applications to hyperbolic paraboloids and elliptical paraboloids. While only a limited number of loading conditions is amenable to algebraic solution, the paper has treated the cases of practical importance. Thus, not only the solutions are carried out with mathematical rigor, but the structural behaviors of these shells are also clearly explained in engineering terms.

Since the paper suggests the use of difference equations and relaxation method for the solution of other shells of double curvature for which the classical solutions are either extremely complicated or plainly unavailable, it may be desirable to point out also that such techniques can be adapted to hyperbolic and elliptical paraboloids with loadings other than uniform vertical load and with different boundary conditions. By considering w_x and w_y as components of force in the direction of x- and y-axis respectively, acting at the center of the element in Fig. 1 of the paper, equations (5) to (9) can be generalized as follows:

$$\frac{\partial T_{xP}}{\partial x} + \frac{\partial S_P}{\partial y} + W_x = 0 \qquad (5)$$

$$\frac{\partial T_{yP}}{\partial y} + \frac{\partial S_P}{\partial x} + W_y = 0 \qquad (6)$$

Equations (7a), (7b) and (7c) remain unchanged. Then, by introducing the stress function F so that

$$T_{xP} = \frac{\partial^2 F}{\partial y^2} - \int_{x_o}^{x} W_x \, dx \qquad (8a)$$

$$T_{yP} = \frac{\partial^2 F}{\partial x^2} - \int_{y_o}^{y} W_y \, dy \qquad (8b)$$

$$S_P = -\frac{\partial^2 F}{\partial x \, \partial y} \qquad (8c)$$

---

22. Asst. Prof. of Eng. Mechanics, Univ. of Detroit, Detroit, Mich.

These values satisfy equations (5) and (6), and reduce equation (7c) to the following:

$$\frac{\partial^2 F}{\partial y^2}\frac{\partial^2 z}{\partial x^2} + \frac{\partial^2 F}{\partial x^2}\frac{\partial^2 z}{\partial y^2} - 2\frac{\partial^2 F}{\partial x\,\partial y}\frac{\partial^2 z}{\partial x\,\partial y} = -w_z + w_x\frac{\partial z}{\partial x} + w_y\frac{\partial z}{\partial y} + \frac{\partial^2 z}{\partial x^2}\int_{x_o}^{x} w_x\,dx + \frac{\partial^2 z}{\partial y^2}\int_{y_o}^{y} w_y\,dy \qquad (9)$$

Solutions of these equations, either by algebraic or numerical method, for hyperbolic paraboloids subjected to several types of lateral loads are well known in European literature,(1) but they have been dismissed by others(2) as only of academic significance because the distribution of lateral forces is generally simplified and assumed in a mathematically convenient manner. While the assumption of the distribution of wind pressure in these solutions may not meet the requirements of the American building codes, the effect of an earthquake can be similated by distributed horizontal force. The latter type of problem is probably not academic, and the same approach has been used to compute earthquake stresses in spherical domes and in cones.(3)

Finally, there is one minor point in the paper which is perhaps not pertinent in practical applications, but nevertheless should be clarified. In the derivation of equation (13) for hyperbolic paraboloids with moderate rise, it is stated that "because the differential S_p with respect to y and x is zero, it is seen from the relationships in equations (5) and (6) that $T_{xp} = T_{yp} = 0$." Actually, from the derivation, the following equations are obtained:

$$T_{xp} = f(y)$$
$$T_{yp} = f(x)$$

The functions f(y) and f(x) become zero if and only if the boundary conditions indicate that no normal forces are acting on the edges. Hence, it is the boundary conditions of free edges that prescribe the constants of integration, and equation (13) represents only one of the many possible edge conditions. This point is not lost in sight by the author since the terms f(y) and f(x) are included in equations (16) and (17) respectively for hyperbolic paraboloids with great rise.

REFERENCES

1. See, for instance, K. G. Tester: "Beitrag zur Berechnung der hyperbolischen Paraboloidschale," Ingenieur-Archiv, v. 16, 1947, pp. 39-44.

2. F. Candela: "Structural Applications of Hyperbolic Paraboloidical Shell," Journal of American Concrete Institute, v. 26, No. 5, pp. 379-415, January, 1955.

3. E. P. Popov: "Earthquake Stresses in Spherical Domes and in Cones," Journal of Structural Division, ASCE, Proc. Paper 974, May 1956.

W. WATTERS PAGON,[23] M. ASCE.—The Society is to be complimented on having published this presentation. The hyperbolic paraboloid has taken the fancy of some architects and engineers, and it is well to have an authoritative presentation of such structures, since Fluegge's book (W. Fluegge, Statik und Dynamik der Schalen, 1934, Julius Springer, and 1943 photolithograph reproduction by Edwards Brothers, Ann Arbor, Mich.) is out of print and not easily accessible.

It would be well if the author would enlarge upon his subject. For instance, there is no discussion of the deflections of such double curved shells, and although the hyperbolic paraboloid is considered to be very rigid, because of the opposing parabolic elements, there is no statement as to the limiting flatness.

In roof structures usually dead load and snow are the essential loadings, and for domes a wind load (which the publications of which I know all deal with as an antisymmetrical wind loading, whereas the true wind loading in the lee is not the inverse of that on the upwind side) seldom will have a marked influence. However, there are two other load conditions which are not dealt with, namely (a) earthquake loading, and (b) uniform radial pressure. The writer had occasion last year to determine the dead load stresses for an ellipsoid whose axis of symmetry was horizontal, and it was only a month or so thereafter that Separate 974 appeared, dealing with horizontal earthquake forces on a spherical dome (Earthquake stresses in spherical domes and cones, E.P. Popov). - - - - - - - There is however still another loading, namely radial uniform pressure or suction. Last year the writer had occasion to design a building to be used to house a jet engine test facility, in which one of the design conditions was a large unit load per square foot, either inside pressure or inside suction, which caused large stresses and large structural members that could have been avoided had a domed structure been used.

There is still another comment, made in the hope that the author can amplify as mentioned above. The paper, as with all others with which the writer is familiar, deals only with a roof slab of square or rectangular plan form. Why would not the hyperbolic paraboloid (for example) be used to house a cylindrical structure, or a structure of (say) hexagonal or octagonal shape (the latter preferably because of full symmetry)?

The author would greatly increase the utility of his paper by adding these topics.

SANDI PADO BANNERJEE,[24] A.M. ASCE.—The formulation of the equations and also the method normally adopted for their solution have been ably exposed in the paper.

The dead load w_z of a hyperbolic-paraboloid shell with reasonably great rise has been represented by equation (14a) as

$$w_z = \frac{w}{\cos \phi . \cos \psi},$$

23. Cons. Engr., Baltimore, Md.
24. Cons. Engr., Calcutta, India.

where w is the constant weight of shell membrane per unit area. The equation is also applicable to doubly curved shells of other shapes. The writer finds that as the elements in the shell away from the origin form oblique angles 'ω' between their adjacent sides, the relationship between the variable load w_z on the projected area and the unit weight w should be represented by

$$w_z = \frac{w}{\cos\phi . \cos\psi} \cdot \sin\omega$$

instead of eqn. (14a). The subsequent related equations presented in the paper also require to be modified accordingly.

With regard to the solution of the three fundamental equations 5, 6 and 7c for three unknowns, it is customary, as has been shown in the paper, to reduce them to 'one equation with one unknown' by suitably introducing a stress function F. Mathematical solution of such an equation becomes extremely involved and therefore Relaxation or similar other iterative method is applied for a practical solution of F. Herein again the operations are time-consuming having to guess the initial values to commence the iteration process.

The writer, however, has found it more convenient to solve the three equations simultaneously after representing them through algebraic expressions obtained from the geometry of the shell form. As a result the solution is more direct.

To illustrate the procedure, an hyperbolic-paraboloid may be considered. The fundamental equations are given in 5, 6 and 7c. Proceeding thereafter, the representative equation of shell form is given by eqn. (10) as

$$z = \left[\frac{h}{ab}\right] xy = C.xy \qquad (A)$$

Thus,
$$\left.\begin{aligned} &\frac{\partial z}{\partial x} = Cy, \qquad \frac{\partial z}{\partial y} = Cx, \\ &\frac{\partial^2 z}{\partial x^2} = \frac{\partial^2 z}{\partial y^2} = 0 \text{ and } \frac{\partial^2 z}{\partial x . \partial y} = C \end{aligned}\right\} \qquad (B)$$

Also,
$$\tan\phi = \left[\frac{h}{b} . y\right] \frac{1}{a} = Cy,$$

and
$$\tan\psi = \left[\frac{h}{a} . x \quad \frac{1}{b}\right] = Cx .$$

Thus
$$\left.\begin{aligned} &\phi = \tan^{-1} Cy \\ &\text{and} \quad \psi = \tan^{-1} Cx \\ &\text{Also} \quad \omega = \cos^{-1}(\sin\phi . \sin\psi) \end{aligned}\right\} \qquad (C)$$

From eqn. 7c after substitution of values,

$$2.S_p .C = - w_z$$

$$\therefore \quad S_p = \frac{w_z}{2\,C} \qquad (D)$$

When w_z varies due to constant weight w of shell slab, then

$$w_z = w \left[\frac{\sin \omega}{\cos \phi . \cos \psi} \right] = w.m \qquad (E)$$

and then eqn. (D) becomes

$$S_p = - w \left[\frac{m}{2C} \right] = - w.r \qquad (F)$$

From eqn. 5 of paper

$$T_{xp} = - \int \frac{\partial S_p}{\partial y} . dx + f(y)$$

$$= w \frac{\partial r}{\partial y} . dx + f(y)$$

The conditions at the boundaries require that at $x = a$, $T_{xp} = O$.

$$\therefore \quad f(y) = - w \int_o^a \frac{\partial r}{\partial y} . dx$$

$$= - w . \delta x \sum_o^a \frac{\partial r}{\partial y}$$

$$= - w . \delta x . K_x$$

where $K_x = \sum_o^a \frac{\partial r}{\partial y}$ (along boundary) (G)

$$\therefore \quad T_{xp} = w . \delta x \left[\sum_o^x \frac{\partial r}{\partial y} - K_x \right] \qquad (H)$$

Similarly, from eqn. 6,

$$T_{yp} = w . \delta y \left[\sum_o^y \frac{\partial r}{\partial x} - K_y \right] \qquad (J)$$

where $K_y = \sum_o^b \frac{\partial r}{\partial x}$ (along boundary) (K)

The equations (F), (H) and (J) replace equations 15, 16 and 17 of the paper, and for purposes of solution are suitable for representation in 'Finite Difference' forms.

The numerical values of r at each nodal point of the working grid on the x-y plane having been known from the geometry of the shell form (eqns. C, E and F), the values of $\frac{\partial r}{\partial x}$ and $\frac{\partial r}{\partial y}$, and thus those of the unknowns S_p, T_{xp} and T_{yp} are easily obtained.

Similar equations as derived above can also be formed for doubly curved shells of other shapes. The working of an example through these equations will be found in an article by the writer under publication by The Indian Concrete Journal.

M. G. SALVADORI,[25] M. ASCE.—Growing interest is being shown in the United States in translational shells which cover rectangular areas. Dr. Parme is to be congratulated for his clearly presented, simple and practical paper on membrane stresses in such type of shells. The writer had numerous opportunities of designing shells of this kind in the shape of elliptic paraboloids both in the United States and abroad, and he finds that rarely, if ever, do membrane stresses create difficulties even for very large spans. The shell thickness is never determined by membrane stresses, but by stresses due to bending, temperature and buckling. The determination of this kind of stresses presents usually great mathematical difficulties, but, luckily, approximate solutions based on the so-called Geckeler assumption (1) lead to very simple formulas which are more than adequate for practical purposes.

Bending Stresses Due to Loads

The discrepancy between the membrane displacements of the shell and the displacements of the sustaining arches introduces bending disturbances in the neighborhood of the boundary which can be easily determined by cylindrical shell theory. Assuming that the transverse shear carries the entire load in the immediate neighborhood of the arches, indicating by R the radius and by h the thickness of the shell at the boundary, it is found that the shear at the boundary has the value:(2)

$$Q_0 = -qc \tag{1}$$

and the maximum bending moment has the value:

$$M_0 = -(\tfrac{1}{2})\, qc^2, \tag{2}$$

where:

$$c = 1/\beta = 0.76\sqrt{Rh} \tag{3}$$

The normal stress parallel to the arch at the boundary is zero since the whole load q is carried by the transverse shear. Figure 1 indicates the amount of load carried by the transverse shear, which peters out rapidly as one moves away from the arch. In the example No. 2 of the paper the maximum radii and the thickness have values:

$$R_x = 102', \; R_y = 156', \; h = 0.25'$$

hence:

$$c_x = 0.76 \sqrt{102 \times 0.25} = 3.84'$$

$$c_y = 0.76 \sqrt{156 \times 0.25} = 4.75'$$

and with a load q = 60 psf:

$$Q_x = -0.023 \text{ k/ft.}, \; Q_y = -0.287 \text{ k/ft.}$$

$$M_x = -0.440 \text{ k.ft./ft.}, \; M_y = -0.682 \text{ k.ft./ft.}$$

The total load carried by the transverse shear is obtained by multiplying Q_x

25. Prof. of Civ. Eng., Columbia Univ., N.Y., N.Y.; and Associate, Paul Weidlinger, Cons. Engr., N.Y., N.Y.

and Q_y by the length of the corresponding sides it amounts to:

$$W_Q = 2(0.230 \times 70 \times 2.87 \times 100) = 89.50 \text{ k}$$

and represents 37.6 per cent of the total load of 420 k on the shell.

Bending Moment Due to Temperature Difference Between Shell and Arch

If the shell is at a temperature ΔT^oF higher than the arches and were free from them, the shell would have a displacement:

$$w_o = -\alpha R \, \Delta T \tag{4}$$

where α is the coefficient of thermal expansion of concrete (8×10^{-6}). Cylindrical shell theory proves that, if this displacement is prevented by the arches, the following boundary shear and moment are developed:

$$Q_o = \frac{\alpha Ehc}{a} \Delta T; \quad M_o = \frac{\alpha Ehc^2}{2a} \Delta T \tag{5}$$

For the shell of example 2 of the paper these formulas give:

$$M_x = 63.0 \, \Delta T; \quad M_x = 62.8 \, \Delta T$$

It is seen that if a temperature differential of only 10^o occurs, the bending moments at the boundary become fairly high. In fact, it is often impossible to absorb them, since an increase in thickness of the shell at the boundary produces an increase in c. Provided sufficient reinforcing be available at the boundaries in a direction orthogonal to the arches, it is often necessary, and quite proper, to let plastic rotation take care of the excess moment.

Stresses Due to the Difference in Temperature Between the Outer and the Inner Surface of the Shell

These stresses can be approximately evaluated by assuming that the shell is spherical with a radius equal to the average of the two maximum radii. It is found[3] that the outer and inner fiber stresses have the following values:

$$\sigma_o = (1/2) \, \alpha E \, (1 - 2/3 \, \frac{h}{r}) \, \Delta T$$

$$\sigma_i = (1/2) \, \alpha E \, (1 + 2/3 \, \frac{h}{r}) \, \Delta T \tag{6}$$

In the case of example No. 2 of this paper we obtain the following values:

$$\sigma_{o,i} = 12(1 \mp 0.0016) \, \Delta T$$

Such stresses do not usually require special care, but may lead to an increase of temperature reinforcement above the minimum required by codes.

Reinforcement

The fundamental assumption in the derivation of membrane stresses is that the supporting arches cannot react horizontally. This assumption is responsible for the supposedly infinite value of the tangential shear at the corners, but as mentioned above, in the neighborhood of the arches, the load is not carried by tangential shear, and if one subtracts from the total load,

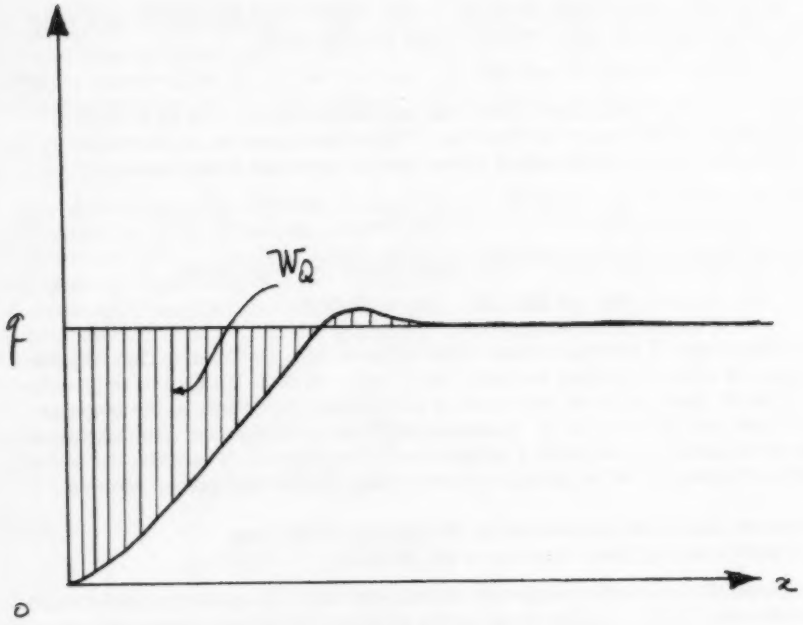

Fig. 1.

the load carried by the transverse shear, it is found that the tangential shear at the corners is not infinite.(4) These shears can be evaluated by the equations for the total vertical equilibrium of the shell, as shown in reference No. 5.

On the other hand, the assumption that the arches do not react horizontally is not satisfied in the neighborhood of the corners, where each arch is supported horizontally by the two adjoining arches at right angles. In order to make the arch as flexible as possible in a horizontal plane, it is advisable not to connect the diagonal reinforcement at the corners with the reinforcement of the arches.

Buckling

An approximate evaluation of the buckling value of the load q can be found by approximating the elliptical paraboloid once more by a tangent sphere. The critical value of a uniform pressure q on a sphere is given by:(4)

$$q_{cr} = \frac{2E}{\sqrt{3}} \left(\frac{h}{r}\right)^2$$

With an average radius of 129', the formula gives:

$$q_{cr} = 3250 \text{ psf}$$

Even if we assume that the modulus of concrete is reduced to 1/6 of its original value (3×10^6 psi), we obtain a safety factor of over 8. It is seen that buckling is not usually a real problem even for very thin shells.

It is hoped that a knowledge of bending and membrane stresses due to loads and temperature will give more confidence to the designing engineer, who will thus be in a position to cover very large areas at costs which cannot be met by any other type of structure at the present time.

BIBLIOGRAPHY

1. Timoshenko, S., "Theory of Plates and Shells," Chapter XI, Sec. 81.
2. Timoshenko, S., "Theory of Plates and Shells," Chapter XII, Sec. 95.
3. Timoshenko, S., "Theory of Elasticity," Chapter XI, Sec. 115.
4. Fruban, K., "Biegetheorie der Translations-flächen und ihre anwendung im Hallenbau," Acta Technica Academiae Scientiarium Hungaricae Tomus VII, 1953.
5. Salvadori, M. G., "Analysis and Testing of Translational Shells," Proceedings ACI, June 1956, Vol. 25, No. 10.

Discussion of
"MOMENT DISTRIBUTION CONSTANTS FROM MODELS"

by Otakar Ondra
(Proc. Paper 1058)

JOHN C. MURPHY,[26] J.M. ASCE.—Many numerical methods have been introduced to provide solutions for the determination of stiffness factors, carry-over factors and fixed end moments. The method of column analogy provides a general solution which lends itself to most problems of varying sections. The column analogy may be modified by taking subdivisions at convenient intervals on the analogous column to approximate values of area and moment of inertia.

The author's concept of using a solid model is a physical application of the principles of the column analogy to replace the mathematical computations required for determination of the properties and loading on the analogous column.

The advantage of the author's method are most apparent when the case of a haunched beam uniformly loaded over a portion or the complete span is considered. This problem is believed to be common in the design of reinforced concrete structures.

The sketch for the analogous column for the exact solution shows the pressure solid which has to be considered. The volume of the pressure solid may be found for this case by integrating over the areas A and B. Volume A is a solid with a constant base width and varying in height as the square of the distance from the center line. Volume B is a solid whose base width varies as the cube of the distance measured from its origin and whose height varies in the same relationship as for Volume A.

For this type of beam and loading, probably the most expedient method of determining the beam constants and fixed end moments would be to assume subdivisions of the solid both for base widths and vertical heights on the pressure solid. These assumptions are shown in the sketch of the analogous column for the approximate solution.

In a study made by the writer on this particular beam the value of the fixed end moment at the left end of the beam for the type of loading shown was found to be $.0398qL^2$ by using the properties found by using the approximate method. The exact value of the fixed end moment was found by integrating for the areas and volumes on the analogous column. The exact value was found to be of the order of $.0345qL^2$. Comparisons of these values indicates that errors of the magnitude of 15% may be involved when the approximate method is used alone. The magnitude of this error will be a result of the judgment of the individual, the refinement of the method and the complexity of the problem.

The use of the solid model in the situation where a complex pressure solid is involved will provide a less tedious method of analysis or a good check on

---

26. Eng. Dept., Pittsburgh-Des Moines Steel Co.

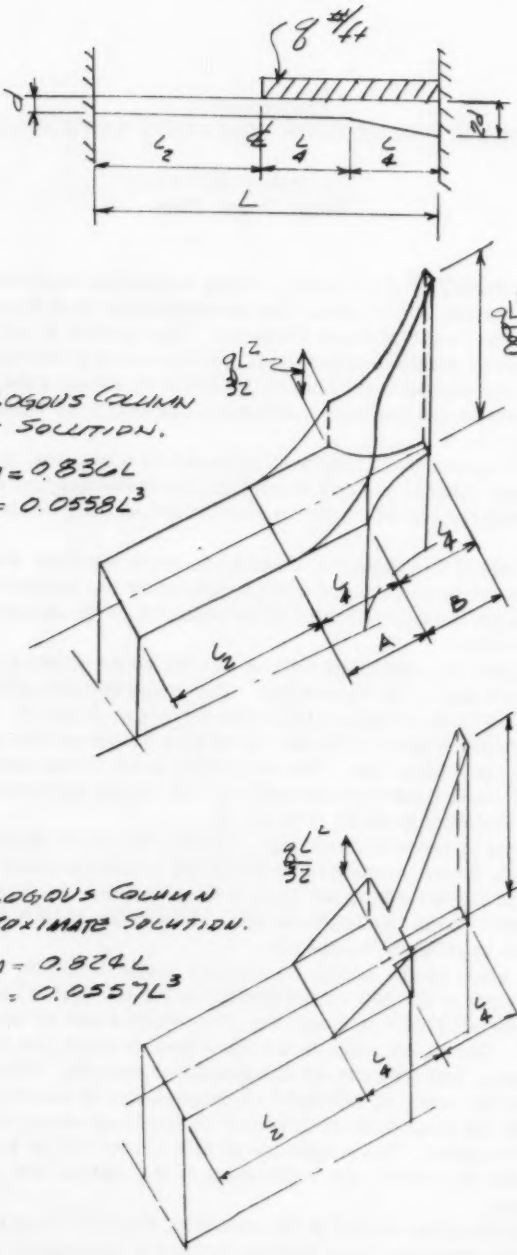
ANALOGOUS COLUMN
EXACT SOLUTION.
AREA = 0.836L
I = 0.0558L³
ANALOGOUS COLUMN
APPROXIMATE SOLUTION.
AREA = 0.824L
I = 0.0557L³

Fig. 1.

the approximate method of solution. As was commented by the author, two solids will be required for the determination of all the desired constants.

THOMAS D. Y. Fok,[27] A.M. ASCE.—The author is to be commended for his exploration of moment distribution constant determinations by model experiment procedures. With the aide of the "Pressure Solid" the effect of a varying moment of inertia upon the moment distribution constants can be easily visualized. Indirectly, the manipulation for determining the moment distribution constants by "Column Analogy" is more easily understood as a result of this method.

In order to appraise the merit of this method two points will be stressed. (1) Accuracy of the results obtained by the experimental method in comparison with the "exact" analytical method, and the "approximate" method ordinarily used in design office practice. (2) The time factor, as a basis for comparing the advantage of the method over other procedures. In the "approximate" method the properties of the analogous column section of the member under consideration are determined, first, by dividing the member into segments. Then, the moment of inertia of each segment is assumed to be uniform, and the value obtained by averaging the varying moments of inertia of the segment.

Degree of accuracy in the computation of moment distribution constants is mainly determined by the type and function of the structure under consideration. In the design of a member in a structure, moment, shear, and axial stress values used are dependent upon the physical properties of the member. That is, the modulus of elasticity, the moment of inertia, and the accuracy of the dimensions of the member, etc. The accurate determination or estimation of the physical properties, and their influence upon the final results of analysis has been the subject of debate for many years, and continues so.

Good practice in design dictates that the selection of values of modulus of elasticity and moment of inertia be those that give conservative design. In keeping with this, the accuracy of results obtained by model experiment or analytical methods can then be compared on a basis of the properties assumed.

Accuracy of Results

A The results obtained by model experiment are dependent upon
a) measurement of the dimensions of model
b) b) homogeneity of the material used for the model
c) c) accuracy of balancing and weighing
d) accuracy of arithmetical computations

Since moment distribution constants are functions of the four factors mentioned, the relative errors of the results is the sum of the relative errors of the individual factors which are independent of each other. The reduction of the relative error in one factor will reduce the relative error of the final result proportionately.

B The error of the results for moment distribution constants obtained by an exact analytical procedure—either by the integration method or the Column

27. Design Engr., Richardson, Gordon and Associates, Pittsburgh, Pa.

Analogy method—is subject only to the error of arithmetical computation, and can be controlled by the "rounding off" of values. Accuracy can be to any degree desired. Results obtained by this method are used in making a comparison with the author's method.

C The error occurring in the determination of moment distribution constants by the approximate method results from the variation of moment of inertia in adjacent segments of a member being analyzed. The error can be reduced, somewhat, by increasing the number of segments used in the determination of the moment of inertia, but depends on the type and shape of the structure, and the type of loading to which the structure is subjected. The magnitude of the error changes accordingly. Design office practice is to use data that has been compiled in tabular or chart form-based on approximate methods of calculation- either approximate integration or Column Analogy.

If errors occurring in the four items listed above under A can be reduced with little effort, and to a greater extent than those obtaining in the approximate analytical method, then the advantage of the model experimental method is readily apparent—at least in comparison of accuracy.

To compare the accuracy of the determination of moment distribution constants by the exact analytical method with the approximate analytical method, an example of a haunched beam is used. See Figure 1.

For computation by the approximate method the beam is divided into ten segments of one foot length. Moment distribution constants and fixed end moments due to a one Kip per foot uniform load are determined by both the exact and the approximate methods. The results have been tabulated in Table I, and are compared with values obtained from tabular data published by the Portland Cement Association,[28] and by Column Analogy, where the properties were obtained by the approximate method.

A comparison of the errors resulting from the experimental "Pressure Solid" method and the "Cardboard Model" method are shown in Table II.

In comparing the relative errors in Tables I and II, the accuracy of the results obtained by the approximate analytical method is better than those resulting from the model experimental method. It should be noted, however, that this occurs in a member of simple shape, with simple loading, and only two or three different values of moment of inertia. Under such conditions the approximate analytical method furnishes more accurate results than model experimental procedures. With members of complex shapes (arches, etc.), and with complicated loadings the accuracy of the approximate method is reduced. Use of the exact analytical method requires increased labor and becomes quite involved. In such cases, model experimental methods will serve an important role in the determination of moment distribution constants, and will give much more accurate results with no increase in effort.

It is shown in Table II that the average accuracy of the results obtained from cardboard models is lower than those from the Pressure Solid method. The choice of method will ordinarily depend upon the time and expense required to construct the models, to test them, and to make the required computations. Cardboard models can be more readily furnished than the wooden models used in the Pressure Solid method. However, if Plaster of Paris, paraffin or other readily molded materials can be used, the construction of models will not necessarily govern the selection of the method used for obtaining the desired information.

---

28. Handbook of Frame Constants published by P.C.A.

It should be noted that the influence line for fixed end moment can be determined by one set up of end rotation by use of a cardboard model, whereas several pressure solids should be used in the other model method. Construction and weighing of the Pressure Solid model requires more time than the measurement of a deflected curve of the cardboard model.

Time Factor in Obtaining Final Results

Time required depends upon the skill of the computer. If the type of member and loading are simple the approximate or exact analytical methods will give results more rapidly and accurately than those derived from model experiments. With complicated types of structures, such as an arch with variable cross section, time consuming and laborious computations become necessary. In addition, there is loss of accuracy. If equal time is required to determine final results by the approximate analytical method and the model method, then the latter method should be used because of the gain in accuracy. Time, cost and accuracy are the governing factors in the selection of the method to be used. A satisfactory determination would probably require a rather comprehensive study.

In the determination of fixed end moments due to a uniform load by the method of Column Analogy, the use of the moment area with parabolic curve as a load becomes necessary. The determination of loads and moments on the analogous column is thereby complicated. In the case mentioned, a modified method, as shown by the author in section 8—Fixed end moments—can be used.

As an example, the beam shown in Figure 2, with a uniform load of one Kip per foot, illustrates the use of the modified column section to determine load and moment on the analogous column. In order to make the structure statically determinate for the application of Column Analogy, the support at A is removed and the beam acts as a cantilever, fixed at B. The moment diagram is shown in Figure 2. The moment area is applied as a load on the analogous column. The magnitude of the load and its moment about the center line of the analogous column is determined as shown below.

$$\text{Area} = 1x5 + 0.5x5 = 7.5$$

$$\bar{X} = \frac{5x2.5 + 2.5x7.5}{7.5} = 4.17'$$

P = Load on analogous column

$= P_1\,(abcd) + P_2\,(aefg)$

$= 1/3x12.5x5x0.5 + 1/3x50x10x0.5$

$= 10.43 + 83.30 = \underline{93.73}$

M = Moment of load about center line of analogous column section.

$M = 10.43x - (4.17-3.75) + 83.30x(7.5-4.17)$

$= 277.66-4.38 = \underline{273.28}$

The same problem can be solved by the substitution of prismatic solids for the solid with parabolic curve, again using the modified method for the determination of loads and moments on the analogous column. The solution is shown on Figure 3.

If the modified analogous column section is used, the moment diagram can

be determined from M = WX, and the width of the analogous column is equal to (x/2 x 1/EI).

The load on the analogous column will be

$$P = \text{Volume } P + \text{Volume } P$$
$$= 1/3x5x2.5x5 + 5/3x(1.25x5 + 2.5x10 + \sqrt{156.25}\ )$$
$$= 20.80 + 73.0 = 93.80$$

M = Moment of load about center of original analogous column

$$= -20.80x(4.17-3.75) + 73.00x3.86 = \underline{273.26}$$

In arch analysis the member under consideration is usually one of variable cross section. For the determination of stiffness, carry over factors, and fixed end moments, due to concentrated or uniform loads, the approximate method for final design purposes may not be of sufficient accuracy unless an increased number of segments are used. Since a solution by integration is tedious and laborious, either Eney's method or the Pressure Solid method can be used. The selection of method will depend upon the knowledge and experience of the analyst.

One disadvantage of the Pressure Solid method that the writer wishes to emphasize is that in order to determine fixed end moments due to concentrated loads at different points on the structure, different pressure solids must be used. This requires more time than Eney's method, in which one distortion at the end support will give influence ordinates simply by measuring the deflection curve of the structure.

Without regard to the time required for the determination of stiffness, carry over factors, and fixed end moments for indeterminate structures by the Pressure Solid method, the author is to be congratulated for having further explored means of solving for these factors by a unique experimental procedure. It is hoped that a paper dealing with application of the method to arches will soon be made available.

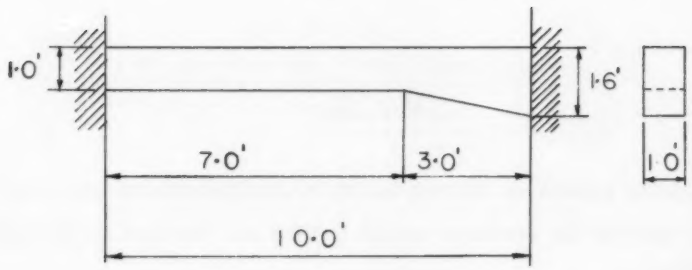

FIG. 1

TABLE I

Moments Distribution Constants and Fixed Moments

	(1)	(2)	(3)	(4)
Stiffness S_A	0.448	0.458	0.010	2.23%
Stiffness S_B	0.684	0.702	0.018	2.64%
Carry Over Factor C_{AB}	0.704	0.716	0.012	1.71%
Carry Over Factor C_{BA}	0.461	0.466	0.005	1.09%
*Fixed End Mom. M_{AB}	6.90	-6.84	-0.06	0.87%
*Fixed End Mom. M_{BA}	1.162	1.164	0.002	0.17%

(1) By exact analytical method. P.C.A. Handbook of Frame Constants

(2) By approximate method with column analogy.

(3) Difference of (2) and (1). Error resulting from the approximate method.

(4) Percentage of error in terms of exact analytical method.

* Fixed End Moment in Kip Ft.

TABLE II

Relative Errors of Moment Distribution Constants and Fixed End Moments by Pressure Solid Method and by Cardboard Model Method.

	(1)	(2)
Stiffness	5.0%	-8.3%
Carry Over Factor	3.9	4.0
Fixed End Moments	2.1	4.5
Impressed Distortion	1.8	*

(1) By Pressure Solid Method. Maximum values used.

(2) Data from article, Page 816, Engineering News Record, Dec.12, 1935, "Fixed Ended Moments by Cardboard Models", W.J. Eney.

* Not computed in data.

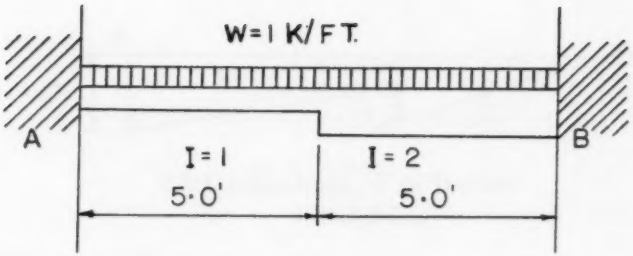

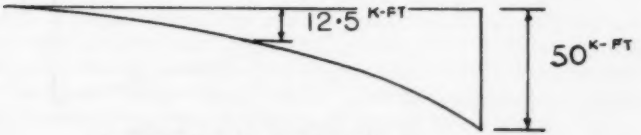

MOMENT DIAGRAM
FOR CANTILEVER AB

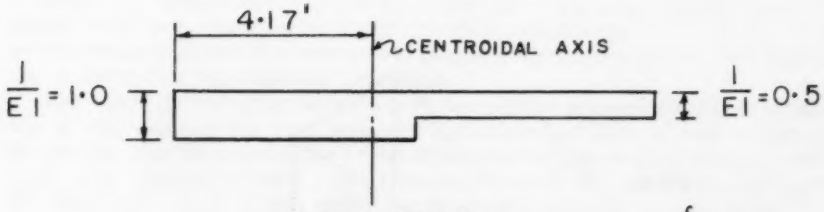

ANALOGOUS
COLUMN

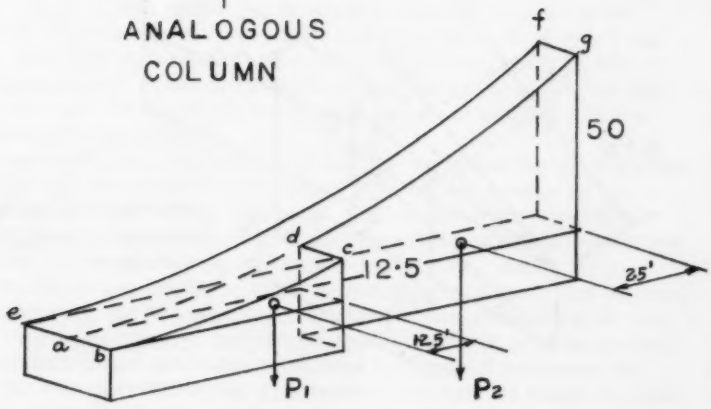

FIG. 2

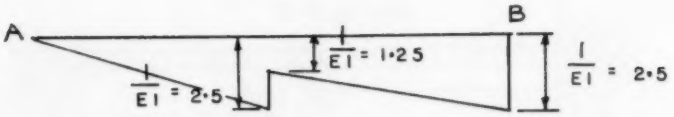

MODIFIED ANALOGOUS COLUMN

MODIFIED MOMENT DIAGRAM

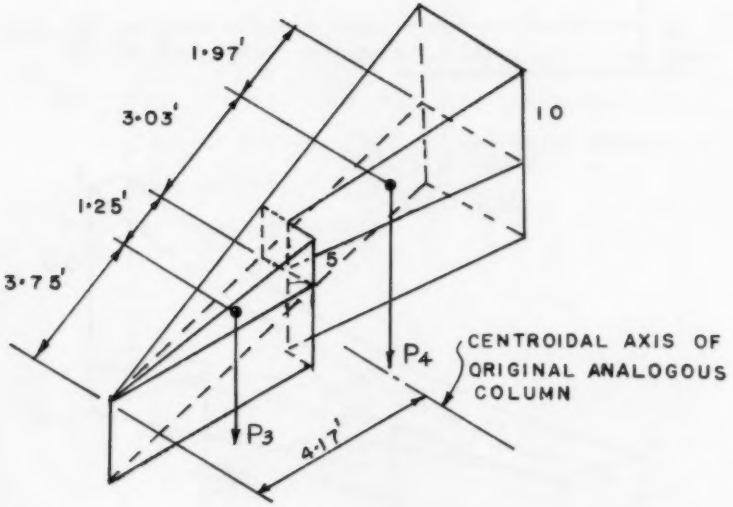

FIG. 3

Discussion of
"THE PAINTING OF STRUCTURAL STEEL"

by E. J. Ruble
(Proc. Paper 1100)

LUDWIG ADAMS,[29] M. ASCE.—Mr. Ruble's paper serves, among other things, to focus the structural engineer's attention on the economic importance of corrosion protection and to clear away some of the mystery on paint and painting. Past poor practice was not due so much to indifference to painting as a necessary evil but rather to a general lack of understanding of the corrosion problem and a scarcity of correlated reliable data, based upon laboratory and field service tests, which could be used in determining the best painting system, from the standpoint of annual maintenance cost.

It is grossly inadequate, and actually negligent, to merely specify, "All steel shall be thoroughly cleaned by approved means, shop painted with one coat of suitable rust inhibitive primer, and field painted, after erection, with one coat of weather resistant paint of a color to be selected by the owner." Typically, the pages of a voluminous specification are often replete with much detail on working loads, design stresses, welding or other joining processes, qualification of operators, inspection procedures, etc., but painting is covered in one impotent paragraph

How many specification writers have been lulled into low first cost thinking by such panacea as, "Our specially formulated patented primer requires no special surface preparation or pretreatment, can be applied directly over rust, as on weathered steel, has a coverage of about 600 square feet per gallon and costs only $3.00 per gallon. It forms a firm base for and can be finished with any topcoat but we recommend our coverall enamel which has a coverage of about 800 square feet per gallon and does not chalk or fade in any normal atmosphere?" Disconcertingly enough the above statement may very well be true—but the structure could show extensive rusting within a few months in a rural atmosphere.

Since the engineer's ultimate purpose is to give the client the most for his money, the paint system should be engineered with the same care as the functional design of the structure. The paint system should be consistent with the intended service, and based upon past experience as modified by new developments in improved paint materials and application. Above all it should be specified as a complete system, including adequate surface preparation, surface pretreatment if necessary, suitable primers, intermediate and topcoats, as many as necessary, and proper application with good equipment by trained operators under favorable conditions to required minimum dry film thicknesses with correct drying time between the various coats of paint.

As emphasized by Mr. Ruble, the Steel Structures Painting Council Painting Manual, particularly Volume 2, provides the engineer with as much detail as he may see fit to use in his specifications but it is entirely adequate to

---

29. Research Engr., Pittsburgh-Des Moines Steel Co.

select, say, Paint System 1 (SSPC-PS1-55T), to provide the client with a complete specification and afford him reasonable assurance that his structure will have suitable corrosion protection.

One of the most important accomplishments of the various SSPC specifications is the criterion of performance. It should no longer be necessary, for example, for the client to insist that by blast cleaning he meant cleaning to "white metal" whereas the contractor assumed and insists "brush-off" cleaning is sufficient for the purpose and based his price upon same. The engineer would merely have to specify SSPC-SP6-52T, "Commercial Blast Cleaning" and there remains no ambiguity or ground for disagreement. Furthermore all contractors would be bidding on the same basis and a more equitable contract can be made. Similarly the client's inspector cannot arbitrarily insist on more paint to be applied if his thickness gauge indicates that the dry film meets the minimum specified in the contract.

In addition to being in the Painting Manual, all of the SSPC Specifications are available as separates and as such could be made available to inspectors, as necessary, to avoid misunderstanding as to performance and acceptance. Currently available specifications cover nine on surface preparation, including solvent cleaning, hand cleaning, power tool cleaning, flame cleaning, blast cleaning to white metal, commercial blast cleaning, brush-off blast cleaning, pickling, and weathering-cleaning. Four pretreatment specifications include wetting-oil treatment, cold phosphate treatment, basic zinc-chromate vinyl butyral washcoat, and hot phosphate surface treatment. The paint application specification covers shop, field, and maintenance painting. Nine paint system specifications include oil base systems for weather exposure, alkyd systems for weather exposure, high humidity, and infrequent immersion; phenolic systems for fresh water immersion, alternate immersion, high humidity and condensation, and weather exposure; vinyl systems for chemical exposure, fresh and salt water immersion, alternate immersion, high humidity and condensation, and weather exposure; paint systems for hand cleaned water immersed steel; one-coat shop paint systems for structural steel; rust preventive compounds, thick film; and bituminous coatings including enamels, cold applied mastics, and emulsions. There are also twenty specifications covering various primers, intermediate, and topcoats.

As a convenience, the Painting Manual includes an index of applicable A.S.T.M. and U.S. Government specifications on paint and paint materials.

The final proof of the painting is in its actual service life. Field tests, such as those so well described by Mr. Ruble on railway bridge applications, are indispensible as an engineering tool to determine which of several suitable paint systems are the most economical for a specific structure in a given locality. Local service and weather conditions, type of atmosphere, whether rural, industrial, or marine, and established paint maintenance policy make each application a unique one. There are no general solutions, except very expensive but uneconomical ones. The final solution is often one of trial and error. Mr. Ruble has pointed out how you can converge toward the final solution.

Discussion of
"SIMPLIFIED ANALYSIS OF RIGID FRAMES"

by Robert M. Barnoff
(Proc. Paper 1106)

THEIN WAH,[30] A.M. ASCE.—The analysis of bridge piers is generally laborious, even in such cases as a two-column pier. Any simplification of the procedure should be welcomed by practicing engineers. Mr. Barnoff's formulas and charts should prove a valuable addition to the designer's repertoire.

However, it is the writer's opinion that the structural engineering profession tends to be overburdened with charts, curves and tables. In many instances these aids to analysis are a necessity and the time taken to understand and use these charts is well worthwhile. The use of such aids ceases to be meaningful, however, when extended to cases which might be analyzed by well-understood procedures in common use.

The method presented by the author requires nine charts for the relatively simple cases covered in the paper. One can well imagine the multiplicity of diagrams that a designer would need to have at hand in order to analyze some of the more complicated cases—such as frames with non-prismatic members —met with in practice. This is not to be construed as a criticism of the paper but it is an essential drawback of the method that has to be pointed out.

The author states that it is usually necessary to solve at least four moment distribution problems for a complete analysis of a frame used as a bridge pier. Actually, by using well-known procedures, it is possible to analyze a two-column symmetrical frame with no more than two distributions, and a three-or four-column symmetrical frame with no more than three distributions. Only in the case of a five-column symmetrical frame does one need to go through four distributions. The procedure referred to is merely the old one of using influence coefficients.

As an illustration consider the frame in the author's Fig. 3. All that is necessary is to carry out the distributions for the cases shown in Figs. (A) and (B):

In Fig. (A) are shown the balanced moments in the frame for a 100^{k} horizontal load; the results are obtained by ordinary moment distribution and the designer's sign convention has been used. Fig. (B) shows the balanced moments in the frame for a 100^{kl} external moment applied to joint B. For the sidesway correction, the results of Fig. A are used. The moments in Fig. (C) are written down by inspection from the values in Fig. (B). Figs. (A), (B) and (C) furnish all the information necessary to analyze any case involving horizontal or vertical loads.

The fixed-end moments due to vertical loads, as given by the author for the illustrative example, cause an unbalanced clockwise moment of 123^{kl} on

---

30. Asst. Prof. of Civ. Eng., Univ. of Connecticut, Storrs, Conn.

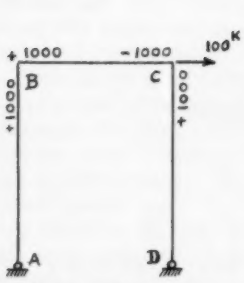

Fig. (A)

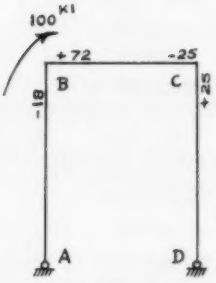

Fig. (B)

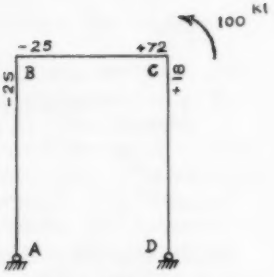

Fig. (C)

joint B, and an unbalanced counterclockwise moment of 70kl on joint C. The final balanced moment in the column can be written by using the results in Figs. (B) and (C) as:

$$M_{BA} = \frac{123}{100}(-18) + \frac{70}{100}(-25) = -40^{kl}$$

This is close to the author's result of -41kl (the 61kl shown in the author's paper is clearly a typographical error). For the horizontal load of 20k applied at the top, the result is, from Fig. (B)

$$M_{BA} = \frac{1000}{100} \times 20 = 200^{kl}$$

For the shrinkage of the cap, the fixed-end moment at the top for the given Δ is $\frac{3EI\Delta}{2} = 114^{kl}$. This is a clockwise unbalanced moment at joint B. Similarly a counterclockwise moment of 114kl exists at joint C. Hence, from Figs. B and C

$$M_{BA} = 114 - \frac{114}{100}(18) - \frac{114}{100}(25)$$

$$= 65^{kl}$$

It is evident that Figs. (A), (B) and (C) may be used for any position of the live load. They could also furnish influence coefficients for shears in the members, if desired. The writer believes they are particularly flexible as applied to bridge piers. For example, the AASHO specifications require that certain lateral wind forces be applied at a definite height above top of pier. Since such forces must cause a horizontal force as well as a couple to act on the pier, Figs. (A) and (B) may be combined to give the solution.

PROCEEDINGS PAPERS

The technical papers published in the past year are identified by number below. Technical-division sponsorship is indicated by an abbreviation at the end of each Paper Number, the symbols referring to: Air Transport (AT), City Planning (CP), Construction (CO), Engineering Mechanics (EM), Highway (HW), Hydraulics (HY), Irrigation and Drainage (IR), Power (PO), Sanitary Engineering (SA), Soil Mechanics and Foundations (SM), Structural (ST), Surveying and Mapping (SU), and Waterways and Harbors (WW) divisions. Papers sponsored by the Board of Direction are identified by the symbols (BD). For titles and order coupons, refer to the appropriate issue of "Civil Engineering." Beginning with Volume 82 (January 1956) papers were published in Journals of the various Technical Divisions. To locate papers in the Journals, the symbols after the paper numbers are followed by a numeral designating the issue of a particular Journal in which the paper appeared. For example, Paper 1113 is identified as 1113 (HY6) which indicates that the paper is contained in the sixth issue of the Journal of the Hydraulics Division during 1956.

VOLUME 82 (1956)

MARCH: 906(WW1), 907(WW1), 908(WW1), 909(WW1), 910(WW1), 911(WW1), 912(WW1), 913 (WW1)[c], 914(ST2), 915(ST2), 916(ST2), 917(ST2), 918(ST2), 919(ST2), 920(ST2), 921(SU1), 922(SU1), 923(SU1), 924(ST2)[c].

APRIL: 925(WW2), 926(WW2), 927(WW2), 928(SA2), 929(SA2), 930(SA2), 931(SA2), 932(SA2)[c], 933(SM2), 934(SM2), 935(WW2), 936(WW2), 937(WW2), 938(WW2), 939(WW2), 940(SM2), 941 (SM2), 942(SM2)[c], 943(EM2), 944(EM2), 945(EM2), 946(EM2)[c], 947(PO2), 948(PO2), 949(PO2), 950(PO2), 951(PO2), 952(PO2)[c], 953(HY2), 954(HY2), 955(HY2)[c], 956(HY2), 957(HY2), 958 (SA2), 959(PO2), 960(PO2).

MAY: 961(IR2), 962(IR2), 963(CP2), 964(CP2), 965(WW3), 966(WW3), 967(WW3), 968(WW3), 969 (WW3), 970(ST3), 971(ST3), 972(ST3)[c], 973(ST3), 974(ST3), 975(WW3), 976(WW3), 977(IR2), 978(AT2), 979(AT2), 980(AT2), 981(IR2), 982(IR2)[c], 983(HW2), 984(HW2), 985(HW2)[c], 986(ST3), 987(AT2), 988(CP2), 989(AT2).

JUNE: 990(PO3), 991(PO3), 992(PO3), 993(PO3), 994(PO3), 995(PO3), 996(PO3), 997(PO3), 998 (SA3), 999(SA3), 1000(SA3), 1001(SA3), 1002(SA3), 1003(SA3)[c], 1004(HY3), 1005(HY3), 1006 (HY3), 1007(HY3), 1008 (HY3), 1009 (HY3), 1010 (HY3)[c], 1011 (PO3)[c], 1012 (SA3), 1013 (SA3), 1014(SA3), 1015(HY3), 1016(SA3), 1017(PO3), 1018(PO3).

JULY: 1019(ST4), 1020(ST4), 1021(ST4), 1022(ST4), 1023(ST4), 1024(ST4)[c], 1025(SM3), 1026 (SM3), 1027(SM3), 1028(SM3)[c], 1029(EM3), 1030(EM3), 1031(EM3), 1032(EM3), 1033(EM3)[c].

AUGUST: 1034(HY4), 1035(HY4), 1036(HY4), 1037(HY4), 1038(HY4), 1039(HY4), 1040(HY4), 1041(HY4)[c], 1042(PO4), 1043(PO4), 1044(PO4), 1045(PO4), 1046(PO4)[c], 1047(SA4), 1048 (SA4)[c], 1049(SA4), 1050(SA4), 1051(SA4), 1052(HY4), 1053(SA4).

SEPTEMBER: 1054(ST5), 1055(ST5), 1056(ST5), 1057(ST5), 1058(ST5), 1059(WW4), 1060(WW4), 1061(WW4), 1062(WW4), 1063(WW4), 1064(SU2), 1065(SU2), 1066(SU2)[c], 1067(ST5)[c], 1068 (WW4)[c], 1069(WW4).

OCTOBER: 1070(EM4), 1071(EM4), 1072(EM4), 1073(EM4), 1074(HW3), 1075(HW3), 1076(HW3), 1077(HY5), 1078(SA5), 1079(SM4), 1080(SM4), 1081(SM4), 1082(HY5), 1083(SA5), 1084(SA5), 1085(SA5), 1086(PO5), 1087(SA5), 1088(SA5), 1089(SA5), 1090(HW3), 1091(EM4)[c], 1092 (HY5)[c], 1093(HW3)[c], 1094(PO5)[c], 1095(SM4)[c].

NOVEMBER: 1096(ST6), 1097(ST6), 1098(ST6), 1099(ST6), 1100(ST6), 1101(ST6), 1102(IR3), 1103 (IR3), 1104(IR3), 1105(IR3), 1106(ST6), 1107(ST6), 1108(ST6), 1109(AT3), 1110(AT3)[c], 1111(IR3)[c], 1112(ST6)[c].

DECEMBER: 1113(HY6), 1114(HY6), 1115(SA6), 1116(SA6), 1117(SU3), 1118(SU3), 1119(WW5), 1120(WW5), 1121(WW5), 1122(WW5), 1123(WW5), 1124(WW5)[c], 1125(BD1)[c], 1126(SA6), 1127 (SA6), 1128(WW5), 1129(SA6)[c], 1130(PO6)[c], 1131(HY6)[c], 1132(PO6), 1133(PO6), 1134(PO6), 1135(BD1).

VOLUME 83 (1957)

JANUARY: 1136(CP1), 1137(CP1), 1138(EM1), 1139(EM1), 1140(EM1), 1141(EM1), 1142(SM1), 1143(SM1), 1144(SM1), 1145(SM1), 1146(ST1), 1147(ST1), 1148(ST1), 1149(ST1), 1150(ST1), 1151(ST1), 1152(CP1)[c], 1153(HW1), 1154(EM1)[c], 1155(SM1)[c], 1156(ST1)[c], 1157(EM1), 1158 (EM1), 1159(SM1), 1160(SM1), 1161(SM1).

FEBRUARY: 1162(HY1), 1163(HY1), 1164(HY1), 1165(HY1), 1166(HY1), 1167(HY1), 1168(SA1), 1169(SA1), 1170(SA1), 1171(SA1), 1172(SA1), 1173(SA1), 1174(SA1), 1175(SA1), 1176(SA1), 1177(HY1)[c], 1178(SA1), 1179(SA1), 1180(SA1), 1181(SA1), 1182(PO1), 1183(PO1), 1184(PO1), 1185(PO1)[c].

MARCH: 1186(ST), 1187(ST), 1188(ST), 1189(ST), 1190(ST), 1191(ST), 1192(ST)[c], 1193(PL), 1194(PL), 1195(PL),

c. Discussion of several papers, grouped by Divisions.

AMERICAN SOCIETY OF CIVIL ENGINEERS

OFFICERS FOR 1957

PRESIDENT

MASON GRAVES LOCKWOOD

VICE-PRESIDENTS

Term expires October, 1957:
FRANK A. MARSTON
GLENN W. HOLCOMB

Term expires October, 1958:
FRANCIS S. FRIEL
NORMAN R. MOORE

DIRECTORS

Term expires October, 1957:
JEWELL M. GARRELTS
FREDERICK H. PAULSON
GEORGE S. RICHARDSON
DON M. CORBETT
GRAHAM P. WILLOUGHBY
LAWRENCE A. ELSENER

Term expires October, 1958:
JOHN P. RILEY
CAREY H. BROWN
MASON C. PRICHARD
ROBERT H. SHERLOCK
R. ROBINSON ROWE
LOUIS E. RYDELL
CLARENCE L. ECKEL

Term expires October, 1959:
CLINTON D. HANOVER, Jr.
E. LELAND DURKEE
HOWARD F. PECKWORTH
FINLEY B. LAVERTY
WILLIAM J. HEDLEY
RANDLE B. ALEXANDER

PAST-PRESIDENTS

Members of the Board

WILLIAM R. GLIDDEN

ENOCH R. NEEDLES

EXECUTIVE SECRETARY
WILLIAM H. WISELY

TREASURER
CHARLES E. TROUT

ASSISTANT SECRETARY
E. L. CHANDLER

ASSISTANT TREASURER
CARLTON S. PROCTOR

PROCEEDINGS OF THE SOCIETY

HAROLD T. LARSEN
Manager of Technical Publications

PAUL A. PARISI
Editor of Technical Publications

DANIEL GOTTHELF
Asst. Editor of Technical Publications

COMMITTEE ON PUBLICATIONS

JEWELL M. GARRELTS, *Chairman*

HOWARD F. PECKWORTH, *Vice-Chairman*

E. LELAND DURKEE

MASON C. PRICHARD

R. ROBINSON ROWE

LOUIS E. RYDELL